University of Glasgow | Institute of Molecular, Cell & Systems Biology

An Investigation of the Molecular Pharmacology of G protein-coupled receptor 35

Amanda Elaine Mackenzie
M.Sc., B.Sc. (Hons) IP

A thesis submitted
in fulfilment of the requirements for the Degree of
Doctor of Philosophy

Supervised by Professor Graeme Milligan

May 2015

Abstract

G protein-coupled receptors (GPCRs) are seven-pass integral membrane proteins that act as transducers of extracellular signals across the lipid bilayer. Their location and involvement in basic and pathological physiological processes has secured thier role as key targets for pharmaceutical intervention. GPCRs are targeted by many of the best selling drugs on the market yet there are a substantial number of GPCRs that are yet to be characterised and could offer interest for therapeutic intervention. GPR35 is one such receptor that, as a result of gene knockout and genome wide association studies, has attracted interest through its association with cardiovascular and gastrointestinal disease. Elucidation of the basic physiological function of GPR35 has, however, been difficult due a paucity of potent and selective ligands and a lack of consensus on the endogenous ligand. Herein, a focussed drug discovery effort was carried out to identify agonists of GPR35. Various *in vitro* cellular assays were employed in conjunction with N- or C-terminally manipulated forms of the receptor to investigate GPR35's signalling profile and to provide an assay format suitable for the characterisation of newly identified ligands. Although GPR35 associates with both $G\alpha_{i/o}$ and $G\alpha_{13}$ families of small heterotrimeric G proteins, the G protein independent β-arrestin-2 recruitment format was found to be the most suited to drug screening efforts. Small molecule compound screening, carried out in conjunction with the Medical Research Council Technology, identified compound 1 as the most potent ligand of human GPR35 reported at that time. However, the lower efficacy and potency of compound 1 at the rodent species orthologues of GPR35 prevented its use in *in vivo* studies. A subsequent effort carried out with Novartis, focussing on mast cell stabilisers as putative agonists of GPR35, revealed lodoxamide and bufrolin as highly potent agonists that activated human and rat GPR35 with equal potency. This finding offered – for the first time – the opportunity to employ the same GPR35 ligand between species, an important factor to consider when translating rodent *in vivo* functional studies to those in man. Additionally, using molecular modelling and site directed mutagenesis studies, these newly identified compounds were used to aid characterisation of the ligand binding pockets of human and rat GPR35 to reveal the molecular basis of species selectivity at this receptor. In summary, this research effort presents GPR35 tool compounds that can now be used to dissect the basic biology of GPR35 and investigate its contribution to disease.

Contents

Page Number:

Abstract ... ii

List of Tables ... x

List of Figures ... xii

Acknowledgements ... xv

Author's Declaration ... xvi

Abbreviations ... xvii

Chapter One: An Introduction to drug discovery, G protein-coupled receptors and GPR35 ... 1

1.1 An overview of therapeutic targets and drug discovery ... 2

1.1.1 *GPCRs and their relevance to drug discovery* ... 2

1.2 Classical and reverse pharmacology for drug discovery at GPCRs ... 5

1.2.1 *GPCR deorphanisation efforts* ... 6

1.2.2 *There are many routes to becoming a therapeutic target: orphan GPCRs and ligands* ... 7

1.3 The orphan GPCR GPR35 as a novel therapeutic target ... 9

1.3.1 *Gene expression analysis and tissue distribution profile of GPR35* ... 9

1.3.2 *Chromosomal location of GPR35 and exon usage* ... 11

1.3.3 *Diseases associated with GPR35: cardiovascular disease* ... 13

1.3.4 *Diseases associated with GPR35: metabolic and gastrointestinal diseases* ... 15

1.3.5 *Diseases associated with GPR35: inflammation* ... 16

1.4 The function and structure of GPCRs ... 17

1.4.1 *GPCR signalling* ... 17

1.4.2 *GPCR structure* ... 20

1.4.3 *Lessons of GPCR activation from the prototypical GPCRs* ... 22

1.4.4 *GPR35 and the prototypical GPCRs* ... 25

1.5 Receptor pharmacology ... 28

1.5.1 *The plasticity of GPCRs and the effects of ligand binding* ... 28

1.5.2 *The assessment of ligand properties through physiochemical parameters* 28
1.5.3 *Ligands acting at GPR35: proposed endogenous ligands* 30
1.5.4 *Ligands acting at GPR35: synthetic ligands* 36
1.7 Aim of Ph.D. 41
Chapter Two: Materials and Methodology 42
2.1 Materials 43
2.2 Pharmacological test compounds 43
2.3 DNA constructs and plasmids 44
2.4 Molecular biology protocols 46
2.4.1 *Preparation of Luria Bertani broth and agar* 46
2.4.2 *Preparation of chemically competent XL-1 Blue cells* 47
2.4.3 *Preparation of yeast peptone dextrose* 48
2.4.4 *Preparation of chemically competent Saccharomyces cerevisiae cells* 48
2.4.5 *Transformation of S. cerevisiae by heat-shock method* 49
2.4.6 *RNA isolation and two-step reverse-transcription polymerase chain reaction* 50
2.4.7 *DNA gel electrophoresis* 52
2.4.8 *In vitro site-directed mutagenesis* 53
2.4.9 *PCR cloning and DNA Ligation using T4 DNA Ligase* 55
2.4.10 *Transformation of XL-1 Blue by heat-shock method* 56
2.4.11 *The Wizard Plus SV Miniprep System for isolation of plasmid DNA from XL-1 Blue* . 57
2.4.12 *Quantification of nucleic acid purity by UV spectrophotometry* 58
2.4.13 *DNA sequencing* 58
2.4.14 *Isolation of plasmid DNA using the QIAfilter Plasmid Maxi kit from QIAGEN* 59
2.5 Mammalian Cell Culture 60
2.5.1 *Maintenance of cell culture* 60
2.5.2 *Cell lines and cell culture* 60
2.5.3 *Passaging of cells* 61
2.5.4 *Transient transfection* 62
2.5.5 *Generation of a Flp-In™ T-REx™ HEK293 stable cell line* 62
2.6 Biochemical assays and procedures 64
2.6.1 *Cell harvesting* 64
2.6.2 *Isolation of cellular lysates* 64

2.6.3 *Sodium dodecyl sulphate polyacrylamide gel electrophoresis (SDS-PAGE)* 64
2.6.4 *Western blot* 65
2.6.5 *Isolation of cellular membranes* 66
2.6.6 *Estimation of protein concentration by the bicinchoninic acid method* 67
2.6.7 *[^{35}S]GTPγS filtration binding assay* 68
2.6.8 *Mammalian Gα$_{13}$ [^{35}S]GTPγ[S] (guanosine 5'-[γ-[^{35}S]thio]triphosphate)-binding assay* 69
2.7 Cell based assays 70
2.7.1 *The S. cerevisiae Yeast Assay using chimeric G proteins* 70
2.7.2 *Inositol Phosphate (IP-One) accumulation assay using chimeric Gα protein subunits* 71
2.7.3 *Detection of β-arrestin recruitment using BRET technology* 73
2.7.4 *Measuring the kinetics of β-arrestin recruitment using BRET technology* 75
2.7.5 *Cell surface enzyme-linked immunosorbent (ELISA) assay* 75
2.7.6 *Receptor internalisation by high content imaging (ArrayScan™)* 76
2.7.7 *Visualisation of receptor internalisation by ZEISS VivaTome spinning disk confocal microscopy* 77
2.7.8 *Dynamic mass redistribution using the Corning® Epic®BT system* 78
2.8 Data analysis 79
2.8.1 *Analysis of agonist functional data* 79
2.8.2 *Analysis of functional antagonist competition experiments* 80
2.8.3 *Global Gaddum/Schild EC$_{50}$ analysis* 80
2.8.4 *Analysis of ligand bias by calculation of the log (dose response) ratio* 82
2.8.5 *Statistical analysis* 83
Chapter Three: Identification of drug screening formats for GPR35 84
3.1 Investigating G protein signal transduction pathways associated with GPR35 85
3.1.1 *Investigating zaprinast-induced G protein coupling at human and rat GPR35 in the yeast assay* 87
3.1.2 *Investigation of G protein coupling to human GPR35 using zaprinast in the [^{35}S]GTPγS assay* 89
3.1.3 *Assessing Gα$_{13}$ coupling to human GPR35 using a [^{35}S]GTPγS assay with an immunoprecipitation step* 94

3.1.4 *Using chimeric Gαq proteins in a mammalian system: GPR35 IP-One assay* 96
3.1.5 *Assessment of cell number on IP_1 accumulation at human GPR35* 97
3.1.6 *Assessment of ligand incubation time on IP_1 accumulation* 97
3.1.7 *Assessment of agonist potency using $G\alpha_q$ chimeras at human and rat GPR35* 99
3.1.8 *Assessing agonist-induced responses at species orthologues of GPR35 using $G\alpha_{q13}$ in the IP-One assay* 99
3.1.9 *Assessment of constitutive activity of GPR35 using the IP-One assay system with ML-145 and CID-2745687* 101
3.2 Investigating the GPR35 internalisation process 107
3.2.1 *Measuring the kinetics of β-arrestin recruitment* 107
3.2.2 *Measuring agonist potency at GPR35 species orthologues using the BRET-based β-arrestin-2 recruitment assay* 109
3.2.3 *An assessment of GPR35 internalisation following agonist stimulation* 110
3.3 Assessing GPR35 agonism in an endogenous cell system 116
3.3.1 *Assessment of* GPR35 *expression using RT-PCR in the HT-29 cell line* 116
3.3.2 *Optimisation of the DMR assay format for GPR35 agonism in HT-29 cells* 117
3.3.3 *GPR35 agonists induce DMR in HT-29 cells* 120
3.3.4 *Zaprinast mediated DMR in HT-29 cells through activation of GPR35* 120
3.4 Discussion 121
3.4.1 *The yeast assay reveals GPR35 G protein profile but caution must be taken when using G protein chimeras* 121
3.4.2 *The yeast assay reveals a lack of species selectivity for G protein coupling and hints toward an important involvement for N-linked glycosylation at GPR35* 122
3.4.3 *Limitations of [^{35}S]GTPγS incorporation with filtration assay for GPR35* 124
3.4.4 *[^{35}S]GTPγS incorporation with immunoprecipitation step* 125
3.4.5 *A GPCR-G protein fusion construct that does not enhance signalling* 125
3.4.6 *IP_1 accumulation assays reveal different patterns of species selectivity depending on the chimera employed* 127
3.4.7 *IP_1 accumulation provides an assay format to assess constitutive activity* 127
3.4.8 *ML-145 and CID-2745687 are inverse agonists of human GPR35* 128
3.4.9 *The BRET-based β-arrestin recruitment assay reveals a distinct GPR35-β-arrestin trafficking pattern* 129

3.4.10 *The BRET-based β-arrestin recruitment assay and IP-One assays reveal distinct species selective profiles of GPR35* 131

3.4.11 *The DMR system provides a platform to assess ligand responses in an endogenous cell system without the requirement for manipulated receptor constructs* 133

3.4.12 *Conclusion* 134

Chapter Four: GPR35 Drug Discovery 136

4.1 High-throughput screening identifies distinct chemical subtypes that activate GPR35 137

4.1.1 *A background to compound library screening in collaboration with MRCT* 137

4.1.2 *Characterising GPR35 MRCT library hits using the BRET assay at species orthologues of GPR35* 138

4.1.3 *Characterising GPR35 MRCT library hits using the IP-One assay at species orthologues of GPR35* 141

4.1.4 *An assessment of pathway bias between β-arrestin-2 recruitment and IP_1 accumulation* 144

4.1.5 *Assessment of the interaction of MRCT compounds with human GPR35* 146

4.2 An assessment of mast cell stabilisers as GPR35 agonists 150

4.2.1 *Mast cell stabilisers display species selectivity at GPR35 orthologues in the BRET assay* 150

4.2.2 *Mast cell stabilisers induce G protein coupling at human GPR35* 154

4.2.3 *Transduction coefficients assess pathway bias between β-arrestin-2 and IP_1 pathways* 157

4.2.4 *Lodoxamide and bufrolin do not conform the rules of simple competitive antagonism* 157

4.3 A pharmacological characterisation of GPR35 agonist responses in a cell system endogenously expressing *GPR35* 161

4.3.1 *Profiling of GPR35 agonist responses in HT-29 cells using DMR technology* 161

4.3.2 *Confirmation that zaprinast and lodoxamide-induced signals are via GPR35 using ML-145 in the DMR assay* 165

4.3.3 *A calculation of agonist bias between β-arrestin-2, IP_1 accumulation, and DMR pathways* 165

4.4 Discussion 169

4.4.1 *Screening of MRCT's compound library and assessment of a subset of mast cell stabilisers indicate that the carboxyl group is a common structural property of*

GPR35 ligands 170

4.4.2 *What is the relevance of GPR35 ligands having mast cell stabilising properties?* 171

4.4.3 *Ligand bias at GPR35* 173

4.4.4 *Species selectivity at GPR35* 175

4.4.4.1 *Why is species selectivity so pronounced at GPR35?* 175

4.4.4.2 *What are the residues that are regulating species selectivity at GPR35?* 177

Chapter Five: Investigating Species Orthologue Selectivity of Ligands at GPR35 180

5.1 Using GPR35 species selectivity to elucidate the basis of ligand-receptor interactions ... 181

5.1.1 *Investigating the mode of ligand binding using GPR35 ligands with various species selectivity profiles* 181

5.1.2 *Identification of residues involved in ligand binding at human and rat GPR35* 182

5.1.3 *Arginine residues 164, 6.58, and 7.32 play a role in ligand binding in human GPR35* 188

5.1.4 *Arginine residues 6.58 and 7.32 act to mediate ligand responses at human GPR35* 191

5.1.5 *Addition of arginine residues 161, 6.58 and 7.32 increase human selective ligand potency at rat GPR35* 191

5.1.6 *Arginine 4.62 plays an important role in ligand binding at rat GPR35* 194

5.2 A conserved network of residues at GPR35 act in a species selective manner 199

5.2.1 *Mutation of Y3.32L perturbs ligand induced β-arrestin-2 recruitment at human and rat GPR35* 199

5.2.2 *R4.60 expression is critical for β-arrestin-2 recruitment at both human and rat GPR35* 200

5.2.3 *Mutation of D7.43A affects responses at rat GPR35 in a ligand-specific basis* 205

5.2.4 *Site directed mutagenesis efforts reveal residues involved in the activation of rat GPR35* 205

5.3 Discussion 209

5.3.1 *A conserved carboxylic acid binding arginine residue at position 3.36* 211

5.3.2 *ECL2 plays a role in ligand binding at human GPR35* 212

5.3.3 *ECL3 is critical for ligand binding at human GPR35* 215

5.3.4 *Y3.32 and D7.43 are species conserved residues at human and rat GPR35 that*

are generally involved in GPCR activation 217

5.3.5 *Conclusions* 219

Chapter Six: Final Discussion 221

6.1 General comments, findings and future perspectives 222

References 226

Appendices 260

Appendix A: Antagonists of GPR35 display high species ortholog selectivity and varying modes of action 261

Appendix B: High-throughput identification and characterisation of novel, species-selective GPR35 agonists 274

Appendix C: The antiallergic mast cell stabilizers lodoxamide and bufrolin as the first high and equipotent agonists of human and rat GPR35 285

Appendix D: American Society of Pharmacology and Experimental Therapeutics Copyright permission form 299

List of Tables

Table 1.1 *Gα protein sub-families, expression and function* 21

Table 1.2 *Purported endogenous ligands for GPR35* 32

Table 1.3 *Selection of potent GPR35 ligands* 37

Table 2.1 *GPR35 cDNA construct history and information* 45

Table 3.1 *Zaprinast couples GPR35 to $G\alpha_{i/o}$, $G\alpha_{13}$ and $G\alpha_{16}$ yeast-mammalian G proteins in the yeast assay* 91

Table 3.2 *Zaprinast and pamoic acid but not cromolyn display GPR35 species selectivity in the IP-One assay* 103

Table 3.3 *ML-145 and CID-2745687 inhibit both basal activity and agonist-induced responses at human GPR35 in the IP-One assay* 112

Table 3.4 *Agonists display species selectivity at GPR35 in the BRET-based β-arrestin-2 recruitment assay* 109

Table 3.5 *GPR35 agonists zaprinast, cromolyn and pamoic acid induce receptor internalisation* 114

Table 3.6 *GPR35 agonist responses in DMR: comparisons with IP-One and BRET assays* 119

Table 4.1 *Potency, efficacy, and selectivity of compounds 1-5 generated via the β-arrestin-2 recruitment system* 140

Table 4.2 *Potency, efficacy, and selectivity of compounds 1-5 generated via the IP-One system* 143

Table 4.3 *Transduction coefficient calculated between BRET and IP-One assays indicate some bias between β-arrestin-2 recruitment and IP_1 accumulation pathways* 145

Table 4.4 *ML-145 acts in a competitive manner with compounds 1-3* 149

Table 4.5 *Mast cell stabilisers display various species selectivity profiles at GPR35* ... 153

Table 4.6 *IP_1 accumulation responses of GPR35 agonist and mast cell stabilisers* 156

Table 4.7 *GPR35 agonists display limited pathway bias between β-arrestin-2 recruitment and IP_1 accumulation* 158

Table 4.8 *ML-145 does not appear to compete with lodoxamide or bufrolin in a*

simple competitive manner 160

Table 4.9 *GPR35 agonists mediated DMR from HT-29 cells and a comparison with the IP-One and BRET systems in HEK293 cells* 164

Table 4.10 *An assessment of GPR35 agonist pathway bias generated through the BRET, IP-One and DMR assays* 168

Table 5.1 *GPR35 agonist potency and efficacy at human, mouse and rat orthologues in the β-arrestin-2 recruitment assay* 184

Table 5.2 *$R^{164}S$, R6.58Q, and R7.32 play a role in human GPR35 ligand selectivity in the β-arrestin-2 recruitment assay* 190

Table 5.3 *R6.58Q and R7.32 act together to mediate ligand responses at human GPR35* 193

Table 5.4 *Human selective ligands increase in potency following expression of $S^{161}R$, Q6.58R and S7.32R at rat GPR35* 196

Table 5.5 *Expression of R4.62 enhanced β-arrestin-2 recruitment at rat GPR35* 198

Table 5.6 *Y3.32 plays a role in ligand induced β-arrestin-2 recruitment at human and rat GPR35* 202

Table 5.7 *R4.60 is involved in ligand-induced β-arrestin-2 recruitment at human and rat GPR35* 204

Table 5.8 *D7.43A plays a variable role in ligand induced β-arrestin-2 recruitment at rat GPR35* 207

List of Figures

Figure 1.1 *G protein-coupled receptors display a characteristic membrane spanning structural motif* 3

Figure 1.2 *The human GPR35 gene region at chromosome 2q37.3 produces two alternatively spliced transcripts to encode GPR35a or GPR35b* 12

Figure 1.3 *GPR35 couples selectively to $G\alpha_{i/o}$ and $G\alpha_{13}$ families of G proteins, and interacts with β-arrestin-1 and β-arrestin-2* 18

Figure 1.4 *The GRAFS phylogenetic system groups human GPCRs within five families* 23

Figure 3.1 *GPR35 agonist and antagonist structures* 86

Figure 3.2 *Yeast control strains are not stimulated following overnight zaprinast treatment* 88

Figure 3.3 *Human and rat GPR35 selectively couple to $G\alpha_{i/o}$, $G\alpha_{13}$, and $G\alpha_{16}$ in the yeast assay* 90

Figure 3.4 *Assessment of zaprinast-induced G protein coupling to human GPR35 using [^{35}S]GTPγS incorporation* *93*

Figure 3.5 *Investigating $G\alpha_{13}$ coupling at human GPR35 using a [^{35}S]GTPγS immunoprecipitation assay* 95

Figure 3.6 *Optimisation of the IP-One assay using $G\alpha_{qi1/2}$ and $G\alpha_{q13}$ chimeras with human GPR35* 98

Figure 3.7 *Zaprinast-induced coupling of $G\alpha_{qi1/2}$ and $G\alpha_{q13}$ chimeras at human and rat GPR35 assessed in the IP-One assay* 100

Figure 3.8 *Agonist-induced $G\alpha_{q13}$ coupling to human and rat GPR35 measured in the IP-One assay* 102

Figure 3.9 *ML-145 and CID-2745687 are inverse agonists at human but not rat GPR35* 105

Figure 3.10 *Human GPR35 and FFA4 generate a higher BRET response at β-arrestin-2* 108

Figure 3.11 *eYFP expression and β-arrestin-2 recruitment profiles at GPR35 species orthologues* 111

Figure 3.12 *High content imaging reveals the GPR35 agonists induce GPR35 internalisation* 113
Figure 3.13 *HT-29 cells endogenously express human GPR35 and respond to ligand treatment as measured using the DMR system* 118
Figure 4.1 *Compounds 1-5 display species selectivity in the β-arrestin-2 recruitment assay* 139
Figure 4.2 *Compounds 1-5 generate species selectivity in the IP-One accumulation assay* 142
Figure 4.3 *ML-145 acts in a competitive manner with compounds 1-3 in the BRET and IP-One assays* 148
Figure 4.4 *The chemical structure of mast cell stabilising compounds assessed for GPR35 agonism* 151
Figure 4.5 *Mast cell stabilising compounds display species selectivity in the BRET assay* 152
Figure 4.6 *Mast cell stabilisers generate various responses in the IP-One assay* 155
Figure 4.7 *The antagonism of lodoxamide and bufrolin by ML-145 does not conform to the rules of competitive antagonism* 159
Figure 4.8 Different *GPR35 agonists display similar kinetic traces in the DMR assay* .. 162
Figure 4.9 *GPR35 agonists produce responses in a concentration-dependent manner in the DMR assay using HT-29 cells* 163
Figure 4.10 *ML-145 is competitive with zaprinast and lodoxamide in the DMR assay* ... 166
Figure 4.11 *CXCL17 sequence alignment indicates shared sequence between species* .. 178
Figure 5.1 *The species selectivity profiles of GPR35 agonists as displayed in the BRET assay* 183
Figure 5.2 *GPR35 ligands tend to contain a carboxyl group or a carboxylic acid isostere* 185
Figure 5.3 *Arginine 3.36 is conserved at the hydroxycarboxylic, oxoeicosanoid, and GPR35 receptors* 186
Figure 5.4 *Arginine residues that differ in sequence between human and rat GPR35* 187
Figure 5.5 *Arg^{164}, R6.58 and R7.32 play a role in ligand selectivity at human GPR35* .. 189
Figure 5.6 *R6.58 and R7.32 act together at human GPR35 to recruit β-arrestin-2* 192

Figure 5.7 *Expression of $S^{161}R$, Q6.58R and S7.32R improve human-selective ligand potency at rat GPR35* 195
Figure 5.8 *R4.62 plays a role in ligand-induced β-arrestin-2 recruitment at rat GPR35* 197
Figure 5.9 *Y3.32 plays a role in ligand-induced β-arrestin-2 recruitment at human and rat GPR35* 201
Figure 5.10 *Expression of R4.60 is critical for β-arrestin-2 recruitment at human and rat GPR35* 203
Figure 5.11 *D7.43A has various effects on ligand responses at rat GPR35* 206
Figure 5.12 *Alterations of GPR35 sequence can induce constitutive activity at rat but not human GPR35* 208
Figure 5.13 *Lodoxamide and bufrolin interact with a distinct subset of residues between species to achieve their equipotent responses* 210
Figure 5.14 *Hydroxycarboxylic acid binding GPCRs contain a conserved arginine residue at position 3.36 that is not conserved across all carboxylic acid-binding GPCRs* 213
Figure 5.15 *Hydroxycarboxylic acid binding GPCRs contain a 'CxSF' motif in ECL2 that is critical for ligand function* 214
Figure 5.16 *Receptor homology model of human GPR35 based on PAR1 with 'ECL4' depicted* 218

Acknowledgements

I would firstly like to thank Prof. Graeme Milligan for all the support, guidance, direction and supervision given to me over the past four years, in addition to the opportunity to carry out my research in such a fantastic laboratory. I would also like to thank Graeme for part-funding my trip to EB2013 in Boston, which was an absolutely incredible experience. I wish to thank my laboratory supervisor, Dr. Brian Hudson, for his help with planning experiments, providing technical assistance, and critiquing of both my research efforts and thesis. Thanks to Laura Jenkins for GPR35 expertise, training with calcium and BRET assays, and general support; to Dr. Nicola Smith, for my initial introduction to the lab and training with the yeast assay; to Dr. Gianluigi Caltabiano, for generating images pertaining to the receptor homology modelling effort at GPR35; to Dr. Richard Ward, for continuous expertise in all lab-related matters; to Dr. John Pediani, for all microscope-related experiments; and to Eugenia Sergeev, for help with drawing the mathematical equations. I extend this thanks to Dr. Elisa Alvarez-Curto, Dr. Chantevy Pou, Dr. Sara Marsango, Dr. Maria Jose Varela, Dr. Kenneth Watterson, Dr. Terry Xu, Despoina Aslanoglou, and Nik Harries, whom have offered advice and support while working in the Milligan lab.

I would like to thank my Industrial CASE supervisors Dr. Debbie Taylor and Dr. Craig Southern for their help, encouragement and support throughout my project and during my three-month studentship at the MRCT. I also extend this thanks to Zaynab Neetoo-Isseljee, for training, advice, and knowledge. For DMR and pharmacology-related matters I thank Jeff Jerman and Dr. Paul Wright; for ADME studies I'd like to thank Dr. David Tickle and Sadhia Mahmood; and for Chemistry, Dr. Ed McIver.

I would like to thank Prof. Shanta Persaud and Prof. Peter Jones for inviting me to their laboratory at KCL, and to Zoheb Hassan for supervising me during this visit and helping with experiments. I'd like to thank Prof Gwyn Gould for training, advice, and providing provisions for the glucose uptake assay. I'd like to thank the MRCT and BBSRC for funding my studentship, and in particular to the MRCT for arranging and funding my travel to Heidelberg. Lastly, I'd like to offer my thanks to my friends and family for their continuous support during my PhD, I appreciated this immensely.

Author's Declaration

I declare that, except where explicit reference is made to the contribution of others, that this thesis is the result of my own work and has not previously been submitted for a degree or diploma at the University of Glasgow or at any other institution.

Signature: _____

Name: _____ Date: _____

Abbreviations

AFU	Arbitrary fluorescence units
AP-2	Adapter protein 2
BRET	Bioluminescence resonance energy transfer
cDNA	Complementary deoxyribonucleic acid
cGMP	Cyclic guanosine monophosphate
COPD	Chronic obstructive pulmonary disease
C-terminus	Carboxyl terminus
DAPI	4',6-diamidino-2-phenylindole
DNA	Deoxyribonucleic acid
DMEM	Dulbecco's modified eagle's medium
DMSO	Dimethyl sulfoxide
DPM	Disintegrations per minute
ECL	Extracellular loop
ELISA	Enzyme-linked immunosorbent assay
ERK	Extracellular-signal regulated kinase
eYFP	Enhanced yellow fluorescent protein
FBS	Foetal bovine serum
FDA	Food and Drug Administration
FISH	Fluorescence *in situ* hybridisation
FFA	Free fatty acid
FRET	Förster or Fluorescence resonance energy transfer
gDNA	Genomic deoxyribonucleic acid
G protein	Guanine nucleotide-binding protein
GAP	Guanosine triphosphatase-activating protein
GDP	Guanosine diphosphate
GEF	Guanine nucleotide exchange factor
GPCR	G protein-coupled receptor
GPD	Glyceraldehyde-3-phosphate dehydrogenase
GRK	G protein-coupled receptor kinase
GTP	Guanosine-5'-triphosphate
GTPase	Guanine nucleotide triphosphatase
GWAS	Genome wide association study
HCA	Hydroxycarboxylic acid receptor
HIF-1	Hypoxia-inducible factor-1
HEK293	Human embryonic kidney cell line 293
HIV-1	Human immunodeficiency virus-1
HTRF®	Homogeneous time-resolved fluorescence
IBD	Inflammatory bowel disease
IBS	Irritable bowel disease
ICAM	Intracellular adhesion molecule 1
ICL	Intracellular loop
IFN-γ	Interferon gamma
iNKT Cells	Invariant natural killer like T cells
LB	Luria Bertani

LPA	Lysophosphatidic acid
LPC	Lysophosphatidylcholine
LPS	Lipopolysaccharide
mRNA	Messenger ribonucleic acid
MRCT	Medical Research Council Technology
NAM	Negative allosteric modulator
NINDS	National Institute of Neurological Disorders and Stroke
NME	New molecular entity
NOP	Nociceptin receptor, also known as orphanin FQ
N-terminus	Amino terminus
PAM	Positive allosteric modulator
PAR1	Proteinase-activated receptor subtype 1
PBS	Phosphate-buffered saline
PCR	Polymerase chain reaction
PDE	Phosphodiesterase
PLCβ	Phospholipase Cβ
PTX	*Bordella pertussis* toxin
Poly(A)	Polyadenylation
PSC	Primary sclerosing cholangitis
qRT-PCR	Quantitative reverse transcription polymerase chain reaction
RGS	Regulators of G protein signalling
Rluc	*Renilla* luciferase
RNA	Ribonucleic acid
RT-PCR	Reverse transcription polymerase chain reaction
RPM	Revolutions per minute
SNP	Single nucleotide polymorphism
T2D	Type two diabetes
TM	Transmembrane
TNF-α	Tumour necrosis factor alpha
UAG	Unacylated ghrelin
UV	Ultra violet
UVT	Ultra violet transmissible
VNTR	Variable number tandem repeat
7TM	Seven transmembrane receptor

Chapter One

An Introduction to drug discovery, G protein coupled receptors, and GPR35

1.1 An overview of therapeutic targets and drug discovery

Drug research is a multidisciplinary effort that has contributed more to the progress of medicine than any other scientific factor during the past century (Drews, 2000). Nonetheless, currently marketed drugs mediate their effects through only a small number of the potential human target proteins, estimated to be between 200 and 300 in number, targeted by some 1000 pharmaceutical agents (Drews and Ryser, 1997; Golden, 2003; Imming et al., 2006; Overington et al., 2006; Rask-Andersen et al., 2011). Human drug targets, separated from the pharmaceutical arm of anti-infectives, include receptors (G protein-coupled receptors (GPCRs), ligand gated ion channels, receptor tyrosine kinases, and nuclear receptors), which form the largest group of drug targets at 44 % market share, followed by enzymes (29 %), and the transporter proteins (voltage gated ion channels, symporters, antiporters and uniporters), (15 %) (Rask-Andersen et al., 2011).

Considerable efforts have been undertaken to expand target diversification, with emphasis on first-in-class products and new molecular entities (NMEs) (Paul et al., 2010; Barker et al., 2013; Sharma and Tan, 2013). Oncology drug discovery has paved the way in this regard and is followed by orphan drugs for the treatment of rare diseases, which together these account for an approximate 60-70 % share of approved applications by the Centre for Drug Evaluation and Research (Mullard, 2012, 2013, 2014). Treatment of other disease states including cardiology, respiratory, endocrinology and metabolism, however, have had a relatively low success rate (approximately 10 % each) (DiMasi et al., 2010) with approval of novel treatments falling behind demand (Mullard, 2013).

1.1.1 *GPCRs and their relevance to drug discovery*

GPCRs are the most successful group of drug targets, and account for some 30 to 40 % of approved drugs on the market today (Drews, 2000, Hopkins and Groom, 2002; Rask-Andersen et al., 2011). Indeed, several GPCR ligands are among the worldwide 100 best-selling pharmaceuticals (Zambrowicz and Sands 2003). GPCRs are the largest and most versatile membrane-bound protein family in mammals, sharing a characteristic seven transmembrane (7TM) domain structure (**Fig 1.1**) (Bockaert and Pin, 1999). The success of GPCRs as therapeutic targets stems from their versatility, location at the cell surface, ability

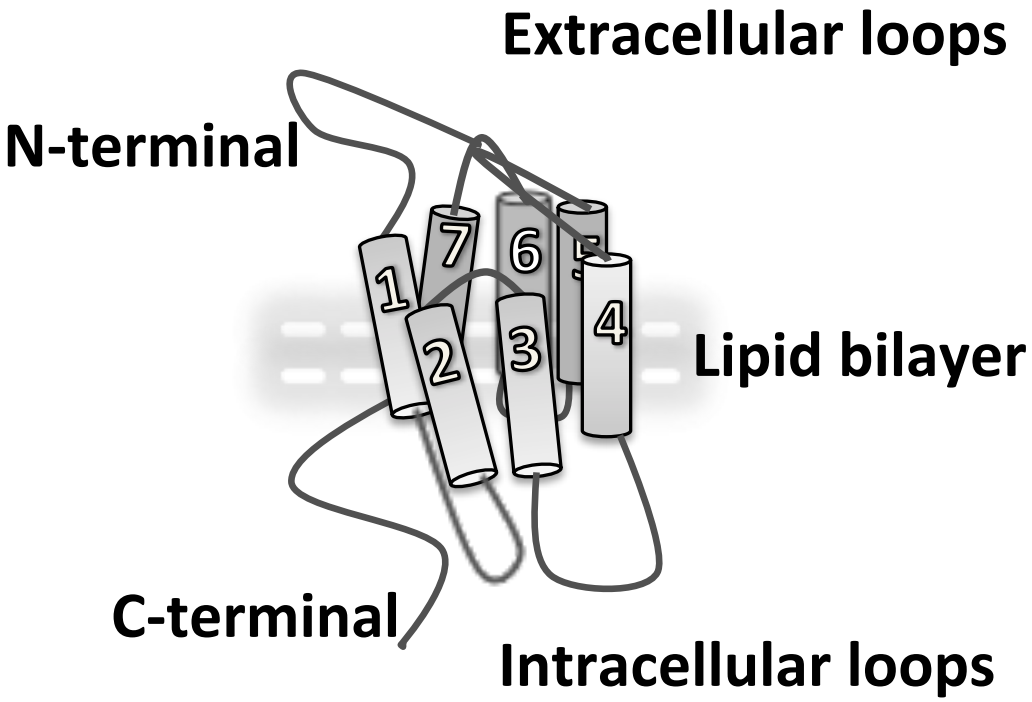

Figure 1.1 G protein-coupled receptors display a characteristic membrane spanning structural motif GPCRs are integral membrane proteins that share a seven alpha-helical domain structural motif. By virtue of this structure, GPCRs are also known as seven transmembrane proteins (7TMs), serpentine or heptahelical receptors. In addition to containing seven α-helical hydrophobic transmembrane (TM) domains that span the lipid bilayer, the GPCR structure is connected by a series of three extracellular loops (named ECL1-3) and three intracellular loops (ICL1-3), capped by an extracellular amino (N-) terminus and an intracellular carboxyl (C-) terminus.

to modulate intracellular interactions, ubiquitous nature, and often their direct contribution to diseases including heart failure and cardiovascular disease (Jensen et al., 2014; Hall et al., 2014) HIV-1 (Stambouli et al., 2014), asthma, allergy, and inflammation (Kawano et al., 2014; Penn et al., 2014; Baker et al., 2014; Vischer et al., 2014), cancer (O'Hayre et al., 2014), diabetes and obesity (Milligan et al., 2014; Bouvier, 2014; Miller et al., 2014; Kimple et al., 2014), and many others. Equally, the ligands that activate GPCRs are as diverse as the receptors and the functions that they modulate, thereby creating vast potential to modulate intracellular signalling and abrogate disease.

GPCR ligands include endogenous molecules such as neuropeptides, amino acids, biogenic amines, chemokines, lipid mediators, nucleotides, polypeptide hormones and exogenous molecules including viruses, photons of light, olfactory and gustatory molecules (Civelli et al., 2013). GPCR ligands include endogenous molecules such as neuropeptides, amino acids, biogenic amines, chemokines, lipid mediators, nucleotides, polypeptide hormones, and exogenous molecules including viruses, photons of light, olfactory and gustatory molecules (Civelli et al., 2013). Synthetic counterparts of these molecules account for up to 90 % of FDA approved drugs (Koehn, 2009); the majority of which are synthetic small compounds. This is, in part, due to the increased likelihood of small molecules of being orally bioavailable (i.e. conforming to Lipinski's Rule of Five; Liprinski, 1997) and because they are suitable for enhancement through chemical engineering to deliver a high degree of specificity into the structure (Mason et al., 2012). Small peptides, proteins and lipids also act as ligands at GPCRs, although they typically have proven more difficult to progress as drugs given the inherent increased size for the former, and increased lipophilicity associated with non-specificity for the latter. Additionally, peptides tend to be more expensive to produce and are often administered subcutaneously, which limits their usefulness. The therapeutic area of biologics, however, has bolstered the success of peptides as drug candidates, and also in some cases, small molecules, through the generation of humanised monoclonal antibody-peptide or monoclonal antibody-small molecule chimeras that act to target the ligand to a specific tissue or receptor (Feng et al., 2014). The antibody provides highly specific targeting to the desired site, increasing the specificity of the therapeutic counterpart and reducing off-target complications (Murad et al., 2013). Monoclonal antibodies themselves can also act endogenously upon GPCRs and have recently proved successful as therapeutics, with a notable example being Herceptin® (trastuzumab)

for the treatment of human epidermal growth factor receptor 2 (HER2)-positive breast cancer (Piccart-Gebhart et al., 2005).

Despite the increased ingenuity associated with the delivery of therapeutics, however, characterisation of therapeutic targets and success in validating these targets has fallen dramatically. Indeed, it is estimated that only 59 of 370 non-olfactory GPCRs have been utilised as successful drug targets, suggesting that either the remainder are either unsuitable or, perhaps, that there still remains great potential within the 'GPCRs as therapeutic targets' arena (Sams-Dodd, 2005; Gashaw et al., 2011; Garland, 2013). Calls for more innovative techniques to expand the understanding of GPCR function have been met with considerable and significant milestones: the outcome of the genome sequencing project (International Human Genome Sequencing Consortium, 2004) which revealed putative, previously unidentified, GPCRs based on their 7TM sequence; and crystallisation of the first active-state GPCR (Lander et al., 2001; Venter et al., 2001; Abdellah et al., 2004), which presented a snap-shot of the nature of GPCR activation, a process that had been poorly understood previously, to revolutionise the field of GPCR structural biology.

1.2 Classical and reverse pharmacology for drug discovery at GPCRs

In historical terms, the manner in which ligands and GPCRs were paired was through the 'classical pharmacological approach' whereby previously identified ligands were associated with their cognate receptor. Two cases in point are adrenaline and histamine, molecules that were well characterised in terms of their physiological response, but the identity of their endogenous receptor remained undetermined for nearly a century (Branch, 1939; Bennett, 1999), and are now known to activate the α_1, α_2, β_1, β_2, and β_3 adrenoceptors and H_1 to H_4 histamine receptors, respectively (Wallukat, 2002; Lomasney et al., 1991; Hough, 2001). During the 1970s, there existed approximately 50 endogenous ligands that remained to be paired with their cognate receptors, however, advances in molecular biology approaches led to a concerted effort during the eighties and nineties that identified novel GPCRs with homology to previously identified sequences using the polymerase chain reaction (PCR) with degenerate primers. Such an example of GPCRs identified in this manner includes the β2-adrenergic receptor (Dixon et al., 1986), which has since emerged as a prototypical GPCR.

More recently, and with completion of the genome sequencing project, a new era in the pharmaceutical industry commenced (Im, 2002), with an additional 120 putative GPCRs identified based on sequences suggestive or predictive of a 7TM structure (Levoye and Jockers, 2008; Yoshida et al., 2012). However, many of these GPCRs shared limited sequence identity with previously identified GPCRs, making it difficult to decode their physiological function and predict their endogenous ligands. Furthermore, there began to amass many more GPCRs than endogenous ligands (Civelli et al., 2013) and techniques such as gene expression profiling, tissue extraction, and pharmacological screening assays became widely used in an effort to increase the repertoire of endogenous ligands (Im, 2002; Brown et al., 2003; Kotarsky and Nilsson, 2004). As a result, small molecule compound libraries were formed that contained both new and previously identified endogenous compounds (Civelli et al., 2013). These compound libraries were central to screening efforts aiming to associate newly identified putative GPCRs with their endogenous ligand; however, they were also valuable for identification of chemically related hit structures that could be used to deduce information pertaining to the structure of the endogenous ligand (Im, 2002). Most recently, information-based approaches have become available that compare novel and known GPCRs based on sequence or pharmacology to infer function (Tunaru et al., 2005; Kotarsky et al., 2003). Together these practices were collectively termed 'the reverse pharmacology approach' (Libert et al., 1991; Civelli et al., 2013), which is a summary term describing the situation in which the GPCR sequence was identified first, followed by a search for the endogenous ligand. After an initial 'boom' in the late 1990s and early 2000s, however, progress to associate newly-identified GPCRs with their endogenous ligands had slowed, and approximately 92 GPCRs remain today without a defined endogenous ligand (Davenport and Harmar, 2013; Davenport et al., 2014).

1.2.1 *GPCR deorphanisation efforts*

Orphan GPCRs are receptors that have not yet been associated with an endogenous ligand, and many of these were identified from their putative 7TM structure identified through the genome sequencing project (Wise et al., 2004). Efforts to deorphanise these GPCRs have had many successes, which have resulted in reclassification and creation of new GPCR subfamilies. This is exemplified by the endothelial differentiation gene (EDG) family,

which was recategorised into the endogenous lipid lysophosphatidic acid (LPA_{1-6}) and lysophospholipid ($S1P_{1-5}$) families following endogenous ligand identification (Erickson et al., 1998; An et al., 1998; Im et al., 2000; Lee et al., 1998; An et al., 1997; Sato et al., 2000). New family members have also been added to previously established families, including receptors that had limited sequence identity but a shared pharmacology, such as the histamine H_4 receptor, which was added to the histamine receptor family (Nakamura et al., 2000; Zhu et al., 2001; Morse et al., 2001; Liu et al., 2001; Nguyen et al., 2001; Zampeli and Tiligada, 2009) or the converse, receptors that shared a high degree of sequence identity but not pharmacology, as in the case of the nociceptin/orphanin FQ (NOP) receptor, which was added to the opioid receptor family (Mollereau et al., 1994; Meunier et al., 1995; Reinscheid et al., 1995; Henderson and McKnight, 1997). Moreover, deorphanisation efforts have also lead to the identification of completely novel GPCRs families and ligands, as was the case for the metabolic intermediates succinate and the free fatty acids, of which succinate was paired with GPR91 (which was subsequently renamed the succinate receptor (He et al., 2004)) and the free fatty acids were paired with GPR40 (renamed FFA_1), GPR41 (FFA_3), GPR43 (FFA_2), GPR120 (FFA_4) and GPR84 receptors (Briscoe et al., 2003; Brown et al., 2003; Itoh et al., 2003; Kotarsky et al., 2003; Le Poul et al., 2003; Hirasawa et al., 2005; Wang et al., 2006b). Novel endogenous peptides and novel receptors were also paired, including ghrelin with the ghrelin receptor GHSR1a (Kojima et al., 1999), and orexin-A and orexin-B that act at the hypocretin receptor type 1 and 2, respectively (renamed orexin receptor type 1 (OX_1) and orexin receptor type 2 (OX_2)) (de Lecea et al., 1998; Sakurai et al., 1998).

1.2.2 *There are many routes to becoming a therapeutic target: orphan GPCRs and ligands*

Not all orphan GPCRs, or GPCRs in general, are suitable as therapeutic targets. A druggable GPCR must display a therapeutically relevant and restricted expression profile, and exhibit a physiological role that can be manipulated for disease treatment (Kotarsky and Nilsson, 2004). However, the validity of a good drug target also depends on the indication for which the target is considered (Gashaw et al., 2011). Evidence to this can be taken from the ghrelin receptor, which was indicated for numerous applications but failed in the majority of clinical trials (Strasser, 2012). Through its ability to regulate food intake and adiposity, the ghrelin receptor was assessed as a therapeutic target for: chronic heart failure

(Okumura et al., 2002; Kishimoto et al., 2012), chronic obstructive pulmonary disease (COPD) (Leviston and Gertner, 2012; Miki et al., 2013), cancer (Fujitsuka et al., 2011), renal failure (Laviano et al., 2010), and cystic fibrosis (Monajemzadeh et al., 2013). In regulating gastrointestinal motility, ghrelin receptor agonist TZP-101 was trialled for the treatment of postoperative ileus, but failed recently in phase III clinical trials due to lack of efficacy (Ejskjaer et al., 2010; Hoveyda et al., 2011). However, a second ghrelin receptor agonist, RM-131, has been assessed for the closely related function of gastroparesis and chronic constipation and is currently in phase I clinical trials (Shin et al., 2013; Van der Ploeg et al., 2014). Ghrelin receptor deficient mice displayed improvements in glucose tolerance (Sun et al., 2006) and insulin sensitivity (Sun et al., 2008b), which suggested that antagonism of the ghrelin receptor could be therapeutically beneficial. Subsequently, ghrelin receptor inverse agonist PF-5190457 was developed and has now entered clinical trials for the treatment of type 2 diabetes (T2D) (Bhattacharya et al., 2014).

The converse of the ghrelin receptor is perhaps exemplified by the orexin OX_1 and OX_2 receptors, which although by no means any less multi-factorial therapeutic targets (Xu et al., 2013a) these receptors have achieved great success in clinical application. With the observation that narcoleptics have only 10 % functioning orexin neurons (Thannickal et al., 2000) and studies from orexin deficient mice indicating severe sleepiness and an inability to maintain wakefulness (Chemelli et al., 1999; Mochizuki et al., 2004; Diniz Behn et al., 2010) antagonism of the OX_1 and OX_2 receptors emerged as treatment for sleep disorders (Riemann and Spiegelhalder, 2014). Subsequently, clinical candidate submissions from almost all major pharmaceutical companies followed (Scammell and Winrow, 2011). To date, two dual orexin receptor antagonist compounds have proved successful in clinical trials (Cox et al., 2010; Renzulli et al., 2011; Bettica et al., 2012), with Merck's Suvorexant obtaining FDA approval in August 2014 (Michelson et al., 2014).

There are also some interesting examples of cases where 1) the endogenous ligand and 2) the therapeutic target have not been identified prior to entering into clinical trials. In both cases however, a strong pathophysiological profile must be altered to give validity to furthering research efforts without a thorough knowledge of the pharmacology of the target. An example an orphan receptor in clinical trials is the bombesin receptor subtype-3 (BRS3) (Battey et al., 1991), which presented with reduced metabolic rate, increased feeding efficiency and subsequent hyperphagia in knockout mice (Ohki-Hamazaki et al., 1997).

Furthermore, application of BRS3 agonist MK-5046 induced a favourable anti-obesity profile in rats and dogs (Guan et al., 2011), and subsequently progressed to phase I human clinical trials (Reitman et al., 2012). An example of an orphan ligand is unacylated ghrelin (UAG), which is a distinct form of ghrelin from that mentioned previously, and accounts for 50-90 % of the total ghrelin concentration in plasma that does not activate the ghrelin receptor GHSR1a (Kojima et al., 1999; Delhanty et al., 2014). Upon administration of UAG analogue AZP531, mice fed a high fat diet were protected from: increasing body fat and mass, glucose intolerance and insulin resistance, proinflammatory effects in white adipose tissue, and lipid accumulation in brown adipose tissue (Delhanty et al., 2013). This led to the entry of AZP531 to human phase I clinical trials for the treatment of T2D (under clinical trial identifier NCT02040012).

1.3 The orphan GPCR GPR35 as a novel therapeutic target

With a reduction in the rate of GPCRs being verified as therapeutic targets, orphan GPCRs have provided a means by which to expand this repertoire with initial characterisation efforts in some instances revealing novel pathways, signalling molecules and disease states. One such orphan GPCR that was billed as a therapeutic target is GPR35, since it presented with a therapeutically relevant gene expression profile and was genetically linked to a number of disease states. This included metabolic and inflammatory diseases, such as ulcerative colitis, irritable bowel syndrome (IBS), gastric cancer, diabetes, heart failure and atherosclerosis. However, despite this disease association, in the sixteen years since its discovery, GPR35 remains poorly characterised and has been slow to amass interest. This has stemmed from a lack of selective and potent tool compounds with which to probe GPR35 pharmacology and pathophysiology, with added complications including significant species selectivity issues and the lack of a selective and potent endogenous ligand hampering research efforts.

1.3.1 *Gene expression analysis and tissue distribution profile of GPR35*

GPR35 was first identified in 1998 alongside GPR30 (renamed the estrogen GPCR) and GPR14 (renamed the urotensin-II receptor) (O'Dowd et al., 1998; Carmeci et al., 1997;

Filardo et al., 2000; Ames et al., 1999; Liu et al., 1999). Mapping of *GPR1* using fluorescence *in situ* hybridisation (FISH) technology revealed that *GPR1* (located on chromosome 15 q21.6) cross-hybridised with a locus on chromosome 2. In an effort to reveal the basis of this cross-hybridisation, degenerate oligonucleotide primer sequences based on *GPR1* transmembrane (TM)2 and TM7 were employed and subjected to PCR amplification from genomic DNA (gDNA) (O'Dowd et al., 1998). Insertion of the PCR fragment into a Bluescript™ plasmid enabled screening of a human genomic library, which led to the identification of a sequence predicted to encode a 309 amino acid protein, named GPR35. GPR35 was found to share little homology with GPR1, GPR30, or GPR14 (less than 26 % overall identity). GPR35 does however share sequence homology with GPR23 (renamed as LPA_4) (32 % overall identity), HM74 (subsequently reclassified as the hydroxycarboxylic acid HCA_2 and HCA_3 receptors) (30 % overall identity), GPR55 (30 % overall identity) and some purinergic receptors (approximately 29 % overall identity) (O'Dowd et al., 1998).

Although no data was shown in the short communication, O'Dowd and colleagues described rat *GPR35* messenger RNA (mRNA) transcripts to be expressed within the rat intestine, but not within the heart, spleen, liver, lung, ovary, kidney, or whole brain; with human *GPR35* mRNA transcripts not detected in the caudate-putamen, thalamus, frontal cortex, pons, cortex, midbrain, medium pons, lung, or adrenal, using Northern blot analysis with poly(A) RNA isolated from various tissues (O'Dowd et al., 1998). More recently, and with a more sensitive means of mRNA transcript detection, Wang et al., (2006a) used quantitative reverse transcriptase PCR (qRT-PCR) analysis, presented relative to glyceraldehyde-3-phosphate dehydrogenase mRNA levels on human and mouse DNase I digested tissues. This revealed expression of *GPR35* in human small intestine, colon, spleen, foetal spleen, peripheral leukocytes and stomach, with lower levels in monocytes, mast cells, T cells, neutrophils, dendric cells, eosinophils, adipose, thymus, kidney, liver, and caudate nucleus. Independent studies also identified upregulation of human *GPR35* following immunoglobulin E (IgE) stimulation of mast cells (Yang et al., 2010) and expression within the lung, skeletal muscle and pancreas (Horikawa et al., 2000). In mouse, Wang et al., reported much higher mRNA levels, with the mouse spleen generating a signal over 100 times higher than that of the human, in addition to expression within the lymph node, small intestine, lung, colon, and pancreas, and lower levels in the medulla oblongata, trachea, adipose, thyroid and thymus (Wang et al., 2006a). Further analysis using *in situ* hybridisation

with *GPR35* RNA probes directed against a mouse tissue array revealed that *GPR35* was expressed the denum, jejunum, ileum, cecum, colon, and rectum, and in various regions of the intestine *GPR35* was primarily expressed within epithelial cells located in the crypts of Lieberkhün, with lower levels in the intestinal villi (Wang et al., 2006a), as well as expression in the dorsal root ganglion (Cosi et al., 2011). Using qRT-PCR analysis from rat total tissue RNA, *GPR35* was found in uterus, small intestine, colon, dorsal root ganglion, stomach, and lung, with lower levels in the spinal cord, heart, liver, bladder, whole brain and cerebrum (Taniguchi et al. 2006; Ohshiro et al., 2008). More recently, and despite initial results to the contrary suggesting that GPR35 was not expressed in the brain (O'Dowd et al., 2008), *GPR35* expression was detected in specific synaptic regions within the hippocampus of mouse and rat (Berlinguer-Palmini et al., 2013; Alkondon et al., 2015), in mouse cortical astrocytes (Berlinguer-Palmini et al., 2013).

1.3.2 *Chromosomal location of GPR35 and exon usage*

FISH analysis performed on metaphase chromosomes prepared from lymphocytes using a biotinylated phage probe in conjunction with DAPI banding indicated that *GPR35* was encoded from chromosome 2q37.3 in man (O'Dowd et al., 1998). Mouse GPR35, sharing 73.4 % overall protein sequence identity with human GPR35, translated into a protein of 307 amino acids from chromosomal locus 1D (Taniguchi et al., 2006), while rat GPR35, sharing 72 % overall homology with man and 85 % overall homology with mouse, encoded a protein of 306 amino acids from a chromosome location of 9q36 (Taniguchi et al., 2006). A number of years after the initial discovery of GPR35, in a study aiming to identify novel factors involved in the transformation process leading to formation of gastric cancer, two alternatively spliced *GPR35* transcripts were identified from human gastric cancer tissue: the original 309 amino acid transcript identified by O'Dowd et al., (1998) and a longer transcript containing a 31 amino acid N-terminal extension (Okumura et al., 2004). As a result of this finding the authors named the GPR35 short variant GPR35a and the long, GPR35b (Okumura et al., 2004). Using sequence analysis it was found that GPR35a was expressed from non-coding exon six and coding exon seven, while GPR35b used non-coding exons one, two, three and four, and coding exons five and seven (**Figure 1.2**); GPR35b was, therefore, suggested to be an alternatively spliced variant of GPR35a produced by alternative transcription site usage

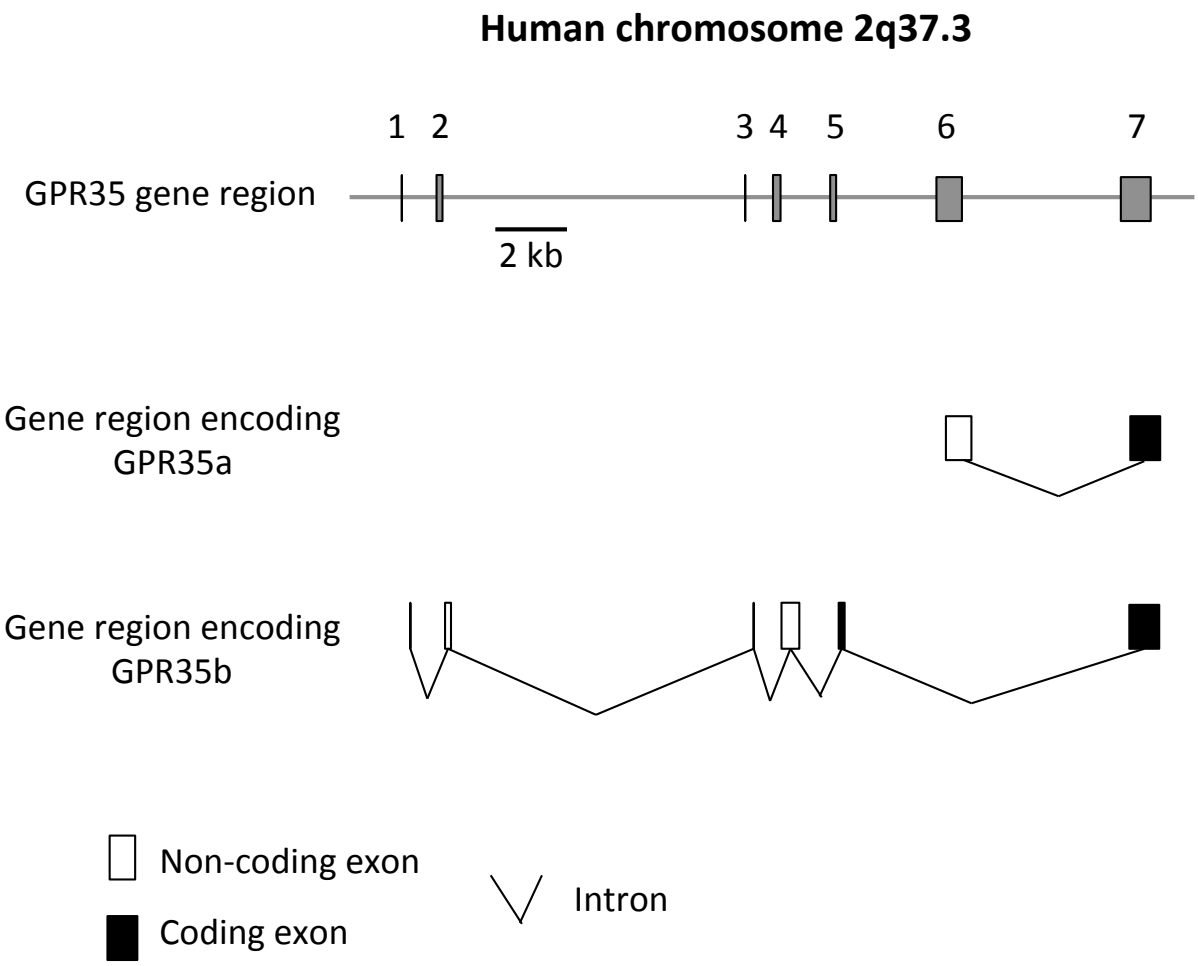

Figure 1.2 The human GPR35 gene region at chromosome 2q37.3 produces two alternatively spliced transcripts to encode GPR35a or GPR35b The short variant of GPR35 (GPR35a), encoded by transcript variant 1, produces a protein of 309 amino acids from the open reading frame in exon 7 (exon 6 is non-coding). The long variant (GPR35b) is encoded by two transcript variants. Both GPR35b transcript variants require non-coding exons 1, 2, 3, 4, and coding exons 5 and 6; the difference between these variants lies within exon 4, which is shorter in transcript variant 2 than in transcript variant 3 (not shown). The gene product, GPR35b, contains an N-terminal extension of 31 amino acids, encoded by exon 5, that is absent from GPR35a. Adapted from Okumura et al., 2004.

(Okumura et al., 2004). Aside from the N-terminal length difference, these two transcripts differ in that GPR35b contains an intronic sequence between exon five and seven while the coding sequence of GPR35a is intronless (Okumura et al., 2004).

In total, three transcript variants of *Homo sapiens GPR35* exist (one encoding GPR35a and two encoding GPR35b), three transcript variants of *Mus musculus* and one of *Rattus norvegicus*, of which the rodent isoforms encode only the short version of GPR35 (information from the National Centre for Biotechnology Information database). *GPR35* and its surrounding region is highly polymorphic, with over 1000 single nucleotide polymorphisms (SNPs) identified following the 1000 genomes project. Upstream (5') of *GPR35* there exists a highly unstable variable number tandem repeat (VNTR) region (VNTR2) and a perfect 19 base pair repeat VNTR1 region, both of which are 3' to neighbouring gene *CAPN10* exons 14 and 15 (Horikawa et al., 2000).

The majority of efforts to elucidate the pharmacological and physiological properties of GPR35 have primarily focussed on GPR35a. Nevertheless, from the few studies that have investigated the pharmacology and function of GPR35b, there has been a suggestion of a higher transforming capability in NIH3T3 cells with a more prominent expression profile of GPR35b than GPR35a in various human gastric cancers compared with the healthy, non-tumorous, surrounding tissue (Okumura et al., 2004). In primary cardiomyocytes however, GPR35a and GPR35b were found to be expressed to similar levels and to respond in a similar manner to external stimuli (Ronkainen et al., 2014). Previously, GPR35b was found to generate pharmacological responses that were similar but more variable than those associated with GPR35a (Guo et al., 2008). GPR35b was also found to produce a lower efficacy than GPR35a following agonist stimulation in *in vitro* test systems (Mackenzie et al., 2014), but the potency of both transcript variants was found to be similar (Guo et al., 2008; Zhao et al., 2010; Mackenzie et al., 2014).

1.3.3 *Diseases associated with GPR35: cardiovascular disease*

Although the gene expression profile described for *GPR35* mRNA suggested an expression that was primarily restricted to the immune and gastrointestinal tissues, early indications as to the pathophysiology of GPR35 were identified through an attempt to identify novel risk factors contributing to coronary artery calcification in non-Hispanic White

sibships (Sun et al., 2008a). This study identified a SNP within *GPR35* positioned at rs3749172, which encoded a non-synonymous alteration from serine to arginine at position 294 (Sun et al., 2008a). Since this SNP encodes an amino acid located at the C-terminal region of GPR35, a region important for intracellular signalling events that follow post receptor activation, and altered a potential phosphorylation site, the authors suggested that the SNP could have considerable implications for the downstream signalling of the receptor (Sun et al., 2008a). In an *in vitro* setting however, this SNP was found not to directly affect ligand potency or β-arrestin-2 recruitment to human GPR35 in a HEK293 cell system (Mackenzie et al., 2014), perhaps suggesting a system dependent effect.

More recently, in a study aiming to identify novel therapeutic targets for treatment of the late stages of heart failure, Min et al., (2010) isolated RNA from twelve patients with severe late stage chronic heart failure and subjected the samples to global microarray analysis. *GPR35* was found to be upregulated compared to two non-failing heart disease control samples and as a result was adenovirus transfected into primary cardiomyocytes isolated from neonatal rats (Min et al., 2010). Assessment of cardiomyocyte cellular morphology revealed that upregulation of *GPR35* decreased cell viability and presented with a hypertrophic cellular morphology, while knock-out *GPR35* mice revealed, through insertion of a catheter to the right carotid artery, a left-ventricular systolic pressure that was 37.5 mmHg higher than wild type littermates (Min et al., 2010).

Thus, although there is an association between GPR35 and cardiovascular disease, the basic profile of GPR35 and its role within the physiology of the heart remained to be clarified. Researchers at the University of Oulu, Finland, began to elucidate the basic profile of GPR35 function within the cardiovascular system with the revelation that mouse *GPR35* expression was extremely sensitive to hypoxia, implicating a role of GPR35 in the acute phase of myocardial infarction during pressure-load induced progressive cardiac hypertrophy (Ronkainen et al., 2014). Furthermore, it was revealed that hypoxia-inducible factor-1 (HIF-1) bound to and activated mouse *GPR35* through interaction with a hypoxia response element sequence in the *GPR35* promoter region that increased the number and density of GPR35 at the cell surface (Ronkainen et al., 2014). Furthermore, overexpression of mouse *GPR35* was found to be associated with membrane ruffling and retraction fibre formation in cultured neonatal mouse cardiomyocytes, leading to a disruption of the cellular actin fibre network and loss of sarcomeric-like structures (Ronkainen et al., 2014).

1.3.4 *Diseases associated with GPR35: metabolic and gastrointestinal diseases*

In addition to cardiovascular disease, GPR35 has been suggested as a risk factor for chronic inflammatory disorders of the gastrointestinal tract including early-onset inflammatory bowel disease (IBD) and ulcerative colitis. This association was primarily reported as a result of a genome wide association study (GWAS) that identified a SNP at rs4676410, which is an upstream intron variant of *GPR35* that is altered from a cytosine to a thymine in European and North American suffers of early-onset IBD (Imielinski et al., 2009). This study also found that rs4676410 was associated with *CAPN10* (Calpain 10, a Ca^{2+}-regulated intracellular cysteine protease involved in cytoskeletal remodelling and signal transduction), *KIF1A* (kinesin family member 1A protein, an anterograde motor protein that transports membranous organelles along axonal microtubules), and *RNPEPL1* (arginyl aminopeptidase B-like 1, a zinc metallopeptidase with preference for methionine, glutamine and citrulline residues, inhibited by Ca^{2+}) in a linkage disequilibrium block (Imielinski et al., 2009). While expression levels of *KIF1A* and *RNPEPL1* were not significantly altered in the GWAS, *CAPN10* was found to be expressed at a significantly lower level in ulcerative colitis cases than in genetically related non-IBD controls (Imielinski et al., 2009).

CAPN10 and *GPR35*, neighbouring genes on chromosome 2, have previously been associated and linked to disease through GWAS studies, respectively (Horikawa et al., 2000). In 2000, in a GWAS of T2D Mexican-Americans native to Mexico, four non-synonymous SNPs were identified within the coding region of *GPR35*: alanine 25 threonine, valine 291 isoleucine, threonine 253 methionine, arginine 125 serine, and serine 294 arginine, of which only the latter was found to be associated with T2D (Horikawa et al., 2000). The S294R SNP also associates *GPR35* with cardiovascular disease, but at least within an *in vitro* setting, none of the aforementioned *GPR35* SNPs affect agonist-induced β-arrestin-2 recruitment in HEK293 cells (Mackenzie et al., 2014).

Further links between GPR35 and ulcerative colitis were provided in an effort to identify risk factors for primary sclerosing cholangitis (PSC), a chronic cholestatic liver disease of unknown etiology that is frequently presented with the comorbidity of ulcerative colitis (Ellinghaus et al., 2013). This study combined two independent GWAS studies that were subsequently integrated to identify risk factors for PSC and ulcerative colitis (Ellinghaus

et al., 2013). In a population of German decent, two *GPR35* SNPs (rs3749171 and rs4676410) were identified that showed association and linkage disequilibrium with PSC (Ellinghaus et al., 2013). The rs3749171 SNP encoded a non-synonymous change in the GPR35 protein from methionine to threonine at position 108, located within the third intracellular loop of the receptor, and highly correlated with the rs4676410 SNP located within a *GPR35* intronic region. Although nothing is currently known about GPR35 in the pathogenesis of PSC, the authors suggested that GPR35 could be involved in the regulation of inflammation in both the gastrointestinal and biliary tract (Ellinghaus et al., 2013).

1.3.5 *Diseases associated with GPR35: inflammation*

GPR35 has been linked to inflammation, primarily in studies whereby addition of GPR35 agonists has attenuated inflammatory processes, leading to the suggestion that GPR35 can modulate inflammatory conditions. Currently, there is considerable interest in the interface between dietary influence of the gut microbiome and its effect upon human health and disease. In addition to other metabolite sensing GPCRs ($FFA_{1\text{-}4}$, GPR81, HCA_2, and the succinate receptor) GPR35 has been linked to immune health through dietary intake and digestion of tryptophan containing foodstuffs including red meat, fish, eggs and vegetables, which can be broken down to generate serotonin, melanin, kynurenic acid, and nicotinamide (Thorburn et al., 2014). In the gut kynurenic acid can be liberated from dietary protein through the activity of *Escherichia coli* and transported to the extracellular milieu and blood where it elicits broadly anti-inflammatory effects (Kuc et al., 2008).

Kynurenic acid acts as a glycine and allosteric site antagonist of the glutamate N-methyl-d-aspartate (NMDA)-receptor ion channel complex and as a non-competitive antagonist at the α7 nicotinic acetylcholine receptor (Hilmas et al., 2001; Stone, 2001; Prescott et al., 2006), in addition to being one of the proposed endogenous agonists of GPR35 (Wang et al., 2006a). The concentration of kynurenic acid varies significantly in the periphery, from an estimated 0.003 μM in human saliva to 16.1 μM in the rat ileum mucus, and has been found to increase in disease states including IBD, ulcerative colitis and Crohn's disease (Forrest et al., 2002; Forrest et al., 2003). Levels of kynurenic acid were also increased in the kidney, lung, intestine, spleen, and muscles in rats suffering chronic renal

failure (Pawlak et al., 2001), in spontaneously hypertensive rats (Mizutani et al., 2002), and in the urine of T2D primates (Patterson et al., 2011).

The actions of the purported GPR35 agonist kynurenic acid and the surrogate reference agonist zaprinast have also provided links between GPR35 and inflammation. Kynurenic acid was found to attenuate lipopolysaccharide (LPS)-induced tumour necrosis factor-α (TNFα) secretion in human peripheral blood mononuclear cells and purified peripheral blood $CD14^+$ (cluster of differentiation 14+) monocytes (Wang et al., 2006a). In an independent study, kynurenic acid and zaprinast were added to human invariant natural killer like T (iNKT) cells pre-stimulated with the super-agonist α-Gal-Cer (a chemically synthesised α-galactosylceramide) (Fallarini et al., 2010). Using an Enzyme-Linked Immunosorbent assay (ELISA), kynurenic acid and zaprinast were shown to reduce interleukin-4 (IL-4) release into the culture medium in a dose-responsive and Pertussis toxin sensitive manner without significantly reducing levels of interferon-γ (INFγ) (Fallarini et al., 2010). (Activated iNKT cells are involved in the maturation of dendric cells and can counter-regulate autoimmunity by secreting the cytokines IL-4, IL-5 and transforming growth factor-β (TGF-β) or exacerbate autoimmunity through secretion of the pro-inflammatory cytokine, INFγ). Lastly, kynurenic acid treatment of monocytes and neutrophils was shown to mediate firm arrest of ICAM-1 (intracellular adhesion molecule 1) expressing monolayers of human umbilical vein endothelial cells (Barth et al., 2009). This signal was diminished by Pertussis toxin treatment and reduced by small hairpin-RNA delivery targeting GPR35, implicating GPR35 as a direct mediator of leukocyte adhesion (Barth et al., 2009). The physiological functions reported for GPR35 are therefore beginning to be unravelled (**Fig 1.3**), with implications in actin remodelling, membrane ruffling, and Pertussis toxin sensitivity being suggestive of coupling between GPR35 and $G\alpha_{13}$ and $G\alpha_{i/o}$ pathways. Further investigation of these processes will be crucial to the elucidation of GPR35's basic physiological function.

1.4 The function and structure of GPCRs

1.4.1 GPCR signalling

GPCRs are named as a result of their function: originally described as proteins that interact with and modulate the activity of the heterotrimeric family of guanine nucleotide

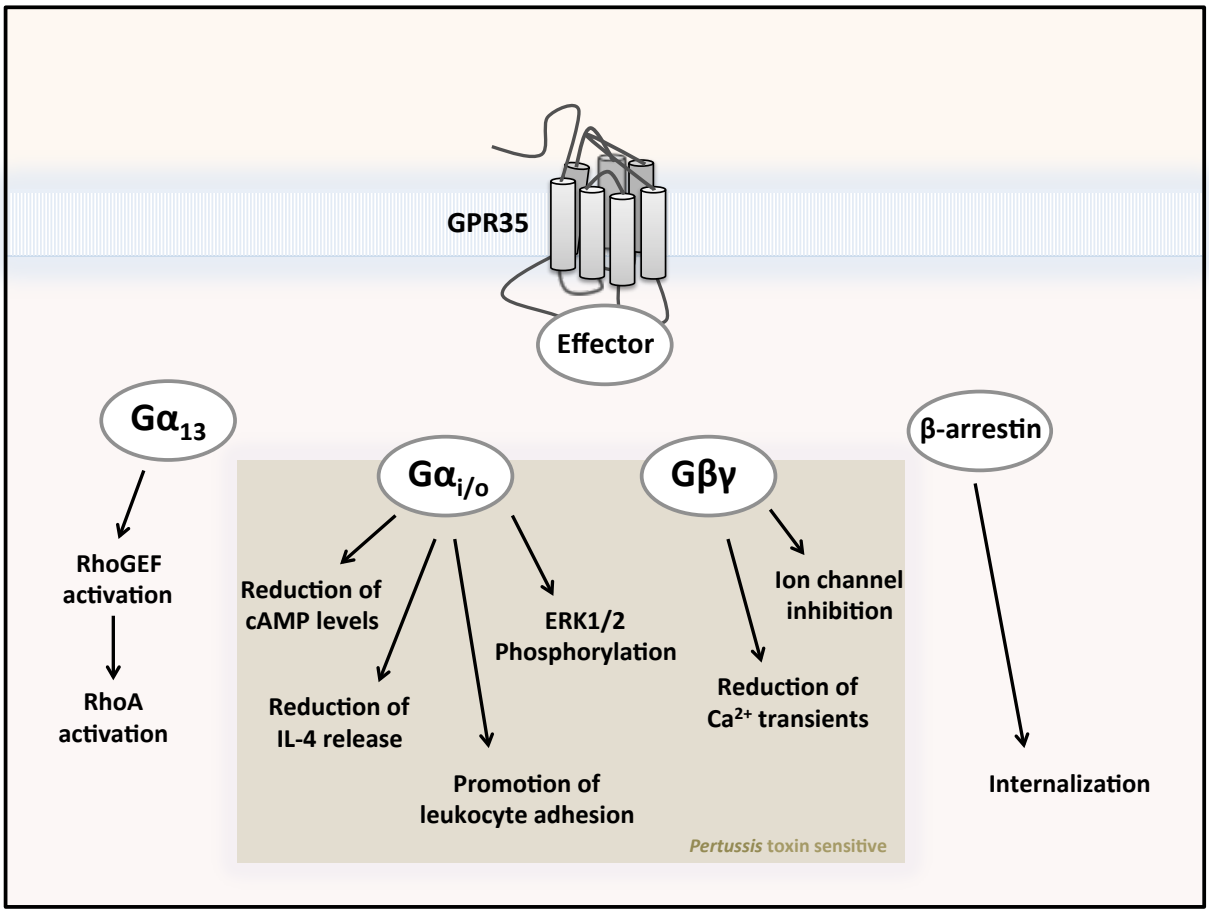

Figure 1.3 GPR35 couples selectively to $G\alpha_{i/o}$ and $G\alpha_{13}$ families of G proteins, and interacts with β-arrestin-1 and β-arrestin-2 The majority of studies that have revealed functional effects following GPR35 activation have used Pertussis toxin to indicate the involvement of $G\alpha_{i/o}$ and its corresponding $\beta\gamma$ subunits in the transduction of GPR35's signal (Ohshiro et al., 2008; Barth et al., 2009; Fallarini et al., 2010; Cosi et al., 2011). The studies indicating an involvement of $G\alpha_{13}$ are fewer in number (Jenkins et al., 2011; Jenkins et al., 2010) since there are no specific inhibitors of this G protein; however downstream effectors can be inhibited to reveal signalling through this pathway (Oka et al., 2010; Deng et al., 2012a). While there are no functional studies indicating recruitment of β-arrestin at GPR35 in native cells, this effector couples highly efficiently to GPR35 *in vitro* when using manipulated forms of this receptor, with β-arrestin translocation assays being employed for almost all drug screening efforts at GPR35 (Zhao et al., 2010; Southern et al., 2013; Neetoo-Isseljee et al., 2013; Funke et al., 2014). GPR35 is located in the lipid bilayer (blue) with the extracellular (orange) and intracellular (pink) regions distinguished. Each effector (grey circles) and the signalling proteins they interact with following GPR35 activation are indicated. RhoGEF, Ras guanine nucleotide exchange factor; RhoA, Ras homologue gene family member A; cAMP, 3'-5'-cyclic adenosine monophosphate; IL-4, interleukin-4; ERK1/2, extracellular-signal regulated kinase 1/2; Ca^{2+}, calcium.

binding (G) proteins. G proteins contain α, β, and γ subunits that are essentially the transducers of the extracellular stimuli that act upon receptors, relaying signals to intracellular effector proteins. This process is critical for an organism's survival, as for a cell to adapt to its environment it must be able to receive extracellular cues and elicit appropriate and integrated intracellular responses. There are hundreds more GPCRs than there are G proteins and, as such, G proteins must be able to interact in a selective manner with more than one GPCR: there are some 800 identified GPCRs in man and only 21 Gα, 6 Gβ, and 5 Gγ protein subunits. Thus, G protein interaction with any given GPCR is controlled through the specificity of their sequence, their structure and their electrostatic potential (Baltoumas et al., 2013). G protein and GPCR interactions can also be controlled spatially and temporally, through controlled expression levels and distribution profiles, which may be distinct between cell types and tissues (Downes and Gautam, 1999). This complexity is the key to the multiplicity of GPCR signals. Additional control is provided by the rate of GTP hydrolysis occurring upon Gα dissociation that dictates the length of time that the G protein is active. This can be accelerated by the effector target or by the Regulators of G protein Signalling (RGS) proteins, which serve as GTPase-activating proteins (GAPs) for some classes of Gα subunits (McCudden et al., 2005).

G proteins are activated following ligand binding and receptor activation, but they can also be constitutively recruited to receptors that are active in the absence of ligand. The classical model of G protein recruitment is that the activated GPCR recruits the $G\alpha_{GDP}$ subunit, which forms part of an inert membrane-bound heterotrimeric complex with Gβγ (Lambright et al., 1996; Wall et al., 1995). Since the GPCR is as guanine nucleotide exchange factor (GEF) and the $G\alpha_{GDP}$ subunit is a substrate for the activated GPCR, a catalytic exchange process occurs upon their interaction that replaces $G\alpha_{GDP}$ with $G\alpha_{GTP}$ (Rasmussen et al., 2011). Upon binding of $G\alpha_{GTP}$, a conformational change occurs within the Gα subunit that enables the release of Gα from both the GPCR and the Gβγ subunit (Coleman et al., 1994; Lambright et al., 1994). The Gα and Gβγ subunits are then free to modulate specific downstream processes (Hamm et al., 1998; Cabrera-Vera et al., 2003). Gα is a guanine nucleotide triphosphatase (GTPase) and so it slowly hydrolyses back to $G\alpha_{GDP}$ in a process that re-associates Gα with Gβγ and reunites the G protein in an inactive state at the cell surface (Kimple et al., 2011).

The Gα subunits couple receptors to effectors including adenylyl cyclase (AC), cGMP phosphodiesterase, phospholipase Cβ (PLCβ), and the small Rho GTPases (Kristiansen, 2004; Hewavitharana and Wedegaertner, 2012), and are grouped into four distinct sub-families based their sequence similarities: $G\alpha_s$, $G\alpha_{i/o}$, $G\alpha_{q/11}$, and $G\alpha_{12/13}$ (**Table 1.1**). Of these G proteins, GPR35 has been found to couple specifically to $G\alpha_{i/o}$ and $G\alpha_{13}$ although the exact details of the emanating signalling pathways and processes have not been fully elucidated (Wang et al., 2006a; Jenkins et al., 2011; Mackenzie et al., 2011).

GPCR activation and G protein recruitment sets in motion a process that ultimately leads to the attenuation of the initiation of signalling. Activated GPCRs must be rapidly inactivated in order to prevent uncontrolled signalling. The first step in this process is phosphorylation of the receptor, which is often carried out by GPCR kinases (GRKs) at the C-terminus and third intracellular loop of the GPCR (Kohout and Lefkowitz, 2003; Moore et al., 2007). This is followed by recruitment of an arrestin molecule to the phosphorylated GPCR. The arrestins include the visual arrestins (arrestin-1 in rod cells, and arrestin-4 in cone cells) and β-arrestins (β-arrestin-1 and β-arrestin-2 also called arrestin-2 and arrestin-3, which are ubiquitously expressed in mammals) (Kang et al., 2014). Interaction between an arrestin molecule and the phosphorylated GPCR occludes the heterotrimeric G protein binding site, which prevents further G protein coupling and terminates G protein-dependent signalling at the cell-surface (Shukla et al., 2013). Additionally, the arrestins facilitate internalisation of GPCRs by acting as scaffolding proteins for clathrin and the clathrin adaptor protein AP-2 to promote clathrin-mediated receptor endocytosis, which mechanically removes the receptor from the cell surface (Tian et al., 2014). In some cases the arrestins are also involved in signalling processes independent of G protein coupling. This finding has led to the observation that certain ligands can 'bias' a receptor to signal via a G protein *or* a β-arrestin pathway, and offers the opportunity to selectively design therapeutics with reduced side-effects (Rives et al., 2012; Tao, 2014; Whalen et al., 2011).

1.4.2 *GPCR structure*

The 7TM topology of membrane proteins that is associated with GPCRs is found in all eukaryotic species (Schöneberg et al., 2007), with representatives present in fungi, yeast, and plants (Bockaert and Pin, 1999; Strotmann et al., 2011; Krishnan et al., 2012). Within the

Table 1.1 Gα protein sub-families, expression and function.

G protein sub-family	G protien sub-type	Molecular Mass (kDa)	Expression	Function
$G\alpha_s$	$G\alpha_{s(S)}$	44	Ubiquitous	Activate adenylate cyclase and Ca^{2+} channels
	$G\alpha_{s(L)}$	46	Ubiquitous	
	$G\alpha_{s(olf)}$	45	Olfactory neuroepithelium	Activate adenylate cyclase
$G\alpha_{i/o}$	$G\alpha_{oA}$	40	neurons, neuroendocrine cells, heart	Inhibit adenylate cyclase and Ca^{2+} channels, activate PLC-β and K^+ channels
	$G\alpha_{oB}$	40	neurons, neuroendocrine cells, heart	
	$G\alpha_{i1}$	40	nearly ubiqutous	
	$G\alpha_{i2}$	40	ubiquitous	
	$G\alpha_{i3}$	40	nearly ubiquitous	
	$G\alpha_z$	41	platlets, brain, neurons, neurosensory cells	Inhibit adenylate cyclase
	$G\alpha_{t1}$	40	retinal rods, taste buds	Activate cyclicGMP phosphodiesterases
	$G\alpha_{t2}$	40	retinal cones	
	$G\alpha_{gust}$	40	taste buds and airways	Activate PDEs
$G\alpha_{q/11}$	$G\alpha_q$	42	nearly ubiquitous	Activate PLC-β
	$G\alpha_{11}$	42	nearly ubiquitous	
	$G\alpha_{14}$	42	lung, kidney, liver, spleen, testis	
	$G\alpha_{15}$	43	hematopoietic cells	
	$G\alpha_{16}$	44	hematopoietic cells	
$G\alpha_{12/13}$	$G\alpha_{12}$	44	ubiquitous	Regulate Na^+/H^+ voltage dependent Ca^{2+} channels, eicosanoids, JNK/SAPK, cytoskeleton, cell growth
	$G\alpha_{13}$	44	ubiquitous	

metazoan phyla, GPCRs have evolved within five structurally distinct protein families: the glutamate (G), rhodopsin (R), adhesion (A), frizzled/taste2 (F) or secretin (S) GPCRs, which are clustered using the GRAFS phylogenetic classification system (Fredriksson et al., 2003; Fredriksson and Schioth, 2005; Josefsson, 1999), (**Fig 1.4**).

GPR35 is placed within the rhodopsin 'class A' family, which is the largest, most studied, and therapeutically targeted family of GPCRs. Although the extracellular sequences of these GPCRs are inherently diverse and receptors typically only share 25 % sequence identity in their TM helices, there are some sequence motifs that are highly conserved. These motifs have been used to generate a system of amino acid nomenclature for GPCRs, known as the Ballesteros and Weinstein numbering system (Ballesteros and Weinstein, 1995). This system numbers the most highly conserved amino acid in each TM domain with the number 50, which decreases (i.e. 49) or increases (i.e. 51) toward the N or C terminus, respectively. Incorporation of the TM in question gives rise to the format for TM1 amino acid 50 as '1.50'. Accordingly, the most highly conserved amino acids and motifs are $N^{1.50}$, $LxxxD^{2.50}$, $E/DR^{3.50}Y$, $W^{4.50}$, $P^{5.50}$, $CWxP^{6.50}$ and $N/DP^{7.50}xxY$.

Other conserved features include a disulphide bridge between ECL2 and the top of TM3 that tethers ELC2 to the helical bundle and provides conformational constraint, sculpting the topography of ligand entry to the binding pocket (Wheatley et al., 2012; Venkatakrishnan et al., 2013). Although the ligand binding pockets of GPCRs are inherently diverse, for most small molecule ligands the binding pocket is situated within the helical bundle, while for peptide ligands the N-terminus and extracellular loops of the receptor play a more prominent role in ligand binding. Despite the inherent differences of GPCR ligands and their mode of binding however, a recent bioinformatics study indicated that while distinct ligands penetrate to different extents within the ligand-binding pocket, all class A GPCRs are likely to form contacts with their ligands at topologically equivalent residues in TM3, TM6, and TM7 at positions 3.32, 3.33, 3.36, 6.48, 6.51 and 7.39 (Venkatakrishnan et al., 2013).

1.4.3 *Lessons of GPCR activation from the prototypical GPCRs*

The structure of the GPCR is integral to its function and facilitates its dynamic nature within the phospholipid membrane. Indeed, many GPCRs are inherently unstable outwith

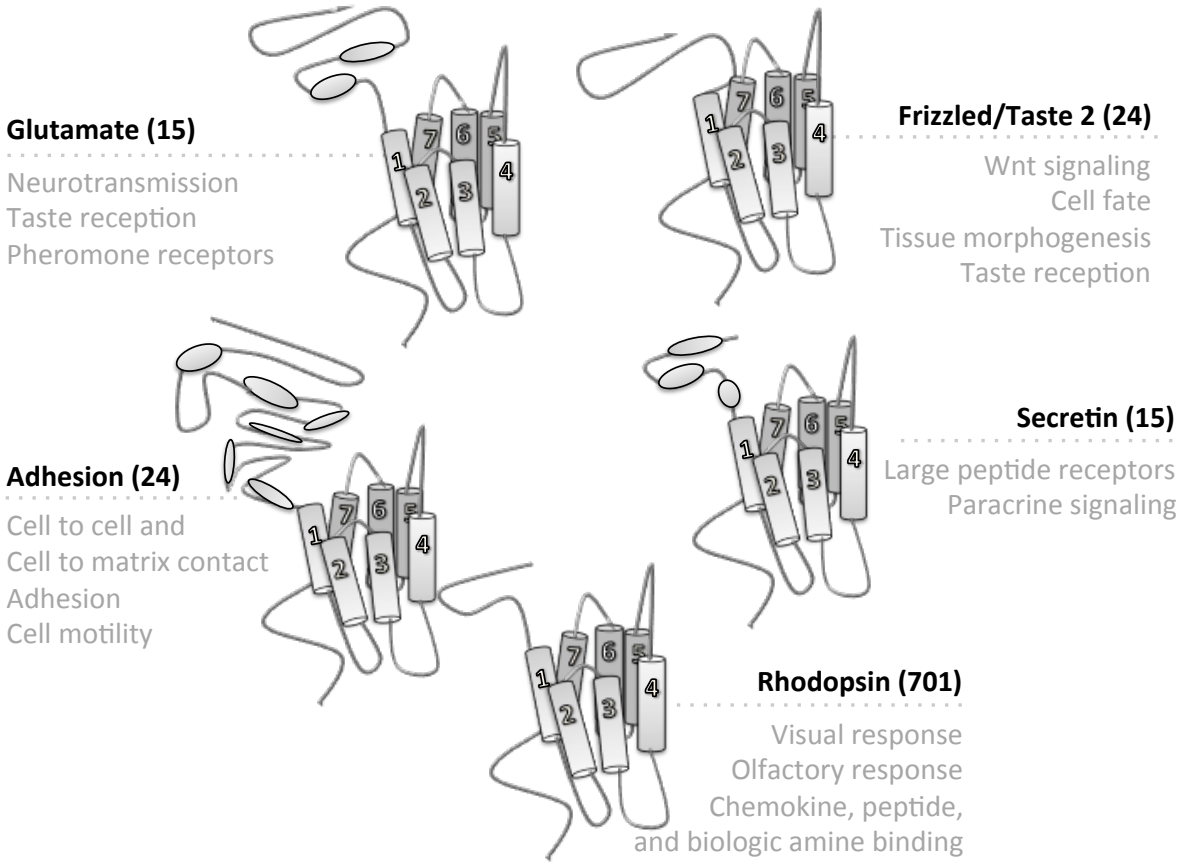

Figure 1.4 The GRAFS phylogenetic system groups human GPCRs within five families Each family name is indicated in bold with the number of members included in brackets. In grey is an overview of some of the functions carried out by members of the associated family. The cartoon GPCR is as described in **Figure 1.1** but with differences in the N-terminal region between each family depicted.

the lipid environment, and despite being ubiquitously expressed, exist in relatively low abundance within cell membranes. This adds to the difficulty associated with obtaining correctly folded and functional GPCR structures in detergents. As a result of this, and despite rapid advances in the biology and pharmacology of the rhodopsin family of GPCRs, progress in the area of elucidating GPCR structure has been slow. Indeed, unlike the enzyme class of therapeutic targets, GPCRs have only relatively recently been subject to large scale successful crystallisation efforts, which were achieved by recent advances in protein engineering, crystallography methods, and X-ray diffraction methods. The ramifications associated with these efforts are tremendous, and as such a new research area has opened up that is focussed on the study of GPCR structure/function and ligand binding dynamics at GPCRs.

The first GPCR to be identified was rhodopsin in 1878 (although it was not recognised as a GPCR at this time). This early identification was aided by the relatively high abundance of rhodopsin, which eased the isolation process. Other GPCRs however, are expressed at much lower levels and, as a result, it was over a century later before the hamster β2-adrenoceptor (β2-AR) (Dixon et al., 1986) and rat muscarinic acetylcholine receptor (Kubo et al., 1986) were cloned. Both rhodopsin and the β2-AR serve as prototypical class A GPCRs and have been relatively well characterised in physiological, pharmacological, structural, and biophysical terms.

Recent crystallisation studies of rhodopsin, the β2-AR, and the adenosine A_{2A} receptor in their inactive and active states revealed that a conserved series of conformational changes ensues following receptor activation. Ligand binding, whether initiated by interaction with the extracellular loops or within the ligand binding pockets, must form contacts with TM3 and TM6 to initiate the structural movements involved in GPCR activation (Rosenkilde et al., 2010; Doré et al., 2011), as TM3 and TM6 directly contact all other helices in the TM bundle with the exception of TM1 (Doré et al., 2011). The largest structural change that occurs during receptor activation is the movement and rotation of TM6 between 7-14 Å, accompanied by movement of TM5 as part of the previously proposed global toggle-switch mechanism (Schwartz et al., 2006; Lebon, et al., 2011; Rasmussen et al., 2011; Manglik and Kobilka, 2014). During activation, there is also movement of TM7 and TM1 inward toward the TM bundle and a lateral upward movement of TM3 (Katritch et al., 2013). The movements of TM3 and TM6 appear to be facilitated by breakage of the ionic

interaction occurring between the arginine of DR$^{3.50}$Y motif and E$^{6.30}$ that connects the intracellular ends of these TMs in the inactive state, although this is not conserved in all class A GPCRs (Vogel et al., 2008; Moukhametzianov et al., 2011; Katritch et al., 2013). Additionally, a salt bridge present in the inactive state between the side chain of D/E$^{3.49}$RY and DR$^{3.50}$Y was found to break during the activation process to enable interaction with the C-terminal helix of the Gα subunit (Scheerer et al., 2008; Standfuss et al., 2011; Choe et al., 2011; Lebon et al., 2011). Like the DRY motif, which is conserved in 96 % of class A receptors, the NPxxY motif, conserved in 97 % of such receptors, serves as a microswitch for GPCR activation, whereby Y$^{7.53}$ is altered from its inactive position, pointing toward TM1, TM2 or the aliphatic intracellular helix 8, to form interactions with side chains of amino acids in TM6 and TM3. This subsequently enables Y$^{7.53}$ to point toward the middle of the TM bundle (Katritch et al., 2013). Overall, therefore, ligand binding and receptor activation act to open a cleft in the intracellular surface of the GPCR that enables G proteins (or other effectors) to bind to the receptor.

Despite sharing conserved sequence motifs, the biophysical studies of rhodopsin and the β2-AR have provided evidence for the existence of two distinct receptor activation models. Rhodopsin, which is unique in that it exists in a stable two-state conformation (inactive or active) with a series of transient intermediates, does not require the binding of a Gα protein to stabilise the active state, which is already pre-formed once 11-*cis*-retinal has isomerised to all-*trans*-retinal. In contrast, the β2-AR, which exists in an ensemble of low energy conformations with different functional properties is not fully activated by agonist binding, and requires the presence of a Gα protein to achieve its fully active state (Bockenhauer et al., 2011; Nygaard et al., 2013).

1.4.4 *GPR35 and the prototypical GPCRs*

It is important to point out that the majority of crystallisation efforts have been focussed on rhodopsin and the β2-AR and that these receptors bear little similarity to GPR35 in terms of their shared sequence identity or ligand binding properties. A sequence comparison between GPR35 and rhodopsin reveals that these receptors share only 20 % sequence homology, and this includes many of the highly conserved residues and motifs found in class A GPCRs. There are significant deviations between rhodopsin and GPR35

within TM1 and TM2, in which GPR35 lacks a proline at position 1.48 (and has a leucine instead) and contains an additional proline residue at 2.58 (a serine in rhodopsin). Moreover, GPR35 and the β2-AR share even less sequence identity (14 %), but they do share key conserved residues at positions $N^{1.50}$, $D^{2.50}$, $R^{3.50}$, $W^{4.50}$, $P^{5.50}$ and $P^{6.50}$. Importantly, GPR35 lacks a proline within the highly conserved NPxxY motif of TM7, and instead presents with a 'DAICY' series of residues. Since proline residues can cause kinks and bends in the TM helix structure that can also affect neighbouring TM helices, GPR35 appears unlikely to display a similar overall topology to the prototypical GPCRs.

Indeed, in homology modelling projects of GPR35, it was suggested that the TM7 of GPR35 would be straighter than that of the rhodopsin, β2-AR, and adenosine A_{2A} receptors (Lane, 2011). However, the positioning of a proline residue at 2.58 instead of at 2.59 is predicted to compensate for the distortion of TM7. While this may be true, the positioning of proline at 2.58 creates a tightly wound kink that is not present in the β2-AR, which instead contains a relaxed, broad turn at P2.59 (**Fig 1.5**) (Zhao et al., 2014). This has the effect that GPR35 and the β2-AR project a completely different series of residues toward the receptor binding pocket, with the GPR35 residues projected toward this space being buried in the TM2-TM3 interface of the β2-AR (Zhao et al., 2014). Further to this, the lack of a conserved proline residue at position 4.60 may cause a conformational change in the TM4 of GPR35, moving the extracellular end of TM4 closer to TM5 and enabling the ECL2 of GPR35 to be longer than that of the prototypical GPCRs (Lane, 2011; Zhao et al., 2014).

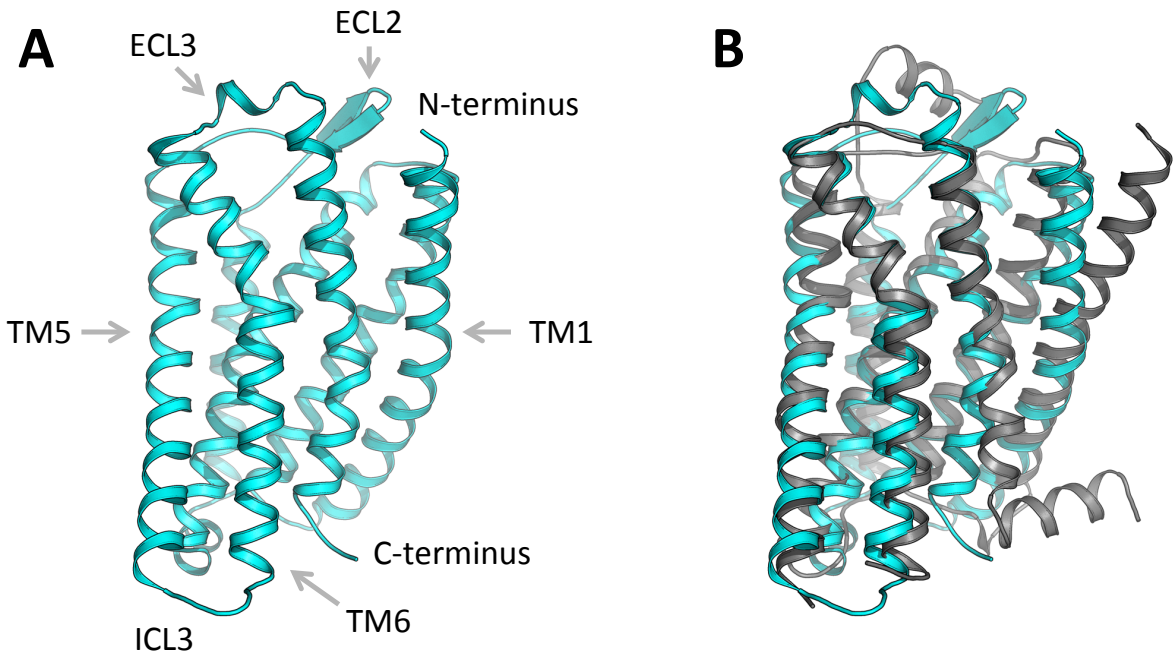

Figure 1.5 GPR35's structure can be distinguished from the prototypical GPCRs. Receptor homology modelling image depicting the topology of GPR35 (cyan), based on the published crystalised structure of the Proteinase-activated receptor subtype 1 (PAR1) receptor (Zhang et al., 2012; Mackenzie et al., 2014) (**A**). Superimposing GPR35 with the depicted crystalised structure of the β2-adrenoceptor (β2-AR) (grey) (Rasmussen et al., 2007; Cherezov et al., 2007) (**B**) enables a qualitative comparison to be made surrounding the overall topology of these two GPCRs. Modelling performed by Dr. Gianluigi Caltabiano.

1.5 Receptor pharmacology

1.5.1 The plasticity of GPCRs and the effects of ligand binding

The fact that the β2-AR exists in multiple distinct receptor conformations is in direct contrast to the canonical two-state receptor model, which states that GPCRs exist either inactive (R) or active (R*) states, and that all ligands with functional capabilities would share a common receptor conformation (Wisler et al., 2014). In fact, the conformational complexity and downstream signalling processes emanating from receptor activation are inherently more complicated than originally surmised (Deupi and Standfuss, 2011; Kenakin, 2013). Indeed, recent mass spectrometry approaches applied to monitor the conformational changes of the β2-AR indicated that functionally distinct ligands evoke distinct receptor conformations once bound (Kahsai et al., 2011; West et al., 2011) and that pharmacologically distinct ligands regulate receptor activity by shifting the conformational equilibrium and shape of the energy landscape associated with the receptor towards a specific state (Deupi and Kobilka, 2010; Nygaard et al., 2013). Moreover, it emerged that constitutively active receptors, unbiased ligands, G protein-biased ligands, and β-arrestin-biased ligands stabilise distinct conformations of the receptor (Kahsai et al., 2011; Rahmeh et al., 2012; Kenakin, 2013; Correll and McKittrick, 2014).

1.5.2 The assessment of ligand properties through physiochemical parameters

The concept of ligand efficacy, therefore, has changed completely from its original description as a property of agonists that cause tissue activation, and now represents the property of a ligand to change the behaviour of a receptor towards the cell (Kenakin, 2013). Efficacy is a term used to define the properties of a ligand alongside ligand affinity for the biological target, and the ability of the ligand to bind for a period of time sufficient to affect target behaviour (dissociation rate, target coverage). Unlike affinity, efficacy is a system dependent parameter and is a reflection of both receptor density and coupling efficiency in a given system. Further to this, not all ligands need to activate all receptors in a given system to elicit a maximal response, leaving some receptors 'spare', a term referred to as receptor reserve.

Agonist molecules preferentially bind to and stabilise the active (R*) population of receptors to generate a system response or efficacy that is attributed to the chemical properties of the ligand. For example, a full agonist will act to generate a system maximum response, while a partial agonist will produce a submaximal response (Kenakin, 2001). Using the β2-AR as an example, it was observed that binding of functionally diverse agonist molecules generated distinct efficacy profiles that could be attributed to the conformational changes imparted to the receptor upon ligand binding. Specifically, noradrenaline (a full agonist) caused breakage of the ionic lock between $R^{3.50}$ and $E^{6.30}$ and engaged the rotamer toggle switch at $W^{6.48}$, effects that were not produced by the agonist salbutamol (a partial agonist that only broke the ionic lock) or catechol (an inverse agonist that only engaged with the rotamer toggle switch) (Bhattacharya et al., 2008). Partial agonists are agonists with low intrinsic activity that may show agonist or antagonist properties depending on receptor density, how well coupled the system is, or whether the endogenous ligand is present (Burris et al., 2002; Yuan et al., 2009). These ligands have particular therapeutic benefit for treatment within systems that are over-stimulated and suffer from receptor desensitisation (Moore et al., 2007), or in systems that require re-balancing of the level of excitation such as the dopaminergic system in schizophrenia (Bolonna and Kerwin, 2005).

Many GPCRs have now been found to display considerable basal activity (Chalmers and Behan, 2002), although the concept of a receptor containing an inherent efficacy of its own emerged in 1989 following the observations of Costa and Herz. Costa and Herz revealed that the basal activity of the δ-opioid receptor could be diminished with the application of the inverse agonist ICI174864. Moreover, the inverse agonism nature of ICI174864 could itself be blocked by the presence of the antagonist MR2266, revealing (importantly) that inverse agonists and neutral antagonists were distinct entities (Costa and Hertz, 1989; Kenakin, 2013). Although initially inverse agonists were thought to be purely of academic interest, many have been found to act with considerable clinical benefit. This includes some of the atypical antipsychotic drugs (such as clozapine), that are inverse agonists of the constitutively active 5-hydroxyryptamine 5-HT_{2C} receptors (Herrick-Davis et al., 2000; Meltzer and Massey, 2011), or the histamine receptor H_1 class of antihistamines, for example (Leurs et al., 2002).

Neutral antagonists impart their function through acting in a competitive or non-competitive manner with an agonist or inverse agonist to impair their efficacy, as neutral

antagonists bind R and R* populations of receptors with equal affinity and hold no efficacy of their own. However, many compounds that were originally classed as neutral antagonists were subsequently re-classified as inverse agonists following characterisation of these compounds in constitutively active cell systems (Khilnani and Khilnani, 2011; Kenakin, 2013). Despite this re-classification, there remain compounds that display neutral antagonism, even in constitutively active systems (Sally et al., 2010; Millan et al., 2011). Competitive antagonists typically interact and compete with endogenous agonist for binding, and can be of use to identify ligand binding to the orthosteric (endogenous ligand binding) site. Conversely, non-competitive but reversible ligands typically bind to a site on the receptor distinct from this, named an allosteric site. Allosteric ligands alter the conformation of the GPCR, resulting in a change in the nature of its interaction with an orthosteric ligand (Langmead and Christopoulos, 2014). Allosteric ligands can possess intrinsic efficacy or impart effects only when in the presence of an orthosteric ligand. In the case of the former, ago-allosteric ligands act on their own, but they can also potentiate the affinity and/or efficacy of the endogenous ligand if both ligands are present together, such as in the case of the FFA2 ago-allosteric ligand 4-CMTB (Smith et al., 2011). In the case of the latter, other allosteric ligands may only impart an effect once an orthosteric ligand is bound to the receptor. There are positive or negative allosteric modulators (PAMs or NAMs), which can impart their effects on the properties of the orthosteric ligand's efficacy or potency (Hudson et al., 2014). PAMs and NAMs offer unique opportunities to manipulate or target receptors that cannot be selectively targeted through orthosteric binding alone (Langmead and Christopoulous, 2014).

1.5.3 *Ligands acting at GPR35: proposed endogenous ligands*

A number of endogenous molecules have now been reported to act as agonists at GPR35 (**Table 1.2**). However, these compounds are unlikely to be produced at concentrations required for GPR35 activation under physiological conditions and/or act non-selectively towards GPR35. An example of the latter, and the most potent of the putative endogenous GPR35 ligands, is LPA (mono-acylglycerol-3-phosphate). LPA consists of a single acyl chain, a glycerol backbone and a phosphate head group, and is the smallest and structurally simplest glycerophospholipid (Yatomi et al., 2013). LPA and choline are

produced through enzymatic cleavage of lysophosphatidylcholine (LPC) in the serum or plasma through the enzyme autotaxin's lysophospholipase D activity (Nakanaga et al., 2010; Nishimasu et al., 2011). LPA exerts its effects through a number of cellular proteins that form a specific sub-family of GPCRs, named LPA_{1-6}, and LPA has been associated with numerous pathological conditions including atherosclerosis (Schober and Siess, 2012), cancer (Gotoh et al., 2012), obesity, impaired glucose homeostasis (Rancoule et al., 2014), and pain (Ueda et al., 2013).

In the study by Oka et al., that identified LPA as a GPR35 agonist, HEK293 cells stably expressing human GPR35 incubated with 2-oleoyl LPA or 2-linoleoyl LPA were found to stimulate intracellular calcium mobilisation above the level of $[Ca^{2+}]_i$ produced by endogenously expressed LPA receptors (Oka et al., 2010). Since GPR35 has not been found to couple to the $G\alpha_q$ pathway (Jenkins et al., 2011; Mackenzie et al., 2011; Jenkins et al., 2012), this study could suggest a novel route for GPR35 stimulated signalling. The level of zaprinast stimulated $[Ca^{2+}]_i$ in GPR35 expressing cells was almost undetectable, and no response to kynurenic acid was detected (Oka et al., 2010), indicating that the mode of action of LPA (if at GPR35) must be distinct from the previously described agonists. Also, these $[Ca^{2+}]_i$ responses were not assessed with a GPR35 antagonist as there was not one available at that time and, therefore, have not been intrinsically linked with GPR35 activity. Lastly, it is important that to note that no other study has reported any effect of LPA as an agonist of GPR35 and one independent study indicated that LPA did not stimulate recruitment of β-arrestin to GPR35, which could be a result of ligand bias (Southern et al., 2013). Nevertheless, there is a requirement for further studies to validate the claim that LPA acts as an endogenous agonist of GPR35.

The first endogenously-generated ligand associated with GPR35 is the L-kynurenine metabolite kynurenic acid (4-oxo-1H-quinoline-2-carboxylic acid), which acts as a neuroprotective modulator through its antagonist action at the AMPA (α-amino-3-hydroxy-5-methyl-4-isoxazole propionic acid), Kainate, NMDA and α7 nicotinc receptors and as an agonist of the aryl hydrocarbon receptor (Hilmas et al., 2001; Stone, 2001; Marchi et al., 2002; Prescott et al., 2006; DiNatale et al., 2010). Importantly however, it remains unclear whether any of the ion channels are actually blocked by kynurenic acid under normal physiological conditions, as levels of kynurenic acid in the brain have been reported under steady-state conditions to be within the 15-150 nanomolar range (Moroni et al., 1988;

Table 1.2 Purported endogenous ligands for GPR35

Name	Structure	Action	Potency (EC_{50})	Comments	References
LPA	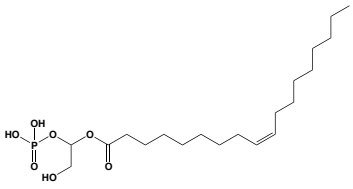	Unknown	Not determined	Phospholipid derivative; Elevates [Ca2+]i through an unknown mechanism; activity at GPR35 not confirmed with a GPR35 antagonist; does not recruit β-arrestin-2	Oka et al., 2010; Southern et al., 2013
Kynurenic acid	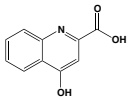	Partial agonist (Human) Full agonist (Rat)	Human: **217 µM** Rat: **66 µM**	Metabolite of L-tryptophan	Wang et al., 2006; Jenkins et al., 2011
cGMP	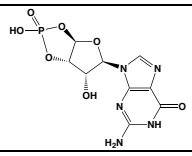	Partial agonist	Human: **131 µM**	Cyclic nucleotide derived from GTP	Southern et al., 2013
DHICA	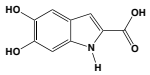	Partial agonist	Human: **22 µM** (DMR 24 µM)	Intermediate in the biosynthesis of melanin	Deng et al., 2012c
Reverse T3	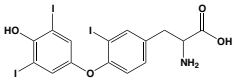	Full agonist	Human: **100 µM** (DMR 6 µM)	Hormone produced in the thyroid gland, liberated from precursor T4	Deng et al., 2012c

Action describes compound efficacy compared with reference compound zaprinast; potency values highlighted in bold were generated in β-arrestin-2 recruitment assays.

Arnaiz-Cot et al., 2008), based on assays of human cerebrospinal fluid (Erhardt et al., 2001) and on microdialysis studies in rats and mice (Turski and Schwarcz, 1988; Swartz et al., 1990; Wu et al., 2007), while micromolar concentrations of kynurenic acid are required to block both the glutamatergic and α7 nicotinic receptors in addition to activation of GPR35 (Mackenzie et al., 2015).

Many of the effects of kynurenic acid in the central nervous system (CNS) have not considered a role for GPR35 since early studies suggested that this receptor was not highly expressed in the brain (O' Dowd et al., 1998; Wang et al., 2006a). However, recent functional studies carried out in rats and mice revealed expression of *GPR35* within specific synaptic regions of the hippocampus as well as in astrocytes (Berlinguer-Palmini et al., 2013; Alkondon et al., 2015). Thus future investigations in the field of kynurenic acid research may wish to consider GPR35 as a contributor to the effects of kynurenic acid in the CNS (Mackenzie et al., 2015).

Although the early studies did not focus on a role of GPR35 in the CNS, GPR35 has begun to receive attention as a potential modulator of kynurenic acid's effects in the periphery since *GPR35* was found to be highly expressed within the gastrointestinal tract and in various immune cell populations (Mackenzie et al., 2011). As mentioned in **Section 1.3.5**, kynurenic acid can be liberated from dietary products via the action of *Escherichia coli* in the gut and is released into the blood and extracellular milieu (Kuc et al., 2008; Moroni et al., 2012; Thorburn et al., 2014). However, as with the estimated levels of kynurenic acid in the CNS, the level of kynurenic acid reported to occur and the concentration required to activate GPR35 in the periphery also do not appear to overlap, at least in humans under normal physiological conditions (Jenkins et al., 2011; Milligan, 2011). Although this is the case, a number of researchers believe the concentration of kynurenic acid reported is artificially low (Moroni et al., 2012) since estimates of this molecule are limited technologically, and there is reason to believe that the actual level of kynurenic acid is much higher in astrocytes where kynurenic acid is liberated from precursor kynurenine (Albuquerque and Schwarcz, 2013).

The need to accurately estimate the levels of kynurenic acid is of considerable clinical importance as relatively minor fluctuations in the level of kynurenic acid have been found to exert profound effects upon the release of glutamate, dopamine and acetylcholine (Carpenedo et al., 2001; Rassoulpour et al., 2005; Amori et al., 2009, Zmarowski et al., 2009;

Wu et al., 2010). Changes to the levels of kynurenic acid have been associated with a number of disease states including Huntington's disease (Beal et al., 1990), Alzheimer's disease (Baran et al., 1999), schizophrenia (Erhardt et al., 2001; Schwarcz et al., 2001), seizure (Wu and Schwarcz, 1996), malarial infection (Hansen et al., 2004), influenza type A infection (Holtze et al., 2008), and ischemic brain damage (Cozzi et al., 1999; Carpenedo et al., 2002; Moroni et al., 2003).

In an *in vitro* setting, application of kynurenic acid to immunological preparations has had beneficial anti-inflammatory effects, which could be abolished following treatment with Pertussis toxin (Fallarini et al., 2010) or small hairpin-RNA targeting of GPR35 (Barth et al., 2009). In pharmacological assays of GPR35, activation of kynurenic acid was found to mobilise $[Ca^{2+}]_i$ following transfection of GPR35 and a cocktail of $G\alpha_q$ protein chimeras with a half maximal effect (EC_{50}) of 39 μM at human, 11 μM at mouse and 7 μM at rat (Wang et al., 2006a). Thus, between the human and rodent orthologues of GPR35 there is a degree of species selectivity, with kynurenic acid displaying higher potency at rat than at human. This profile was also observed in an independent study using HEK293 cells transiently expressing C-terminally manipulated forms of GPR35 and β-arrestin-2, which recorded half maximal effects using a Bioluminescence Resonance Energy Transfer (BRET) assay of 66 μM rat GPR35-eYFP and > 100 μM at human (Jenkins et al., 2010).

More recently, the second messenger cyclic guanosine 3' 5' monophosphate (cGMP) was identified as a putative endogenous ligand of human GPR35 (Southern et al., 2013). cGMP and derivatives MANT cGMP (2'-O-(N-methylanthraniloyl)-cGMP) and db-cGMP (dibutyryl-cGMP) were identified from a concerted effort to deorphanise a panel of 82 orphan GPCRs by screening 10,500 candidate endogenous ligands using the DiscoveRx PathHunter™ β-arrestin-2 recruitment assay (Southern et al., 2013). MANT-cGMP (EC_{50} 2 μM) was the most potent while cGMP was the least potent (EC_{50} 130 μM) (Southern et al., 2013). Despite this discovery, the functional relevance of these ligands at GPR35 remains to be demonstrated, including whether concentrations of these ligands present *in vivo* would be sufficient to activate GPR35. Notwithstanding, it is interesting to note that cGMP and its associated signalling pathways have received considerable attention recently for the treatment of cardiovascular disorders including hypertrophy, hypertension, ischemia and reperfusion injury (Lukowski et al., 2014; Garcia-Dorado et al., 2009; van Heerebeek et al.,

2012; Greene et al., 2013), and the possible link between GPR35 and cGMP may therefore deserve further attention.

An assessment of tyrosine pathway metabolic intermediates that contain catechol or carboxylic acid groups also revealed that the melanin biosynthesis intermediate DHICA (5,6-dihydroxyindole-2-carboxylic acid) and thyroid hormone synthesis intermediates T3 (3,5,3' triiodothyronine) and reverse T3 (3,3',5'-triiodothyronine) promoted dynamic mass redistribution (DMR) in the human colorectal adenocarcinoma cell line HT-29, which endogenously expresses GPR35 (Deng et al., 2012c). Application of the synthetic GPR35 antagonist CID-2745687 (methyl-5-[(tert-butylcarbamothioylhydrazinylidene)methyl]-1-(2,4-difluorophenyl)pyrazole-4 carboxylate) at a fixed concentration of 64 μM reduced the wavelength shift of each of the aforementioned agonists to almost basal levels, indicating that their activity occurred primarily through GPR35, which is expressed endogenously in these cells. However, confirmation of these responses in an independent assay utilising a β-lactamase reporter gene-based readout of β-arrestin recruitment suggested that only DHICA acted with similar potency to that generated in the DMR format (Deng et al., 2012c). This indicated that T3 and reverse T3, if acting through GPR35, do so in a functionally selective manner. Reverse T3 was found to be the most potent of the tyrosine metabolites assessed, generating DMR in HT-29 cells with an EC_{50} of 5.9 ± 0.4 μM (Deng et al., 2012c). The EC_{50} observed in the Tango™ β-arrestin recruitment assay, however, was substantially higher, at 108 ± 9 μM. T3 was less potent than reverse T3, with an EC_{50} of 50 ± 5 μM in the DMR assay and 513 ± 61 μM in the Tango™ assay (Deng et al., 2012c). As with the previously mentioned putative endogenous ligands however, estimates of the free and total levels of T3 and reverse T3 in the literature (Chopra et al., 1975; Hüfner et al., 1978; Prescott et al., 1979) indicate that it is unlikely that the concentrations of these molecules produced in man could activate GPR35 significantly *in vivo* (Deng et al., 2012c). Nonetheless, it is interesting to note that the levels of reverse T3 were found to increase, and T3 to decrease, following acute myocardial infarction (Friberg et al., 2002) and in advanced heart failure (Hamilton et al., 1990), and have been utilised as a measure to predict survival rates in patients with heart disease (Iervasi et al., 2003).

Thus, although there have been advances in the number of endogenous molecules activating GPR35, because of the low potency of many of these compounds and the fact that it is unlikely that any of them activate this receptor selectively under normal physiological

conditions, the discovery and use of synthetic ligands have been critical to the advancement in the understanding of the pharmacology and function of GPR35.

1.5.4 *Ligands acting at GPR35: synthetic ligands*

Consensus may not have been reached on whether GPR35 is truly activated by any of the aforementioned endogenous ligands *in vivo* (Mackenzie et al., 2011; Milligan, 2011; Divorty et al., 2015), yet progress in the identification of synthetic surrogate ligands for this receptor has been quite successful (**Table 1.3**). Focused compound discovery efforts carried out by both the industrial and academic sectors have reported a number of compounds that display moderate-to-high potency at GPR35, and indeed there now exists a reasonable number of tool compounds with which to probe the basic physiology and pathophysiology of this receptor. Notably, however, as observed for kynurenic acid, many of these synthetic compounds display marked species selectivity.

One of the first ligands documented for GPR35 was the cyclic guanosine monophosphate (cGMP)-phosphodiesterase (PDE) 5/6 inhibitor zaprinast (2-(2-propyloxyphenyl)-8-azapurin-6-one) (Taniguchi et al., 2006), which was originally synthesised during the creation of xanthines for the treatment of allergy (Broughton et al., 1974). Due to zaprinast's success in increasing the amplitude/duration of nitrergic responses, it became a lead compound for the rational drug design of sildenafil (Gibson, 2001). However, although zaprinast is an analogue of cGMP and is structurally similar to sildenafil, cGMP acts only with weak activity at GPR35 (Southern et al., 2013) while sildenafil is inactive (unpublished observations). Zaprinast tends to be employed as a reference agonist for GPR35 since it displays moderate-to-high potency at each of the human, mouse, and rat species orthologs (Taniguchi et al., 2006; Yang et al., 2010; Jenkins et al., 2012), and zaprinast's GPR35-mediated effects can be dissected from those exerted through its inhibition of phosphodiesterases (Taniguchi et al., 2006; Yoon et al., 2005; Choi et al., 2007).

Because zaprinast is the only phosphodiesterase blocker to specifically inhibit PDE6 over PDE5 (Zhang et al., 2005), in a study aiming to elucidate the effects of PDE6 in retinal photoreceptors on light-dependent signal transduction, Du et al., used zaprinast. These authors unexpectedly found that zaprinast altered the metabolic profile of mitochondrial intermediates and amino acids in the retina and brain of mice, acting like mitochondrial

Table 1.3 Selection of potent GPR35 ligands

Name(s)	Structure	Action	Potency (EC_{50}/ IC_{50})	Comments	References
Zaprinast, M&B 22,948	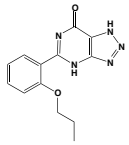	Full agonist	Human: **2-8 µM** Mouse: **1 µM** Rat: **100 nM**	Xanthine derivative; cGMP PDE 5, 6, 9 inhibitor, selective for PDE 5 (IC_{50} 750 nM)	Taniguchi et al., 2006; Jenkins et al., 2012;
Pamoic acid, Pamoate, Embonic acid,	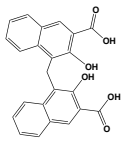	Partial agonist at human, weak activity at rodent	Human: **30-50 nM** Mouse: **Inactive** Rat: **> 100 µM**	Added as an "inert" substance to pharmaceutical agents; inhibits DNA pol β (IC_{50} 9 µM)	Zhao et al., 2010; Jenkins et al., 2010; Neubig, 2010; Jenkins et al., 2012
Cromolyn, Sodium cromoglicate, DSCG	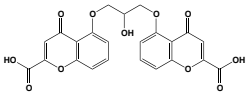	Full agonist	Human: **~ 7 µM** Mouse: **22 - 56 µM** Rat: **~4 µM**	Mast cell stabiliser, prophylactic agent against asthma attacks (Intal®); ophthalmic solution (Opticrom®)	Yang et al., 2010; Jenkins et al., 2010; Deng et al., 2012a
Compound 1	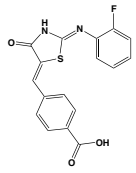	Full agonist at human, partial agonist at rodent	Human: **26 nM** Mouse: **17 µM** Rat: **8 µM**	Novel ligand	Neetoo-Isseljee et al., 2013
PSB-13253	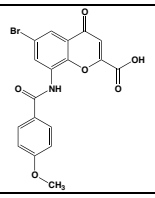	Full agonist at human, partial agonist at rat	Human: **12 nM** Mouse: **Inactive** Rat: **1.4 µM**	Novel ligand; [^{3}H] radiolabelled structure also available with K_D of 5.3 nM	Funke et al., 2013; Thimm et al., 2013
Lodoxamide, ICI 74917	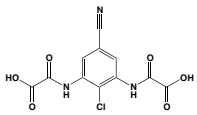	Full agonist	Human: **4 nM** Rat: **13 nM**	Mast cell stabiliser; ophthalmic solution: Alamide® lodoxamide tromethamine, U-42,585E	Mackenzie et al., 2014
Bufrolin, BRL10833	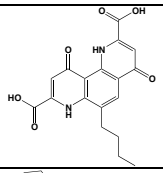	Full agonist	Human: **13 nM** Rat: **10 nM**	Mast cell stabiliser; equipotent at human and rat GPR35	Mackenzie et al., 2014
ML-145, CID-2286812	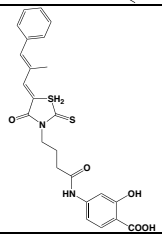	Inverse agonist	Human: **~ 25 nM**	Novel ligand; Displays selectivity towards human GPR35	Heynen-Genel et al., 2010; Jenkins et al., 2012
CID-2745687, SPB05142, ML-194	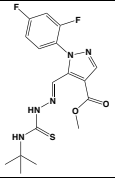	Inverse agonist	Human: **~ 200 nM**	Novel ligand; Displays selectivity towards human GPR35	Zhao et al., 2010; Heynen-Genel et al., 2011; Jenkins et al., 2012

Action describes compound efficacy compared with reference compound zaprinast, potency values were generated in β-arrestin-2 recruitment assays.

pyruvate carriers to stimulate oxidation of glutamate and accumulation of aspartate (Du et al., 2013). Importantly this effect was not due to the PDE activity of zaprinast, and although the authors suggested that this effect was also not due to the effects of GPR35, they used CID-2745687 as an antagonist and pamoic acid as an independent agonist, neither of which function at the mouse orthologue of GPR35 (Jenkins et al., 2012) and as such these conclusions must be viewed with caution. In a separate study zaprinast was found to inhibit hydrogen peroxide-induced lysosomal destabilisation, a step that precedes mitochondrial apoptotic changes and oxidative cell death in cultured astrocytes in a manner independent from cGMP activity (Choi et al., 2007). Further studies have linked zaprinast activity to anti-nociception, with spinal application of zaprinast following formalin-induced nociception dose-dependently reducing the sum of flinches in male Sprague-Dawley rats (Yoon et al., 2005). However, despite the wide application of zaprinast as reference agonist of GPR35, with a potency of between 2 and 8 μM at the human ortholog, concerted efforts have been taken to identify agonists with high potency at human GPR35, and ideally one that acts with similar potency at the human and rodent orthologs.

Indeed, ligands that acted with potencies higher than zaprinast at the human ortholog were subsequently identified (**Table 1.3**). This includes pamoic acid (5-nitro-2-(3-phenylproplyamino) benzoic acid), which was identified independently by two groups following screens of the Prestwick Chemical Library® (Zhao et al., 2010; Jenkins et al., 2010). Pamoic acid is a substance that is added as a counter ion to stabilise drug formulations, including the antihelminthics oxantel pamoate and pyrantel pamoate, the psychoactive compounds hydroxyzine pamoate (Vistaril®) and imipramine pamoate (Tofranil-PM®) and the peptide hormones triptorelin pamoate (Trelstar®) and octreotide pamoate (OncoLar®) (Zhao et al., 2010; Neubig, 2010). Crucially, pamoic acid was added to these formulations as an 'inert' substance, as classified by the US Food and Drug Administration (FDA), and was believed to act only to prolong the activity of the active components before it was identified as a GPR35 agonist (Neubig 2010; Zhao et al., 2010; Jenkins et al., 2010). This, therefore, since pamoic acid is present in the therapeutic formulation, could link GPR35 to the disease states treated by these formulations (Citrome, 2009; Xu et al., 2013b; McCarthy, 2014). Specifically, pyrvinium pamoate was found to inhibit the NADH-fumarate reductase system in mitochondria of a Panc-1 (human pancreatic cancer) cell line, a system involved in delivering nutrients within the hypoxic-hypoglycaemic tumour environment (Tomitsuka et

al., 2012). Pyrvinium pamoate was also found to disable survival of cardiac fibroblasts to ameliorate myocardial contractile dysfunction in a mouse model of myocardial infarction (Murakoshi et al., 2013). While these studies could be attributed to the action of pyrvinium alone, in conjunction with the effect of zaprinast on mitochondrial function and that GPR35 gene expression is extremely sensitive to hypoxia, with a potential role in the acute phase of myocardial infarction, it raises an intriguing potential role for GPR35 in hypoxic metabolism (Ronkainen et al., 2014). Importantly however, *in vitro* analysis carried out in HEK293 cells revealed that pamoic acid activates GPR35 with 1000 fold selectivity toward the human orthologue, with activity at the rodent orthologues being weak to non-existent in the BRET and inositol monophosphate accumulation assays (Jenkins et al., 2010; Jenkins et al., 2012). Thus, caution is required when interpreting pamoic acid data acquired using rodent models of disease. Furthermore, pamoic acid also acts as an inhibitor of DNA polymerase β, but this is at a markedly higher concentration (K_D 9 μM) than that needed to activate human GPR35 (EC_{50} 10-50 nM) (Hu et al., 2004; Hazan et al., 2008; Jenkins et al., 2012).

Unlike zaprinast and pamoic acid, GPR35 agonist cromolyn (disodium cromoglycate) acts at human, mouse, and rat orthologues of GPR35 with almost equal potency; however, its potency significantly less than the other GPR35 ligands, which limits its usefulness (**Table 1.3**) (Yang et al., 2010; Jenkins et al., 2012). Cromolyn has been used clinically for the treatment of asthma since 1967. Although the mechanism of cromolyn's action has not been elucidated, inhalation of cromolyn in patients with allergic asthma blocks allergen-induced bronchospasm, thought to be through inhibition of mast cell degranulation (Oka et al., 2012), which was supported by cromolyn's ability to inhibit the degranulation of rat peritoneal mast cells in response to challenge with IgE (Shin et al., 2004). In keeping with the ligand-associated functions of zaprinast and pamoic acid, cromolyn has been associated with the prevention of superoxide generation in neutrophils (Kilpatrick et al., 1995), reduction of ischemic tissue injury in rats following pulmonary allograft transplant (Chang et al., 2014), and increases apoptosis as part of an anti-cancer therapy (Motawi et al., 2014).

Subsequent to these early discoveries, a number of high potency ligands have been discovered for GPR35, including 'compound 1' (4-{(Z)-[(2Z)-2-(2-fluorobenzylidene)-4-oxo-1,3-thiazolidin-5-ylidene]methyl}benzoic acid) (Neetoo-Isseljee et al., 2013), and PSB-13253 (6-bromo-8-(4-[(3)H]methoxybenzamido)-4-oxo-4H-chromene-2-carboxylic acid) (Funke et al., 2013), which both display potency similar to pamoic acid at human GPR35 and act with

significantly lower potency and efficacy at the rodent orthologs (**Table 1.3**). Compound 1 was identified following a screen of the MRCT 100,000 small molecule compound collection using the DiscoveRx enzyme complementation β-arrestin-2 recruitment assay, as were four other, chemically distinct, GPR35 agonists that display various profiles of species selectivity (Neetoo-Isseljee et al., 2013), (which are described herein in **Chapter Four**), while PSB-13253 was derived from a medicinal chemistry programme based on derivatives of chromen-4-one-2-carboxylic acid (Funke et al., 2013).

The study by Funke and colleagues also presented the first comprehensive assessment of the structure-activity relationship between various chemical structures at human, mouse, and rat orthologs of GPR35. Although noted previously for individual ligands (Neetoo-Isseljee et al., 2013), this study provided collective evidence that GPR35 ligands act with either human-selective, human-and-mouse-selective, human-and-rat-selective or rodent-selective properties, with no ligands found to act with high and equal potency at all three orthologs (Funke et al., 2013). However, shortly after this study was published, two mast cell stabilisers were found to activate human *and* rat in a high and equipotent manner, becoming the first tool compounds reported at GPR35 that could feasibly be employed to translate the findings obtained for the human receptor *in vitro* into *in vivo* physiological studies in rat models of physiology and disease (Mackenzie et al., 2014). In the BRET-based β-arrestin-2 recruitment assay, lodoxamide (2,2'-[(2-chloro-5-cyano-1,3-phenylene)diimino]bis[2-oxoacetic acid]) and bufrolin (6-butyl-4,10-dioxo-1,7-dihydro-1,7-phenanthroline-2,8-dicarboxylic acid) activated human and rat GPR35 with EC_{50}s of 3.6 nM and 12.5 nM at human and 12.5 nM and 10 nM at rat, respectively (**Table 1.3**) (Mackenzie et al., 2014). This study also identified a number of mast cell stabilisers that act with rat-selectivity at GPR35 orthologs, including amlexanox and pemirolast, which are described herein in **Chapter Four**.

1.7 Aim of PhD

The lack of consensus surrounding the endogenous ligand of GPR35 has limited efforts to understand and dissect the basic physiologic function of the receptor. Indeed, as mentioned previously, the majority of reports that suggest GRP35 to be a notable therapeutic target stem from GWAS and gene knock-out studies. In an effort to provide potent tool compounds to elucidate the pharmacology and function of GPR35, I embarked upon a drug discovery effort through a collaborative project with Medical Research Council Technology (MRCT) (Neetoo-Isseljee et al., 2013), and, independently, with Novartis (Mackenzie et al., 2014). The efforts from such studies are presented herein (**Chapter Four**), following optimisation of assay formats for drug screening efforts at GPR35 (**Chapter Three**). Finally, in an effort to understand how these ligands interact with GPR35, and why they display marked species selectivity profiles, a mutagenesis effort was carried out to switch key residues from the human and rat orthologue ligand binding pockets to ascertain their role in ligand binding (**Chapter Five**). At the time of completing this project my efforts, as part of the two aforementioned collaborations, had reported three of the most potent ligands available for human GPR35. Two of which, importantly, activated human and rat GPR35 with similar potency. These findings should considerably benefit the study of GPR35 in rodent models of disease and enable a comparison of research efforts between species, which has not been possible before.

Chapter Two

Materials and Methodology

2.1 Materials

Chemical substances were supplied either by Sigma-Aldrich (Gillingham, UK) or Thermo Fisher Scientific (Waltham, MA) at the highest possible analytical grade. Cell culture reagents were supplied by Life Technologies Ltd, (Paisley, UK), unless specified otherwise. Plasticware including disposable cell culture flasks were from Corning, Costar, (Cambridge MA, USA). Assay plates (96- or 384-well) were sourced from various companies as indicated throughout the text.

2.2 Pharmacological test compounds

Zaprinast (1,4-Dihydro-5-(2-propoxyphenyl)-7H-1,2,3-triazolo(4,5-d)pyrimidin-7-one), **CID-2745687** (1-(2,4-Difluorophenyl)-5-[[2-[[(1,1-dimethylehyl)amino] thioxomethyl]hydrazinylidene] methyl]-1*H*-pyrazole-4-carboxylic acid methyl ester), and **ML-145** (2-Hydroxy-4-[4-(5*Z*)-5-[(*E*)-2-methyl-3-phenylprop-2-enylidene]-4-oxo-2-sulfanylidene-1,3-thiazolidin-3-yl]butanoylamino]benzoic acid) were purchased from Tocris Bioscience (Bristol, UK). **Amlexanox** (2-Amino-7-(1-methylethyl)-5-oxo-5H-[1]Benzopyrano[2,3-b]pyridine-3-carboxylic acid), **compound 48/80** (2-(4-methoxyphenyl)-N-methylethanamine), **cromolyn disodium** (disodium;5-[3-(2-carboxylato-4-oxochromen-5-yl)oxy-2-hydroxypropoxy]-4-oxochromene-2-carboxylate), **doxantrazole** (3-(1H-tetrazol-5-yl)-9H-thioxanthen-9-one 10,10-dioxide monohydrate), **ketotifen fumarate** 4-(1-methylpiperidin-4-ylidene)-4,9-dihydro-10*H*-benzo[4,5]cyclohepta[1,2-*b*]thiophen-10-one), **kynurenic acid** (4-Hydroxyquinoline-2-carboxylic acid), **pamoic acid disodium salt** (4,4'-Methylenebis(3-hydroxy-2-naphthoic acid), **pemirolast potassium** (9-Methyl-3-(1H-tetrazol-5-yl)-4H-pyrido[1,2-a]pyrimidin-4-one potassium salt), **tranilast** (2-[[3-(3,4-Dimethoxyphenyl)-1-oxo-2-propenyl]amino] benzoic acid) were purchased from Sigma-Aldrich (Gillingham, Dorset). **Bufrolin** (6-butyl-4,10-dioxo-1,7-dihydro-1,7-phenanthroline-2,8-dicarboxylic acid) was synthesised in collaboration with Novartis, Horsham UK. **Lodoxamide** (2-[2-chloro-5-cyano-3-(oxaloamino)anilino]-2-oxoacetic acid), **compound 1** (4-{(Z)-[(2Z)-2-(2-fluorobenzylidene)-4-oxo-1,3-thiazolidin-5-ylidene]methyl}benzoic acid), **compound 2** (2,2'-bithiophene-5,59-dicarboxylic acid), **compound 3** (4-chloro-3-(2,5-dimethyl-1H-pyrrol-1-yl)benzoic acid), **compound 4** (4H-thieno[3,2-b]pyrrole-2-carboxylic

acid), and **compound 5** (9-benzyl-5-methyl-3-(4-methylphenyl)-5,9-dihydro-6H-[1,2,4]triazolo[4,3-e]purine-6,8(7H)-dione) were synthesised in collaboration with the MRCT, London, U.K.

With the exception of compound 48/80, ketotifen fumarate, and pemirolast potassium, which were soluble in dH_2O, all other powdered test compounds were re-suspended in dimethyl sulfoxide (DMSO), (Thermo Fisher Scientific, Waltham, MA, # D/4120/PB08) to a 10 mM working stock solution. Note, due to poor solubility, bufrolin was diluted to 1 mM in DMSO.

2.3 DNA constructs and plasmids

Human, rat and mouse GPR35 receptor cDNAs were N-terminally fused with the FLAG epitope tag (sequence DYKDDDDK), with removal of the stop codon and addition of the enhanced yellow fluorescent protein (eYFP) sequence to the C-terminus by PCR cloning yielding a single gene transcript for each species. Each cDNA construct was cloned, in frame, into pcDNA™3.1 or the inducible expression vector pcDNA™5/FRT/TO (Life Technologies Ltd; Paisley, UK) as described in the references included in **Table 2.1**.

As part of this project the FLAG-human GPR35a-*EcoRV*-$G\alpha_{13EE}$ fusion construct was generated by PCR cloning (**Section 2.4.9**) using oligonucleotide primers. This enabled the 3' *NheI* sequence to be adjoined to the KOZAK-FLAG-human GPR35a construct N-terminus (forward 5' TGGAGCTAGCACCATGGATGGACTACAAAGACGATGACGACAAGCTGAGTGG TTCCCGGGC 3') and an *EcoRV* site to be added immediately following the C-terminal sequence of GPR35, removing the stop codon (reverse 5' TTAAGATATCGGCGAGGGTCACGCACAG 3'). To allow a subsequent ligation between GPR35 and $G\alpha_{13EE}$ using the *EcoRV* site, an *EcoRV* sequence was added to the N-terminus of $G\alpha_{13EE}$ (forward: 5' TTAAGATATCGCGGACTTCCTGCCGTC 3') in addition to a stop codon and *NotI* sequence at the C-terminal end of $G\alpha_{13EE}$ (reverse 5' TCCAGCGGCCGCTGACTGT AGCATAAGCTGCTT 3'). The $G\alpha_{13EE}$ construct was purchased from the Missouri S&T cDNA Resource centre (Rolla, Missouri # GNA130EI00) and contained an internal 'Gla-Glu' epitope sequence (EYMPTE) at residues 188-193, which replaced the endogenous 'DYIPSQ' sequence. The construct sequence was confirmed by sequencing (**Section 2.4.13**) and stably transfected into the HEK293 Flp-In™ T-REx™ cell line as described in **Section 2.5.5**.

Table 2.1 GPR35 cDNA construct history and information

Gene Name	Ref Seq	Species	cDNA Length (bp)	Isolated From	Gene Product	Construct	Plasmid	Restriction Sites	Protein Length (aa)	Reference
GPR35 transcript variant 1	NM_005301.3 with a M108T SNP	Human	927	dorsal root ganglion	GPR35a	FLAG-humanGPR35a-eYFP	pcDNA™3.1 and pcDNA™5/FRT/TO	5' *HidIII* 3' *NotI*	309	Taniguchi et al., 2006; Jenkins et al., 2010
GNA13	NM_006572	Human	1140	unknown	$G\alpha_{13EE}$	$G\alpha_{13EE}$ (DYIPSQ residues mutated to EYMPTE to insert internal EE epitope tag at residues 188-193)	pcDNA™3.1	5' *KpnI* 3' *XbaI*	380	Missouri S&T cDNA Resource Centre, GNA130EI00
GPR35-GNA13	not applicable	Human	2093	not applicable	GPR35a-$G\alpha_{13EE}$	FLAG-humanGPR35a-*EcoRV*-Gα13EE	pcDNA™5/FRT/TO	5' *KpnI* 3' *NotI*	697	This study
GPR35 transcript variant 2 or 3	NM_001195381.1, NM_001195382-1	Human	1022	human colorectal adenocarcinoma cells, HT-29	GPR35b	FLAG-humanGPR35b-eYFP	pcDNA™3.1 and pcDNA™5/FRT/TO	5' *HidIII* 3' *NotI*	340	Mackenzie et al., 2014
GPR35 transcript variants 1-3	NM_022320.4, NM_001104529.1, NM_001271766.1	Mouse	923	mouse genomic DNA	GPR35	FLAG-mouseGPR35-eYFP	pcDNA™3.1 and pcDNA™5/FRT/TO	5' *BamHI* 3' *NotI*	307	Jenkins et al., 2012
GPR35	NM_001037359.1	Rat	921	colon	GPR35	FLAG-ratGPR35-eYFP	pcDNA™3.1 and pcDNA™5/FRT/TO	5' *BamHI* 3' *NotI*	306	Taniguchi et al., 2006; Jenkins et al., 2010

Each construct expressed from pcDNA™5/FRT/TO was inserted stably into the HEK293 Flp-In™ T-Rex™ cell line, whereas pcDNA™3.1 expression vectors were used for transient transfections. See references for further information.

Bovine β-arrestin-1-*Renilla* luciferase and β-arrestin-2-*Renilla* luciferase were generated previously by PCR amplification of *Renilla* luciferase-containing plasmid pRL-CMV (Promega, Southampton, UK, # E2261), which was digested with 5' *XbaI* and 3' *NhoI* and subcloned into the respective *β-arrestin* pcDNA™3.1 vector to create *β-arrestin*-Renilla-*luciferase*-pcDNA™3.1 (Jenkins et al., 2011). Chimeric $G\alpha_q$ subunits were previously created by the replacement of last five carboxyl terminal amino acids of $G\alpha_q$ (EYNLV) with those from $G\alpha_i$ (DCGLF) to create $G\alpha_{qi1/2}$ or $G\alpha_{13}$ (QLMLQ) to create $G\alpha_{q13}$ expressed in pcDNA™3.1 (Molecular Devices, Life Technologies, Paisley, UK). These constructs allowed re-routing of human, mouse, and rat $G\alpha_{i1/2}$ and $G\alpha_{13}$ coupled receptors through the $G\alpha_{q/11}$ pathway. pcDNA™ vectors contained the immediate-early Cytomegalovirus (CMV) promoter, and included CAAT and TATA boxes. Additionally, inserted constructs contained the KOZAK enhancer sequence surrounding the ATG initiation codon, which ensured high-level mRNA expression was obtained. In HEK293T cells, which expressed the Simian Virus 40 large T antigen, replication from pcDNA™ plasmids was initiated from the SV40 early promoter sequence, and terminated at the SV40-PolyA sequence. Each pcDNA vector contained a pUC origin of replication and ampicillin resistance gene to enable growth in and selection in bacterial cultures. The p426 glyceraldehyde-3-phosphate dehydrogenase (GPD) vector (ATCC®, Middlesex, UK, # 87361™) was used for yeast expression of FLAG-tagged GPR35 constructs, which were inserted within the poly-linker site using the 5' *BamHI* and 3' *PaeR71* restriction sequences, as described in Jenkins et al., 2010. The p426GPD vector contained the GPD promoter for gene expression initiation, with replication controlled by a 2μ replication origin, and termination was controlled by the *CYC1* (cytochrome C1) polyA sequence. Selective gene markers included the *URA3* and AMP^R genes.

2.4 Molecular biology protocols

2.4.1 *Preparation of Luria Bertani broth and agar*

Luria Bertani medium (LB) or Luria Bertani agar (LB agar) were prepared by reconstitution of LB Broth or LB Agar (Merck Millipore International, Darmstadt, Germany, MILLER # 71753 or # 110283, respectively) with Milli-Q dH_2O, using a plastic-coated

magnetic stir-bar in a 500 mL DURAN® laboratory glass bottle with a plastic screw cap and pouring ring (SCHOTT UK Ltd, Stafford, UK). The homogeneous solution was sterilised using an autoclave (Prestige Medical, Coventry, UK, 2100 series model), with 11 min cycle at 126°C. For LB agar, autoclaved bottles were sealed and placed in an incubator set at 50°C to cool. By use of sterile technique, the plastic pouring ring was flamed using a Bunsen burner and approximately 20 mL LB agar poured into sterile 10 cm^2 Sterilin® single use dishes (Thermo Fisher Scientific, Waltham, MA). Lids were replaced on plates and set at room temperature, before storage overnight at 4°C. LB was stored at room temperature for up to six months. LB agar-Amp or LB-Amp was created by the dilution of filter-sterilised 100 mg/mL ampicillin stock solution (prepared fresh every six months and stored at -20°C in the absence of light) to 100 μg/mL in LB or LB agar solution. LB agar-Amp and LB-Amp solutions were freshly prepared and stored at 4°C in the absence of light.

2.4.2 *Preparation of chemically competent XL-1 Blue cells*

Escherichia coli laboratory strain XL-1 Blue contain *recA1*, *endA1, gyrA96*, *thi-1*, *hsdR17*, *supE44*, *relA1*, *lac* [F' *proAB lacI*^{q}*ZΔM15*, Tn*10* (Tet^r)] mutations to improve the stability, quality, yield, and purity of transformed exogenous DNA vectors. Additionally, tetracycline resistance is conferred, and XL-1 Blue are eligible for blue/white colour selection when grown in the presence of isopropyl-β-D-thiogalactopyranoside (IPTG). XL-1 Blue stock, stored at -80°C, was defrosted on ice and streaked onto a freshly prepared LB agar dish (in the absence of antibiotic) using sterile technique (**Section 2.4.1**). The bacterial culture plate was inverted at incubated at 37°C for 16 h. Using sterile technique, a single colony was isolated and inoculated into a 30 mL Universal containing 5 mL freshly prepared LB (in the absence of antibiotic). Each 5 mL starter culture was incubated overnight (16 h) at 37°C, 250 RPM. To a 1 L PYREX® Erlenmeyer flask containing 100 mL LB, 100 μl starter culture was added and incubated at 37°C, 220 RPM. Once an optical density of 0.48 at 600 nm was obtained, growth was stalled by incubation of cultures on ice for 20 min, before centrifugation in pre-chilled sterile 50 mL centrifuge tubes (2000 x *g*, 10 min at 4°C).

To gently re-suspend the bacterial pellet in freshly prepared solution 1 [CH_3CO_2K (30 mM), RbCl (0.1 M), $CaCl_2$ (10 mM), $MnCl_2$ (50 mM), glycerol (80 % (w/v)), pH 5.8, filter

sterilised using a 0.2 μm filter fitted with a sterile syringe and stored at 4°C] the top of a 1 mL plastic pipette tip was cut, flamed using a Bunsen burner and used to re-suspend pellet in a 1 mL volume, which was then diluted to 20 mL. A total of 20 mL solution 1 was added and cultures incubated on ice for 20 min before a second centrifugation at 2000 x *g*, 10 min at 4°C. Supernatant was poured, carefully, using sterile technique, before re-suspension in 2 mL of solution 2 [MOPS (10 mM, pH 6.5), $CaCl_2$ (75 mM), $RbCl_2$ (10 mM), glycerol (80 % (w/v)), pH 6.5, filter sterilised using a 0.2 μm filter fitted with a sterile syringe and stored at 4°C] using a cut 1 mL pipette tip. The competent bacteria were incubated on ice for 15 min then aliquoted into pre-chilled, sterile 1.5 mL microcentrifuge tubes at a volume of 220 μl and stored immediately at -80°C for up to one year.

2.4.3 *Preparation of yeast peptone dextrose*

Under the same principle for LB and LB-Agar as described in **Section 2.4.1**, yeast peptone dextrose (YPD) media and agar were prepared. Briefly, 1 % (w/v) yeast extract powder (ForMedium™, Norfolk, UK, # YEA02), 2 % (w/v) peptone (Duchefa Biochemie, Haarlem, Netherlands, # P1328) and 2 % (w/v) D-glucose were reconstituted with Milli-Q dH_2O. For YPD-Agar, 2 % micro agar (Duchefa Biochemie, Haarlem, Netherlands, # M1002) was added, and autoclaved as described previously (**Section 2.4.1**). By use of sterile technique, approximately 20 mL YPD-Agar was poured into Sterilin® 10 cm^2 petri dishes. Lids were replaced on plates and set at room temperature before storage overnight at 4°C.

2.4.4 *Preparation of chemically competent Saccharomyces cerevisiae cells*

Frozen stock vials containing laboratory *S. cerevisiae* strain W303-1A (*MAT***a**, *ade2*, *can1*, *his3*, *leu2*, *trp1*, *ura3*), containing a Gpa1-Gα chimera was defrosted on ice. By use of a sterile technique, a pipette tip was used to spread the yeast in a thick layer onto a fresh, pre-warmed, YPD-Agar 10 cm^2 plate. The plate was then turned at a 45°C angle and using a zig-zag method, yeast scraped across the plate. This process was carried out three times, each time with a fresh pipette tip in order to isolate individual *S. cerevisiae* colonies. Plates were incubated for three days, agar side up, at 30°C in a designated yeast incubator.

To generate chemically competent *S. cerevisiae*, using sterile technique, an individual colony was isolated using a sterile pipette tip and inoculated into a 30 mL sterile Universal containing 5 mL sterilised YPD. Starter cultures were incubated overnight at 30°C, 250 RPM in a designated orbital yeast incubator. To a sterilised 2 L PYREX® Erlenmeyer flask containing 200 mL YPD, 2 mL saturated overnight starter culture was added, using sterile technique, and incubated at 30°C, 220 RPM. Absorbance was recorded regularly using a disposable plastic cuvette and UV absorbance quantified at an optical density (OD) of 600 nm using an Eppendorf® BioPhotometer. Following doubling for a minimum of two generations (approximately 2.2 h each), with growth in mid-logarithmic growth phase (OD_{600} between 0.8 – 1.0), the flask was placed on ice. *S. cerevisiae* cells were isolated by transfer to sterile, 50 mL centrifuge tubes and spun at 600 x *g* for 5 min at 4°C on a benchtop centrifuge. Supernatant was discarded and pellets re-suspended in 10 mL freshly prepared and sterilised LiTESorb [LiAc (1 M), Tris-HCL (1 M, pH 7.4), EDTA (0.5 M), sorbitol (2.4 M)], centrifuged at 600 x *g* for 5 min at 4°C. Cell pellets were then gently re-suspended in 4 mL LiTESorb and placed in a shaking incubator at 30°C, 220 RPM, for 1 h. Centrifuge tubes containing *S. cerevisiae* cultures were then placed in a metal rack, housed within a polystyrene box filled with crushed ice, and incubated overnight at 4°C. An equivalent volume (4 mL) of freshly prepared and filter sterilised ice-cold 40 % (w/v) glycerol/0.5 % NaCl was added, mixed gently, and cultures aliquoted into 1.5 mL microcentrifuge tubes, on ice, and stored at -80°C.

2.4.5 *Transformation of S. cerevisiae by heat-shock method*

Chemically competent *S. cerevisiae* strains expressing the endogenous yeast Gα subunit GPA1 or a yeast-mammalian chimeric GPA1 Gα subunit was added (200 µl) with 10 µg vector DNA containing the gene of interest (p426 GPD expressing FLAG-GPCR), into sterile 1.5 mL microcentrifuge tubes. An equivalent volume of sterilised 70 % polyethylene glycol (PEG)-3350 (Sigma Aldrich, Gillingham, UK) was added to cells and incubated in a shaking yeast designated incubator at 30°C, 220 RPM, for 45 min. Cells were then heat-shocked for 20 min at 42°C in a temperature-controlled waterbath, and isolated by centrifugation at 5900 x *g* in a benchtop microcentrifuge for 2 min at room temperature. Using sterile technique, supernatant was discarded and pellets gently re-suspended in 100 µl sterile Milli-

Q dH_2O by pipetting. Transformed cultures, using an ethanol-flamed metal spreader, were plated onto Synthetic Complete (SC) drop-out agar lacking uracil and methionine (ForMedium™, Norfolk, UK # DSCK192). Once dry, the plate was inverted and incubated at 30°C for three days. By use of sterile technique, a single colony was isolated and streaked onto a freshly prepared SC -Ura -Met agar [Yeast Nitrogen Base (6.8 % (w/v)), D-glucose (20 % (w/v)), Kaiser synthetic drop-out mix (1.85 % (w/v)), microagar (2 % (w/v))] plate using a sterile pipette tip before further incubation at 30°C overnight.

2.4.6 *RNA isolation and two-step reverse-transcription polymerase chain reaction*

To isolate cellular RNA from mammalian cell lines, cultures were grown to sub-confluence in 10 cm^2 dishes, prior to trypsinisation as described in (**Section 2.5.3**). The cell pellet was then washed twice with sterile 1X phosphate buffered saline (PBS) before the RNeasy® mini kit from QIAGEN® was used to isolate mRNA (Manchester, UK, # 74124). To prepare the workbench for RNA isolation, surfaces were thoroughly sprayed with RNase*Zap*® Decontamination Solution (Life Technologies Ltd., Paisley, UK, # AM9780). Gilson pipettes and plastic tube racks were also decontaminated prior to use and allowed to air dry. To prevent aerosol contamination, sterile, RNase- and DNase-free filter tips (TipOne®, Starlab Group, Milton Keynes, UK) were used throughout the RNA isolation procedure. Nitrile gloves were worn and changed frequently throughout. All centrifugation steps were carried out on a benchtop centrifuge at room temperature.

To the isolated cell pellet, 600 μl Buffer RLT (containing guanidinium thiocyanate) was added and sample vortexed briefly to ensure protein denaturation, cell lysis, and immediate inactivation of RNases. The cell lysate was homogenised by passing five times through a 20-gauge needle (BD Microlance™) fitted to an RNase-free syringe (BD Plastipack™), before the addition of 600 μl 70 % ethanol to prepare the sample for the silica-based membrane. The sample (600 μl) was transferred to an RNeasy spin column placed within a 2 mL collection tube and centrifuged for 15 sec at 8000 x *g*. Flow-through was discarded and this process was repeated for a second time to process the remainder of the test sample.

To remove contaminating carbohydrates, fatty acids and proteins that non-specifically bound the silica-membrane, the spin column was stringently washed with 700 µl Buffer RW1 (containing guanidine salt and ethanol) and centrifuged for 15 sec at 8000 x *g*. Flow-through was discarded and samples inverted briefly on tissue paper before the column was washed using 500 µl mild washing buffer, Buffer RPE, which contained ethanol and was used to remove any remaining traces of salts situated on the column. The sample was centrifuged for 15 sec at 8000 x *g* before a second wash was carried out using 500 µl Buffer RPE, and centrifuged for 2 min at 8000 x *g* to dry the spin column membrane. The RNeasy spin column was then transferred to an RNase-free microcentrifuge tube (supplied) and 60 µl RNase-free water (supplied) was added directly to the spin column membrane. After standing for 1 min, the sample was centrifuged at 8000 x *g*, for 1 min, with the eluted RNA collected and spun once more through the spin column to increase the RNA concentration. An assessment of RNA concentration was carried out as described in **Section 2.4.12**, with test samples immediately frozen at -80°C and stored for up to one year.

To ensure no contaminating DNA was amplified with RNA during the RT-PCR reaction, samples were treated with a DNase I (Amplification Grade) treatment kit (Life Technologies Ltd., Paisley, UK, # 18068-015) as per manufacturer's instructions. Briefly, samples containing or lacking reverse transcriptase were prepared on ice, in sterile, nuclease-free microcentrifuge tubes to provide a positive and negative sample for reverse transcriptase treatment. For each reaction, RNA sample (1 µg/µl), 10X DNase I Reaction Buffer (1 µl), DNase I (1 µl = 1 unit), and diethylpyrocarbonate (DEPC) treated water (to 10 µl) (Ambion®, Life Technologies Ltd., Paisley, UK, # AM9916) was added, and incubated for 15 min at room temperature. DNase I was inactivated by the addition of 25 mM EDTA (1 µl), mixed gently, and heated at 65°C for 10 min.

Complimentary DNA (cDNA) was generated from DNase treated mRNA using SuperScript™ II Reverse Transcriptase (Life Technologies Ltd., Paisley, UK, # 18064-014), 100 ng mRNA sample (1 µl DNase treated sample), and 50 ng random primer (Promega, Southampton, UK, # C1181). To a nuclease-free microcentrifuge tube, 50 ng random primer (1 µl), 100 ng mRNA (1 µl), 10 mM dNTP mix (1 µl), and DEPC treated water (to 12 µl) was added, mixed, and heated at 65°C for 5 min, before transfer to ice for 2 min. The samples were then centrifuged briefly in a benchtop centrifuge before addition of 5X first-strand

buffer (4 μl) and RNaseOUT™ (1 μl = 40 units), mixed gently and incubated at room temperature for 2 min. To generate single stranded cDNA, SuperScript™ II (1 μl = 200 units), or for minus RT treated samples, 1 μl DEPC treated water was added, and mixed by pipetting gently before incubation at room temperature for 10 min. The reaction was then carried out in a temperature-controlled waterbath at 42°C for 50 min prior to enzyme inactivation by heating at 70°C for 15 min.

The RT-PCR reaction was carried out using GoTaq® DNA polymerase assay kit (Promega, Southampton, UK, # M3005). To a sterile, nuclease-free, thermostable microcentrifuge tube, 5X Green GoTaq® Reaction Buffer (containing blue and yellow dye for gel electrophoresis) (10 μl), 10 mM dNTP mix (1 μl), 10 μM human GPR35 forward (5' GATCAAGCTGGGCTTCTACG 3') and reverse primers (5' CAGGCTGATGCTCATGTACC 3') (0.5 μl), GoTaq® DNA polymerase (0.25 μl = 1 unit), template cDNA (1 μl single stranded cDNA = 5 ng), and DEPC-treated water (to 50 μl) was added, on ice. Tubes were centrifuged briefly (30 sec), vortexed gently, and placed immediately into a MultiGene™ Gradient Thermal Cycler containing a heated lid (Multigene-Labnet International Inc., Edison, NJ). The RT-PCR reaction was carried out in the following steps: preheat 95°C, 2 min; denature, 95°C, 30 sec; anneal, 56°C, 30 min; extend, 72°C, 30 sec (1 min/ kb); repeated for 30-35 cycles and terminated with a final extension at 72°C for 5 min, followed by an indefinite soak at 4°C.

2.4.7 *DNA gel electrophoresis*

To determine gene expression in native and overexpressing cell lines, mRNA was isolated, cDNA prepared, and RT-PCR carried out as described in **Section 2.4.6**. Since the amplified RT-PCR fragments were between 200 to 250 bp in length, a 2 % (w/v) agarose gel was prepared by adding 1 g multi-purpose agarose (Roche, Applied Science, Penzberg, Germany, # 11388991001) to 50 mL 1X Tris/Borate/EDTA (TBE) buffer in a 500 mL PYREX Erlenmeyer flask. 1X TBE was diluted from a 10X TBE stock, stored at room temperature [tris base (1M), boric acid, anhydrous, (0.9 M), $Na_2EDTA \bullet 2H_2O$ (10 mM), Milli-Q dH_20 to 1 liter, final pH 8.3]. To dissolve, the mixture was heated in a microwave for 30 sec, swirled, and this process continued for approximately 2 min until the solution was homogenous. The solution was cooled to 50°C in a temperature-controlled incubator before SYBR® Safe DNA

gel stain (Life Technologies Ltd., Paisley, UK, # S33102) was added (10,000 x concentrated stock, 1 μl per 10 mL) and swirled gently to mix. The agarose was the poured carefully into the centre of a UVT (ultra violet transmissible) tray sealed with dams at either end, placed within a horizontal HORIZON® gel tank (Life Technologies Ltd., Paisley, UK, # 11.14 (medium) or # 58 (small)) containing a 1 mm thick DELRIN® comb with the desired well size.

Once the agarose gel had set, the dams were removed and TBE buffer was added to fill the tank, covering the gel to a depth of 1 to 2 mm, before the comb was removed and samples added. A 50 bp ladder, DNA Molecular Weight Marker XIII (Roche Applied Science, Penzberg, Germany # 11721925001) was added (1 μg) to 5X DNA gel loading buffer and loaded into the first well. Since the Go-Taq™ buffer contained a blue yellow dye, the RT-PCR samples were loaded directly into the bottom of each well in a volume dependent upon the size of the comb used to set the gel. The safety lock lid containing power cables was secured over the gel tank, which was connected to a 250 volts DC power supply. Electric current was provided until the yellow dye-front, which ran ahead of the sample, had reached ¾ length of the tank. The electric current was then switched off before the UVT tray containing the gel removed, excess TBE buffer drained, and DNA fragments visualised under ultraviolet light using a Gel Doc UV transilluminator (Bio-Rad Laboratories Inc., Hercules, CA, # 2000) fitted with Quantity One software to document and quantitate each gel.

2.4.8 *In vitro site-directed mutagenesis*

Site directed mutagenesis was carried out to alter wild type sequence of human or rat *GPR35* by point mutation, amino acid substitution, deletion or addition. Oligonucleotide primer sequences were designed using the online software programme PrimerX (http://www.bioinformatics.org/primerx), and were between 21-25 bases in length, with a GC content below 60 % (when possible), and a T_m of approximately 80°C. Primer self-complimentary and primer dimer formation was assessed using the online software programme (http://www.biocompute.bmi.ac.cn/CZlab/MFEprimer-2.0/index.cgi/check_dimer). Primer sequences were synthesised via the custom DNA de-salted oligonucleotide facility provided by Thermo-Fischer Scientific (Leicestershire, UK),

with dried primer sequences reconstituted in sterile Milli-Q dH_2O to 100 μM and working stock aliquots (10 μM) diluted in sterile Milli-Q dH_2O and stored at -20°C.

Site directed mutagenesis was carried out using the QuickChange® method as per manufacturer's instructions (Stratgene, La Jolla, CA, # 200518). Mutations were induced by thermo cycling using *Pfu* DNA polymerase isolated from *Pyrococcus furiosus* (Promega, Southampton, UK, # M774A), pcDNA™3.1 vectors containing *FLAG-hGPR35-eYFP* or *FLAG-rGPR35-eYFP* DNA constructs, and the oligonucleotide primers containing the mutations of interest. A master mix, prepared on ice using a sterile nuclease-free PCR microcentrifuge tube, contained deoxynucleotide triphosphates (dNTPs) dATP, dTTP, dCTP, dGTP (Promega, Southampton, UK, # U120A, U123A, U122A, U121A, respectively) diluted to 10 μM final concentration; *Pfu* DNA polymerase reaction buffer containing $MgSO_4$ (10x stock, 5 μl addition/reaction) (Promega, Southampton, UK, # M776A); DMSO to reduce formation of secondary structure (2 μl/reaction); and *Pfu* DNA 5'→3' polymerase (1.25 units/reaction) (Promega, Southampton, UK, # M7741), which was added last. All reagents were added to sterile ice-cold Milli-Q dH_2O to generate an individual reaction volume of 50 μl. Template DNA (50 ng/μl), forward and reverse single strand DNA oligonucleotide primers (1 μl/reaction; 200 ng final) were added individually to pre-chilled PCR tubes, on ice, before the addition of master mix. Tubes were centrifuged briefly (30 sec), vortexed gently, and placed immediately into a MultiGene™ Gradient Thermal Cycler containing a heated lid (Multigene-Labnet International Inc., Edison, NJ). The site-directed PCR reaction was carried out in the following stages: preheat, 95°C, 5 min; denature, 95°C, 1 min; anneal, 58°C, 1 min; extend, 72°C, 15 min (2 min/kb of template); repeated for 18 cycles, terminated with a final extension at 72°C for 10 min, and followed by an indefinite soak at 4°C.

Parental DNA, methylated or hemimethylated by Dam^+ XL1-Blue methylases during propagation, was digested by the endonuclease activity of *DpnI*, which digested 5'G^{me}ATC-3' sequences to leave only newly synthesised, mutant, DNA. The reaction was carried out by addition of 1 unit (1 μl) *DpnI* endonuclease (Promega, Southampton, UK, # R6231) to each individual PCR reaction tube. Tubes were gently vortexed and incubated for 6-8 h in a 37°C incubator. After this stage, *DpnI* digested PCR reactions (1 μl) were transformed immediately into XL1 Blue as described in **Section 2.4.10**.

2.4.9 *PCR cloning and DNA Ligation using T4 DNA Ligase*

To clone by PCR, the following was assembled on ice in a sterile nuclease-free PCR microcentrifuge tube: *Pfu* DNA polymerase reaction buffer containing $MgSO_4$ (10x stock, 5 μl addition/reaction) (Promega, Southampton, UK, # M776A), *Pfu* DNA 5'→3' polymerase (1.25 units/reaction) (Promega, Southampton, UK, # M7741), 10 mM dNTP mix (200 μM final concentration), oligonucleotide primers (200 ng final concentration), template cDNA (100 ng), and dH_2O to 50 μl. The PCR reaction was carried out using a MultiGene™ Gradient Thermal Cycler with a heated lid (Multigene-Labnet International Inc., Edison, NJ) as follows: preheat 95°C, 5 min; denature, 95°C, 30 sec; anneal, 55°C, 30 sec; extend, 72°C, 2 min (2 min/ kb); repeated for 30 cycles and terminated with a final extension at 72°C for 10 min, followed by an indefinite soak at 4°C.

To confirm that sufficient amplification of the PCR product had taken place, a 1 % (w/v) analytical agarose gel was generated, (as described in **Section 2.4.7**) by adding 0.3 g multi-purpose agarose to 30 mL TBE. Before restriction digests were initiated, a PCR clean-up step was performed to remove PCR buffers and enzyme using the QIAquick PCR purification kit (QIAGEN, Manchester, UK, # 28106) according to the manufacturer's instructions. To digest, *KpnI*-KOZAK-FLAG-human GPR35a-*EcoRV* (2 μg) was incubated with 1 μl *EcoRV-HF®* (NEB, # R3101S) and 1 μl *KpnI-HF®* (NEB, # R3142S) with CutSmart™ buffer (10X; # B7204S); *EcoRV*-Gα_{13EE}-*NotI* (2 μg) was digested with 1 μl *EcoRV-HF®* and 1 μl *NotI-HF®* (NEB, # R3189S) with CutSmart™ buffer; while pcDNA5™/FRT/TO plasmid was digested using the *KpnI-HF®* and *NotI-HF®* enzymes (1 μl each) with the CutSmart™ buffer. All samples were incubated at 37°C for six hours in a 50 μl volume.

Once digested, each sample was loaded and run on a 1 % (w/v) agarose gel to separate the digested vector from its insert (performed as described in **Section 2.4.7**). To isolate DNA from the agarose, the QIAGEN QIAquick Gel Extraction kit (# 28706) was employed and used as per manufacturer's instructions. To determine the relative concentration of each fragment, a second 1 % (w/v) agarose gel was set up and loaded using 4 μl DNA and 1 μl 5X dye alongside a 1 kb HyperLadder™ molecular weight marker (BIOLINE, London, UK, # BIO-33053). Comparison of the intensity between sample and the

HyperLadder™ under UV light enabled an approximation of the DNA concentration of each sample, which was used to set up the DNA ligation reaction.

Ligation of the *KpnI*-FLAG-GPR35a and pcDNA™5/FRT/TO was carried out in a 1:4 ratio. The reaction was compiled as follows: 50 ng vector, approximately 30 ng insert (depending on the sample), ligase 10X buffer (2 μl) (Promega, Southampton, UK, # C126A), T4 DNA ligase (Promega, Southampton, UK, # M180A), final volume 20 μl, with the reaction incubated overnight at 16°C. Next, the *KpnI*-FLAG-GPR35a-pcDNA™5/FRT/TO plasmid was digested with *EcoRV* and *NotI* and ligated in a 4:1 ratio as for the previous reaction to insert *EcoRV*-Gα_{13EE}-*NotI*. Following ligation, the fusion construct was transformed according to **Section 2.4.10**; DNA isolated using the SV Wizard miniprep system (**Section 2.4.11**); DNA quantified (**Section 2.4.12**); sent for sequencing (**Section 2.4.13**); and stably transfected into an inducible Flp-In™ T-REx™ HEK293 cell line as described in **Section 2.5.5**.

2.4.10 *Transformation of XL-1 Blue by heat-shock method*

Chemically competent *Escherichia coli* laboratory strain XL-1 Blue prepared as described in **Section 2.4.2** were defrosted on ice. Using sterile technique, DNA (between 1-10 ng or 1 μl of restriction digested PCR sample), and XL-1 Blue (50 μl/tube) were added to a pre-chilled sterile microcentrifuge tube and incubated for 20 min on ice. Samples were carefully placed in a floating foam tube rack and heat-shocked at 42°C for 90 sec, then immediately transferred to ice and cooled for 2 min. After addition of 450 μl LB-Amp using sterile technique, samples were incubated at 37°C for 1 h at 250 RPM to induce *Bla* gene expression. This confers ampicillin resistance to XL-1 Blue cells successfully transformed with pcDNA™3.1 or pcDNA5/FRT/TO vectors. To isolate cells, samples were centrifuged at 5900 x *g* for 2 min. After removal of supernatant, the bacterial pellet was gently re-suspended by pipetting to a volume of 100 μl, added to a freshly prepared, pre-warmed LB-Amp plate and spread using an 70 % ethanol-flamed metal spreader using sterile technique. Dry plates were inverted and incubated for 12-16 h at 37°C in a bacterial-designated incubator.

2.4.11 *The Wizard® Plus SV Miniprep System for isolation of plasmid DNA from XL-1 Blue*

Plasmid DNA was isolated from 5 mL overnight cultures of *Escherichia coli* XL-1 Blue using the Wizard® *Plus* SV Miniprep DNA Purification System, as per the manufacturer's instructions (Promega, Southampton, UK # A1460). Bacterial cells were isolated by centrifugation at 3184 x *g* for 5 min at room temperature using a benchtop centrifuge. Supernatant was removed by pouring, and 30 mL Universal tubes were inverted on tissue paper to remove excess media. Cells were re-suspended via the addition of 250 μl Cell Suspension Solution [Tris-HCL (50 mM, pH 7.5), EDTA (10 mM), RNase A (100 μg/mL)], homogenised by pipetting, and vortexed briefly before transfer to a sterile 1.5 mL microcentrifuge tube. Post addition of 250 μl Cell Lysis Buffer, [NaOH (200 mM), sodium dodecyl sulphate (SDS; 1 % (w/v)] each tube was inverted four times and incubated for 4.5 min at room temperature. Cellular proteins were inactivated by the addition of Alkaline Protease Solution (10 μl) [isolated from *Bacillus licheniformis*], mixed by inversion four times and incubated for 5 min at room temperature. This reaction was deactivated by the addition of 350 μl Neutralisation Solution, [guanidine hydrochloride (409 mM), CH_3CO_2K (759 mM), glacial acetic acid (212 mM), pH 4.2] with each tube inverted four times and centrifuged to remove cellular debris (16,100 x *g*, 10 min, room temperature).

Cleared lysate (approximately 750 μl) was carefully transferred to a Spin Column inserted into a 2 mL Collection Tube and centrifuged at 14,000 x *g* for 1 min at room temperature. Column flow-through was discarded by pouring into a waste beaker and washed using 750 μl Column Wash Solution [CH_3CO_2K (162.8 mM), Tris-HCL (22.6 mM, pH 7.5), EDTA (0.190 mM, pH 8.0) ethanol (95 %, 60 % final (w/v)), pH 7.4] by centrifugation at 16,100 x *g* for 1 min at room temperature. This process was repeated, but with the second addition of Column Wash Solution at a volume of 250 μl. Each Spin Column was transferred to a sterile, 1.5 mL microcentrifuge tube, Nuclease-Free Water (100 μl) was added and plasmid DNA eluted by centrifugation at 16,100 x *g* for 1 min at room temperature. Isolated DNA concentration was assessed by UV spectrophotometry as described in **Section 2.4.12**.

2.4.12 *Quantification of nucleic acid purity by UV spectrophotometry*

Isolated DNA or RNA was assessed for concentration and purity by UV spectrophotometry using an Eppendorf® BioPhotometer, via the addition of 5 μl sample to 995 μl Milli-Q dH_2O. Assessment of absorbance/transmission of light through a quartz cuvette at the maximal UV absorbance wavelength for nucleic acid (260 nm) provided DNA concentration values. Quantification of the UV absorbance/transmission values maximally absorbed by protein (280 nm) in a ratio with nucleic acid absorbance, (A_{260}/A_{280}) generated an estimate of sample purity, with ratio between 1.8 and 2.0 indicative of highly pure nucleic acid. Before sample assessment the UV spectrophotometer was switched on for 10 min, and the machine blanked between reads using 1 mL Milli-Q dH_2O. The quartz cuvette was rinsed thoroughly with Milli-Q dH_2O and excess liquid removed with by inversion on tissue paper prior to analysis of each sample. Once nucleic acid concentration was recorded, DNA samples were stored at -20°C while RNA samples were transferred immediately to storage at -80°C.

2.4.13 *DNA sequencing*

DNA samples were diluted to a concentration of 500 ng/30 μl using sterile Milli-Q dH_2O, added to 1.5 mL microcentrifuge tubes and packaged in a padded envelope before being sent for DNA sequencing under standard postal conditions. Sequencing was carried out by DNA Sequencing and Services™ (Dundee University, Dundee, UK) using an automated ABI PRISM® capillary DNA sequencer (Applied Biosystems®, Life Technologies Ltd, Paisley, UK, # 3730), and Big-Dye® terminator cycle sequencing kit (Applied Biosystems®, Life Technologies Ltd, Paisley, # 3.1) to analyse fluorescently labelled DNA fragments by capillary electrophoresis. Forward sequencing reactions were primed using the CMV oligonucleotide sequence provided by DNA Sequencing and Services™, while the reverse eYFP oligonucleotide primer was designed in-house and provided at 3.2 pm/μl in sterile Milli-Q dH_2O in a volume of 10 μl. The presence of the desired sequence alteration from processed sequencing reactions was assessed using the online ClustalW2 software package

(http://www.ebi.ac.uk/Tools/msa/clustalw2), by aligning wild type sequences with analysed sequencing data.

2.4.14 *Isolation of plasmid DNA using the QIAfilter Plasmid Maxi kit from QIAGEN*

For DNA purification of plasmid DNA from *Escherichia coli* laboratory strain XL-1 Blue of up to 500 μg, the QIAfilter Plasmid Maxi kit (QIAGEN, Manchester, UK, #12165) was used, as per manufacturer's instructions. The QIAGEN method of plasmid DNA purification was carried out after isolation of a single colony grown overnight from LB Agar plates containing 100 μg/μl ampicillin. By use of sterile technique, an individual colony was inoculated into a 30 mL Universal containing 5 mL LB-Amp. This culture was incubated overnight (16 h) in an orbital incubator at 37°C, 250 RPM. To a sterile 1 L PYREX® Erlenmeyer flask containing 100 mL LB-Amp, 100 μl overnight starter culture was added, incubated overnight (16 h) at 37°C, 250 RPM in an orbital incubator. Bacterial cells were isolated by centrifugation at 6000 x *g* for 15 min in a pre-chilled ultracentrifuge with a Beckman™ rotor at 4°C.

Pellets were then re-suspended in 10 mL Buffer P1 [Tris-HCL (50 mM), EDTA (10 mM), RNase A, (100 μg/μl), pH 8.0]. Cell lysis was carried out by the addition of 10 mL Buffer P2 [NaOH (200 mM), SDS (1 % (w/v)] mixed by inversion four times, and incubated for 5 min at room temperature. SDS was neutralised by addition of CH_3CO_2K to form a KDS precipitate containing protein, phospholipid, chromosomal DNA, and cell debris, via addition of 10 mL pre-chilled Buffer P3 [CH_3CO_2K, (3 M) pH 5.5]. This was mixed by inversion four times, poured immediately into the barrel of a QIAfilter Cartridge, and incubated for 10 min at room temperature.

During this incubation time, a QIAGEN-tip coated with a DEAE (diethylaminoethyl) anion-exchange resin was calibrated by addition of 10 mL Buffer QBT [NaCl (750 mM), MOPS (50 mM), isopropanol (15 % (v/v)) pH 7.0], which travelled through the column by gravity flow. After 10 min, a plunger was inserted into the QIAfilter Cartridge and approximately 25 mL bacterial solution gently pushed through the QIAGEN-tip.

In order to remove any residual cellular protein, RNA or DNA contaminants, the QIAGEN-tip was rinsed twice using the medium-salt wash of 30 mL Buffer QC [NaCl (1 M), MOPS (50 mM), isopropanol (15 % (v/v)), pH 7.0]. Then, upon placing a 50 mL centrifuge

under the QUIAGEN-tip, plasmid DNA was eluted using a high-salt wash by addition of 15 mL Buffer QF [NaCl (1.25 M), Tris-HCL (50 mM), isopropanol (15 % (v/v)), pH 8.5].

To desalt and precipitate DNA 10.5 mL isopropanol was added, mixture vortexed and centrifuged at 5000 x *g* for 60 min at 4°C. Supernatant was carefully removed and clear pellets washed with 70 % ethanol, vortexed, and centrifuged at 3110 x *g*, 30 min, 4°C. Upon ethanol removal, the pellet was air-dried at room temperature for 30 min, re-dissolved in 500 µl sterile Milli-Q dH_2O, and transferred to sterile 1.5 mL microcentrifuge tube. DNA concentration was calculated by UV spectrophotometry as described in **Section 2.4.12**.

2.5 Mammalian Cell Culture

2.5.1 *Maintenance of cell culture*

Prior to use, all cell culture reagents were pre-warmed to 37°C by heating in a temperature-controlled waterbath for approximately 30 min. All cell cultures were maintained in vented cell culture treated $T75^2$ flasks with canted necks (Corning™, Tewksbury, MA, # 10-126-31) containing 10-15 mL medium with phenol red and heat inactivated foetal bovine serum (FBS) (GE Healthcare, Fairfield, CT, EU Approved, # A15-101). Cells were incubated a designated cell culture facility in an inCu saFe® SANYO humidified incubator supplied with 5 % CO_2 and maintained at 37°C. Media was replaced by aspiration under sterile conditions in a Faster UltraSafe class II laminar flow biosafety cabinet every two-to-four days.

2.5.2 *Cell lines and cell culture*

Adherent HEK293T cells constitutively expressing the large simian virus 40 large T antigen clone 17 were purchased from ATCC® (Middlesex, UK, # CRL-11268™) and were maintained in Dulbecco's modification of Eagle's medium (DMEM) (Sigma-Aldrich, Gillingham, UK # D5671) supplemented with 0.292 g/L L-glutamine (Sigma-Aldrich, Gillingham, UK, # G7513), 1X penicillin/streptomycin mixture (Sigma-Aldrich, Gillingham, UK, # PO781) and 10 % (v/v) FBS. HEK293T cells (passage 4-30) were supplemented with fresh

media every two days, passaged upon reaching 80 % confluence, and dissociated by use of 0.25 % trypsin•EDTA (Sigma-Aldrich, Gillingham, UK, # T4049).

Doxycycline inducible Flp-In™ T-REx™ HEK293 cells (Life Technologies Ltd, Paisley, UK, # R780-07) stably expressing human, mouse and rat GPR35 receptor constructs were created previously (see references detailed in **Table 2.1** for information). Stable cell lines (passage 2-25) were maintained in DMEM (Life Technologies Ltd, Paisley, UK, # 41965) containing 10 % (v/v) FBS, 15 μg/mL blasticidin (Life Technologies Ltd, Paisley, UK # A1113903) and 200 μg/mL hygromycin B (Roche Applied Science, Penzberg, Germany, # 10843555), passaged routinely at 85-90 % confluence, and dissociated by use of 0.25 % trypsin•EDTA.

Human colorectal adenocarcinoma cell line HT-29 was purchased from ATCC® (Middlesex, UK, # HTB-38™), maintained in McCoy's 5A (Modified) Medium (Life Technologies Ltd, Paisley, UK # 26600-023) supplemented with 10 % (v/v) FBS and 1X penicillin/streptomycin mixture. HT-29 cells were supplemented with fresh media every two days, and passaged at 70 % confluence. Due to strong adherence, HT-29 cells were first washed with sterile 1X PBS before addition of 0.25 % trypsin•EDTA and incubation for 5 min at 37°C + 5 % CO_2.

2.5.3 *Passaging of cells*

Upon reaching the desired confluence, medium was aspirated under sterile conditions inside a laminar flow cabinet by use of a Corning® 5 mL pipette connected to an exterior 5 liter plastic drum (containing 1 liter Rely+On™ Virkon® (DuPoint™, Wilmington, DE)) fitted with a KNF Neuberger VP Series vacuum pump. Unless otherwise described, pre-warmed 0.5 % trypsin•EDTA was added (3 mL per T75 cm^2 flask or 2 mL per 10 cm^2 dish) and evenly distributed to ensure coverage, before incubation at room temperature (between 30 sec – 5 min depending on adherence of the cell line). Flasks were tapped gently to ensure complete cell dissociation from the plasticware. Proteolytic cleavage was inhibited and cells re-suspended by addition of pre-warmed medium containing serum (typically 5 mL for T75 cm^2 flask and 10 cm^2 dishes) by use of a sterile 10 mL pipette, before transferring to a sterile 15 or 50 mL Corning® centrifuge tube. Cell pellets were isolated following centrifugation at

3110 x *g*, (5 min, room temperature) re-suspended in 1 mL medium using a Gilson pipette and sub-cultured at the desired density into fresh plasticware.

2.5.4 *Transient transfection*

One T75 cm^2 flask containing confluent HEK293T cells was split, as described in **Section 2.5.3**, and distributed (1:4) into a 10 cm^2 dish to a volume of 9 mL. Sixteen to 24 h later, at a minimum of 80 % confluence, cells were transfected by use of the cationic DNA complexing agent polyethyleneimine (PEI) (Polysciences Incorporated, Eppelheim, Germany, linear, mw 2500). In a category II laminar flow biosafety cabinet, under sterile conditions, two separate reaction mixtures were generated. The first contained DNA to a total of 5 μg and 250 μl NaCl (150 mM in Milli-Q dH_2O, sterilised, pH 7.4). The second was prepared by carrying out a 1:6 dilution of PEI (1 mg/mL) with NaCl (250 μl, 150 mM). The two mixtures were added together and vortexed for approximately 30 sec. Following a 10 min incubation at room temperature, the DNA/PEI mixture was added, drop-wise, to a freshly supplemented 10 cm^2 transfection dish containing 8 mL pre-warmed complete medium. Transfection plates were returned to the cell culture incubator and maintained for a minimum of 24 h before use. In every experimental system a control transfection was carried out via transfection of pcDNA™3.1 or pcDNA™5/FRT/TO as required.

2.5.5 *Generation of a Flp-In™ T-REx™ HEK293 stable cell line*

The Flp-In™ T-REx™ HEK293 cell line (Life Technologies Ltd; Paisley, UK, # R780-07) facilitates rapid and homologous expression of cDNA constructs when expressed from a Flp-In™ vector such as pcDNA™5/FRT/TO (Life Technologies Ltd; Paisley, UK, # V6520-20), which contains the hygromycin resistance gene and a flippase recognition target (FRT) site that enables selection of transformants that are inserted via DNA recombination by Flp recombinase at the FRT-site. The Flp recombinase is constitutively expressed from the pOG44 plasmid under control of the human CMV promoter. Prior to transfection, Flp-In™ T-REx™ HEK293 cells were maintained in DMEM (Life Technologies Ltd, Paisley, UK, # 41965) containing 10 % (v/v) FBS, 15 μg/mL blasticidin (Life Technologies Ltd, Paisley, UK # A1113903), (Roche Applied Science, Penzberg, Germany, # 10843555), Zeocin™ 100 μg/mL,

and 1X penicillin/streptomycin mixture (Sigma-Aldrich, Gillingham, UK, # PO781). Zeocin™ maintains selection of a stably inserted pFRT/lacZeo sequence that contains a lacZ-Zeocin™ fusion gene and an FRT site that serves as the binding and cleavage site for the Flp recombinase.

Two days prior to transfection Zeocin™ must be removed from the medium to allow recombination and stable insertion of the pcDNA™5/FRT/TO construct into the HEK293 genome at the FRT site. Insertion of pcDNA™5/FRT/TO at the pFRT/lacZeo site brings the SV40 promoter and the ATG initiation codon from pFRT/lacZeo into frame with the hygromycin resistance gene on the pcDNA™5/FRT/TO plasmid, which inactivates the lacZ-Zeocin™ gene and induces hygromycin resistance. To begin the stable insertion of FLAG-humanGPR35a-*EcoRV*-Gα_{13EE}, Flp-In™ T-REx™ HEK293 cells are subcultured as described (**Section 2.5.3**) into 10 cm^2 plates. Upon reaching 80 % confluence, the pOG44 plasmid and the pcDNA™5/FRT/TO vector containing FLAG-humanGPR35a-*EcoRV*-Gα_{13EE} were transiently cotransfected in a 4:1 ratio using PEI (as described, **Section 2.5.4**). Twenty-four hours after transfection the cells were subcultured in 1:10, 1:5, 1:3 ratios to ensure that the cell confluence would be low enough to allow hygromycin to kill the non-transfected cells. Twenty-four hours later, the media containing 200 μg/mL hygromycin B was added and replaced every three-to-four days to remove dying cells. Once cell death was complete, resistant colonies were identified and sub-cultured together to generate a homologously expressing FLAG-humanGPR35a-*EcoRV*-Gα_{13EE} cell line. To determine the concentration of doxycycline required to induce maximal expression of the FLAG-humanGPR35a-*EcoRV*-Gα_{13EE} construct, unlike with previous GPR35 stable cell lines that were tagged with eYFP and doxycycline concentration determined by quantifying maximal eYFP expression, the FLAG-humanGPR35a-*EcoRV*-Gα_{13EE} construct expression was assessed via Western blot (**Section 2.6.4**) using an M2 anti-FLAG® antibody (Sigma-Aldrich, Gillingham, UK, # F1804) following overnight expression with various concentrations of doxycycline. A concentration of 100 ng/mL was employed for all experiments described herein.

2.6 Biochemical assays and procedures

2.6.1 Cell harvesting

Twenty-four h post transfection or doxycycline induction, cells were harvested by aspiration of medium and replacement with 10 mL ice-cold sterile PBS (1X). On ice, cells were dislodged from plasticware by scraping. Cell suspensions were added to ice-cold 50 mL Corning® tubes and pellets isolated by centrifugation (3110 x *g*, 5 min, 4°C). Following re-suspension of cell pellets in 1 mL ice-cold PBS on ice, a further 9 mL PBS was added, cells were vortexed briefly and re-centrifuged as before. This process was repeated once more, before all supernatant was aspirated and cells transported on ice to storage at -80°C.

2.6.2 Isolation of cellular lysates

Cells were harvested as described in **Section 2.6.1**. Isolated cell pellets were re-suspended in 500 μl 1x radioimmunoprecipitation (RIPA) buffer, which was diluted from a 2X RIPA stock (HEPES (10 mM), NaCl (300 mM), Triton X-100 (2 % (v/v)), sodium deoxycholate (1 % (w/v)), SDS (0.2 % (w/v)), pH 7.4) on the day of use, and supplemented with sodium fluoride (0.5 M), EDTA (0.5 M), $NaPO_4$ (0.2 M), ethylene glycol (5 % (v/v)), and 1 EDTA-free cOmplete™ protease cocktail inhibitor tablet per 50 mL buffer (Roche Applied Science, Penzberg, Germany, # 11873580001). Lysates were placed within a rotating wheel and rotated for 1 h at 4°C, before centrifugation at 14,000 x *g* at 4°C for 30 min to pellet cellular debris. Supernatants were isolated, and protein concentration quantified by the bicinchonic acid method as described in **Section 2.6.6**. Samples were then frozen at -20°C until required.

2.6.3 Sodium dodecyl sulphate polyacrylamide gel electrophoresis (SDS-PAGE)

Using the property of electrophoretic mobility, whole cell lysates were separated by SDS-PAGE and used in conjunction with Western blotting to identify and resolve protein samples of interest. Pre-cast NuPAGE® Novex® 4-12 % Bis-Tris protein gels (1 mm, 10 well)

(Life Technologies Ltd, Paisley, UK # NP0321BOX), stored at 4°C were removed from the plastic casing, the well separator removed, rinsed with Milli-Q dH_2O and inserted into a XCell SureLock™ mini-cell electrophoresis gel tank system (Life Technologies Ltd., Paisley, UK, # EI0001). If only one pre-cast gel was to be used, then an empty cassette was inserted into the other side of the gel tank, with wells facing inward, and the gel tension wedge locked. Prior to use, NuPAGE® Novex® MOPS SDS running buffer (20X) (Life Technologies Ltd., Paisley, UK, # NP0001) was diluted in Milli-Q dH_2O and poured into the buffer core. Once it was ensured that there was no leak, the outside of the gel tank was filled to a suitable level and samples loaded.

Cell lysates were defrosted on ice, and diluted to the required concentration before warmed 2X concentrated Laemmli buffer [SDS (4 % (v/v)), glycerol (20 % (v/v)), 2-mercaptoethanol (10 % (v/v)), bromophenol blue (0.0004 % (v/v)), Tris-HCL (0.125 M), pH 6.8] was added to each sample. To allow estimation of protein size, a pre-stained full range molecular weight Rainbow™ marker was added (10 μl) (GE Healthcare, Buckinghamshire, UK, # RPN800E) to the first well, followed by each sample to be analysed. Any empty wells were filled via the addition of 1X Laemmli buffer. Before the gel tank lid was replaced, MOPS buffer was added to top-up the buffer core. An electrophoresis current at 200 volts DC was applied until the dye front reached the base of the gel.

2.6.4 *Western blot*

Following separation of cellular proteins using SDS-PAGE, samples were transferred from the Bis-Tris gel to a nitrocellulose blotting membrane (Amersham Protran 0.45 NC, GE Healthcare, Buckinghamshire, UK), using an XCell II™ Blot module (Life Technologies Ltd., Paisley, UK, # EI9051). The nitrocellulose membrane and sponges were soaked in 1X transfer buffer [glycine (0.2 M), Tris (25 mM), methanol (20 % (v/v))], before being placed with the Bis-Tris gel into the XCell II™ blot module. The cassette was locked in place and the gel tank filled with 1X transfer buffer. A fixed voltage of 30 volts was applied for 90 min to allow protein transfer to take place. Transfer of the molecular marker usually represented complete protein transfer from the gel to the membrane. To block non-specific binding, the membrane was incubated in PBST [PBS containing Tween-20 (0.1 % (v/v))] containing Marvel skimmed powdered milk (5 % (w/v)), at room temperature for 60 min on a benchtop shaker.

Primary antibody was incubated overnight at 4°C in TBST containing 5 % (w/v) low-fat milk, on a benchtop shaker. Following a minimum incubation of 16 h, primary antibody was removed and the membrane washed four times for 5 min in PBST under gentle agitation at room temperature. Horseradish peroxidase (HRP) conjugated secondary antibody, diluted in PBST containing 5 % (w/v) low-fat milk was added to the membrane and incubated at room temperature for 60 min under gentile agitation. Antibodies used herein were the monoclonal anti-FLAG® M2 antibody (Sigma-Aldrich, Gillingham, UK, # F1084), and monoclonal anti-$G\alpha_{13EE}$ (raised in-house), which were detected with anti-mouse IgG secondary antibody conjugated to HRP (Cell Signalling, Danvers, MA, # 7076). Sheep anti-GFP polyclonal antibody was synthesised in-house and detected using a HRP conjugated anti-goat IgG secondary antibody (GE Healthcare, Buckinghamshire, UK, # 45001213).

Post removal of the secondary antibody, the membrane was washed four times for 5 min using PBST under gentle agitation at room temperature. Excess liquid was removed by blotting on tissue paper and the membrane placed on Saran wrap to which a working solution of Enhanced Chemiluminescent (ECL) HRP substrate was added by mixing a 1:1 ratio of Enhanced Luminol Reagent and Oxidising Reagent, components of the SuperSignal™ West Pico Chemiluminescent Substrate kit (Thermo Fisher Scientific, Waltham, MA, # PI-34078). Luminol was oxidised by the HRP-conjugated secondary antibody and thus light emitted was directly proportional to the amount of protein bound to the nitrocellulose membrane. Using the SuperSingal™ kit, this signal was stable for 6-8 h. Once the membrane was coated for approximately 5 min, excess ECL reagent was removed and the membrane placed within a plastic coating inside a developing cassette. All air pockets were smoothed out and the plastic coating taped in place. Once inside a dark room, under red light, a sheet of Carestream® KODAK® BioMax® Light film was placed inside the developing cassette, removed after the desired exposure time and processed through a KODAK® X-OMAT® Film Developer.

2.6.5 *Isolation of cellular membranes*

Cell culture pellets, previously washed three times in 1X PBS and frozen at -80°C, were defrosted on ice. Defrosted cell pellets were re-suspended in membrane buffer first by

passing through a 19-gauge needle (BD Microlance™) fitted to a sterile syringe (BD Plastipack™), followed by passing through a 25-gauge sterile needle (BD Microlance™). The membrane buffer consisted of ice-cold 1X Tris-EDTA (pH 8.0) and protease inhibitor cocktail (1X cOmplete EDTA-free tablet per 50 mL buffer). Dependent upon the volume of the membrane preparation, either the cell suspension was passed manually 50 times through a Teflon-in-glass homogeniser, or sheered mechanically (while on ice) using an electronic Janke and Kunkel Ultra T45 Turax® homogeniser for approximately 2 min.

Unbroken cells, nuclei and larger organelles were removed by centrifugation at 3110 x *g*, 5 min, 4°C followed by the careful removal of supernatant and addition to an ultracentrifuge tube (Beckman Coulter, Palo Alto, CA). Each tube weight was normalised using a Satorius fine balance to three decimal places by the addition of membrane buffer prior to being secured in an evenly balanced Optima TLX Ultracentrifuge rotor (Beckam Coulter, Palo Alto, CA). Post ultracentrifugation at 20,000 x *g* for 1 h at 4°C, the isolated pellet was re-suspended in Tris-EDTA membrane buffer, passed 10 times through a 19-gauge needle and 10 times through a 25-gauge needle on ice, until homogeneous. Generally pellets were re-suspended in a volume of 500 μl membrane buffer (for 10 cm^2 dish isolations) prior to an estimation of protein concentration via the bicinchoninic acid method (**Section 2.6.6**). Unless otherwise stated, each sample was diluted to a concentration of 1 mg/mL stock concentration and added to a pre-chilled sterile 1.5 mL microcentrifuge tube in 250 μl volume aliquots for storage at -80°C for up to six months.

2.6.6 *Estimation of protein concentration by the bicinchoninic acid method*

The bicinchoninic acid (BCA) method utilised two chemical reactions (the reduction of cupric ions by peptide bonds in alkaline solution and chelation of the resulting cuprous ions by BCA reagent) in order to estimate protein concentration. First, bovine serum albumin standards at set concentrations (0.2, 0.4, 0.6, 0.8, 1.0, 1.2, 1.4, 1.6, 1.8, 2.0, and 2.2 mg/mL, diluted in Milli-Q dH_2O, and stored at 4°C) were added to a clear 96 well, non-sterile, flat bottom polystyrene plate in triplicate (10 μl volume) (Sigma-Aldrich, Gillingham, UK, # M2186), followed by addition of test sample (10 μl) in triplicate. Secondly, BCA reagent (Sigma-Aldrich, Gillingham, UK, # B9643) in a 50:1 ratio with copper sulphate was vortexed

briefly and immediately added (200 μl) using an Eppendorf Repeater® manual handheld dispenser (Eppendorf, Hauppauge, NY, # 022260201) to each sample. Test plate was covered using a disposable plate seal (Perkin-Elmer, Norwalk, CT, TopSeal™ # 6050195) and incubated at 37°C for 10 min. Absorbance values generated at 560 nm for each BSA standard were determined using a POLARstar Omega microplate reader (BMG Labtech, Ortenberg, Germany) and used to plot a standard curve. By linear regression analysis the protein concentration of each test sample could be calculated and diluted accordingly prior to storage at -80°C.

2.6.7 *[^{35}S]GTPγS filtration binding assay*

HEK293T cells transiently co-transfected with FLAG-GPR35-eYFP-pcDNA3.1 and a $G\alpha_{i/o}$ construct containing the cysteine 351 isoleucine modification to render insensitivity to Pertussis toxin treatment as per instructions detailed in **Section 2.5.4**. Twenty-four h after transfection cells were treated with *Bordella pertussis* toxin (PTX; 100 ng/mL) and incubated overnight in a humidified cell culture incubator (37°C + 5 % CO_2). Cells were then harvested and membranes prepared as described in **Section 2.6.1** and **Section 2.6.5**, respectively. To glass test tubes, ligand, prepared in GTPγS Filtration buffer [HEPES, (20 mM), NaCl (100 mM), $MgCl_2$ (6 mM), BSA (0.1% (w/v)), pH 7.4], was added to 1 mL GTPγS Filtration buffer, 10 μg/tube cellular membrane, 10 μM GDP, 0.1 nM [^{35}S]GTPγS and incubated for 1 h at 25°C in a temperature-controlled waterbath covered with foil to minimise evaporation.

The [^{35}S]GTPγS reaction was terminated by rapid filtration through GF/C filters (Brandel, Brandel, Gaithersburg, MA, # 800-948-6506) pre-soaked in ice-cold 1X PBS using a cell harvester (Brandel, Gaithersburg, MA) and washed three times before being air-dried. Filter areas containing test sample were isolated using and placed into a plastic scintillation tube. Ultima Gold™ XR scintillation cocktail (Perkin-Elmer, Norwalk, CT) was added at 3 mL/vial and tubes vortexed before being placed in a Tri-Carb® liquid scintillation counter to quantify [^{35}S] DPM following a 5 min quantification time.

2.6.8 *Mammalian $G\alpha_{13}$ [^{35}S]GTPγ[S] (guanosine 5'-[γ-[^{35}S]thio]triphosphate)-binding assay*

To detect G protein activation via the $G\alpha_{13}$ pathway, Flp-In™ T-REx™ HEK293 cells were transiently transfected with an internal 'EE' (EYMPME) epitope-tagged $G\alpha_{13EE}$ construct as described in **Section 2.5.4**. As a modification to standard [^{35}S]GTPγS binding assay, $G\alpha_{13EE}$ incorporation was isolated using an immunoprecipitation step (Jenkins et al., 2010). To a Fisherband glass test tube (Fisher Scientific, Loughborough, UK, # 14-961-26) test compound, prepared at 5x final assay concentration in GTPγS assay buffer [HEPES (20 mM), $MgCl_2$ (3 mM), NaCl (100 mM), GDP (1 μM), ascorbic acid (0.2 mM), pH 7.4] was added to GTPγS assay buffer (300 μl), and 50 nCi [^{35}S]GTPγS (Perkin-Elmer, Norwalk, CT, # NEG030X) followed by isolated cellular membrane (25 μg/point), prepared as described in **Section 2.6.1**. All tubes were placed in a plastic tube rack in a temperature-controlled waterbath at 25°C for 1 h, covered with foil to minimise evaporation, before the reaction was terminated by addition of 500 μl ice-cold GTPγS assay buffer containing an EDTA-free cOmplete protease inhibitor cocktail.

Following centrifugation at 16,100 x *g* for 10 min at 4°C, resulting pellets were re-suspended in Solubilisation buffer [Tris (100 mM), NaCl (200 mM), EDTA (1 mM), Nonidet P-40 (1.25 % (v/v)), SDS (0.2 % (w/v)), pH 7.4] before pre-clearance using 60 μl PANSORBIN® cells (Merck Millipore, Hertfordshire, UK, # 507858) in Bead Buffer [BSA (2% (w/v)), sodium azide (0.1 % (w/v)), pH 7.4] for 60 min at 4°C in a rotating incubator. To remove cellular pellets, samples were centrifuged at 16,100 x *g* for 10 min at 4°C. Immunoprecipitation was carried out on isolated supernatant via the addition of 50 μl Protein G Sepharose 4 Fast Flow beads (GE Healthcare, Buckinghamshire, UK, # 17-0618-05) supplemented with mouse anti-$G\alpha_{13EE}$ anti-sera (at a 1:1000 dilution), and rotated for a further 60 min at 4°C. To isolate the enriched [^{35}S]GTPγS samples, beads were pelleted by centrifugation at 16,100 x *g* for 5 min at 4°C, and washed with four times with 500 μl ice-cold solubilisation buffer. Following the final centrifugation step, pellets were dissolved in 1 mL Ultima Gold™ XR scintillation cocktail (Perkin-Elmer, Norwalk, CT), which was added to each microcentrifuge tube, vortexed and placed within a Tri-Carb® liquid scintillation counter (Perkin-Elmer, Norwalk, CT, # 2910TR) to quantify [^{35}S] disintegrations per minute (DPM) following a 5 min read-time.

2.7 Cell based assays

2.7.1 The S. cerevisiae Yeast Assay using chimeric G protein

Haploid MAT**a** *S. cerevisiae* strain W303-1A stably expressing chimeric Gpa1-Gα_x subunits at the *TRP1* locus were generated by GlaxoSmithKline, as described (Dowell and Brown, 2009). To assess functional coupling between agonist induced receptor activation and functional response, the pheromone response pathway of *S. cerevisiae* was manipulated by removal of *FAR1* to prevent cell cycle arrest, forcing pathway responses toward the mating pathway through activation of the *FUS1* promoter. Subsequent activation of *FUS1-lacZ* produced reporter-gene readout, measurable through β-galactosidase activity.

An individual colony from a freshly transfected *S. cerevisiae* strain transiently expressing FLAG-GPCR-p426GPD and stably expressing Gpa1-Gα_x subunit was isolated from agar containing selective media (SD –Ura –Met) and inoculated into a 30 mL Universal containing 5 mL SD –Ura –Met. Following an overnight incubation at 30°C at 220 RPM, saturated yeast cultures were diluted 1/1000 to generate an approximate optical density of 0.0025/mL in Assay Medium. Assay Medium was generated per 100 mL as follows:

- SD growth medium without Ura or His (75 mL) : Kasier Synthetic Drop-out Mix (1.85 %), 40 % D-glucose (50 mL), 10X Yeast Nitrogen Base (100 mL), pH 7.0, autoclaved;
- 10x BU Salts (10 mL): $Na_2HPO_4.7H_2O$ (70 %), NaH_2PO_4 (30 %), pH7.0, 0.2 μm filter sterilised;
- 10x Yeast Nitrogen Base, (10 mL), 0.2 μm filter sterilised;
- 40 % D-glucose, (5 mL), 0.2 μm filter sterilised;
- 3-amino-1,2,4-triazole (3-AT) (200 μl) (Sigma-Aldrich, Gillingham, UK, # A8056), made fresh in sterile Milli-Q dH_2O, 0.2 μm filter sterilised, and protected from light;
- Fluorescein Di-β-D-Galactopyranoside (FDG), (50 μl) (Molecular Probes®, Life Technologies Ltd., Paisley, UK, # F-1179), reconstituted in sterile Milli-Q dH_2O to 20 mM, protected from light

Reconstituted yeast cells were distributed into sterile 96 well deep block plates and thoroughly re-suspended before addition to assay plate. Ligand, prepared at 10x final assay concentration, was diluted in Assay Medium with DMSO concentration (below 1 %)

normalised throughout. Using sterile technique, 11 μl test compound was added to black solid bottomed 96 well plates (Greiner® Bio One International AG, Kremsmuenster, Austria) using a multichannel pipette. Yeast culture was subsequently added (100 μl/well) and plates incubated at 30°C overnight in a designated yeast incubator, without agitation.

Following a 16 h incubation, fluorescence, occurring upon sequential hydrolysis of FDG to fluorescein monogalactosidase and fluorescein by β-galactosidase, was gain adjusted using the well with the highest treatment of ligand concentration, and subsequently quantified using a top reading function using a 2x2 grid with an excitation of 490 nm and an emission of 514 nm using a PHERAstar *FS* plate reader (BMG Labtech, Durham, NC). Emission at 514 nm, reported as arbitrary fluorescence units (AFU), was used to plot concentration response curves.

2.7.2 *Inositol Phosphate (IP-One) accumulation assay using chimeric Gα protein subunits*

In order investigate G protein signalling, GPR35 was coupled through the $G\alpha_{q/11}$ pathway and agonist induced response quantified using the IP-One HTRF® Tb assay, according to manufacturer's instructions (Cisbio Assays, Codolet, France # 62IPAPEC). IP-One, a competitive immunoassay, used HTRF (homogeneous time resolved fluorescence resonance energy transfer) between a (donor) terbium cryptate labelled monoclonal anti myo-inositol 1 phosphate (IP_1) antibody and d2 (acceptor dye) labelled IP_1. To begin, HEK293T cells were transiently transfected under sterile conditions as described in (**Section 2.5.3**).

Post 24 h incubation HEK293T cells transfected with 2.5 μg FLAG-GPR35-eYFP-pcDNA3.1 and 2.5 μg G protein chimera ($G\alpha_{qi1/2}$ or $G\alpha_{q13}$) were visually assessed by microscopic analysis using a Nikon inverted microscope to confirm cell surface receptor-eYFP expression. Under sterile conditions, in a category II laminar flow biosafety cabinet, medium was aspirated from each $10cm^2$ dish and mechanically dislodged by pipetting. Following centrifugation, isolated cell pellet was re-suspended in 1 mL sterile PBS (1X) and re-centrifuged at 3110 x *g*, 5 min at room temperature. Upon aspiration of supernatant, cells were re-suspended in 1 mL IP-One Stimulation Buffer [HEPES (10 mM), $CaCl_2$ (1 mM), $MgCl_2$ (0.5 mM), KCL (4.2 mM), NaCl (146 mM), D-glucose (5.5 mM), LiCl (50 mM), pH 7.4], which was either commercially supplied or generated in-house. To reduce constitutive activity,

some assays were carried out where the cells had not been prepared in buffer containing LiCl (indicated in the text). To ensure that the concentration of LiCl was kept constant with the cells that were prepared in LiCl-containing buffer, twice the final assay concentration of LiCl was added to the ligand preparation. This ensured that the final LiCl concentration was kept at 50 mM in assays with cells re-suspended in stimulation buffer with or without LiCl.

Cell number was quantified via the addition of trypan blue (10 μl) to cell suspension (10 μl), using a plastic chamber and a Countess™ automated cell counter (Life Technologies Ltd, Paisley, UK). The concentration of cells was adjusted to 10,000 cells/7 μl in IP-One Stimulation Buffer. Agonist, prepared fresh on the day of assay, was diluted to twice the final assay concentration in IP-One Stimulation Buffer, DMSO normalised throughout, and added at 7 μl/well using a low-volume multichannel pipette to a white, solid bottom, low volume OptiPlate™-384 microplate (Perkin-Elmer, Norwalk, CT, # 6007299). A series of internal assay standards were also prepared in IP-One Stimulation Buffer and added at 14 μl/well. This included a positive control, a negative control, and a standard curve that was used to calibrate the assay. Upon addition of test compound and control, the microplate was centrifuged briefly (900 x *g*, 30 sec) at room temperature to ensure compound settled at the bottom of each well. This was followed by the addition of diluted cells (7 μl/well) using an Eppendorf Repeater® manual handheld dispenser to wells containing test compound only. The plate was centrifuged briefly, wells covered using a TopSeal™ to prevent evaporation, and cells incubated for 2 h at 37°C.

For antagonist assays, test compound was prepared at four times final assay concentration, added at 3.5 μl/well using a low volume multichannel pipette and centrifuged briefly. Transiently transfected HEK293T cells were diluted as for agonist assay format, at 10,000 cell/well, and added at 7 μl/well using an Eppendorf Repeater®. The proxy-plate was centrifuged briefly, covered with a TopSeal™ and incubated for 15 min at 37°C to facilitate receptor-antagonist equilibrium. Agonist test compound, prepared at four times final assay concentration, was added at 3.5 μl/well and incubated for 2 h at 37°C as described previously.

To detect IP_1 accumulation, the HTRF® reagents IP_1-d2 and anti-IP_1 Lumi4™-Tb cryptate were diluted (1/20 or 1/5 dependent upon the assay kit) in Cell Lysis Buffer, and mixed gently by pipetting to avoid bubble formation. IP_1-d2 was added to all wells (at 3

μl/well) using an Eppendorf Repeater® with the exception of the negative control, to which only Cell Lysis Buffer was added (3 μl). The anti-IP_1 Lumi4™-Tb cryptate was added in the same fashion at 3 μl/well to all wells including the negative control. Plates were centrifuged briefly for 30 sec at 86 x *g*, covered with a fresh TopSeal™, and incubated for 1 h at room temperature.

With the plate seal in place, HTRF® occurring between Lumi4™-Tb cryptate and IP_1-d2 was quantified using the fluorescence ratio of acceptor emission at 665 nm/ donor emission at 620 nm, following excitation at 337 nm. Emission was measured following a 50 μs delay with an integration time of 400 μs, with the number of flashes totalling 53. The 665 nm and 620 nm reads were measured simultaneously using a PHERAstar *FS* plate reader (BMG-Labtech, Germany). IP_1 accumulation (nM) was generated by calculation of the fluorescence ratio, which was calibrated by plotting a four-parameter curve fit through a standard curve (concentrations of 11,000 nM, 2750 nM, 688 nM, 43 nM and 11 nM). Generally, assay data were plotted as a percentage of maximum internal reference control, with each dataset representing a minimum of three independent experiments carried out in duplicate.

2.7.3 *Detection of β-arrestin recruitment using BRET technology*

Under sterile conditions, poly-D-lysine hydrobromide, (MW 70,000-150,000, Sigma-Aldrich, Gillingham, UK # P6407) was reconstituted in Milli-Q dH_2O to a concentration of 1 mg/mL, and diluted 1:20 in serum free DMEM (Sigma-Aldrich, Gillingham, UK, # D5796). To coat plates, poly-D-lysine was added at 50 μl/well to white OptiPlate™-96 microplates and stored overnight at 4°C (Perkin-Elmer, Norwalk, CT). Prior to use, pre-coated 96 well plates were warmed to room temperature. Following a 24 h incubation between HEK293T cells and PEI transfected constructs (total 5 μg DNA in a ratio of 4:1 FLAG-GPR35-eFYP to β-arrestin-*Renilla* luciferase), cells were visually assessed to determine confluence and cell surface receptor-eYFP expression by microscopic analysis using a Nikon inverted microscope. Under sterile conditions, in a category II laminar flow biosafety cabinet, medium was aspirated from each $10cm^2$ dish and trypsinised as described previously (**Section 2.5.3**). Following centrifugation, each pellet was re-suspended in 20 mL fresh pre-warmed complete

media (**Section 2.5.1**) and added at 100 μl/well to poly-D-lysine coated plates. Cells were settled at room temperature for 30 min before 24 h incubation at 37°C + 5 % CO_2 in a humidified incubator.

Test compounds were prepared on the day of use, diluted to 10x final assay concentration in Hanks' balanced salt solution (HBSS) containing Mg^{2+} and Ca^{2+}, pH 7.4, (Gibco™, Life Technologies Ltd, Paisley, UK, # 14025-050) and DMSO normalised throughout. For agonist assays the final assay DMSO concentration was typically 0.1 % and for antagonist assays, 1.1-2 %. Post 24 h incubation, cell culture medium was aspirated and cells washed twice with room temperature HBSS (100 μl/well). Transfected HEK293T wells were incubated in a final volume of 80 μl/well HBSS (agonist assay) or 70 μl/well (antagonist assay) and incubated at 37°C for 30 min.

A quantitative measure of eYFP was gathered by measurement of eYFP fluorescence (excitation 500-10 nm, emission 530-10) using the POLARstar Omega (BMG Labtech Ltd., Alyesbury, UK) to ensure receptor expression. For antagonist assay only, antagonist compound was added (10 μl/well) and plates incubated for 5 min at 37°C. Next, and initially for the agonist assay format, luciferase substrate coelenterazine-h, diluted to a concentration of 25 μM in HBSS and protected from light, was added (10 μl/well) using an Eppendorf Repeater® manual handheld dispenser. To allow oxidation to coelenteramide, plates were covered with aluminium foil and incubated for 10 min at 37°C. Agonist (10 μl/well) was then added using a 2-20 μl multichannel pipette and cells incubated for a further 5 min at 37°C in the absence of light.

Subsequently, after a 10 min incubation with substrate, luminescence was read simultaneously for the acceptor at 535 nm (with an optical bandpass of 10 nm) and donor at 475 nm (with an optical bandpass of 10 nm), for 1 s using the PHERAstar *FS* plate reader (BMG Labtech Ltd., Alyesbury, UK). Each assay was gain adjusted using the β-arrestin-*Renilla* luciferase/pcDNA™3.1 transfected cells, which normalised for cell number variation between experiments. Data are calculated from the BRET ratio between eYFP acceptor emission at 535 nm divided by luciferase donor emission at 475 nm. The net BRET ratio was then calculated as the ratio of cells co-expressing *Renilla* luciferase and eYFP minus the ratio of cells expressing only *Renilla* luciferase in the same experiment, which was multiplied by 1000 to generate mBRET values. Generally, herein, data are expressed as a percentage of a

reference control agonist rather than raw mBRET values in order to normalise data between experiments.

2.7.4 *Measuring the kinetics of β-arrestin recruitment using BRET technology*

To assess the temporal kinetics of β-arrestin-1-*Renilla* luciferase or β-arrestin-2-*Renilla* luciferase, the BRET system of protein/protein interaction was employed. Briefly, transiently co-transfected HEK293T cells were prepared as described in **Section 2.7.3**. Coelenterazine-h was diluted to a concentration of 25 μM in HBSS, added at 10 μl/well using an Eppendorf Repeater®, and incubated for 10 min at 37°C + 5 % CO_2, protected from light. Using the PHERAstar *FS* plate reader, a single maximally active concentration of agonist was added. BRET was measured over a 45 min timeframe by simultaneously monitoring the dual luminescence emissions at 475 nm and 535 nm. Data was normalised between experiments using zaprinast as a reference agonist and represent two independent experiments.

2.7.5 *Cell surface enzyme-linked immunosorbent (ELISA) assay*

To quantify cell surface receptor expression, an ELISA assay was performed using a cell impermeable horseradish peroxidase (HRP) substrate TMB (3,3',5,5'-tetramethylbenzidine) (Thermo Fisher Scientific, Waltham, MA, # 34018) and a monoclonal antibody (mouse anti-FLAG® M2, Sigma-Aldrich, Gillingham, UK, # F1804) directed toward the N-terminal region of the tagged GPCR. Typically, cells that were prepared for the β-arrestin-2 recruitment assay as described in **Section 2.7.3** were used for the cell surface ELISA to provide a quantification of cell surface receptor expression level. From a 10 cm^2 dish containing HEK293T cells transiently co-transfected with FLAG-GPR35-eYFP (4 μg) and β-arrestin-2 (1 μg), cells were trypsinised, centrifuged at 3110 x *g* for 5 min at room temperature, and re-suspended in 20-22 mL complete media before addition at 100 μl/well to poly-D-lysine coated 96 well black, clear bottom plates (Greiner® Bio One International AG, Kremsmuenster, Austria, # 655090). Cells were settled at room temperature for 30 min before incubation for 24 h at 37°C + 5 % CO_2.

On the day of assay, medium was aspirated and replaced with 100 μl pre-warmed serum-free DMEM #D5671 containing anti-FLAG® M2 (1 μg/mL), and incubated for 30 min + 5 % CO_2. Cells were then washed twice with pre-warmed PBS before addition of 100 μl pre-warmed serum-free DMEM containing HRP-conjugated anti-mouse IgG secondary antibody (Cell Signalling, Danvers, MA, # 7076, 1:2500 dilution) and the cell permeant nucleic acid stain Hoechst 33342 trihydrochloride (100 ng/mL) (Molecular Probes®, Life Technologies, Paisley, UK # H1399). Cells were incubated for 30 min + 5 % CO_2, washed twice with 100 μl pre-warmed PBS, and Hoechst fluorescence quantified using the ratio of excitation at 355 nm /emission at 460 nm using 100 flashes per well on a POLARstar Omega plate reader (BMG Labtech, Durham, NC). PBS was completely aspirated and replaced with 100 μl room temperature TMB, which acted as a hydrogen donor for HRP reduction of hydrogen peroxide to water. After incubation at room temperature for 10 min, protected from light, absorbance was measured at 650 nm using 20 flashes per well on the POLARstar Omega.

Cell surface expression was quantified per cell by Hoechst/absorbance, which had non-specific binding, calculated from empty wells containing pcDNA™3.1 or TMB only, deducted, and data normalised accordingly. Each experiment was carried out in sextuplicate, and data represent a minimum of three experiments carried out independently.

2.7.6 *Receptor internalisation by high content imaging (ArrayScan™)*

Under sterile conditions, poly-D-lysine hydrobromide, (1mg/mL stock in Milli-Q dH_2O) was diluted 1:20 in serum free DMEM (Life Technologies Ltd, Paisley, UK # 41965) in a category II laminar flow cabinet under sterile conditions. To coat plates, poly-D-lysine was added at 50 μl/well to black, clear bottomed 96 well plates (Greiner® Bio One International AG, Kremsmuenster, Austria, # 655090) and stored overnight at 4°C. Human GPR35a-eYFP Flp-In™ T-REx™ HEK293 cells were seeded at a density of 80,000 cells/well in complete media (**Section 2.5.1**) using a multi-channel pipette under sterile conditions. After settling at room temperature for 30 min, a 6 h incubation was carried out in a humidified atmosphere at 37°C + 5% CO_2, to allow cells to adhere sufficiently. To induce receptor expression, media was aspirated from each well and replaced with complete media containing 100 ng/mL doxycycline. Following a 24 h incubation, cell surface eYFP expression was assessed by visual

inspection using a Nikon inverted microscope. Media was then completely aspirated under sterile conditions and washed twice with pre-warmed serum free DMEM (Life Technologies Ltd, Paisley, UK, # 41965), before a final addition of 90 μl serum free media. Cells were incubated for a minimum of 30 min before test compound, prepared at 10X final assay concentration in serum free media, was added at 10 μl/well using a multichannel pipette. After a 45 min incubation at 37°C + 5 % CO_2, medium was completely aspirated and cells fixed via the addition of 4 % paraformaldehyde in 1X PBS (100 μl) and subsequent 40 min incubation at room temperature. Paraformaldehyde was removed by aspiration and cells washed 3 times with 100 μl 1X PBS. Plates were then wrapped in Saran wrap to minimise evaporation and stored at 4°C overnight.

To assay, cells were incubated with Hoechst 33342 trihydrochloride nuclear stain, diluted to 500 nM in 1X PBS (100 μl/well) and incubated for 30 min at room temperature protected from light. Hoechst 33342 was removed by aspiration and cells washed three times with 100 μl 1X PBS before assessment of receptor internalisation using the ArrayScan™ II High Content Analyser (Cellomics, Boston, MA), Receptor Internalisation and Trafficking application. Cell nuclei (measured using Hoechst nuclear stain) were detected as a surrogate measure of cell number, while fluorescence intensity was used to monitor internalised receptor. Cells were automatically detected using a 10X objective lens, before exposure for a fixed duration. Using an internalisation vesicle inclusion form factor of 1.0 and a TopHat transformed algorithm to remove background interference, four images/well were taken simultaneously to provide an assessment of receptor internalisation per cell.

2.7.7 *Visualisation of receptor internalisation by ZEISS VivaTome spinning disk confocal microscopy*

Glass coverslips (30 nm) were sterilised in 100 % ethanol and air-dried under sterile conditions in a category II laminar flow cabinet. Each coverslip was coated with poly-D-lysine hydrobromide (1 mg/mL) and air-dried. Approximately 30,000 Flp-In™ T-REx™ HEK293 human GPR35-eYFP cells were added in 500 μl to the centre of each coverslip in complete media, housed within a six well plate. Plates were carefully transported to a humidified cell culture incubator and incubated for 30 min at 37°C + 5 % CO_2 to allow cells to settle. Cells were then carefully rotated incubated for 2 h at 37°C + 5 % CO_2. To induce receptor

expression, each well was flooded with 2 mL complete media containing 100 ng/mL doxycycline and incubated overnight at 37°C + 5 % CO_2. The next day, media was carefully aspirated and replaced with 500 µl HBSS containing 10 mM D-glucose.

Coverslips were placed into a microscope chamber containing physiological saline solution [NaCl (130 mM), KCl (5 mM), $CaCl_2$ (1 mM), $MgCl_2$ (1 mM), HEPES (20 mM), and D-glucose (10 mM), pH 7.4]. Ligand (2X final assay concentration) was added to the microscope chamber and fluorescent images were acquired at 15 min intervals using a spinning disk structured illumination Viva Tome device attached to the bottom port of a ZEISS Axio Observer.Z1 invert microscope (Carl Zeiss Ltd, Cambridge, UK). Narrow band 490/20 nm excitation light was reflected through a 63X, oil immersion Plan-Apochromat objective lens to excite eYFP and the resulting emitted light was detected at 536 nm/ 540 nm using an Axiocam MRm CCD camera (Carl Zeiss Ltd, Cambridge, UK). All experiments were carried out with Dr John Pediani.

2.7.8 *Dynamic mass redistribution using the Corning® Epic®BT system*

HT-29 cells were plated in complete medium McCoy's 5A (Modified) Medium (Life Technologies Ltd, Paisley, UK, # 26600-023) at a density of 30,000 cells/well into black, fibronectin coated, glass bottomed Epic® 384 well plates (Corning®, Tewksbury, MA # 5042), at a volume of 50 µl/well using an electronic multichannel pipette. Each plate was centrifuged at 3110 x *g*, for 30 sec and plates kept at room temperature for 30 min to allow cells to settle prior to incubation for 24 h at 37°C in a humidified atmosphere containing 5 % CO_2. At 95 % confluence, the cells were washed three times with serum free McCoy's 5A (Modified) Medium containing 25 mM HEPES using a Biomek® FX^P automated liquid handling system (Beckman Coulter, Palo Alto, CA, # A31845), before a final addition (40 µl) of serum free medium containing 0.01 % DMSO to equilibrate the cells.

HT-29 cells were temperature and DMSO adjusted by incubation for 90 min at room temperature (26°C) in the Epic® Bench Top (BT) system (Corning, Tewksbury, MA, # 5053) followed by the acquisition of basal data for 2 min using the whole cell scanning function. Plates were then removed from the Epic®BT system and agonist, five times concentrated in serum free media and normalised for DMSO concentration (0.01 %), was added using the Biomek® FX^P at a volume of 10 µl/well. Immediately following agonist addition, plates were

returned to the Epic®BT system. Change in refractive index upon dynamic mass redistribution within the cell is reflected by the resonant waveguide grating biosensor located within the glass base of each well. Simultaneous illumination of each biosensor was carried out using a laser light source that using a charged coupled device camera captured pixilated spectral images every 2 sec with a spatial resolution of 150 nm to record changes in pm shift over 60 min at 26°C.

For antagonist assays, antagonist (5 µl/well) was added using the Biomek® FX^P liquid handling system, and plates returned to the Epic®BT for 30 min prior to agonist addition (5 µl/well). DMR data was gathered for a further 60 min. DMR values obtained 5 min post ligand addition (agonist) or 35 min (antagonist) were baseline corrected by deducting control wells (DMSO only treated cells), which were distributed across the middle row of each plate, from ligand treated cells. All DMR assays were carried out on the premises of the MRCT during CASE placement (London, UK), with data representing three independent experiments carried out in quadruplicate.

2.8 Data analysis

All data analysis was carried out using GraphPad Prism version 5.0b (GraphPad Software Inc. San Diego, CA).

2.8.1 *Analysis of agonist functional data*

A series of eight-point agonist concentration responses (where the last point was a vehicle-only control and was plotted one log unit lower than the lowest concentration of test ligand assessed) were fit to the (agonist) versus response (variable slope) three-parameter nonlinear regression analysis in GraphPad Prism. The three-parameter curve fit assumed that the concentration response had a standard slope, equal to a Hill slope of 1.0, with a formula:

$$Response = Bottom\ \frac{(Top - Bottom)}{1 + 10^{LogEC50-X}}$$

In which Top is the maximal asymptote of the curve, or the E_{max}; Bottom is the vehicle only control response; $logEC_{50}$ is the negative logarithm of the agonist's EC_{50}, (the concentration of ligand that generates the half maximal response); X is the agonist concentration.

The pEC_{50} values were obtained from the three-parameter curve fit 'best-fit' analysis. This analysis was performed individually for each experiment and pEC_{50}s from each experiment were then used to calculate the mean ± standard error of the mean (SEM). This gave a grouped pEC_{50} ± SEM value for each ligand's response.

2.8.2 *Analysis of functional antagonist competition experiments*

To determine antagonist activity, agonist responses were measured at a fixed EC_{80} concentration of the reference agonist (zaprinast) in the presence of a series of concentrations of antagonist. An agonist-only response was also performed. Analysis was performed using the equation described in **Section 2.8.1**, except that the IC_{50} (the concentration whereby 50 % of the agonist response was inhibited) was calculated rather than the EC_{50}. Such that:

$$Response = Bottom\ \frac{(Top - Bottom)}{1 + 10^{LogIC50-X}}$$

The pIC_{50} values were obtained from the 'best fit' curve-fit from each individual experiment, which was performed a minimum of three times and each value was used to calculate the pIC_{50} ± SEM in the same way as described in **Section 2.8.1**.

2.8.3 *Global Gaddum/Schild EC_{50} analysis*

To determine if the interaction between newly discovered GPR35 agonists and GPR35 antagonists (ML-145 or CID-2745687) was competitive, Schild analysis was carried out, based on the model described by Arunlakshana and Schild, 1959. The Schild analysis performed herein used the GraphPad Prism global non-linear regression curve fit. For BRET and IP-One assays, eight-point concentration responses of agonist (where the last point is a vehicle-only control) were assessed in duplicate against five fixed concentrations of

antagonist in a 96- or 384-well plate, respectively. An agonist only concentration-response curve was also performed. To obtain the Top and Bottom values of the agonist-only control a three-parameter curve fit analysis (**Section 2.8.1**) was performed. Antagonist competition data was then fit to the Gaddum/Schild EC_{50} shift global fit analysis using GraphPad Prism, with the formula:

$$Response = Bottom + \frac{(Top - bottom)}{1 + \left(\frac{10^{LogEC50}[1 + ({}^{[B]}/_{10^{-pA_2}})^S]}{[A]}\right)^{Hillslope}}$$

Where A is the agonist concentration; B is the antagonist concentration; EC_{50} or the negative logarithm of the EC_{50} is the concentration of agonist that generates a half maximal response in the absence of inhibitor; pA_2 is the negative logarithm of the concentration of antagonist needed to shift the agonist concentration response curve by a factor of 2; the Hill Slope is the steepness of the family of curves (with a Hill Slope of 1.0 being standard); the Schild Slope (S) quantifies if the shift in the agonist's response with increasing antagonist concentration that corresponds to the prediction of competitive interaction, (if the antagonist is competitive then the Schild Slope would be equal to 1.0); Top is the maximal asymptote of the curve; Bottom is the basal response.

To normalise the Schild analysis data between and within BRET experiments, using GraphPad Prism's normalise function, the Top and Bottom values obtained from the agonist-only control curve were set to 0 and 100 %, respectively, such that any reduction in the maxima of the antagonist competitions were not artificially constrained to 100 %. For IP-One assays, where the basal values decreased with increasing antagonist/ inverse agonist concentration, basal and maximal values had to be constrained to 0 and 100 % for each concentration of antagonist assessed, which negated the Schild analysis but allowed visualisation of the rightwards shift of the agonist concentration response with increasing antagonist concentration.

2.8.4 *Analysis of ligand bias by calculation of the log (dose response) ratio*

All equations and analytical procedures outlined below were performed in accordance with those described previously (Kenakin and Christopoulos, 2013), and the GraphPad Prism file containing the formulae was kindly provided by Prof. Arthur Christopoulos, University of Monash, Australia. To quantify ligand bias, agonist activity was measured in two or more pathways (such as β-arrestin-2 recruitment or IP_1 accumulation) with functional concentration-response data analysed using a modified version of the Black and Leff operational model of agonism (detailed in Kenakin et al., 2012):

$$Response = Basal + \frac{(E_m - Basal)[A]^n \tau^n}{[A]^n \tau^n + ([A] + K_A)^n}$$

Where [A] is the agonist concentration; E_m is the maximal possible response of the system and basal is the vehicle-only response; K_A is the equilibrium dissociation constant of the agonist; τ is the operational agonist efficacy of the agonist (and is defined as R_T/K_E (where R_T is the receptor density and K_E is the intrinsic efficacy of the agonist in a particular signalling pathway); *n* is the transducer slope for the function between agonist occupancy and measured responses. E_m and *n* are cell-type specific and are shared by all agonists that act on the same receptor in the same pathway. $Log(\tau/K_A)$ is defined as the transduction coefficient for a particular agonist in a particular signalling pathway.

To determine the difference between pathways, $\Delta log(\tau/K_A)$ values are calculated by subtracting the $log(\tau/K_A)$ value of the test compound from the $\Delta log(\tau/K_A)$ of the reference agonist (usually the endogenous agonist but in this case, zaprinast). For each agonist, $\Delta\Delta log(\tau/K_A)$ values are calculated by subtracting the $\Delta log(\tau/K_A)$ value from pathway one from the corresponding $\Delta log(\tau/K_A)$ value from the second pathway. Bias is then quantified as $10^{\Delta\Delta log(\tau/KA)}$. If the value of $10^{\Delta\Delta log(\tau/KA)}$ was 1, then the agonist was unbiased between the two pathways, if the value was larger than 1 the agonist was biased towards pathway one, or if it was less than 1 the agonist was biased towards pathway two.

Step 1: Concentration response curves were generated using a modified version of the Black and Leff operational model, as described by Kenakin et al., 2012.

Step 2: The transduction coefficient difference $\Delta\log(\tau/K_A)$ between different ligands in the same pathway were calculated by subtracting transduction coefficient of the test sample from the reference compound (zaprinast):

$$\Delta Log\left(\frac{\tau}{K_A}\right) = Log\ \left(\frac{\tau}{K_A}\right)\ of\ sample - Log\ \left(\frac{\tau}{K_A}\right)\ of\ reference$$

Step 3: The difference between transduction coefficients $\Delta\Delta\log(\tau/K_A)$ were calculated between different pathways for the same test ligand by subtracting the $\Delta\log(\tau/K_A)$ for pathway one from that of pathway two:

$$\Delta\Delta Log\left(\frac{\tau}{K_A}\right) = \Delta Log\ \left(\frac{\tau_1}{K_{A1}}\right) - \Delta Log\ \left(\frac{\tau_2}{K_{A2}}\right)$$

Step 4: The bias factor was calculated as:

$$Bias = 10^{\Delta\Delta log\left(\frac{\tau}{K_A}\right)}$$

2.8.5 *Statistical analysis*

Statistical analysis was performed using a one-way analysis of variance (ANOVA) when comparing the means of multiple treatment groups. Tukey's post-hoc analysis was used to determine significance between treatment groups versus the control group, with a p value <0.05 deemed statistically significant.

Chapter Three

Identification of drug screening formats for GPR35

3.1 Investigating G protein signal transduction pathways associated with GPR35

At the beginning of 2011, when this project commenced, there were few ligands available for assessing the pharmacology of GPR35. Of those that were available, most were of modest potency, were non-selective with prominent off-target effects, or displayed marked species selectivity between the human and rodent orthologues (Wang et al., 2006a; Taniguchi et al., 2006; Jenkins et al., 2010; Jenkins et al., 2011; Zhao et al., 2010). Indeed, the proposed endogenous ligands, the L-tryptophan metabolite kynurenic acid (Wang et al., 2006a) and the phospholipid derivative lysophosphatidic acid (Oka et al., 2010), suffered from the above issues, with kynurenic acid acting with low potency at the human orthologue (Jenkins et al., 2011) and with lysophosphatidic acid responses being irreproducible by independent investigators (Southern et al., 2013; my unpublished findings).

In this first results chapter, five synthetic ligands were used to characterise assay systems suitable for drug discovery efforts at GPR35 (**Fig 3.1**). These were zaprinast, the GPR35 reference agonist and cGMP PDE 5/6 inhibitor (Taniguchi et al., 2006; Jenkins et al., 2012); pamoic acid, a GPR35 agonist previously believed to be an inert substance that was added as a counter ion to drug formulations (Neubig, 2010; Zhao et al., 2010); cromolyn, a GPR35 agonist with mast cell stabiliser properties (Yang et al., 2010; Jenkins et al., 2010); and two novel GPR35 antagonist molecules, ML-145 and CID-2745687 (Heynen-Genel et al., 2010; Heynen-Genel et al., 2011).

In addition to drug discovery, at the beginning of this project, a number of groups had investigated the function of GPR35 using Pertussis toxin (isolated from *Bordetella pertussis*, abbreviated as PTX), to abolish GPR35 signalling by ADP-ribosylation of the $G\alpha_{i/o}$ protein carboxyl terminus, suggesting that GPR35 coupled to the $G\alpha_{i/o}$ family of G proteins (Wang et al., 2006a; Taniguchi et al., 2006; Barth et al., 2009; Zhao et al., 2010; Fallarini et al., 2010). Subsequently, it emerged that GPR35 also selectively coupled to the RhoA and Src family kinase activator $G\alpha_{13}$ but not to the closely related $G\alpha_{12}$ G protein subunit (Jenkins et al., 2011). This presented GPR35 as a $G\alpha_{13}$ and $G\alpha_{i/o}$ selective GPCR.

Herein, I began my research efforts through identification of assay formats that would be suitable for subsequent GPR35 drug discovery and characterisation efforts. To this end, the heterologous *Saccharomyces cerevisiae* yeast system that employed yeast-mammalian G protein chimeras was used to reassess the published GPR35 G protein

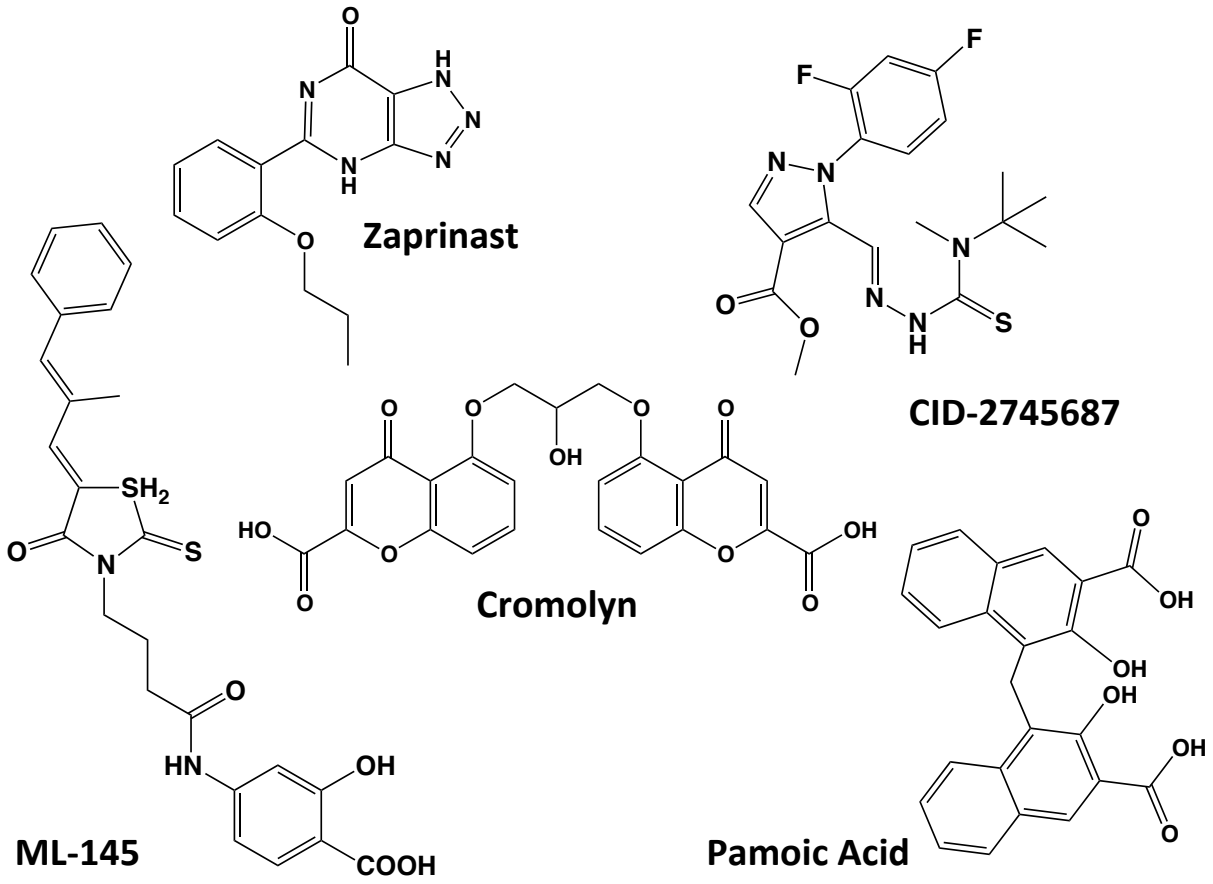

Figure 3.1 GPR35 agonist and antagonist structures Schematic depicting the molecular structures of zaprinast, cromolyn and pamoic acid, which are agonists of GPR35, displayed alongside antagonists ML-145 and CID-275687. Structures were constructed using ChemDraw Ultra.

coupling profile. Subsequently, distinct [^{35}S]GTPγS incorporation, second messenger, β-arrestin recruitment, and receptor internalisation assays were investigated as drug screening formats. To characterise GPR35 responses in an endogenous cell line, a label-free system was employed to assess cellular dynamic mass redistribution (DMR). Finally, species orthologue responses were assessed where appropriate in order to characterise ligand responses but also to identify any species selectivity issues that could hinder future drug development efforts.

3.1.1 *Investigating zaprinast-induced G protein coupling at human and rat GPR35 in the yeast assay*

In order to reassess the published G protein coupling preference of GPR35, I employed a previously described *S. cerevisiae* yeast system (Dowell and Brown, 2009). In this system a W303-1A strain is manipulated to chromosomally express the endogenous yeast Gα subunit, *Gpa1*, or a yeast-mammalian chimeric G protein from the *trp* locus (Dowell and Brown, 2009). Yeast-mammalian G protein chimeras were generated by replacement of the last five carboxyl terminal amino acids of Gpa1 with the corresponding mammalian G protein sequence to couple mammalian GPCR responses through the yeast mating response pathway (Dowell and Brown, 2009). In cases where the carboxyl amino acid sequences were identical between different G proteins (such as for $G\alpha_{i1}$/$G\alpha_{i2}$ and $G\alpha_{oA}$/$G\alpha_{oB}$) the emanating responses were non-distinguishable and were thus presented as a single incorporated response. Stimulation of this pathway resulted in the induced production of β-galactosidase, which cleaved the cell permeable substrate fluorescein-di-β-galactopyranoside (FDG) to fluorescein and generated a fluorescent readout for agonist stimulation (**Section 2.7.1**).

This yeast assay has previously been employed to characterise $G\alpha_{13}$ responses at human and rat GPR35 (Jenkins et al., 2011) and had been optimised for this purpose. Nonetheless, negative control strains were employed to ensure selectivity following overnight treatment with varying concentrations of zaprinast (**Fig 3.2**). These were empty p426GPD vector strains lacking GPR35 but containing each G protein chimera to assess for receptor-independent activity, or Gpa1 only with p426GPD vector, human GPR35, or rat

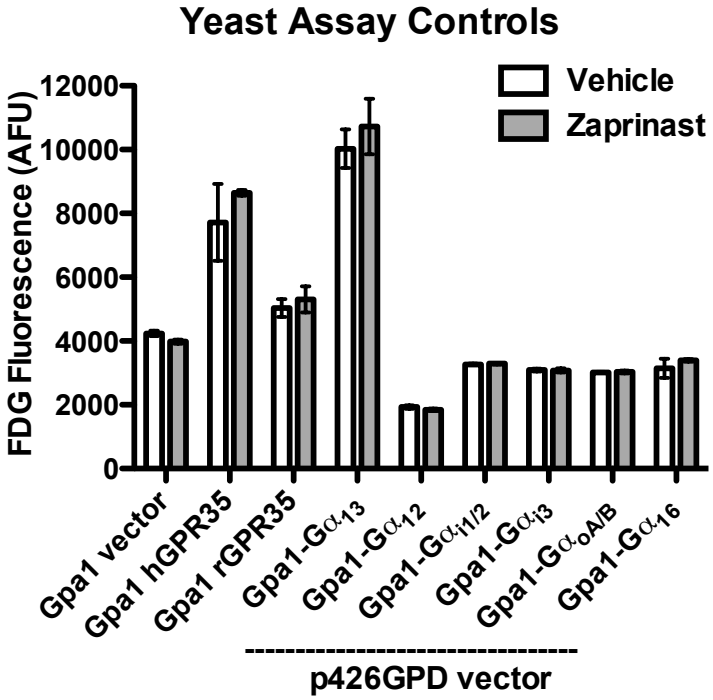

Figure 3.2 Yeast control strains are not stimulated following overnight zaprinast treatment *S. cerevisiae* cells stably expressing empty yeast expression vector p426GPD or p426GPD vectors containing human (h) or rat (r) FLAG-GPR35 were grown to confluence in the absence or presence of zaprinast overnight at 30 °C (see **Section 2.7.1** for details). Each receptor strain also stably expressed a yeast-mammalian chimera that, if activated following zaprinast treatment, would signal through the Gpa1 pathway to induce β-galactosidase expression and generate fluorescence proportional to ligand activation. Samples were treated with zaprinast at 100 μM or DMSO, 0.01 %. Data are presented as raw arbitrary fluorescence units (AFU) from two independent experiments carried out in triplicate with distinct single colonies.

GPR35 strains to control for G protein-independent activity. In all these cases, no difference was observed between vehicle and zaprinast treatment.

Following overnight incubation with varying concentrations of zaprinast, human and rat GPR35 Gpa1-Gα_{13} strains acted to generate fluorescence with a half-maximal response (pEC_{50}) that was similar for each species orthologue (**Fig 3.3A**; **Table 3.1**). This response was selective for Gpa1-Gα_{13}, since Gpa1-Gα_{12} failed to generate an increase in AFU via either human or rat GPR35 (**Fig 3.3B**). Meanwhile, zaprinast acted at the Gpa1-G$\alpha_{i1/2}$ strains with significantly higher potency at rat than at human GPR35 ($P \leq 0.05$) (**Fig 3.3C**). At the Gpa1-Gα_{i3} and Gpa1-G$\alpha_{oA/B}$ strains however, the potency of zaprinast was not significantly different between species orthologues (**Fig 3.3D/E**). For the final Gpa1-G$\alpha_{i/o}$ family member Gpa1-Gα_{z}, there was no stimulated increase in AFU following zaprinast treatment, indicating that zaprinast induced G protein coupling selectively within the Gpa1-G$\alpha_{i/o}$ and Gpa1-G$\alpha_{12/13}$ families of G proteins (**Table 3.1**). For the Gpa1-Gα_{16} strain various concentrations of zaprinast induced a response at human but not rat GPR35, for which only the highest concentration (100 μM) elicited a response (**Fig 3.3F**; **Table 3.1**). There was not an increase in AFU following zaprinast stimulation of Gpa1-Gα_{s}, Gpa1-Gα_{q}, and Gpa1-Gα_{14} human or rat GPR35 strains, indicating that zaprinast acted with specificity toward Gpa1-Gα_{13}, Gpa1-G$\alpha_{i1/2}$, Gpa1-Gα_{i3}, Gpa1-G$\alpha_{oA/B}$, and Gpa1-Gα_{16} chimeras in the yeast assay.

3.1.2 *Investigation of G protein coupling to human GPR35 using zaprinast in the [^{35}S]GTPγS assay*

To determine whether the profile of G protein coupling observed in the heterologous yeast system translated into a mammalian assay format, and to establish a mammalian G protein drug screening system, distinct [^{35}S]guanosine-5'-O-(3-thio)triphosphate ([^{35}S]GTPγS) assays were employed. The premise of the [^{35}S]GTPγS assay is to monitor receptor activation at the level of the exchange process occurring between GDP and GTP at the Gα protein subunit, which relies on the slower dissociation properties of GTPγS, a poorly hydrolysable analogue of GTP that is radiolabelled for detection purposes using [^{35}S]. The [^{35}S]GTPγS assay format is ideally suited to assessment of G$\alpha_{i/o}$ responses as G$\alpha_{i/o}$ proteins are expressed at higher level and display a faster GDP/GTP exchange rate compared with

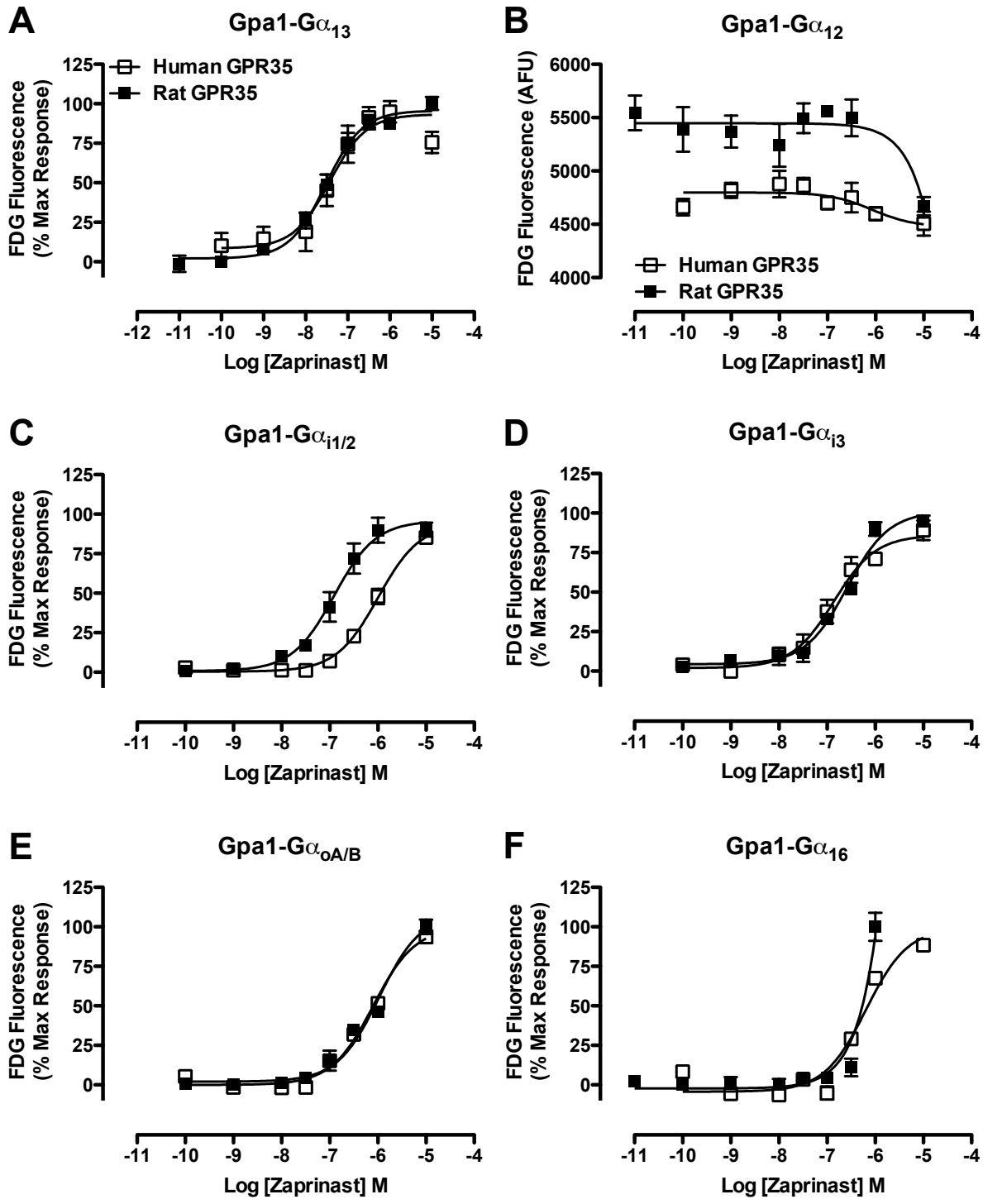

Figure 3.3 Human and rat GPR35 selectively couple to $G\alpha_{i/o}$, $G\alpha_{13}$, and $G\alpha_{16}$ in the yeast assay *S. cerevisiae* cells stably expressing human or rat FLAG-GPR35 were grown to confluence in the absence or presence of zaprinast overnight at 30°C. Signalling through the Gpa1 pathway induced β-galactosidase expression and generated fluorescence proportional to ligand activation for Gpa1-$G\alpha_{13}$ (**A**), $G\alpha_{12}$ (**B**), $G\alpha_{i1/2}$ (**C**), $G\alpha_{i3}$ (**D**), $G\alpha_{oA/B}$ (**E**), and $G\alpha_{16}$ (**F**). Data are normalised to the maximum ligand best-fit response and are the mean ± SEM of three independent experiments carried out with distinct single colonies, with the exception of $G\alpha_{12}$, which is presented as raw data.

Table 3.1 Zaprinast couples GPR35 to $G\alpha_{i/o}$, $G\alpha_{13}$ and $G\alpha_{16}$ yeast-mammalian G proteins in the yeast assay

	Yeast Assay pEC_{50}[a]	
Gpa1 G protein chimera	**FLAG-Human GPR35**	**FLAG-Rat GPR35**
$G\alpha_{13}$	7.43 ± 0.19	7.52 ± 0.08
$G\alpha_{12}$	Inactive	Inactive
$G\alpha_{i1/2}$	6.01 ± 0.05	6.91 ± 0.11***
$G\alpha_{i3}$	6.86 ± 0.13	6.59 ± 0.08
$G\alpha_{oA/B}$	6.01 ± 0.08	5.98 ± 0.05
$G\alpha_{z}$	Inactive	Inactive
$G\alpha_{s}$	Inactive	Inactive
$G\alpha_{q}$	Inactive	Inactive
$G\alpha_{14}$	Inactive	Inactive
$G\alpha_{16}$	6.19 ± 0.14	<6

[a] A significant difference in the potency of zaprinast between human and rat GPR35 denoted by P *** ≤ 0.001
Data are the mean ± SEM of three independent experiments carried out in triplicate using distinct single colonies on each occasion

other G protein subunits. As a result, the [^{35}S]GTPγS assay was the format of choice to assess G$\alpha_{i/o}$ coupling and also to dissect which specific G$\alpha_{i/o}$ subunits interacted with human GPR35 following treatment with zaprinast.

The [^{35}S]GTPγS assay was carried out on membranes prepared from cells transfected to express G$\alpha_{i/o}$ proteins that contained the C^{351}I mutation (**Section 2.6.7**). Application of PTX to cells results in ADP ribosylation of all endogenously expressed G$\alpha_{i/o}$ G proteins present within the cell but not the mutant G$\alpha_{i/o}$ proteins containing C^{351}I, which would remain active and able to incorporate [^{35}S]GTPγS. Systematic assessment of each G$\alpha_{i/o}$-C^{351}I protein in the presence of PTX therefore provides a means to dissect G$\alpha_{i/o}$ G protein recruitment to GPR35. Membranes were prepared from HEK293T cells transiently co-transfected with FLAG-human GPR35-eYFP or pcDNA3.1 and assessed in the absence of PTX for [^{35}S]GTPγS incorporation following a one hour treatment with zaprinast (**Section 2.6.7**). This enabled an assessment of endogenous G protein coupling following zaprinast treatment in the presence or absence of GPR35. Quantification of [^{35}S]GTPγS incorporation by liquid scintillation spectrometry revealed that there was a difference in the relative amount of [^{35}S]GTPγS incorporation between human GPR35 and pcDNA3.1 in vehicle (DMSO, 0.1%) treated samples (**Fig 3.4A**). When stimulated with zaprinast however, there was no further increase in [^{35}S]GTPγS incorporation in membranes expressing human GPR35 (**Fig 3.4A**). This indicated that the low level of [^{35}S]GTPγS incorporation associated with GPR35 did not occur as a result of zaprinast stimulation.

To specifically assess induced G$\alpha_{i/o}$ recruitment, membranes were prepared from HEK293T cells transiently co-transfected to overexpress individual G$\alpha_{i/o}$-C^{351}I subunits alongside FLAG-human GPR35-eYFP or bovine free fatty acid (FFA) receptor 2-eYFP, a receptor that endogenously couples to the G$\alpha_{i/o}$ family of G proteins (Hudson et al., 2012b). Although there was no zaprinast-induced enhancement of [^{35}S]GTPγS incorporation for any of the G$\alpha_{i/o}$-C^{351}I subunits assessed following PTX treatment for GPR35 (**Fig 3.4B**), there was an increase in [^{35}S]GTPγS incorporation via bovine FFA2 following stimulation with valeric acid (**Fig 3.4B**). This indicates that zaprinast does not stimulate [^{35}S]GTPγS incorporation of G$\alpha_{i/o}$ G proteins through activation of human GPR35.

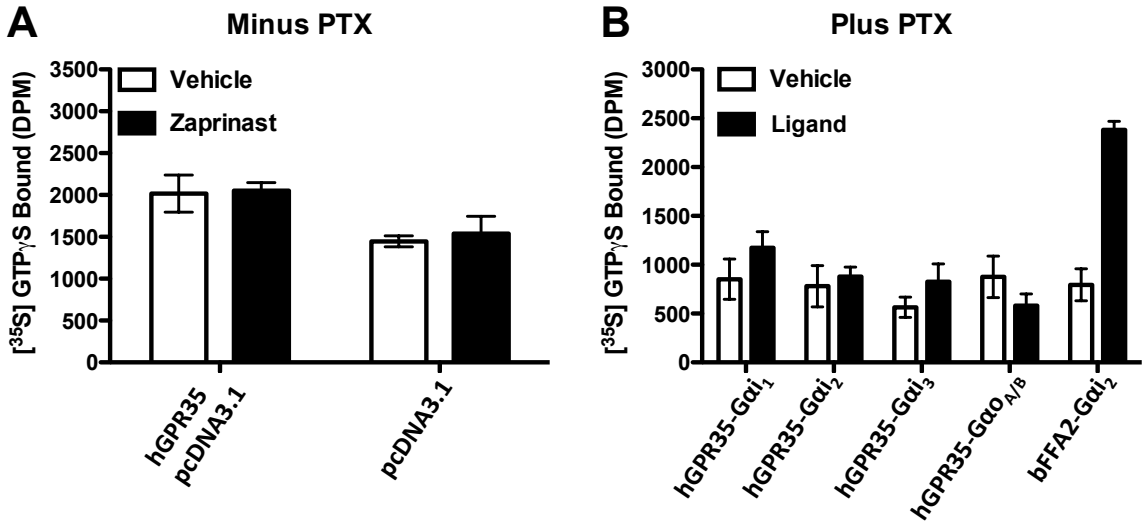

Figure 3.4 Assessment of zaprinast-induced G protein coupling to human GPR35 using [^{35}S]GTPγS incorporation HEK293T cells were transiently co-transfected with FLAG-human GPR35-eYFP, bovine-FFA2-eYFP, or pcDNA3.1, along with $G\alpha_{i/o}$ proteins modified with the $C^{351}I$ mutation that is insensitive to Pertussis toxin (PTX). Membranes were prepared from cells as described (**Section 2.6.5**). Ten μg membrane protein was incubated at 25°C with ligand for 1 hour in the [^{35}S]GTPγS assay (as described in **Section 2.6.7**). In the absence of PTX treatment, zaprinast (100 μM) or vehicle (DMSO, 0.1%) were incubated with human GPR35 or pcDNA3.1 and [^{35}S]GTPγS incorporation monitored (**A**). Following overnight treatment with PTX (100 ng/mL), agonist induced [^{35}S]GTPγS incorporation was assessed relative to vehicle control in membranes containing human GPR35 $G\alpha_{i1\text{-}C351I}$, $G\alpha_{i2\text{-}C351I}$, $G\alpha_{i3\text{-}C351I}$, or $G\alpha_{oA/B\text{-}C351I}$ alongside bovine FFA2 with $G\alpha_{i2\text{-}C351I}$. GPR35 and FFA2 samples were incubated with a maximally effective concentration of zaprinast (100 μl) or valeric acid (10 mM), respectively (**B**). Data represent the mean of two independent experiments carried out in triplicate ± SEM.

3.1.3 *Assessing $G\alpha_{13}$ coupling to human GPR35 using a [^{35}S]GTPγS assay with an immunoprecipitation step*

Despite the inability to detect $G\alpha_{i/o}$ G protein subunit recruitment to GPR35 in the [^{35}S]GTPγS assay, I continued with the [^{35}S]GTPγS format but moved to a [^{35}S]GTPγS assay that incorporated an immunocapture step to enrich for $G\alpha_{13}$ (**Section 2.6.8**), since this had previously been employed with limited success to characterise ligand responses at GPR35 (Jenkins et al., 2010). For this assay an internally EE-epitope tagged form of $G\alpha_{13}$ was overexpressed that allowed for the EE tag to be used in the immunoprecipitation step. Flp-In™ T-REx™ HEK293 inducible stable cells (**Section 2.3**), were transiently transfected with $G\alpha_{13EE}$ and incubated overnight in the absence or presence of 100 ng/mL doxycycline, which was used to induce expression of FLAG-GPR35-eYFP. Membranes prepared from these cells were treated with zaprinast, and [^{35}S]GTPγS incorporation was monitored after an anti-EE immunocapture step to enhance the $G\alpha_{13EE}$ response. Membranes expressing FLAG-human GPR35-eYFP and $G\alpha_{13EE}$ showed a clear increase in [^{35}S]GTPγS incorporation relative to $G\alpha_{13EE}$ alone, FLAG-human GPR35-eYFP alone, or empty vector pcDNA5/FRT/TO (**Fig 3.5A**). Zaprinast induced [^{35}S]GTPγS incorporation via FLAG-human GPR35-eYFP with a pEC_{50} of 7.08 ± 0.37 (**Fig 3.5A**).

In an effort to increase the signal window in the [^{35}S]GTPγS assay a fusion construct was generated. Fusion proteins between GPCRs and G proteins have been shown to increase signalling efficiency since the two polypeptides are expressed within close proximity to each other (Milligan, 2003a). The fusion was generated between FLAG-human GPR35 and $G\alpha_{13EE}$ and contained an *EcoRV* restriction site sequence between the receptor and G protein (**Section 2.3**). This construct was stably inserted into the genome of a Flp-In™ T-REx™ HEK293 cell line and expressed on demand following overnight incubation with 100 ng/mL doxycycline (**Section 2.5.5**). Since the anti-EE antibody did not appear to detect the fusion construct, as indicated in the immunoblot presented in **Figure 3.5B**, the immunocapture step in the [^{35}S]GTPγS assay was carried with an anti-FLAG antibody.

Membranes prepared from Flp-In™ T-REx™ HEK293 cells containing FLAG-human GPR35-$G\alpha_{13EE}$ displayed a concentration dependent increase in [^{35}S]GTPγS incorporation following zaprinast treatment as compared with non-induced Flp-In™ T-REx™ HEK293

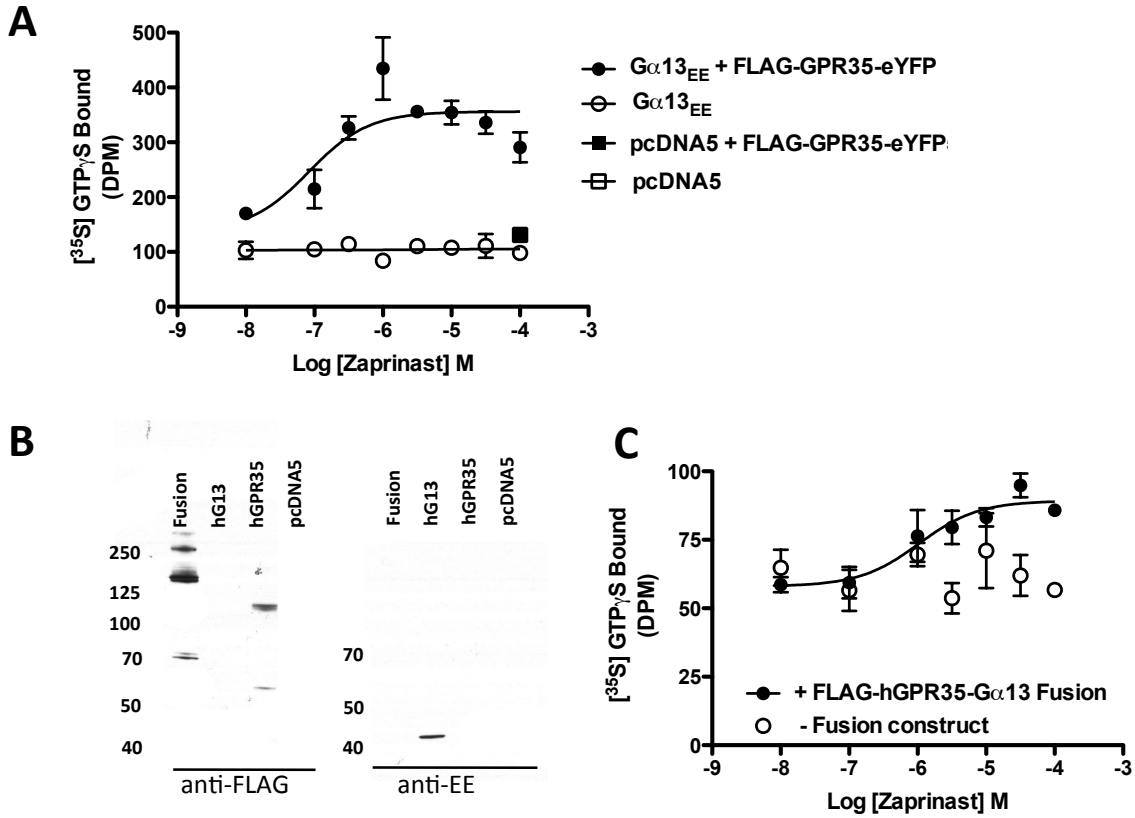

Figure 3.5 Investigating $G\alpha_{13}$ coupling at human GPR35 using a [^{35}S]GTPγS immunoprecipitation assay $G\alpha_{13EE}$ or pcDNA™5/FRT/TO constructs were transiently transfected into Flp-In™ T-REx™ cells that were incubated in the presence (black symbols) or absence (open symbols) of doxycycline. Overnight incubation with 100 ng/mL doxycycline induced FLAG-human GPR35-eYFP receptor expression. Membranes prepared from these cells were treated with or without zaprinast and assessed for their ability to recruit $G\alpha_{13EE}$ using the [^{35}S]GTPγS assay with an anti-EE immunocapture step (**Section 2.6.8**). All reactions were performed at 25°C for 1 h using 25 μg protein. Negative controls were assessed using a single high concentration of zaprinast only (100 μM) (**A**). For the Western blot, 10 μg of membrane protein was added per lane. Approximate sizes of the proteins are indicated on the left of the blots (in kDa). Flp-In™ T-REx™ membranes containing the FLAG-human GPR35-$G\alpha_{13EE}$ fusion construct (78 kDa) was detected with the anti-FLAG but not the anti-$G\alpha_{13EE}$ antibody. HEK293T membranes containing $G\alpha_{13}$ (44 kDa), FLAG-human GPR35-eYFP (61 kDa), or pcDNA3.1 were employed as controls (**B**). The Western blot is a representative example and details of the assay are described in **Section 2.6.4**. (**C**), as for (**A**), but with membranes prepared from Flp-In™ T-REx™ cells uninduced or doxycycline induced (100 ng/mL) to express the FLAG-human GPR35-$G\alpha_{13EE}$ fusion construct, which was immunoprecipitated using an anti-FLAG antibody. [^{35}S]GTPγS data represent the mean of two independent experiments carried out in triplicate ± SEM.

membranes (**Fig 3.6B**). Importantly however, the signal window associated with the fusion construct was not greater than that of the previously described FLAG-human GPR35-eYFP and $G\alpha_{13EE}$ [^{35}S]GTPγS immunoprecipitation experiment (**Fig 3.6A/B**). Furthermore, the potency generated by zaprinast was lower at the fusion construct (pEC_{50} 5.98 ± 0.3) than that generated when the FLAG-human GPR35-eYFP and $G\alpha_{13EE}$ proteins when individually expressed (pEC_{50} 7.08 ± 0.37). This indicated that individual expression of GPR35 and $G\alpha_{13EE}$ would be superior to employing the fusion construct for future [^{35}S]GTPγS immunoprecipitation assays. However, given the low magnitude of the signal window and the low throughput nature of the [^{35}S]GTPγS immunoprecipitation assay, this format was not employed for drug screening efforts herein.

3.1.4 *Using chimeric Gαq proteins in a mammalian system: GPR35 and the IP-One assay*

To obtain a higher throughput G protein output for drug screening efforts in a mammalian cell system, I returned to the chimeric G protein approach, this time using transiently transfected HEK293 cells. To this end $G\alpha_{qi1/2}$ and $G\alpha_{q13}$ chimeras were employed, which expressed the full length $G\alpha_q$ sequence but with the last five residues replaced with the corresponding residues from the $G\alpha_{i1/2}$ or $G\alpha_{13}$ C-terminus. For drug screening efforts the IP-One approach was chosen rather than intracellular calcium mobilisation, since IP-One offered the option of a long ligand incubation period coupled with an accumulative response rather than a rapid and transient signal associated with the Ca^{2+} assay, which has previously been employed for GPR35 ligand characterisation efforts (Jenkins et al., 2011; Taniguchi et al., 2006; Wang et al., 2006a).

As such, using the $G\alpha_q$ chimeras, GPR35 signalling was transferred through the $G\alpha_{q/11}$ pathway to the inositol phosphate (IP) cascade. The major product of this pathway, inositol 1,4,5 trisphosphate (IP_3), is degraded rapidly and difficult to quantify. However in the presence of lithium chloride, the IP_3 metabolite inositol monophosphate (IP_1) can be maintained and quantified. Thus, agonist stimulation of the $G\alpha_q$ pathway can be measured through accumulation of IP_1. To monitor this process I employed a commercially available IP-One assay kit (see **Section 2.7.2**). The IP-One assay utilises homogeneous time resolved fluorescence (HTRF®) to assess IP_1 accumulation through utilisation of a Cryptate labelled anti-IP_1 antibody that binds endogenously produced IP_1, followed by addition of a dye-

labelled IP_1 molecule that competes with any remaining anti-IP_1. This process generates a competitive quantitative immunoassay that is inversely proportional to the level of endogenously generated IP_1.

3.1.5 *Assessment of cell number on IP_1 accumulation at human GPR35*

To optimise the IP-One assay for GPR35, donor to acceptor transfection ratio, seeding cell density, and incubation time was assessed using both the $G\alpha_{qi1/2}$ and $G\alpha_{q13}$ chimeras. Since various transfection ratios provided similar signal windows (data not shown), a ratio of 1:1 between GPR35 and the $G\alpha_q$ chimera was utilised throughout. A density of 5,000 (**Fig 3.6A**) and 10,000 (**Fig 3.6B**) cells per well was used to assess the effect of cell number upon zaprinast induced IP_1 accumulation. Cells expressing human GPR35, $G\alpha_{qi1/2}$ or $G\alpha_{q13}$ chimeras were treated with zaprinast (100 μM) for two hours and generated an increase in IP_1 accumulation that was greater than the response associated with the vehicle control (DMSO, 0.1 %). Furthermore, in cells expressing GPR35 and G protein chimera, the magnitude of IP_1 accumulation was substantially higher at 10,000 cells per well than that generated at 5,000 cells per well (**Fig 3.6A/B**). Interestingly, the basal signal was higher for human GPR35 when co-expressed in the presence of $G\alpha_{q13}$ in the absence of zaprinast treatment at 10,000 cells per well, indicating constitutive activity between human GPR35 and $G\alpha_{q13}$ in the IP-One cell system (**Fig 3.6B**). Human GPR35/pcDNA3.1 and human GPR35/$G\alpha_q$ failed to significantly increase IP_1 accumulation following zaprinast treatment at either cell density, indicating that the responses generated did not occur as a result of zaprinast induced GPR35-indepenent or $G\alpha_q$-chimera independent signalling through the IP_1 pathway (**Fig 3.6A/B**).

3.1.6 *Assessment of ligand incubation time on IP_1 accumulation*

Although I had initially used the maximum ligand incubation time suggested by the manufacturer when optimising cell number in the IP-One assay, I wanted to justify this decision by ensuring that a shorter time point did not provide a similar magnitude of IP_1 accumulation. Assessment of IP_1 accumulation at one (**Fig 3.6C**) or two (**Fig 3.6D**) hours confirmed that IP_1 accumulation increased with a longer ligand incubation period for both

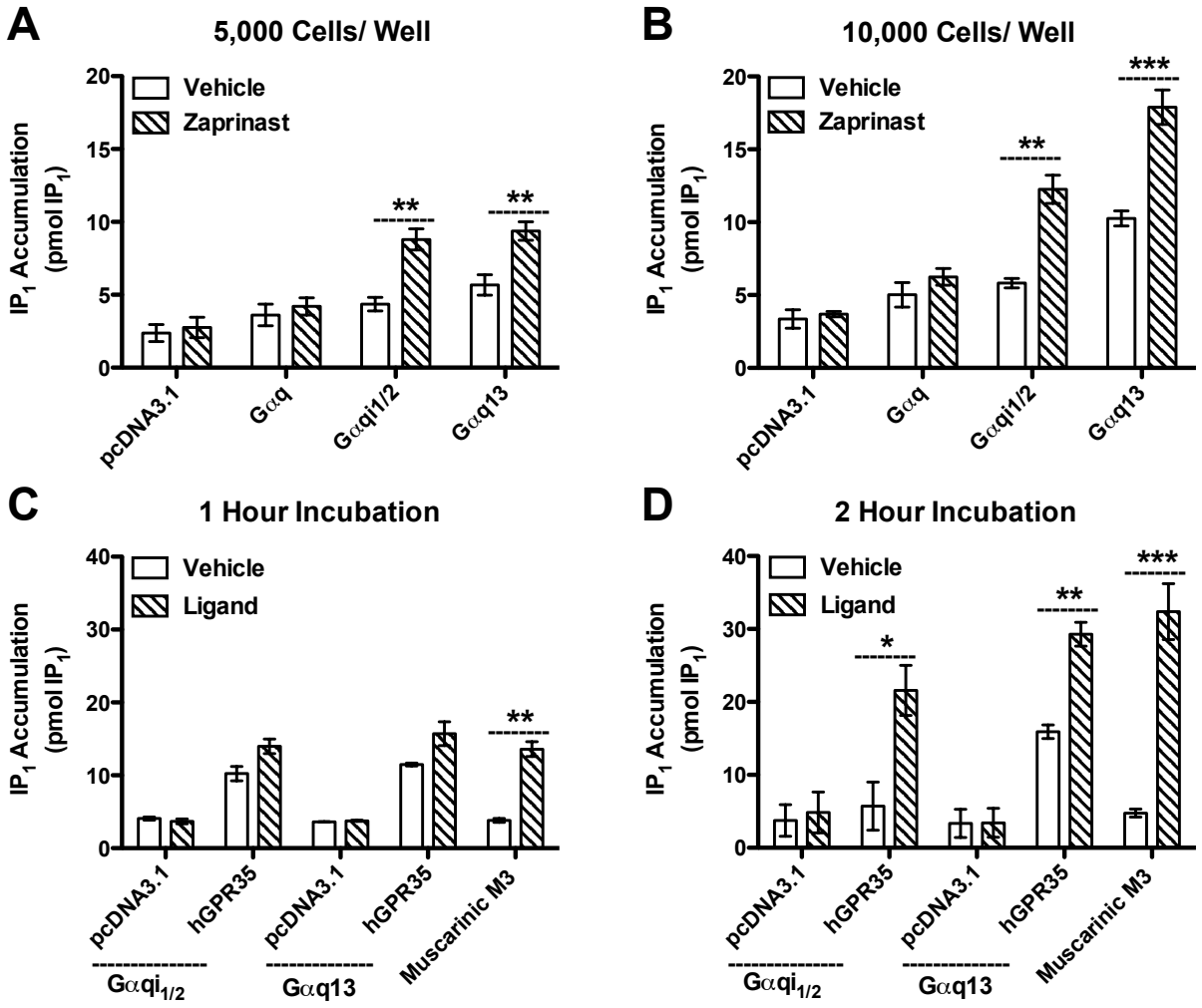

Figure 3.6 Optimisation of the IP-One assay using $G\alpha_{qi1/2}$ and $G\alpha_{q13}$ chimeras with human GPR35

HEK293T cells were transiently co-transfected to express FLAG-human GPR35a-eYFP and a $G\alpha_q$ chimeric G protein $G\alpha_{qi1/2}$ or $G\alpha_{q13}$. The FLAG-muscarinic M3 receptor was transfected as a positive control. The IP-One assay quantified IP_1 accumulation through an immuno-competition occurring between a cryptate labelled monoclonal anti-IP1 antibody (acceptor) and a IP_1 labelled D2 dye (donor) using HTRF® technology, is presented as pM IP_1 accumulation. Following a two-hour incubation at 37°C with zaprinast, IP_1 accumulation was assessed at cell densities of 5,000 (**A**) and 10,000 (**B**) cells per well. Using 10,000 cells per well, ligand incubation time was assessed post zaprinast treatment for one (**C**) or two hours (**D**). Cells expressing the M3 receptor were incubated in the presence or absence of 10 mM carbachol. All other responses were assayed with 100 μM zaprinast or DMSO, 0.1 %. Significance was denoted by *P* = ***≤ 0.001, **≤ 0.01 or *≤ 0.05. Data are presented as mean ± SEM of three independent experiments carried out in triplicate.

the $G\alpha_{q13}$ ($P \leq 0.01$) and $G\alpha_{qi1/2}$ ($P \leq 0.05$) chimeras with human GPR35. Furthermore, in addition to a higher maximal response, the difference between unstimulated and stimulated responses also increased, and generated a higher signal to background ratio after two hours. This was observed for GPR35 and the muscarinic M3 receptor. The M3 receptor was employed as a positive control for IP_1 accumulation as M3 couples to $G\alpha_q$ following incubation with carbachol (Offermanns et al., 1994). Application of carbachol to cells expressing M3 generated HTRF with an increase in IP_1 accumulation of 9.8 pmol at one hour and 27.6 pmol after two hours ($P \leq 0.001$) (**Fig 3.6C/D**). Importantly, there was no zaprinast stimulated increase in IP_1 accumulation for pcDNA3.1-$G\alpha_{qi1/2}$ or pcDNA3.1-$G\alpha_{q13}$, indicating that GPR35 must be present to direct $G\alpha_{i1/2}$ and $G\alpha_{13}$ signalling through the $G\alpha_q$ pathway (**Fig 3.6C/D**).

3.1.7 *Assessment of agonist potency using $G\alpha_q$ chimeras at human and rat GPR35*

To determine which $G\alpha_q$ chimera would be best suited for future drug discovery efforts (to be carried out using both human GPR35 and species orthologues), various concentrations of zaprinast were assessed using $G\alpha_{qi1/2}$ and $G\alpha_{q13}$ chimeras with human and rat GPR35 (**Fig 3.7**). Both the $G\alpha_{qi1/2}$ and $G\alpha_{q13}$ chimera expressing cells displayed similar potency to zaprinast at human (pEC_{50} 6.86 ± 0.19 and 7.09 ± 0.06, respectively) and rat (pEC_{50} 8.38 ± 0.19 and 8.61 ± 0.21, respectively) GPR35. However for both orthologues, the observed response of the $G\alpha_{qi1/2}$ chimera was significantly lower than that of the $G\alpha_{q13}$ chimera ($P \leq 0.01$). This suggested that while either chimera would be suitable for subsequent assays, the $G\alpha_{q13}$ chimera would provide a higher signal (**Fig 3.7A**). Thus, at human and rat GPR35, subsequent IP-One assays were carried out using the $G\alpha_{q13}$ chimera only.

3.1.8 *Assessing agonist-induced responses at species orthologues of GPR35 using $G\alpha_{q13}$ in the IP-One assay*

To determine the activity of the previously identified GPR35 agonists in the IP-One assay format, the responses of pamoic acid and cromolyn were assessed alongside zaprinast

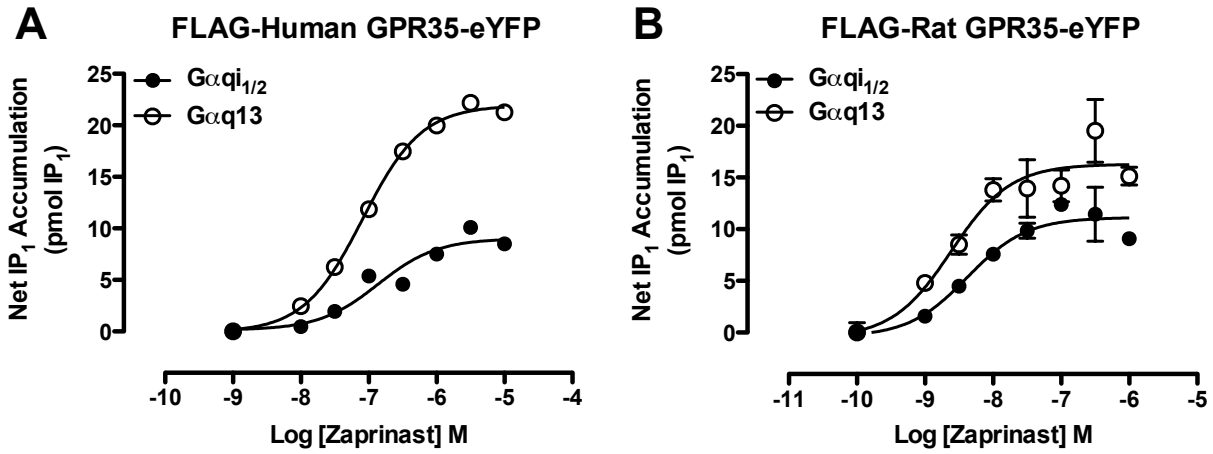

Figure 3.7 Zaprinast-induced coupling of $G\alpha_{qi1/2}$ and $G\alpha_{q13}$ chimeras at human and rat GPR35 assessed in the IP-One assay Concentration responses to zaprinast were generated following a two-hour incubation at 37°C using 10,000 cells per well. FLAG-human GPR35-eYFP (**A**) or FLAG-rat GPR35-eYFP (**B**) were transiently transfected with $G\alpha_{qi1/2}$ (closed circles) or $G\alpha_{q13}$ (open circles). Data represent the mean ± SEM of two independent experiments carried out in duplicate. Efficacy was baseline corrected to normalise for differences in constitutive activity.

using $G\alpha_{q13}$ at human and rat GPR35. Prior to development of the IP-One assay system, measures of potency and efficacy for these agonists at species orthologues had been assessed through the BRET-based β-arrestin-2 recruitment assay, which suggested that different profiles of species selectivity were generated by all three aforementioned agonists (Jenkins et al., 2010; Jenkins et al., 2012).

Within the IP-One system, zaprinast acted with significant, 25-fold, rat selectivity ($P \leq 0.001$) (**Fig 3.8A**; **Table 3.2**). Pamoic acid, conversely, acted with potency that was 195-fold human selective ($P \leq 0.001$), and generated a significant difference in efficacy between human and rat GPR35 ($P \leq 0.001$) compared to zaprinast (**Fig 3.8B**). Cromolyn, distinctly, displayed similar potency at human and rat GPR35 although the efficacy was significantly lower at human GPR35 ($P \leq 0.05$) compared to the zaprinast response (**Fig 3.8C**). Overall, agonist measures of potency and efficacy as generated in the IP-One system were generally higher than those reported from of the BRET-based β-arrestin-2 recruitment assay (Jenkins et al., 2012), although the rank order of potency and profiles of species selectivity were maintained between the two systems. As a result, the IP-One assay format was established as an important G protein dependent output for the assessment of ligand responses at GPR35.

3.1.9 *Assessment of constitutive activity of GPR35 using the IP-One assay system with ML-145 and CID-2745687*

Since the IP-One assay system appeared to detect agonist-independent constitutive activity for human and rat GPR35 in the presence of $G\alpha_{q13}$, the IP-One assay also provided a means to assess the pharmacology of GPR35 antagonists in a constitutively active system. Importantly, the GPR35 antagonists ML-145 and CID-2745687 had previously been reported to act as simple competitive antagonists in the BRET-based β-arrestin-2 system, which fails to display constitutive activity (Mackenzie et al., 2014). To assess antagonist pharmacology of GPR35 using the IP-One system, HEK293T cells containing FLAG-human GPR35-eYFP and $G\alpha_{q13}$ were assayed in the presence of antagonist only, agonist only, or a combination of agonist (at an EC_{80} concentration) and an antagonist.

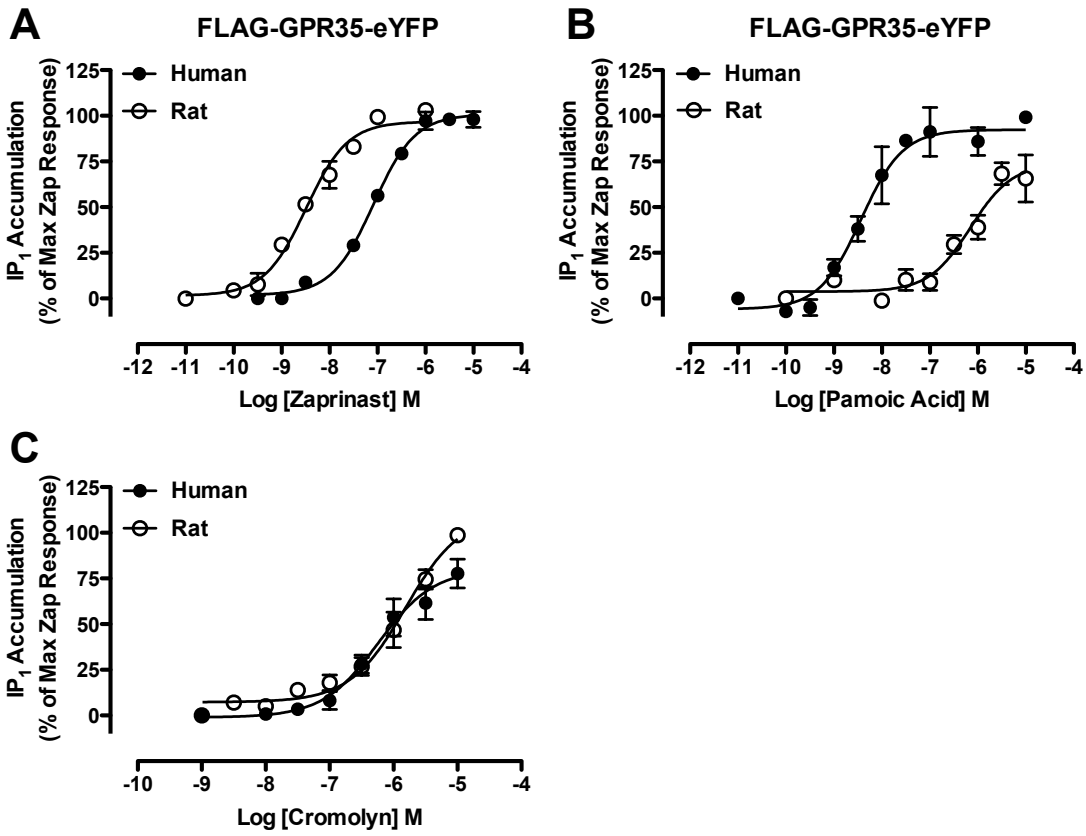

Figure 3.8 Agonist-induced $G\alpha_{q13}$ coupling to human and rat GPR35 measured in the IP-One assay

Human (closed circles) and rat (open circles) GPR35 were transiently transfected alongside $G\alpha_{q13}$ and assessed for ability to accumulate IP_1 following a two-hour incubation with zaprinast (**A**), pamoic acid (**B**) or cromolyn (**C**). Efficacy was normalised to the maximum best-fit zaprinast response generated at each species orthologue. Data are presented as the mean ± SEM of a minimum of four independent experiments carried out in duplicate.

Table 3.2 Zaprinast and pamoic acid but not cromolyn display GPR35 species selectivity in the IP-One assay

	Human	Rat
Ligand	**pEC_{50}[a] and (E_{max})[b]**	
Zaprinast	**7.09 ± 0.05**	**8.49 ± 0.08**
	100.9 ± 1.9	96.8 ± 3.3
Pamoic Acid	**8.44 ± 0.13*** **	**6.15 ± 0.18*** **
	92.4 ± 5.1	73.8 ± 6.9*
Cromolyn	**6.24 ± 0.13** **	**5.82 ± 0.11*** **
	80.1 ± 5.5*	110.2 ± 8.5

[a] Significant differences from the pEC_{50} of zaprinast, denoted with *P* = ***≤ 0.001, ** ≤ 0.01, * ≤ 0.05

[b] E_{max} normalised to the maximum best-fit zaprinast response with significantly different efficacy denoted as *P* = ***≤ 0.001, ** ≤ 0.01, * ≤ 0.05

Data are the mean ± SEM of a minimum of 4 independent experiments carried out in duplicate

ML-145, which was the more potent of the two antagonists (**Table 3.3**), reduced the IP_1 accumulation response below the vehicle level (**Fig 3.9A**). When pre-equilibrated with GPR35 and challenged with 300 nM zaprinast, ML-145 reduced the signalling below the zaprinast-only response to the level associated with ML-145 alone, and toward the level of the pcDNA3.1/$G\alpha_{q13}$ negative control (**Fig 3.9A**). This suggested that ML-145 displayed inverse agonism to reduce basal and agonist-induced responses at human GPR35. Assessment of CID-2745687 resulted in a similar profile of inverse agonism, although responses were less potent than those generated at ML-145 (**Table 3.3**) as noted previously (Jenkins et al., 2012; **Appendix A**). CID-2745687 acted to reduce IP_1 accumulation below the level of the vehicle response, and also in a concentration dependent manner reduced the 300 nM zaprinast response below the agonist-only level (**Fig 3.9B**; **Table 3.3**). As presented initially in the BRET-based β-arrestin-2 assay (**Appendix A**) however, the pharmacology at human GPR35 did not translate to the rat orthologue, as addition of 10 nM zaprinast was not concentration dependently reduced using either ML-145 (**Fig 3.9C**) or CID-2745687 (**Fig 3.9D**). Therefore, these data indicated that the GPR35 antagonist compounds acted with marked human-selectivity in both G protein and β-arrestin-2 recruitment systems as assessed in HEK293T cells, with the IP-One system providing a means to assess ligand-independent GPR35 constitutive activity.

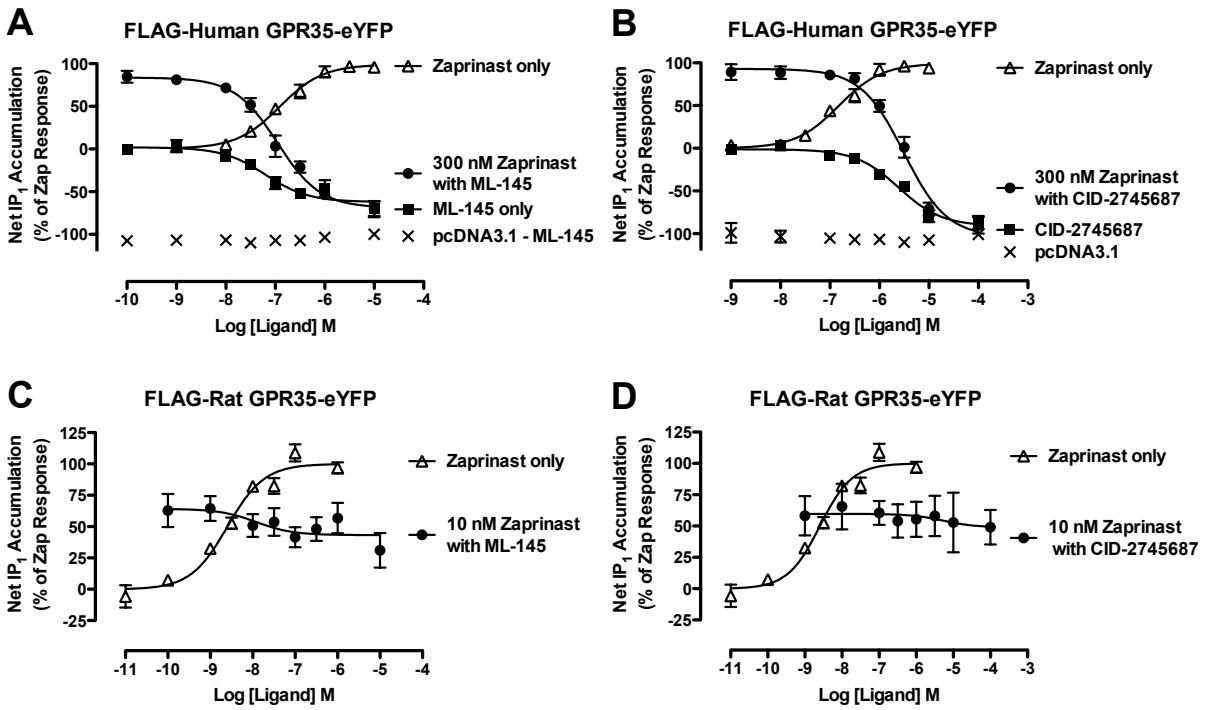

Figure 3.9 ML-145 and CID-2745687 are inverse agonists at human but not rat GPR35 ML-145 and CID-2745687 were pre-incubated with transiently co-transfected HEK293T cells containing $G\alpha_{q13}$ for 15 min at 37°C before a two-hour agonist incubation. At human GPR35, ML-145 (**A**) or CID-2745687 (**B**) were assayed against 300 nM zaprinast (black circles), alongside a zaprinast-only (clear triangles), or antagonist-only (black squares) response. The negative control, pcDNA3.1/$G\alpha_{q13}$, was assessed with antagonist only (crosses). At rat GPR35, zaprinast (10 nM) was incubated with ML-145 (**C**) or CID-2745687 (**D**) (black circles), and is displayed alongside zaprinast-only responses (open triangles). Data represent the mean ± SEM of three independent experiments. Efficacy is normalised as a percentage of the zaprinast response at the GPR35/$G\alpha_{q13}$ transfected cells, with the basal response set to zero.

Table 3.3 ML-145 and CID-2745687 inhibit both basal activity and agonist-induced responses at human GPR35 in the IP-One assay

	pIC_{50} Values - IP-One Assay			
	FLAG-Human GPR35-eYFP		FLAG-Rat GPR35-eYFP	
Ligand	**ML-145**	**CID-2745687**	**ML-145**	**CID-2745687**
Zaprinast	6.96 ± 0.09	5.51 ± 0.08	NA	NA
Antagonist Only	7.20 ± 0.18	5.61 ± 0.10	NT	NT

NA, not applicable; NT, not tested

Data represent the mean ± SEM of three independent experiments carried out in duplicate.

3.2 Investigating the GPR35 internalisation process

The majority of ligand screening at GPR35 has been carried out through assessment of ligand induced β-arrestin-2 recruitment and/or receptor internalisation outputs (Jenkins et al., 2010; Zhao et al., 2010; Deng et al., 2011a; 2011b; Deng and Fang 2012a; Neetoo-Isseljee et al., 2013; Southern et al., 2013), which has provided a robust measure of GPR35 pharmacology *in vitro*. Herein, agonist induced stimulation at the level of β-arrestin recruitment (using BRET technology) and receptor internalisation (using confocal microscopy and high content imaging) were optimised and presented as assay systems for the assessment of novel ligands.

3.2.1 *Measuring the kinetics of β-arrestin recruitment*

BRET technology is based on the principle of nonradiative energy transfer occurring between the electromagnetic dipoles of a luminescent energy donor (*Renilla* luciferase) and a fluorescent energy acceptor (eYFP). Given close proximity occurring between these polypeptides and degradation of luciferase substrate coelenterazine h, energy is emitted and is transferred from donor to acceptor and subsequently re-emitted at a characteristic wavelength, which can be quantified using a luminescence-readout (**Section 2.7.3**). This luminescent signal decays within the order of tens of minutes. The BRET-based β-arrestin recruitment assay employed herein has previously been utilised and optimised extensively for GPR35 (Jenkins et al., 2010; Jenkins et al., 2011; Jenkins et al., 2012; Mackenzie et al., 2014). It employs a C-terminal eYFP molecule linked to GPR35 and a *Renilla* luciferase (Rluc) tagged β-arrestin and these were transiently co-transfected in a 4:1 ratio (see **Section 2.7.3** for details).

To ensure the optimal arrestin subtype and timeframe were employed for drug screening efforts, a kinetic BRET approach was taken to assess zaprinast stimulated β-arrestin recruitment to human GPR35 (**Section 2.7.4**). To this end, zaprinast (10 μM) was added to transiently co-transfected HEK293T cells expressing FLAG-human GPR35-eYFP and β-arrestin-1-Rluc or β-arrestin-2-Rluc proteins and BRET occurring between these proteins monitored over a 45 min period (**Fig 3.10A/B**). Notably, while both β-arrestin-1 and

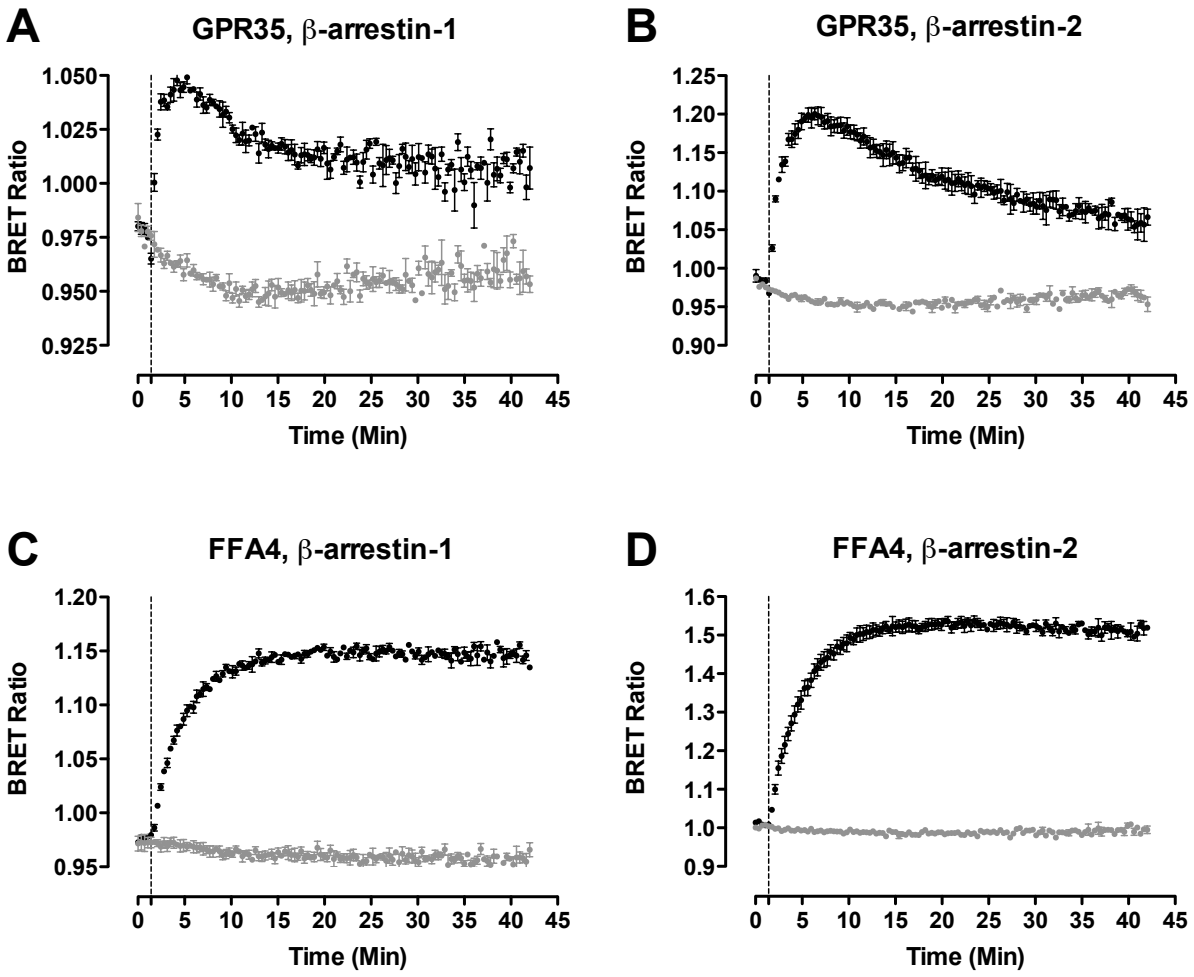

Figure 3.10 Human GPR35 and FFA4 generate a higher BRET response at β-arrestin-2 HEK293T cells were transiently co-transfected with FLAG-receptor-eYFP and β-arrestin-*Renilla* luciferase, with agonist induced coupling monitored kinetically using BRET technology (**Section 2.7.3** and **Section 2.7.4**). Human GPR35 and human FFA4 recruited β-arrestin-1 (**A**/**C**) and β-arrestin-2 (**B**/**D**) following treatment with agonist, (black circles) but not vehicle, 0.01% DMSO (grey circles). Zaprinast (10 μM) or TUG-891 (10 μM) (Hudson et al., 2013c) was used to stimulate BRET at GPR35 or FFA4, respectively. The BRET ratio is calculated by acceptor (luciferase) luminescence divided by donor (eYFP) luminescence. Data are representative of the mean ± SEM of two independent experiments carried out in duplicate.

β-arrestin-2 subtypes were recruited to GPR35, the magnitude of the BRET signal was greater for β-arrestin-2. Despite this, the kinetic profile at GPR35 was similar for both β-arrestin-1 and β-arrestin-2 subtypes with an induced BRET ratio peak that occurred 5 min post addition and subsequently decreased over time. Importantly, β-arrestin recruitment did not ensue following vehicle addition (DMSO, 0.01 %) indicating that the BRET signal measured occurred as a result of zaprinast stimulated receptor activation only (**Fig 3.10A/B**).

To assess whether the gradual decline in BRET signal observed after 5 min of zaprinast treatment was an artefact associated with coelenterazine h oxidation or was indeed a genuine occurrence, the kinetics of β-arrestin interaction with the free fatty acid receptor FFA4 were assessed following stimulation with the synthetic agonist TUG-891 (10 μM) (Hudson et al., 2013c) (**Fig 3.10C/D**). FFA4 was chosen since previous results from within our laboratory indicated that the kinetic profile of the interaction between FFA4 and β-arrestin-2 are maintained over time (Butcher et al., 2014). Indeed, TUG-891 (but not vehicle) stimulated FFA4 to recruit β-arrestin-1 and β-arrestin-2 with a peak at approximately 10 min that was maintained over the 45 min assay duration. These data, therefore, indicate that the kinetics of the GPR35-β-arrestin recruitment interaction display rapid association followed by a slow disassociation, and thus placed a greater emphasis on ensuring that the correct time point was employed to ensure the strongest signal was obtained for subsequent drug screening, set time-point, BRET assays.

3.2.2 *Measuring agonist potency at GPR35 species orthologues using the BRET-based β-arrestin-2 recruitment assay*

Next, since β-arrestin-2 provided a greater magnitude of net BRET as compared with β-arrestin-1, agonist-induced β-arrestin-2 recruitment was quantified following incubation with varying concentrations of agonist. Zaprinast, pamoic acid and cromolyn stimulated β-arrestin-2 BRET has previously been quantified at human, mouse, and rat species orthologues of GPR35 (Jenkins et al., 2012), and this data was therefore used to ensure reproducibility and data quality prior to undertaking subsequent drug screening efforts.

Prior to commencement of the BRET assay, cell surface receptor expression was assessed visually using fluorescence microscopy (data not shown), while total receptor

expression was quantified by measuring eYFP fluorescence (**Fig 3.11A**). Subsequently, agonist-induced β-arrestin-2 BRET was quantified following a 5-minute agonist incubation, and these studies replicated previously published findings (Jenkins et al., 2012). This included zaprinast, which was active at all three species orthologues and acted with significant rat selectivity ($P \leq 0.001$) (**Fig 3.11B**; **Table 3.4**); pamoic acid, which acted with human selectivity ($P \leq 0.001$) and partial efficacy at human GPR35 ($P \leq 0.001$), but recorded weak or no responses at rat and mouse, respectively (**Fig 3.11B**); and cromolyn, which acted at all three species orthologues but generated pEC_{50}s at human and rat that were significantly different from mouse ($P \leq 0.001$), indicating human and rat selectivity (**Fig 3.11D**). These findings suggested that the BRET assay format could be employed to assess ligand induced responses of novel ligands arising through subsequent drug discovery efforts and could complement data obtained through the IP-One assay.

3.2.3 *An assessment of GPR35 internalisation following agonist stimulation*

Since receptor internalisation assays have also been successfully employed at GPR35 for characterisation of ligand-induced responses, two distinct assays were employed herein that monitored the receptor internalisation process. Because transiently transfected GPCRs often suffer from variability in the cell surface expression level within and between transfections and are associated with a higher level of internalised receptor, a doxycycline inducible Flp-In™ T-REx™ HEK293 cell line that stably expressed FLAG-human GPR35-eYFP on demand was employed. Using confocal microscopy, live-cell receptor internalisation was imaged following zaprinast stimulation (100 μM) over a 45-minute period (**Fig 3.12A**) (**Section 2.7.7**). At 0 minutes, prior to zaprinast addition, the majority of eYFP-tagged receptor appeared to localise to the cell surface. Upon application of zaprinast however, definition of the cell surface became less distinct and punctate clusters of receptor began to form within intracellular vesicles, indicating that the receptor internalisation process was underway.

To quantify this process, and to utilise the internalisation output as a measure of agonist-induced potency, an ArrayScan™ high content imager was employed (**Section 2.7.6**). ArrayScan™ technology utilises a proprietary algorithm to quantify receptor internalisation by identifying fluorescence present in endocytic compartments, appearing as punctate

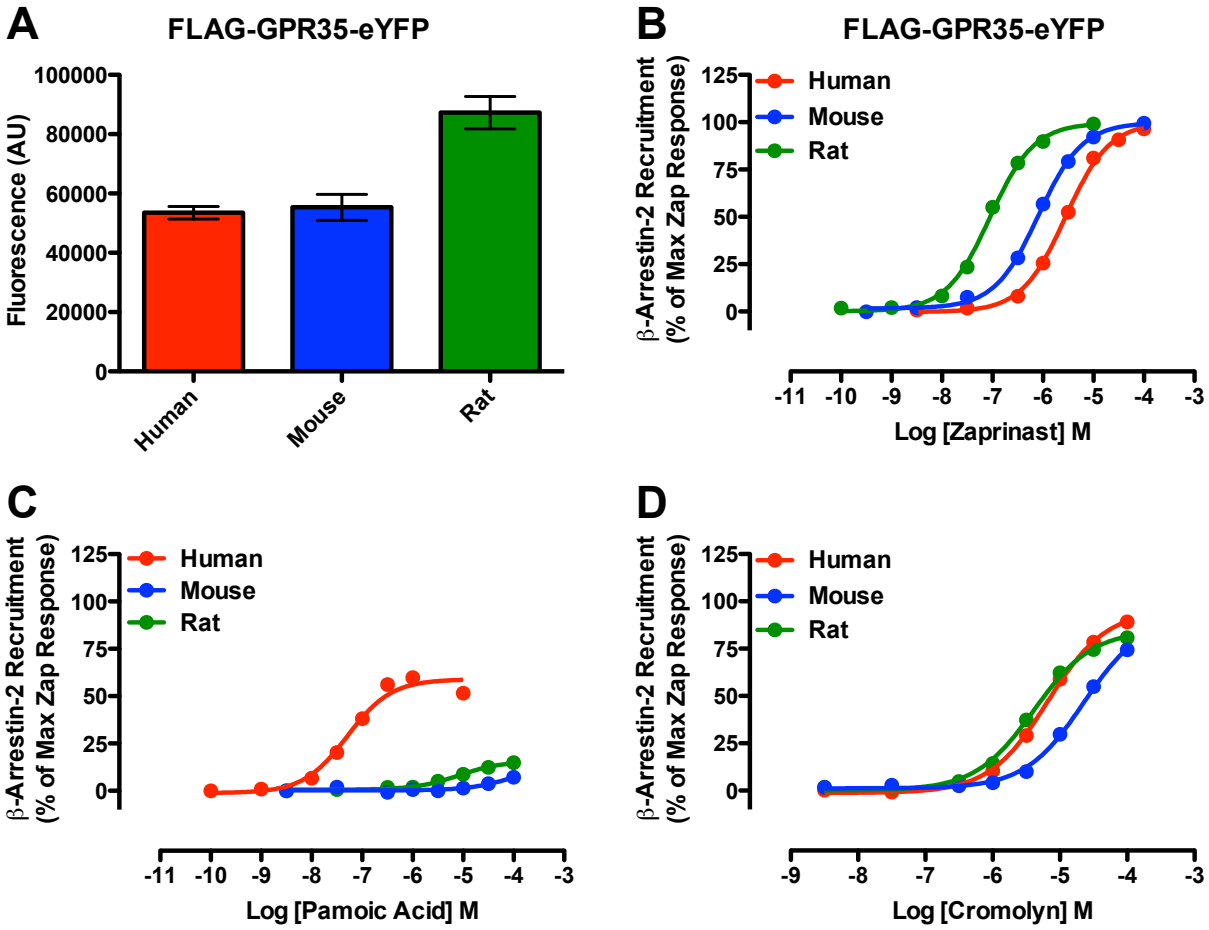

Figure 3.11 eYFP expression and β-arrestin-2 recruitment profiles at GPR35 species orthologues Before BRET analysis was carried out, cells transiently transfected with FLAG-GPR35-eYFP and β-arrestin-2-*Renilla* luciferase constructs were assessed for eYFP fluorescence (**A**), which was gain adjusted on each occasion to the human receptor. Zaprinast (**B**), pamoic acid (**C**) and cromolyn (**D**) induced β-arrestin-2 recruitment to human (red), mouse (blue) or rat (green) GPR35 was quantified using BRET responses 5 min post ligand addition (**Section 2.7.3**). Efficacy was normalised to the maximum best fit zaprinast response, with mean ± SEM presented from a minimum of 6 independent experiments carried out in duplicate.

Table 3.4 Agonists display species selectivity at GPR35 in the BRET-based β-arrestin-2 recruitment assay

	pEC_{50}[a] and E_{max}[b] Values - BRET		
Ligand	**Human**	**Mouse**	**Rat**
Zaprinast	**5.56 ± 0.01**	**6.09 ± 0.02**	**7.01 ± 0.02**
	99.9 ± 0.7	99.8 ± 1.0	99.6 ± 1.0
Pamoic Acid	**7.30 ± 0.06*** **	**Inactive**	**5.08 ± 0.2*** **
	58.9 ± 1.4***	NR	15.8 ± 1.7***
Cromolyn	**5.18 ± 0.02**	**4.65 ± 0.05*** **	**5.39 ± 0.03*** **
	95.5 ± 1.2	91.5 ± 3.5	84.8 ± 1.0*

[a] A statistically different pEC_{50} from zaprinast is denoted, *P* ***≤ 0.001, ** ≤ 0.01, * ≤ 0.05

[b] Efficacy is normalised as a percentage of the maximum best fit zaprinast response. Significantly different responses are denoted, *P* = ***≤ 0.001, ** ≤ 0.01, * ≤ 0.05

Data are a mean ± SEM of a minimum of 6 independent experiments carried out in duplicate

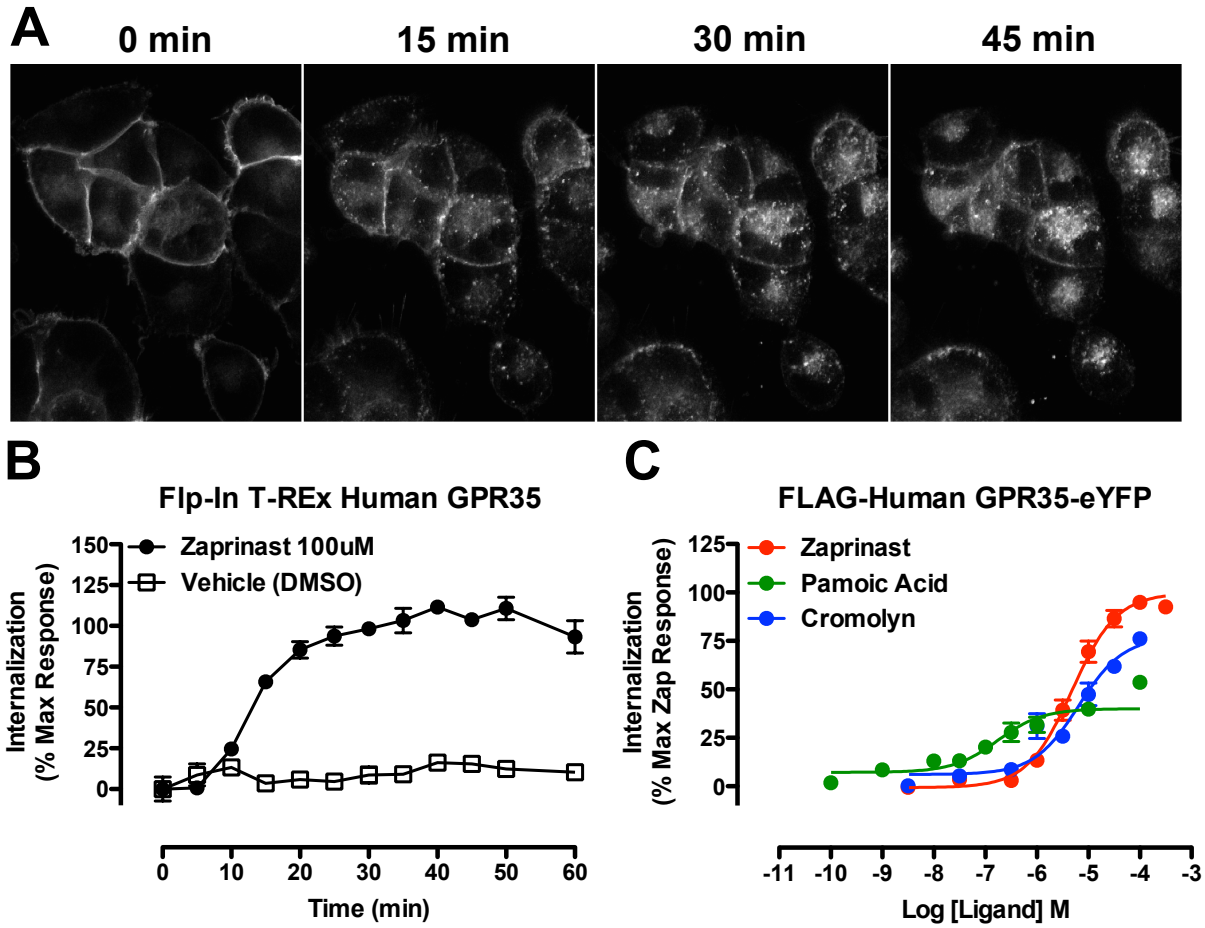

Figure 3.12 High content imaging reveals the GPR35 agonists induce GPR35 internalisation Flp-In™ TREx™ HEK293 cells were doxycycline induced to stably express FLAG-human GPR35-eYFP. Live cell confocal imaging captured agonist-induced GPR35 internalisation over 15 min periods using 100 μM zaprinast (**A**) as described (**Section 2.7.7**), and performed with Dr. John Pediani. For high content imaging using ArrayScan™ technology (**Section 2.7.6**), cells were incubated with agonist, fixed using 4 % paraformaldehyde, and internalisation quantified using the ArrayScan™ incorporated algorithm. An internalisation time-course was carried out using zaprinast, 100 μM (black circles) or vehicle, 0.1% DMSO (clear circles) over a 60 min period (**B**) with subsequent concentration responses to zaprinast (red), pamoic acid (green) and cromolyn (blue) quantified following a 45 min ligand incubation (**C**). Panels **A** and **B** are representative of two independent experiments, while **C** is presented as the mean ± SEM of three independent experiments carried out in triplicate.

Table 3.5 GPR35 agonists zaprinast, cromolyn and pamoic acid induce receptor internalisation

	FLAG-Human GPR35-eYFP	
Ligand	**pEC_{50} [a]**	**E_{max} [b]**
Zaprinast	**5.32 ± 0.07**	**99.7 ± 3.2**
Pamoic Acid	**6.76 ± 0.19*** **	**40.0 ± 3.0*** **
Cromolyn	**5.19 ± 0.11**	**77.0 ± 4.3** **

[a] Pamoic acid generated a statistically different pEC_{50} from zaprinast, denoted P = *** ≤ 0.001

[b] Efficacy is normalised to the maximum best fit zaprinast response (%), with significantly different responses denoted, P = ***≤ 0.001 or ** ≤ 0.01

Data are the mean ± SEM of three independent experiments carried out in triplicate

'spots'. To optimise the ArrayScan™ assay format, a suitable timeframe for agonist stimulation was identified through quantification of zaprinast induced receptor internalisation over a 60-minute period (**Fig 3.12B**). Application of zaprinast (100 μM) generated a substantial increase in FLAG-human GPR35-eYFP internalisation relative to the vehicle control (DMSO, 0.1%) between 20 and 60 minutes with a peak occurring between 40 and 50 minutes.

As a result, subsequent agonist-incubations were carried out for 45 minutes. To perform a comparison of agonist potency, concentration responses to zaprinast, cromolyn and pamoic acid were quantified in their ability to internalise GPR35 using ArrayScan™ technology (**Fig 3.12C**). Importantly, the profile of agonist potency and efficacy was maintained between the BRET-based β-arrestin-2 recruitment and the ArrayScan™ system (**Table 3.5**), with pamoic acid ($P \leq 0.001$) and cromolyn ($P \leq 0.01$) maintaining partial efficacy. Furthermore, the rank order of potency was also shared between ArrayScan™ and IP-One assay formats. As a result of this, the ArrayScan™, IP-One, and BRET assay systems were carried forward for subsequent ligand characterisation efforts at GPR35.

3.3 Assessing GPR35 agonism in an endogenous cell system

The characterisation of GPR35 ligand responses in non-manipulated cell lines that endogenously express *GPR35* has proven difficult since the basic biology surrounding GPR35 signalling downstream from its immediate effectors has not yet been elucidated. Thus, 'label free' technology may offer particular benefit with respect to GPR35 as it offers the ability to simultaneously incorporate signalling from multiple pathways in an endogenous cell system and removes the need for knowledge of the signalling pathways associated with the receptor. Although a number of different label free technologies are available, the dynamic mass redistribution (DMR) format was employed since it had successfully been utilised for GPR35 screening efforts by others using the endogenously expressing immortalised colorectal adenocarcinoma cell line, HT-29 (Deng et al., 2011a; 2011b; 2012a).

The DMR format incorporates refractive waveguide grated optical biosensors within the glass plane of each assay plate that acts to filter polarised broadband light in proportion to DMR occurring approximately 150 nm above the surface of the sensor. Changes in cell shape, morphology, adherence, binding events or intracellular protein movements occurring as a result of ligand addition are captured using a charged coupled device camera as pixelated spectral images, and quantified in terms of picometer (pm) shift. Thus, to identify kinetic DMR traces and potency of GPR35 agonist compounds in an endogenous cell system, zaprinast, pamoic acid and cromolyn were assayed following DMR optimisation steps with the intention of characterising the endogenous 'GPR35' response prior to profiling of novel screening hit compounds.

3.3.1 *Assessment of* GPR35 *expression using RT-PCR in the HT-29 cell line*

Before assessing agonist induced DMR responses using the Epic Bench Top™ (BT) system, confirmation of expression of human *GPR35* messenger RNA in HT-29 cells was carried out using reverse transcriptase (RT)-PCR analysis (**Section 2.4.6**). The RT-PCR approach was taken as although antibodies reported to be directed against GPR35 are commercially available, specific detection of GPR35 was not obtained, despite anti-FLAG and anti-eYFP antibodies being able to detect epitope and fluorescently tagged versions of GPR35 (data not shown). Therefore, efforts to determine that signalling responses emanate

from GPR35 at the protein level have been obtained using GPR35-specific antagonists to silence receptor-mediated agonist-induced signalling.

All RT-PCR samples were assessed with short oligonucleotide forward and reverse internal GPR35 sequence primers. These included a no template control, a minus reverse transcriptase sample (to control for genomic contamination, since the human GPR35 primers used did not span an intron), a plus RT sample and genomic DNA positive control (**Fig 3.13A**). The presence of only one band of the predicted size (which was isolated and sequenced to confirm its identity) for the +RT sample that was not present in the negative controls confirmed *GPR35* mRNA expression in the human HT-29 cell line.

3.3.2 *Optimisation of the DMR assay format for GPR35 agonism in HT-29 cells*

The DMR assay format was optimised for GPR35 using the HT-29 cell system at a room temperature of 26 °C, ± 1 °C (**Section 2.7.8**). Initially, seeding cell density was assessed through quantified outputs of maximal response (**Fig 3.13B**) and potency (**Fig 3.13C**) for zaprinast and pamoic acid. The result of this was that kinetic DMR responses were increased with increasing cell number without an alteration in ligand potency, indicating that increasing cell number could generate an improved DMR signal. Since a maximal response was obtained at 30,000 cells per well, that did not further increase with cell number, subsequent assays were carried out using a cell seeding density of 30,000 cells per well.

Agonist compounds were added using an automated Biomek® FX^P liquid handling system (**Section 2.7.8**) before the plate was returned to the Epic BT™ system. Reference agonists zaprinast, pamoic acid, and cromolyn generated concentration responses with similar kinetic DMR traces, producing a peak that occurred immediately following agonist addition and decreased after a number of minutes (**Fig 3.13D**). To assess which time-point would be most suitable for extrapolation of kinetic responses into concentration response format, potencies generated within the peak DMR response for zaprinast and pamoic acid were presented relative to time (**Fig 3.13E**). The correlation indicated that potency was stable between 4 and 8 minutes and outwith this timeframe potency began to increase (**Fig 3.13D/E**). As a result, kinetic responses obtained at the 5-minute period were converted to concentration response format for each agonist (**Fig 3.13F**).

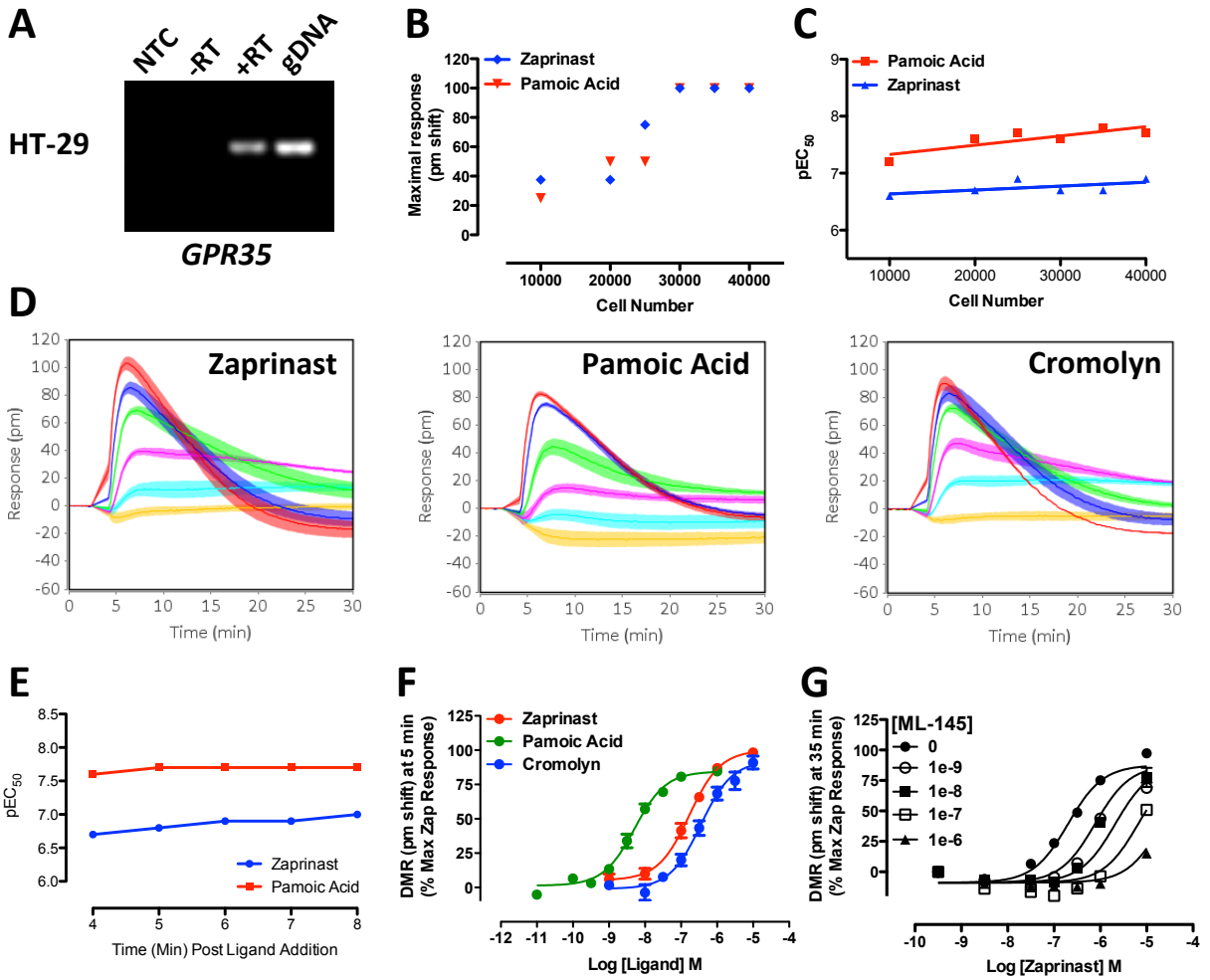

Figure 3.13 HT-29 cells endogenously express human *GPR35* and respond to ligand treatment as measured using the DMR system RT-PCR analysis depicted expression of *GPR35* mRNA transcripts. NTC, no template control, -/+ RT, minus or plus reverse transcriptase, gDNA, genomic DNA (**A**). Various cell-seeding densities were assessed for changes in signal (**B**) or potency (**C**) using zaprinast (blue) or pamoic acid (red). Using 30,000 cells per well label-free dynamic mass redistribution (DMR) kinetic traces (presented as picometer wavelength shift) were monitored over time in HT-29 cells at 26 °C following addition of agonist at 2 min (**D**). pEC_{50}s generated for zaprinast and pamoic acid within the peak DMR response were compared over time to determine a suitable time point for extrapolation of kinetic data into concentration responses (**E**). Agonist data extrapolated at 5 min post ligand addition is presented (**F**) with each concentration data point corresponding to an independent kinetic trace at 5 min as presented in (**D**). To assess whether this response occurred through agonism of GPR35, zaprinast was antagonised with increasing concentrations of ML-145, as indicated (**G**), with data fitted to the Gaddum-Schild EC_{50} shift global analysis. Efficacy was normalised to the maximum best-fit zaprinast response (**F**) or the maximum and minimum best-fit responses to correct for the inverse agonism associated with ML-145 (**G**). Data are the mean ± SEM of three (agonist) or two (antagonist) independent experiments.

Table 3.6 GPR35 agonist responses in DMR: comparisons with IP-One and BRET assays

	GPR35 agonist potency (pEC_{50})[a] and efficacy (E_{max})[b]		
Ligand	**DMR: HT-29 Cells**	**IP-One**	**BRET**
Zaprinast	**6.77 ± 0.07**	**7.09 ± 0.05**	**5.56 ± 0.01*** **
	100.0 ± 3.2	100.9 ± 1.9	99.9 ± 0.7
Pamoic Acid	**8.29 ± 0.06**	**8.44 ± 0.13**	**7.3 ± 0.06*** **
	84.5 ± 2.3	92.4 ± 5.1	58.9 ± 1.4***
Cromolyn	**6.45 ± 0.09**	**6.24 ± 0.13**	**5.18 ± 0.02*** **
	92.3 ± 4.1	80.1 ± 5.5	95.5 ± 1.2

[a] Statistically different pEC_{50}s from the DMR assay, denoted P = *** ≤ 0.001

[b] Efficacy (%), normalised to the maximum best-fit zaprinast response, with a statistically significant difference from the DMR format denoted P = *** ≤ 0.001

Data are the mean ± SEM of three independent experiments carried out in duplicate

3.3.3 *GPR35 agonists induce DMR in HT-29 cells*

Concentration response analysis emanating from the kinetic DMR profiles of zaprinast, pamoic acid, and cromolyn indicated that the rank order of potency was maintained between the endogenous HT-29 cell system and the manipulated HEK293 overexpressing IP-One and BRET systems (**Fig 3.13F; Table 3.6**). With regards to efficacy, pamoic acid recorded a response that was significantly lower than zaprinast ($P \leq 0.05$), and thus retained partial efficacy status, while cromolyn generated full efficacy in the DMR system (**Table 3.6**).

3.3.4 *Zaprinast mediated DMR in HT-29 cells through activation of GPR35*

Since the HT-29 cell system was not manipulated to specifically monitor GPR35 activation then, conceptually, responses could arise through non-GPR35 ligand effects. It was therefore necessary to ensure that the DMR kinetic traces generated were as a result of GPR35 agonism and not of a non-specific nature. A Schild plot experiment, carried out using ML-145, was undertaken to determine if increasing antagonist concentration could abolish the kinetic DMR traces of zaprinast. Indeed, application of increasing, fixed concentrations of ML-145 acted to rightward shift the zaprinast kinetic response to the point of inactivity (**Fig 3.13G**). Given that ML-145 abolished the characteristic 'GPR35 DMR peak' this indicates that zaprinast (and by extension pamoic acid and cromolyn) were inducing DMR as a result of GPR35 agonism.

3.4 Discussion

An important aspect of the early drug discovery process is the design and implementation of high-throughput GPCR functional assays that allow the cost-effective screening of large compound libraries to identify novel drug candidates. For orphan GPCRs this process is particularly valuable as characterisation of hit compounds can provide clues as to what the endogenous ligand may be. At GPR35, previous compound library screening efforts have led to the identification of agonist compounds such as pamoic acid, cromolyn, dicoumarol, niflumic acid and luteolin (Jenkins et al., 2010; Zhao et al., 2010). Orphan GPCRs can be difficult to screen compound libraries against since often little is known regarding the signalling profile of the activated receptor; however, the use of chimeric or promiscuous G proteins, β-arrestin assays, and most recently, label-free technologies, can overcome this problem. In an effort to identify suitable assay systems for drug screening and characterisation efforts at GPR35, a number of distinct experimental outputs were investigated, including a *S. cerevisiae* FDG 'yeast assay' with yeast-mammalian G protein chimeras; two distinct [^{35}S]GTPγS incorporation assays; an IP_1 accumulation assay with $G\alpha_q$ chimeras; a β-arrestin recruitment assay using BRET technology; an automated ArrayScan™ receptor trafficking programme to monitor receptor internalisation; and a 'label free' DMR assay to monitor ligand induced movement within the cell. While all of the assay systems described herein were functional, not all were suited as drug screening systems for GPR35, as discussed below.

3.4.1 *The yeast assay reveals GPR35 G protein activation profile but caution must be taken when using G protein chimeras*

Initial steps taken to assess the profile of G protein coupling at human and rat GPR35 employed the FDG yeast assay with a series of chimeric yeast-mammalian G proteins. Overnight incubation with zaprinast revealed a G protein coupling preference that was shared between human and rat GPR35 through Gpa1 -$G\alpha_{13}$, -$G\alpha_{i1/2}$ -$G\alpha_{i3}$ -$G\alpha_{oA/B}$ (**Fig 3.3**). Importantly this pharmacology appears to translate between yeast and mammalian systems, as GPR35 has been shown to couple to both $G\alpha_{13}$, and $G\alpha_{i/o}$ following zaprinast treatment in mammalian systems (Wang et al., 2006a; Taniguchi et al., 2006; Jenkins et al., 2010; Jenkins

et al., 2011; Deng et al., 2012a). Herein, and in the literature, GPR35 was reported to act in a manner specific for $G\alpha_{13}$ over $G\alpha_{12}$ (Jenkins et al., 2011; Deng et al., 2012a), indicating a selectivity within the $G\alpha_{12/13}$ family.

However, it is important to note that while the coupling profile of GPR35 appears to translate between systems, these yeast-mammalian G protein chimeras contain only the last five carboxyl amino acids of the mammalian G protein (Dowell and Brown, 2009). G protein chimeras do not always represent the true biology of the full-length sequence (Brown et al., 2003; Brown et al., 2011), since at least six other regions of the G protein are also involved in mediating contact and conferring specificity with the GPCR (Kostenis et al., 2005). Therefore, although this system offers considerable potential as a format to screen ligands for pathway bias, care should be taken when interpreting data and subsequent steps employed using full-length G proteins to ensure equivalence between assay systems.

3.4.2 *The yeast assay reveals a lack of species selectivity for G protein coupling and hints toward an important involvement for N-linked glycosylation at GPR35*

Application of zaprinast at GPR35 is usually associated with species selectivity, as zaprinast is reportedly some 25 fold selective for rat over human GPR35 (Taniguchi et al., 2006; Yang et al., 2010; Jenkins et al., 2011; Jenkins et al., 2012). This phenomenon also extends to numerous other ligands acting at GPR35, and is not a zaprinast specific effect (Jenkins et al., 2012; Neetoo-Isseljee et al., 2013; Funke et al., 2013; Mackenzie et al., 2014). Surprisingly, the data arising from the yeast assay revealed that human and rat GPR35 coupled to Gpa1 -$G\alpha_{13}$, -$G\alpha_{i3}$ -$G\alpha_{oA/B}$ with similar potency following zaprinast treatment, with a significant difference noted only for Gpa1-$G\alpha_{i1/2}$ (**Table 3.1**). Although the exact reason for this is unclear, and could indicate that as yet unidentified accessory proteins differentially regulate the human and rat receptors in mammalian systems, this difference could also be a result of the composition of the yeast cell wall. The cell wall of *S. cerevisiae* contains ergosterol rather than cholesterol, and recombinant proteins expressed in yeast are often glycosylated with high-mannose type sugars rather than complex N-linked oligosaccharides (Bonander and Bill, 2012).

The lack of complex N-linked glycosylation occurring in yeast has important ramifications for glycosylated mammalian proteins, which are typically non-functional if re-

expressed in a mammalian system (Wildt and Gerngross, 2005). Notably, rat GPR35 contains the N-linked glycosylation sequence (NxS/T) within ECL2 while human GPR35 does not. In **Chapter Five**, the ECL2 of human GPR35 is shown to play a role in ligand binding and species selectivity. It was previously demonstrated that treatment of human and rat GPR35 HEK293 membranes with PNGase F (Peptide-N-Glycosidase F; which cleaves N-linked glycoproteins) reduces human GPR35 from two distinct bands to one entity of 55 kDa, and rat is reduced to two distinct entities of 47 and 53 kDa from a range of different sizes observed prior to de-glycosylation, as indicated by Western blot analysis (Jenkins et al., 2011). This indicates that human and rat GPR35 are differentially N-glycosylated in HEK293 cells, existing as differently sized proteins before and after de-glycosylation (Jenkins et al., 2011).

While the N-terminus of many class A GPCRs (approximately 60 %) contain N-linked glycosylation, a lesser amount (approximately 32 %) contain a potentially glycosylated sequence within ECL2, where it is predicted that the oligosaccharide chain could be accommodated within the GPCR tertiary fold (Wheatley et al., 2012). Glycosylation in this region can act to pull ECL2 away from the ligand-binding pocket, or simply act to stabilise the conformation of the ECL2 loop (Wheatley et al., 2012). If this is the case at rat GPR35, it would appear that human and rat GPR35 could have a different topological structure in this region. This is supported by recent modelling efforts that predicted the ELC2 of human GPR35 to partially form a lid over the ligand binding pocket but with the ECL2 of rat being less involved in ligand binding (Mackenzie et al., 2014). Thus, in addition to providing a profile of G protein coupling at human and rat GPR35, the yeast system revealed that species selectivity does not occur following zaprinast treatment for the majority of Gpa1 G protein chimeras, and this could be a result of the lack of complex N-linked glycosylation in yeast. Mutating the rat NFS sequence in this region and/or introducing this sequence into human GPR35 (which is currently NFN), followed by assessment of receptor responses in a mammalian system would help clarify this, and is of considerable interest given the marked differences in species selectivity displayed by GPR35 ligands that limit the translatability of *in vitro* and *in vivo* research efforts.

3.4.3 *Limitations of [^{35}S]GTPγS incorporation with filtration assay for GPR35*

The [^{35}S]GTPγS incorporation assay was successfully employed to demonstrate G$\alpha_{i/o}$ coupling of GPR35 following stimulation with kynurenic acid (Wang et al., 2006a). However, as described herein, human GPR35 did not appear to couple to G$\alpha_{i/o}$ following zaprinast stimulation of membranes of HEK293T cells, while bovine FFA2, a receptor that endogenously couples to the G$\alpha_{i/o}$ family (Hudson et al., 2012b), incorporated [^{35}S]GTPγS following stimulation with its endogenous ligand valeric acid, suggesting that the assay format was functional (**Fig 3.4**). It is important to note that the results presented herein only assessed the ability of zaprinast to stimulate [^{35}S]GTPγS incorporation at GPR35, and further analyses should evaluate the kynurenic acid response in GPR35-transfected HEK293T cell membranes to ensure that the lack of the zaprinast response was not a ligand specific effect. However, as zaprinast induced-signalling can be abolished following PTX treatment in *GPR35* endogenously expressing cells (Wang et al., 2006a; Barth et al., 2009; Zhao et al., 2010; Fallarini et al., 2010), it appears that the lack of zaprinast-induced [^{35}S]GTPγS incorporation could be a result of the cell type used to assess the responses, indicating that GPR35 signalling could be influenced by the cellular background it is expressed within. It may be relevant that Chinese hamster ovary (CHO)-K1 cell membranes were employed for the kynurenic acid study (Wang et al., 2006a), while HEK293T cell membranes were utilised herein. Additionally, the kynurenic acid [^{35}S]GTPγS incorporation assay utilised by Wang and colleagues did not employ G$\alpha_{i/o}$ proteins that contained the C^{351}I mutation (Wang et al., 2006a). Given the critical role for the Gα C-terminus in enabling GPCR interaction, it is not surprising that manipulation to this sequence can negatively impact potency, agonist mediated GDP turnover (Carr et al., 1998), and/or efficacy (Wise et al., 1999). Expression of G$\alpha_{i/o}$ proteins in an insect cell system is a method that would enable quantification of full length G proteins without interference or cross-talk from endogenous G protein subunits, since insect G proteins are expressed at a level some 80 % lower than mammalian G proteins, in addition to insect G proteins sharing limited homology to their mammalian counterparts (Knight et al., 2003).

Lastly, it has been demonstrated that the glycosylation profile of recombinant proteins expressed in HEK293 and CHO cell lines differ significantly, with recombinant

proteins from CHO cells containing a higher number of sialic acid residues attached to the glycoproteins (Croset et al., 2012), with implications for cell surface delivery and half-life of the protein (Otto et al., 2004; Wide et al., 2010). Further to this, the CHO cells employed by Wang and colleagues stably expressed GPR35, while I carried out my studies using transiently transfected HEK293T cells. While there is inherent variability in the cell surface expression of GPCRs within and between cells following transient expression, this was the preferred option for these studies since CHO cells are less amenable to transient expression, and the amount of recombinant protein produced in CHO cells is substantially less than that associated with HEK293 cells (Wurm and Bernard, 1999; Pham et al., 2006; Baldi et al., 2007).

3.4.4 *[^{35}S]GTPγS incorporation with immunoprecipitation step*

Unlike the standard [^{35}S]GTPγS incorporation assay, zaprinast has been shown to successfully induce coupling between GPR35 and $G\alpha_{13}$ in a modified version of this assay (Jenkins et al., 2010). In this study, a Flp-In™ T-REx™ HEK293 cell line that stably expressed FLAG-human GPR35-eYFP following doxycycline treatment was transiently transfected with $G\alpha_{13}$ containing an internal 'EE' epitope sequence (EYMPME), to confirm that hits from the Prestwick chemical library activated GPR35 via $G\alpha_{13}$ (Jenkins et al., 2010). However, in order to try and achieve a larger signal window, instead of transfecting only the $G\alpha_{13EE}$ construct, I initially began by transiently transfecting both FLAG-human GPR35-eYFP and $G\alpha_{13EE}$, but came to the same conclusion: zaprinast was able to induce [^{35}S]GTPγS incorporation following an anti-EE immunocapture, but the magnitude of the response was small (**Fig 3.5A**).

3.4.5 *A GPCR-G protein fusion construct that does not enhance signalling*

Since the efficiency of GPCR-G protein coupling depends on the ratio of GPCRs to G protein, the level of expression of each protein, and spatial proximity within cellular membranes (Seifert et al., 1999b), a fusion construct between the C-terminus of GPR35 and the N-terminus of $G\alpha_{13EE}$ was generated. This was with the expectation that the 1:1

stoichiometry, the close proximity of the two polypeptides, and the tethering of $G\alpha_{13EE}$ to the cell membrane would increase the functional output of the response (Milligan, 2003b; Milligan et al., 2007). This has been successful for increasing [^{35}S]GTPγS incorporation at the dopamine D_2/D_3 (Lane et al., 2007), FFA1 (Stoddart et al., 2007) β2-AR (Bertin et al., 1994; Seifert et al., 1999a) and histamine H_4 receptors (Schneider et al., 2009) amongst others (Milligan, 2000). However, unlike in these studies, the GPR35-$G\alpha_{13EE}$ fusion was not found to produce a signal magnitude greater than the individually expressed proteins, and actually recorded a pEC_{50} some 12.5 fold less than that obtained from the non-fusion experiment (**Fig 3.5C**). There are a number of factors that could account for this: the G protein could be constrained by the linker sequence and/or not in the correct orientation for maximal activation (Robinson and Sauer, 1998; Seifert et al., 1999b) (this could also explain the inability to detect $G\alpha_{13EE}$ in the fusion construct with the anti-EE antibody (**Fig 3.5B**)); the 1:1 stoichiometry could prevent multiple G protein coupling and therefore reduce the overall potency and efficacy of the response; the kinetics of the [^{35}S]GTPγS incorporation rate could be increased due to the close proximity of the polypeptides, leading to a lower estimation of potency at the time point measured; or there could be a mechanical or structural requirement for the association of Gβγ subunit for GDP turnover (Iiri et al., 1998; Adjobo-Hermans et al., 2011).

Future efforts to improve the signal from the fusion protein could assess the flexibility between GPR35 and $G\alpha_{13}$ that currently only contains the *EcoRV* linker sequence (GATATC). This translates to aspartic acid and isoleucine: only two amino acids in length. Some studies have used two restriction sites as a linker (Zhang et al., 2006), while yet others have placed an epitope tag and/or proteolytic cleavage sequence in this region, significantly increasing the linker length (Siefert et al., 1999a). The secondary structure of the linker region must also be considered, as sequences encoding α-helical or β-strand structures could alter the conformation of the fusion protein. Distinctly, expression of receptor and G protein in an insect cell line would provide a cell system with limited interference of endogenous mammalian G proteins (Knight et al., 2003) allowing for GPR35-$G\alpha_{13}$ measurement free from competing $G\alpha_{i/o}$ proteins that could ultimately increase the magnitude of $G\alpha_{13}$ [^{35}S]GTPγS incorporation. Nevertheless, considering the aforementioned issues, and the relatively low throughput nature of the assay, the [^{35}S]GTPγS $G\alpha_{13EE}$ assay

would be best suited to selected ligand characterisation efforts, namely to dissect ligand bias or to confirm $G\alpha_{13}$ protein coupling to GPR35 using a full length G protein rather than as a system for ligand screening.

3.4.6 *IP_1 accumulation assays reveal different patterns of species selectivity depending on the chimera employed*

The IP_1 accumulation assay was originally assessed at GPR35 by Yang et al., 2010 in their discovery of cromolyn as a human, mouse and rat GPR35 agonist. Using HEK293 cells transiently co-transfected with GPR35 and $G\alpha_{qoA/B}$, measurement of [^{3}H] inositol stabilised with lithium chloride revealed that cromolyn acted with a pEC_{50} of 7.21 ± 0.14 at human, 6.15 ± 0.31 at mouse and 6.31 ± 0.13 at rat GPR35 (Yang et al., 2010). This indicated that cromolyn displayed human selectivity. However, in the β-arrestin-2 recruitment (**Fig 3.11**) and HTRF® IP_1 accumulation assay using $G\alpha_{q13}$ (**Fig 3.8**) the human and rat cromolyn responses were found to be equipotent (Jenkins et al., 2012). Specifically, in the IP_1 accumulation assay, pEC_{50}s of 6.24 ± 0.13 at human and 5.82 ± 0.11 at rat were generated (**Table 3.2**): lower than those reported by Yang et al. (2010). A further study carried out by Yang, (although not assessing the activity of cromolyn) utilised the $G\alpha_{qoA/B}$ chimera and [^{3}H] inositol to reveal potencies of zaprinast that were almost identical to those presented herein (**Table 3.2**) and lower than those originally published in the 2010 study (Yang et al., 2010; Yang et al., 2012; Jenkins et al., 2012). Thus, while my studies using $G\alpha_{q1/2}$ and $G\alpha_{q13}$ (**Fig 3.7**) found no difference in the potency of zaprinast, this does not mean that there is no G protein chimera selectivity displayed by cromolyn. Assessing this in subsequent research efforts could reveal an interesting pattern of pathway bias.

3.4.7 *IP_1 accumulation provides an assay format to assess constitutive activity at GPR35*

Almost any GPCR can be engineered to become constitutively active through mutational alteration (Tehan et al., 2014), and loss or gain of constitutive activity *in vivo* can lead to disease (Tao, 2008). The level of constitutive activity generally is found to increase linearly with receptor expression level, as a higher level of receptor expression will naturally lead to a greater number of R* receptors. Thus, overexpression of GPCRs can be associated

with increased basal signalling. However, constitutive activity is not merely an artefact of overexpression, as some receptors are constitutively active even in endogenous systems (de Ligt et al., 2000). For GPCRs such as rhodopsin however, there is a strict requirement to maintain the receptor in an inactive state to allow effective perception of light (Milligan, 2003b).

Constitutive activity was initially thought to indicate the presence of an unidentified agonist in the assay preparation, and indeed this may be the case for some GPCRs, such as the free fatty acid receptor FFA1 (Stoddart and Milligan, 2010). However, after ruling out the presence of the endogenous agonist, receptors such histamine H_1 (Bakker et al., 2000), H_2 (Threlfell et al., 2008), H_3 (Rouleau et al., 2002) and H_4 (Wifling et al., 2014), dopamine D_2 (Hall and Strange, 1997), and D_5 (Plouffe et al., 2010), β2-AR, GPR3, GPR6, GPR12, GPR26, and GPR78 (Levoye and Jockers, 2008; Milligan, 2003b) were found to naturally display constitutive activity. GPR35 appears to display constitutive activity when overexpressed in recombinant cell systems (**Fig 3.9**), but also in a cell line endogenously expressing *GPR35* (my unpublished observations). However, since no consensus has been reached as to the endogenous ligand of GPR35 (Mackenzie et al., 2011), one cannot rule out the possibility of the presence of an endogenous agonist existing within the assay preparation. Furthermore, Na^+ and Zn^{2+} ions can allosterically modulate responses at GPCRs, as demonstrated for the A_{2A} adenosine (Liu et al., 2012; Gutiérrez-de-Terán et al., 2013) dopamine D_2 (Selent et al., 2010), β2-AR (Swaminath et al., 2003), GPR39 (Holst et al., 2007) and GPR83 (Müller et al., 2013) receptors; and accessory proteins such as RAMPs (Roux and Cottrell, 2014; Christopoulos et al., 2003); and homo- or heterodimers (Levoye et al., 2006) can also influence the basal activity. Although there has been no suggestion of GPR35 acting as part of a higher order oligomer or with accessory proteins, it would be of interest to assess whether interaction partners with GPR35 species orthologues play a role in the divergent pharmacology observed.

3.4.8 *ML-145 and CID-2745687 are inverse agonists of human GPR35*

Herein, the IP-One assay facilitated the characterisation of GPR35 antagonist compounds in a constitutively active G protein system for the first time. This revealed that ML-145 and CID-2745687 acted as inverse agonists of human GPR35 in systems exhibiting

constitutive activity (**Fig 3.9**). This is not a novel phenomenon, and many antagonist compounds originally identified in systems devoid of basal activity were subsequently reclassified as inverse agonists following assessment within constitutively active systems (Milligan et al., 1995; Milligan, 2003b). Inverse agonism is not solely an academic phenomenon, as inverse agonists can potentially deliver therapeutic benefits over neutral antagonists (Tao, 2008) since they reduce the activity of constitutively active receptors to a greater extent than neutral antagonists. Therapeutically successful inverse agonists include naloxone (Suboxone®) for the management of opioid overdose (Sirohi et al., 2009), and clozapine as an inverse agonist of dopamine D_2 and serotonin $5HT_{2C}$ receptors for the treatment of psychosis (Herrick-Davis et al., 2000). Inverse agonists displaying functional selectivity also offer therapeutic advantages, as demonstrated by the β-blocker carvedilol. Carvedilol is a non-selective β-blocker that at the β2-AR acts as an inverse agonist of $G\alpha_s$ and as an agonist of β-arrestin recruitment and extracellular-regulated kinase (ERK) activity, a profile associated with beneficial implications for the treatment of heart failure (Wisler et al., 2007). From the data presented herein, ML-145 and CID-2745687 could act as G protein selective inverse agonists, although this would require further investigation. Additionally, in order to elucidate whether inverse agonism at GPR35 would be therapeutically favourable, compounds must first be generated with efficacy at the rodent receptors to enable investigation of this idea in *in vivo* models.

3.4.9 *The BRET-based β-arrestin recruitment assay reveals a distinct GPR35-β-arrestin trafficking pattern*

Assessment of kinetic β-arrestin-1 and β-arrestin-2 recruitment towards GPR35 indicated that a rapid and transient interaction was initiated following zaprinast treatment (**Fig 3.10A/B**). This pattern of arrestin recruitment was distinct from that observed following TUG-891 activation of FFA4, which formed a stable interaction with either β-arrestin-1 or β-arrestin-2 that was maintained throughout the time scale of the experiment (**Fig 3.10C/D**). Interactions of this nature have previously been demonstrated for a number of GPCRs, and can be grouped into two distinct categories: transient interactors, named 'class A GPCRs' and sustained interactors that form 'class B GPCRs' (not to be confused with the GPCR subfamily nomenclature, 'Class A, B, C') (Shenoy and Lefkowitz, 2003b). Other receptors in

the class A group include the β2-AR (Shenoy and Lefkowitz, 2003a), the α_{1b}-adrenergic receptor, μ-opioid receptor, endothelin ET_A receptor and the dopamine D_{1A} receptor (Oakley, et al., 2000), while examples of class B receptors include the vasopressin receptor V_2R (Terrillon et al., 2004), angiotensin II type 1A receptor (Anborgh et al., 2000), thyrotropin-releasing hormone receptor (Hinkle et al., 2012), neurotensin 1 receptor and neurokinin NK1 receptor (Oakley, et al., 2000). When expressed at comparable levels, class A GPCRs have been found to a higher affinity for β-arrestin-2 over β-arrestin-1 (Oakley, et al., 2000). This however cannot be stated from the GPR35 data presented in **Figure 3.10** as it is unknown if the two β-arrestin constructs express to similar levels. Indeed, class B GPCRs are reported to non-discriminately interact with β-arrestin-1 and β-arrestin-2. However, the BRET signal of FFA4 is also higher with β-arrestin-2 than with β-arrestin-1, suggesting that perhaps the β-arrestin-1 construct employed herein does not express as well as β-arrestin-2. This may be clarified using Western blot analysis using anti-luciferase or arrestin-specific antisera.

The functional ramifications of the pattern of β-arrestin recruitment presented for GPR35 and FFA4 when linked to either class A or class B GPCRs are differential rates of receptor dephosphorylation, recycling, degradation, and desensitisation. Class B receptors contain clusters of phosphate acceptor sites in their C terminal tails, defined as serine or threonine residues occupying three consecutive positions, or three of four positions, suggested to be responsible for the higher affinity interaction with β-arrestin than that associated with class A GPCRs (Oakley et al., 2000; Tohgo et al. 2003). As a result of this, class B receptors maintain association with β-arrestins during the internalisation process, and β-arrestin is incorporated with the GPCR into endosomes. β-arrestin's scaffolding function subsequently facilitates association with cytosolic proteins within endosomes that can lead to activation of signalling cascades such as ERK or cAMP accumulation (Calebiro et al., 2010); further to this, the association of β-arrestin with the GPCR delays the dephosphorylation and recycling process, resulting in a longer period between successive activation events, and augmenting the receptor desensitisation process (Shenoy et al., 2001; Oakley et al., 2001; Shenoy and Lefkowitz, 2003a). Class A GPCRs, on the other hand, dissociate from β-arrestin post interaction with AP-2 and clathrin, but before entry of the GPCR to the endosome (Hanyaloglu and von Zastrow, 2008). As a consequence of this, class A GPCRs have been associated with a shorter duration between internalisation and recycling

since the rapid dissociation of β-arrestin does not restrict the receptor within endosomes nor does it slow the dephosphorylation process (Shenoy and Lefkowitz et al., 2003b; Oakley et al., 2001).

However, there are exceptions to grouping GPCRs within class A or class B and this definition does not fit all receptor trafficking profiles. For example, the N-formyl peptide receptor requires β-arrestin for recycling but not for internalisation (Vines et al., 2003); the protease-activated receptor-1 (PAR-1) receptor is phosphorylated and internalised but does not require β-arrestin (Paing et al., 2002); while the human somatostatin receptors sst_1 and sst_4 do not recruit β-arrestin and do not internalise (Tulipano et al., 2004). Receptor trafficking profiles can also be distinct depending on the agonist used to stimulate the response, as indicated by the μ-opioid receptor, which is phosphorylated and internalised when treated with etorphine, weakly phosphorylated and poorly internalised following morphine treatment, and not at all phosphorylated nor internalised following herkinorin treatment (Bohn et al., 2004; Groer et al., 2007). This indicates that the conformational ensemble of the receptor is important for receptor trafficking, with the pattern of constitutive receptor internalisation and receptor trafficking also being distinct from agonist-induced internalisation (Segura et al., 2013). Thus, there exists opportunities to selectively engineer ligands to minimise receptor desensitisation and degradation (Woolf and Linderman, 2003), a major issue impacting upon drug efficacy and tolerance (Williams et al., 2013; Hudson et al., 2013c). With regard to GPR35, therefore, it may be of interest to determine whether distinct patterns of β-arrestin trafficking occur following stimulation with a variety of structurally and pharmacologically distinct agonists; whether constitutively internalised receptor trafficking differs from the agonist-stimulated profile presented herein (**Fig 3.11**); and whether human and rat GPR35 display similar or distinct β-arrestin trafficking profiles.

3.4.10 *The BRET-based β-arrestin recruitment assay and IP-One assays reveal distinct species selective profiles of GPR35 ligands*

Herein, agonist-induced activation of GPR35 species orthologues was monitored using two distinct systems: IP_1 accumulation using HTRF® with a chimeric $G\alpha_q$ G protein and β-arrestin-2 recruitment using BRET technology. Importantly, both assay systems, although

distinct, were employed using the same cellular background (transiently transfected HEK293T cells). The data provide an interesting profile of species selectivity at GPR35: cromolyn is essentially equipotent at human and rat GPR35 in both the BRET and IP-One systems and zaprinast retains significant rat selectivity in both assay formats (**Fig 3.8**; **Fig 3.11**). However, while pamoic acid also acts with significant human selectivity in the BRET and IP-One assays, the action of pamoic acid at rat GPR35 is substantially different between BRET and IP-One (**Fig 3.8**; **Fig 3.11**). Pamoic acid recruits β-arrestin-2 weakly at rat GPR35 (pEC_{50} 5.08 ± 0.2; E_{max} 15.8 ± 1.7 %), but in the IP-One system produces close to full agonism (pEC_{50} 6.15 ± 0.18; E_{max} 73.8 ± 6.9 %). This suggests that instead of pamoic acid being inactive at rat GPR35 due to an inability to recruit β-arrestin-2 (Jenkins et al., 2010), in fact this ligand may selectively signal via a GPR35 G protein dependent pathway (Jenkins et al., 2012).

Pamoic acid has been shown to act in an anti-nociceptive manner in a mouse abdominal constriction test (Zhao et al., 2010). If acting through GPR35 in this model, it would be of interest to determine which pathway pamoic acid utilises to this end, as unlike rat GPR35 which gains efficacy and potency in the IP-One assay using the $G\alpha_{q13}$ chimera, mouse GPR35 does not gain function to the same extent, and only begins to display efficacy at 10 μM (with further increases in concentration limited by the solubility of pamoic acid) (Jenkins et al., 2012). However, it is possible that mouse GPR35 could be activated by pamoic acid at GPR35 *in vivo* perhaps even in a $G\alpha_{i/o}$ dependent manner (which was not investigated herein in an *in vitro* format), and implications of this would be interesting to dissect in further detail. At human GPR35, pamoic acid increases in efficacy between the BRET and IP-One systems, from a partial to a full agonist (**Fig 3.8**; **Fig 3.11**). This difference is investigated in further detail in **Chapter Four**, and will not be discussed fully here. Nevertheless, the implications of this appear to be due to the accumulative nature of the IP-One assay system, the longer incubation period, and are a reflection of a better-coupled system as compared to the β-arrestin-2 recruitment assay, rather than a true 'pathway bias'.

3.4.11 *The label free DMR system provides a platform to assess ligand responses in an endogenous cell system without the requirement for manipulated receptor constructs*

Many of the drug discovery campaigns at GPR35 have utilised β-arrestin-2 recruitment assays including the BRET-based method utilised herein (Jenkins et al., 2010, 2011, 2012; Neetoo-Isseljee et al., 2013; Mackenzie et al., 2014), or reporter-based formats such as DiscoveRx's PathHunter® (Southern et al., 2013; Neetoo-Isseljee et al., 2013) or Life Technologies' Tango™ (Deng et al., 2011a; 2011b; 2012b; 2012c; 2012d). These assays, particularly for GPR35, provide a robust means of assessing ligand responses, but they also potentially limit the selection of ligands to those that may bias the receptor toward a β-arrestin-2 pathway. Since there are very limited G protein-based outlets for assessing activation of GPR35 during drug discovery efforts, the extent of β-arrestin bias had perhaps not been realised until DMR assays were employed as a non-biased outlet to identify ligands of GPR35. Recent efforts to this end have been reported by Corning researchers who, utilising the DMR platform with the human colorectal adenocarcinoma HT-29 cells endogenously expressing *GPR35*, revealed ligands that induce DMR in HT-29 cells, which could be at least partially blocked by addition of the GPR35 antagonist CID-2745687 (also known as SPB05142), but failed to recruit β-arrestin-2 in the Tango™ assay (Deng et al., 2011a; 2011b; 2012c; 2012d; Deng and Fang 2012b). These findings generate considerable excitement given the current interest surrounding biased agonism. However, the DMR format is essentially a 'black box' with regard to ligand responses (Fang et al., 2007), and although ligands may induce responses that appear to arise through activation of a given target, it remains difficult to deduce functionally what these responses may be. DMR assays rely heavily on receptor specific antagonists or interfering RNAs to ablate agonist responses or reduce expression of the receptor, respectively, as a measure of ligand specificity. Given that there are at least two widely accepted human-selective GPR35 antagonists, it is concerning that CID-2745687 (the less potent of the two) is primarily utilised for this purpose, as it does not act in a competitive manner with all GPR35 agonists, for example pamoic acid (Jenkins et al., 2012). Thus, important agonist responses may not be suppressed by application of CID-2745687 and could be wrongly identified as being non-specific to GPR35.

Herein, it was of importance to demonstrate that the GPR35 agonists identified and characterised through this drug discovery campaign could do so in a cell line endogenously expressing *GPR35* (**Fig 3.12A**). Importantly, zaprinast, cromolyn and pamoic acid all generated kinetic responses in the DMR assay that resembled one another (**Fig 3.12D**), with potencies following the same rank order as recorded in the HEK293T IP-One and β-arrestin-2 assays (**Table 3.6**). Moreover, the response generated by application of zaprinast could be ablated following ML-145 treatment, suggesting that the zaprinast DMR response was indeed a result of GPR35 activation (**Fig 3.12G**). These traces however, also appeared similar to the kinetic trace displayed by β-arrestin recruitment in HEK293T cells (**Fig 3.10A/B**), indicating that the DMR could be monitoring β-arrestin recruitment, potentially as well as G protein trafficking.

In contrast to this, it is suggested that the DMR kinetic traces are characteristic of G protein coupling to the receptor (Schröder et al., 2010). However, within the same study, two $G\alpha_s$-coupled receptors: the β2-AR (expressed in CHO cells) and the prostaglandin E_1 receptor (expressed in HEK293 cells) displayed negative or positive DMR traces, respectively (Schröder et al., 2010). This indicates that a 'one fits all' kinetic response for each family of G proteins is unlikely, particularly for receptors that couple to more than one family of G protein, the abundance of which may be different between cellular backgrounds (Downes and Gautam, 1999). Comparison of the kinetic traces displayed by zaprinast, cromolyn, and pamoic acid (**Fig 3.12D**) with those published by Schröder match more closely to the '$G\alpha_{i/o}$' response displayed by the prostaglandin D_2 receptor CRTH2 in HEK293 cells rather than the '$G\alpha_{13}$' response of GPR55. Deconvoluting the G protein pathway involved in the DMR response of GPR35 agonists would be of interest given the current lack of characterisation of GPR35's basic signalling profile in endogenously expressing cell lines.

3.4.12 *Conclusion*

The initial assessment of assay systems has identified a number of formats that will be useful and suitable to assess and characterise ligand responses emanating from drug discovery efforts at GPR35. This includes, the IP-One assay using chimeric G proteins, the BRET-based β-arrestin recruitment assay, the ArrayScan™ high content imaging platform,

and the label-free DMR format, which together provide a diverse means of assessing GPR35 function. Each format provides at least some advantages, be it low cost, assay robustness, assessment of G protein function, or a platform to assess endogenous cellular responses; but there are also associated negatives, including high cost, potential pathway bias, the use of chimeric G proteins, and recombinant overexpression of epitope tagged proteins that may not accurately affect native cellular responses. Nonetheless, rather than relying on just one output to assess GPR35 pharmacology, employing a combination of these platforms should even out any issues and reinforce experimental outcomes as a reflection of responses from distinct pathways and cell types.

Chapter Four

GPR35 Drug Discovery

4.1 High-throughput screening identifies distinct chemical subtypes that activate GPR35

Upon commencement of this project, in the absence of a potent and selective endogenous agonist, the identification of novel chemical compounds was required in order to probe the pharmacology and (patho)physiology of GPR35. Initial efforts undertaken employed various pharmacological systems but focused on β-arrestin-2 recruitment methods; namely DiscoveRx's PathHunter® enzyme fragment complementation assay and a BRET-based methodology for measuring protein-protein interactions. These platforms have been highly valuable to the understanding of GPR35 pharmacology, and in association with chimeric G protein based and DMR assays, have been employed for virtually all drug discovery and characterisation efforts at GPR35 (Jenkins et al., 2010; Jenkins et al., 2012; Deng et al., 2012a; 2012b; Deng and Fang 2012a; Southern et al., 2013; Neetoo-Isseljee et al., 2013; Funke et al., 2013; Mackenzie et al., 2014).

Presented herein is the drug discovery effort that led to the identification of some of the most potent agonists currently available at human GPR35: compound 1 (Neetoo-Isseljee et al., 2013), lodoxamide, and bufrolin (Mackenzie et al., 2014). From high-throughput screening (HTS) efforts, the identification of the novel human selective GPR35 agonist, compound 1 ((4-{(Z)-[(2Z)-2-(2-fluorobenzylidene)-4-oxo-1,3-thiazolidin-5-ylidene]methyl} benzoic acid)), is described (Neetoo-Isseljee et al., 2013). Profiling of GPR35 hit compounds generated from HTS efforts revealed that the anti-asthma medication cromolyn, the flavonoids luteolin, ellagic acid and quercetin (Jenkins et al., 2010), and the anti-allergy treatment amlexanox (Neetoo-Isseljee et al., 2013), shared function as mast cell stabilisers. Extending this screening effort to include a further subset of compounds with mast cell stabilising capability led to the identification of lodoxamide and bufrolin as the most potent activators of human and rat GPR35 currently reported (Mackenzie et al., 2014).

4.1.1 *A background to compound library screening in collaboration with MRC Technology*

As an extension to previous screening campaigns of the Prestwick® small molecule chemical library that identified pamoic acid as an agonist of GPR35 (Jenkins et al., 2010; Zhao et al., 2010), collaborators from the MRC Technology (MRCT) screened the commercially available NINDS (National Institute of Neurological Disorders and Stroke) small

molecule library and Sequoia's plant-derived compound library for activity at human GPR35 (Neetoo-Isseljee et al., 2013). Including zaprinast, which was used as a positive control, previous GPR35 agonists from the aforementioned Prestwick® chemical library were identified, such as pamoic acid, cromolyn, dicoumarol, furosemide, and NPPB (5-nitro-2-(3-phenylpropylamino)benzoic acid). Novel hits for human GPR35 included the mast cell stabiliser amlexanox, the anthraquinone derivatives emodic acid and purpurin, and the kynurenic acid derivative 5-fluoroindole-2-carboxylic acid (Neetoo-Isseljee et al., 2013). However, as with previous screens of commercially available compound libraries, most of the compounds are known to have prominent off-target effects and were of modest-to-low potency at GPR35. Thus, in order to identify novel, potent, and distinct chemical structures with which to probe the pharmacology of GPR35, 100,000 small molecule compounds from the MRCT's private compound collection were screened using DiscoveRx's β-arrestin-2 enzyme complementation assay (Neetoo-Isseljee et al., 2013). From these efforts, the majority of hit compounds (39%) generated pEC_{50}s between 4.5 and 5.3; some (11.5%) displayed potencies similar to zaprinast (pEC_{50}s between 5.5 and 6.0), but few (3.9%) generated pEC_{50} values greater than 6.0 (Neetoo-Isseljee et al., 2013).

4.1.2 *Characterising GPR35 MRCT library hits using the BRET assay at species orthologues of GPR35*

Herein, I present compounds 1-5, which were identified as five chemically distinct compounds from the MRCT compound library that activated human GPR35 (Neetoo-Isseljee et al., 2013). Using the BRET-based β-arrestin-2 recruitment assay, I assessed responses of human, mouse, and rat GPR35 to characterise the pharmacology of compounds 1-5. For the BRET-based assay, HEK293T cells were transiently co-transfected with human, mouse, or rat FLAG-GPR35-eYFP and β-arrestin-2-*Renilla* luciferase, which interacted following agonist stimulation to enable BRET between the C-terminal tags of each construct (**Section 2.7.3**). As reported previously (**Section 3.2.2**), zaprinast displayed rat selectivity ($P \leq 0.001$) and acted with moderate to high potency at human, mouse, and rat GPR35 (**Fig 4.1A**; **Table 4.1**).

At human GPR35, compound 1 generated responses that were some 700-fold more potent ($P \leq 0.001$) and with higher efficacy ($P \leq 0.001$) than those generated at mouse or rat

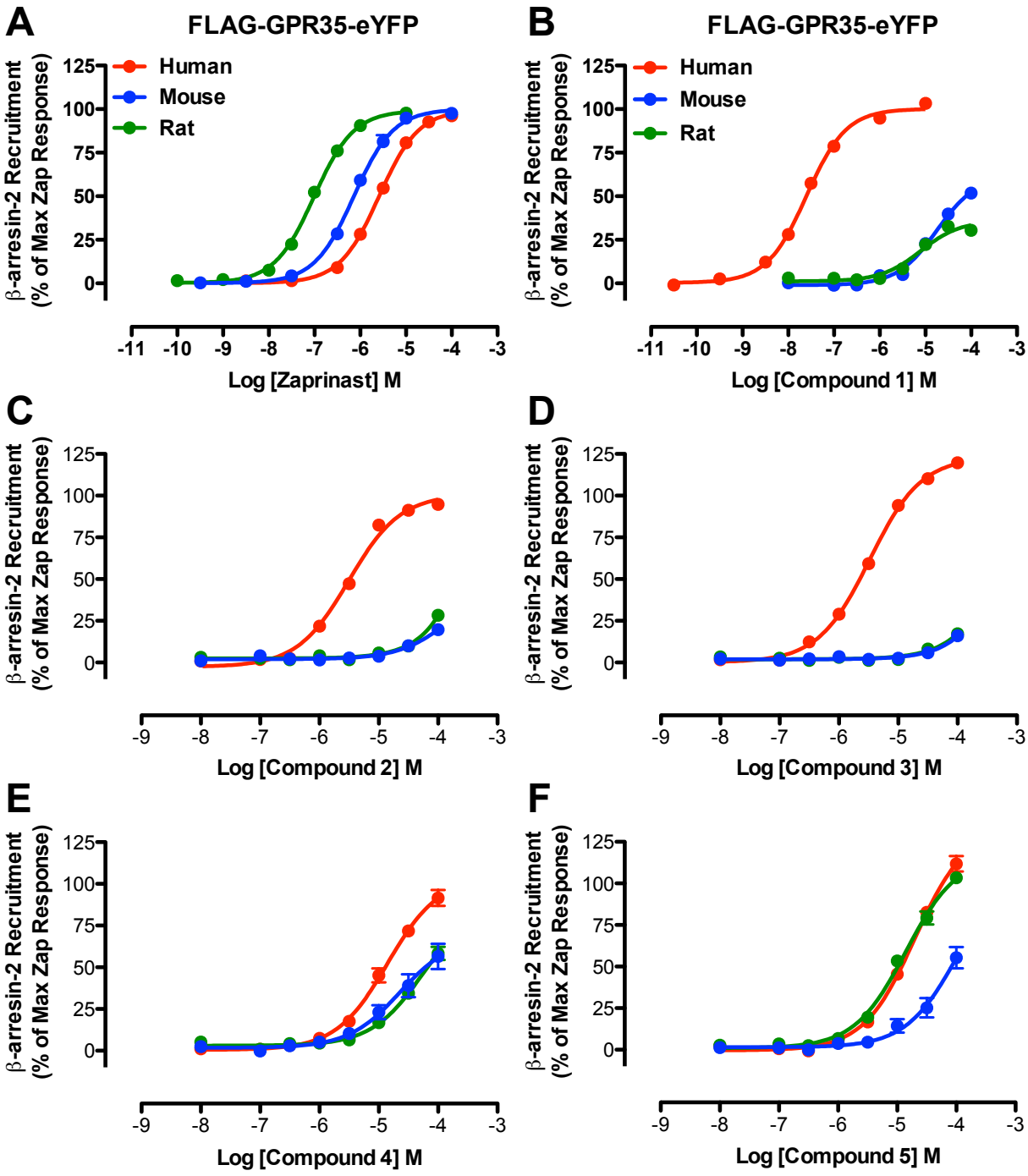

Figure 4.1 Compounds 1-5 display species selectivity in the β-arrestin-2 recruitment assay HEK293-T cells were transiently cotransfected with human (red), mouse (blue), or rat (green) FLAG-GPR35-eYFP and β-arrestin-2-*Renilla* luciferase, with agonist-induced receptor activation assessed via β-arrestin-2 recruitment using BRET. The species selectivity of zaprinast (**A**), compound 1 (**B**), compound 2 (**C**), compound 3 (**D**), compound 4 (**E**), and compound 5 (**F**) is presented. Each dataset represents the mean of a minimum of three independent experiments carried out in duplicate ± SEM. Efficacy is presented as a percentage of the maximum zaprinast response at each orthologue.

Table 4.1 Potency, efficacy, and selectivity of compounds 1-5 generated via the β-arrestin-2 recruitment system

		β-arrestin-2 Recruitment - BRET						
Compound	**Structure**	**Human**	**Mouse**	**Rat**	**Mouse - Human**	**Rat - Human**	**Rat - Mouse**	**Selectivity[b]**
		pEC_{50} ± SEM			**ΔpEC_{50}[a]**			
Zaprinast	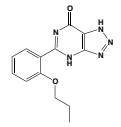	**5.59 ± 0.01**	**6.01 ± 0.03**	**7.01 ± 0.02**	**+ 0.42 ± 0.04****	**+ 1.42 ± 0.03*****	**+ 1.00 ± 0.05*****	**Rat**
		E_{max} (% of max zap response) ± SEM			**ΔE_{max}[c]**			
		99.8 ± 0.7	99.8 ± 1.2	99.3 ± 0.9	NA	NA	NA	
1	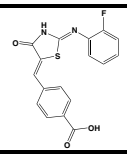	**7.60 ± 0.03**	**4.75 ± 0.06**	**5.12 ± 0.08**	**- 2.85 ± 0.09*****	**- 2.48 ± 0.12*****	**+ 2.30 ± 0.14***	**Human**
		100.2 ± 1.3	61.7 ± 2.5***	36 ± 1.5***	- 38.5 ± 4.0***	- 64.2 ± 2.8***	- 25.7 ± 4.1**	
2	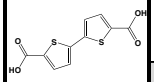	**5.51 ± 0.04**	**Inactive**	**Inactive**	**-**	**-**	**-**	**Human**
		100.8 ± 1.8	NR	NR	-	-	-	
3	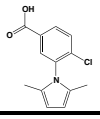	**5.48 ± 0.04**	**Inactive**	**Inactive**	**-**	**-**	**-**	**Human**
		123.1 ± 2.0***	NR	NR	-	-	-	
4		**4.85 ± 0.06**	**4.65 ± 0.17**	**4.27 ± 0.09**	**- 0.20 ± 0.25**	**- 0.58 ± 0.15*****	**- 0.38 ± 0.27***	**Human and Mouse**
		104.3 ± 4.2	68.1 ± 8.0***	88.4 ± 8.0	- 36.2 ± 12.8***	- 15.9 ± 12.8	+ 20.3 ± 16.0*	
5	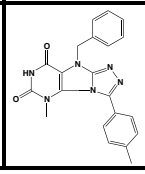	**4.70 ± 0.04**	**<4**	**4.86 ± 0.04**	**≤ 0.7**	**+ 0.16 ± 0.08**	**≤ 0.86**	**Human and Rat**
		134.4 ± 4.1***	NA	116.9 ± 3.8*	-	- 17.5 ± 7.9	-	

[a] ΔpEC_{50} represents the difference in potency between two species, *P* = *** ≤ 0.001, ** ≤ 0.01, * ≤ 0.05

[b] Represents the species for which the highest potency was generated

[c] ΔE_{max} represents the difference in efficacy (%) between two species, *P* = *** ≤ 0.001, ** ≤ 0.01, * ≤ 0.05

NR, no response; NA, not applicable; - , not calculated

Data represent the mean of a minimum of three independent experiments carried out in duplicate ± SEM

GPR35 (**Fig 4.1B**; **Table 4.1**). Compound 2 and compound 3, meanwhile, were active only at the human orthologue (**Fig 4.1C/D**). Compound 4 acted with similar potency at all three species orthologues, but was statistically human ($P \leq 0.001$) and mouse ($P \leq 0.05$) selective. Efficacy was reduced at mouse ($P \leq 0.05$) and rat ($P \leq 0.001$) for compound 4 compared with human GPR35 (**Fig 4.1E**). Compound 5 acted at human and rat with similar effect, but was inactive at mouse GPR35 with a pEC_{50} <4 (**Fig 4.1F**).

4.1.3 *Characterising GPR35 MRCT library hits using the IP-One assay at species orthologues of GPR35*

To ascertain whether compounds 1-5 could also activate GPR35 through a G protein coupled pathway, the IP-One assay was employed using the chimeric G protein $G\alpha_{q13}$ since GPR35 does not couple to $G\alpha_q$ (**Fig 3.6**). The $G\alpha_{q13}$ chimera consists of the full-length sequence of $G\alpha_q$ but with the last five carboxyl residues replaced with the corresponding sequence of $G\alpha_{13}$. This enabled GPR35 to couple to $G\alpha_{13}$ and to signal through the $G\alpha_q$ pathway, with agonist-induced IP_1 accumulation monitored using HTRF® technology (**Section 2.7.2**). In the IP-One assay, zaprinast maintained rat selectivity ($P \leq 0.001$) and acted with moderate potency at human, mouse, and rat GPR35 (**Fig 4.2A**; **Table 4.2**). Compound 1 however, acted with 355-fold selectivity ($P \leq 0.001$) toward human GPR35, but, in comparison with the BRET assay, the difference in potency relative to mouse and rat was reduced (**Fig 4.2B**). Compound 1 also acted at mouse and rat with full agonism in the IP-One assay, while the efficacy at human GPR35 was not significantly different from that generated in the BRET assay (**Fig 4.2B**; **Table 4.2**). Unlike in the β-arrestin-2 recruitment assay, compound 2 generated a response at the mouse and rat orthologues, but acted with 80 to 100-fold selectivity ($P \leq 0.001$) toward human GPR35 (**Fig 4.2C**). Compound 3, however, was poorly active at mouse or rat GPR35 in the IP-One assay, and remained human-selective with a non-significant decrease in efficacy at human GPR35 (**Fig 4.2D**; **Table 4.2**). For compound 4 there was a shift in selectivity from human GPR35 in the BRET system to mouse ($P \leq 0.001$) and rat (**Fig 4.2E**) in the IP-One assay. Compound 5, meanwhile, remained human and rat selective ($P \leq 0.001$), but acted with increased efficacy at mouse GPR35 (**Fig 4.2F**; **Table 4.2**).

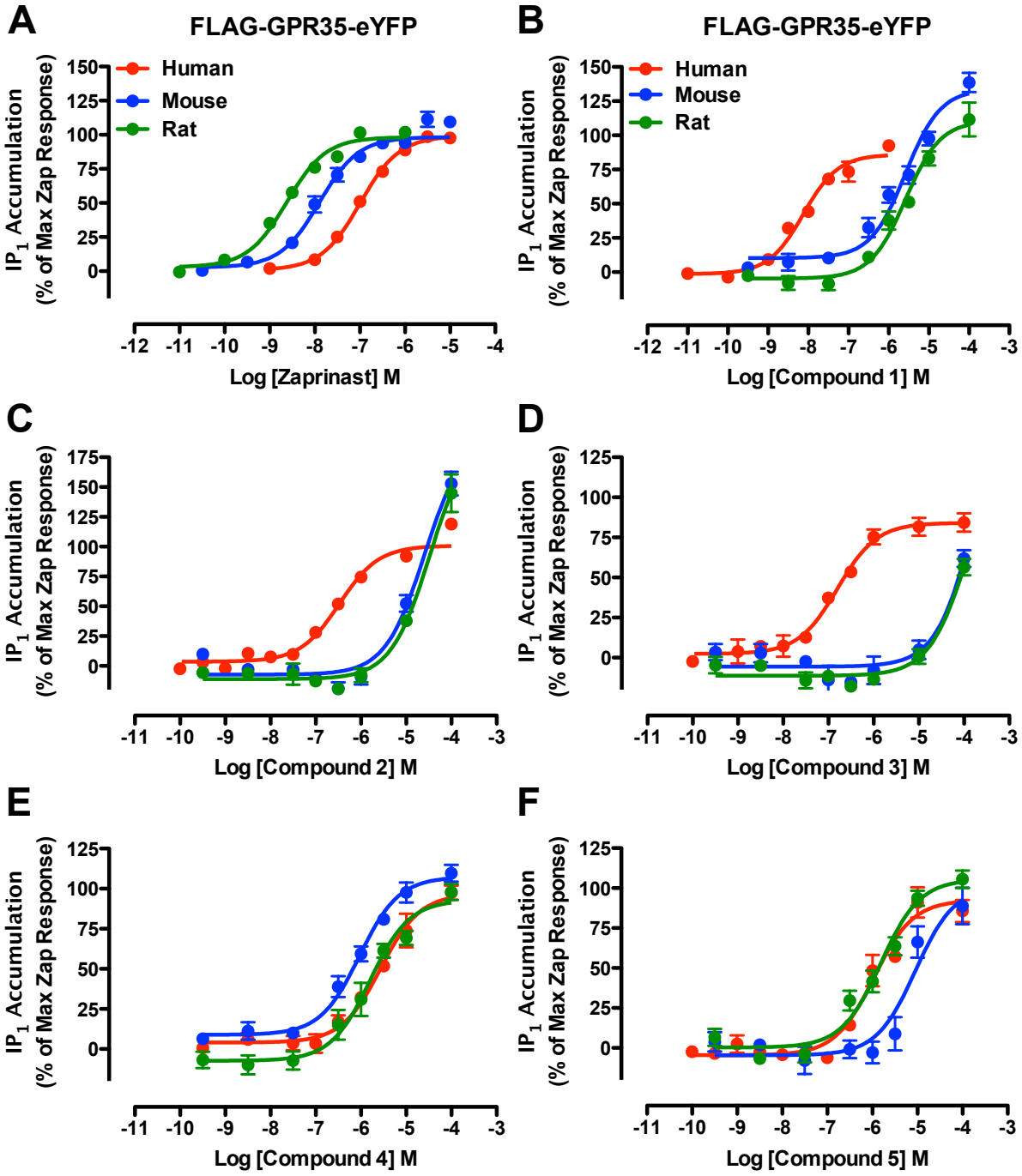

Figure 4.2 Compounds 1-5 generate species selectivity in the IP-One accumulation assay Human (red), mouse (blue), or rat (green) FLAG-GPR35-eYFP constructs and the $G\alpha_{q13}$ chimera were used to assess agonist-induced G protein-mediated signalling via the IP-One accumulation assay. The species selectivity of zaprinast (**A**), compound 1 (**B**), compound 2 (**C**), compound 3 (**D**), compound 4 (**E**), and compound 5 (**F**) is presented. Each dataset represents the mean of a minimum of four independent experiments carried out in duplicate ± SEM. Efficacy is presented relative to the maximum of the reference compound zaprinast, which served as an internal control between experiments.

Table 4.2 Potency, efficacy, and selectivity of compounds 1-5 generated via the IP-One system

		IP_1 Accumulation with $G\alpha_{q135}$ - IP-One Assay						
Compound	**Structure**	**Human**	**Mouse**	**Rat**	**Mouse - Human**	**Rat - Human**	**Rat - Mouse**	**Selectivity[b]**
Zaprinast	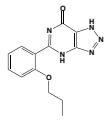	**pEC_{50} ± SEM**			**ΔpEC_{50}[a]**			
		7.00 ± 0.05	**7.90 ± 0.07**	**8.62 ± 0.06**	**+ 0.90 ± 0.12*****	**+ 1.62 ± 0.11*****	**+ 0.72 ± 0.13*****	**Rat**
		E_{max} (% of max zap response) ± SEM			**ΔE_{max}[c]**			
		99.1 ± 1.8	98.4 ± 2.3	98.3 ± 2.2	NA	NA	NA	
1	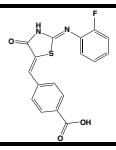	**8.13 ± 0.09**	**5.58 ± 0.09**	**5.58 ± 0.10**	**- 2.55 ± 0.18*****	**- 2.55 ± 0.19*****	**-**	**Human**
		86.0 ± 3.5	133.7 ± 6.1**	110.6 ± 6.3	+ 47.7 ± 10.0***	+ 24.6 ± 10.2	- 23.1 ± 12.4	
2	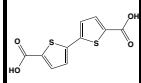	**6.48 ± 0.06**	**4.59 ± 0.11**	**4.48 ± 0.14**	**- 1.89 ± 0.18*****	**- 2.00 ± 0.22*****	**- 0.11 ± 0.25**	**Human**
		100.9 ± 3.1	194.1 ± 14.8***	197.2 ± 3.1***	+ 94.1 ± 21.4***	+ 97.2 ± 6.2***	+ 3.1 ± 21.4	
3	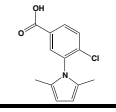	**6.80 ± 0.07**	**<4**	**<4**	**-**	**-**	**-**	**Human**
		84.1 ± 2.6*	NA	NA	-	-	-	
4	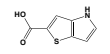	**5.56 ± 0.10**	**6.03 ± 0.08**	**5.80 ± 0.10**	**+ 0.47 ± 0.18*****	**+ 0.24 ± 0.20**	**- 0.23 ± 0.18**	**Mouse and Rat**
		96.8 ± 5.6	107.3 ± 3.8	92.9 ± 5.8	+ 10.5 ± 9.6	- 3.9 ± 11.4	- 14.4 ± 9.8	
5	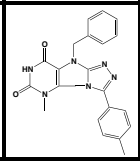	**5.97 ± 0.10**	**5.05 ± 0.16**	**5.82 ± 0.09**	**- 0.92 ± 0.27*****	**- 0.15 ± 0.19**	**+ 0.77 ± 0.26*****	**Human and Rat**
		92.5 ± 5.2	101.4 ± 11.0	105.5 ± 11.2	+ 8.9 ± 17.2	+ 13.0 ± 17.5	+ 4.1 ± 22.2	

[a] The species selectivity of each compound

[b] ΔpEC_{50} represents the difference in potency between two species, *P* = *** ≤ 0.001, ** ≤ 0.01, * ≤ 0.05

[c] ΔE_{max} represents the difference in efficacy (%) between two species, *P* = *** ≤ 0.001, ** ≤ 0.01, * ≤ 0.05

NA, not applicable; - , not calculated

Data represent the mean ± SEM of a minimum of four independent experiments carried out in duplicate

4.1.4 *An assessment of pathway bias between β-arrestin-2 recruitment and IP_1 accumulation*

To determine whether the gain in potency and efficacy associated with full and partial agonists (respectively) in the IP-One assay was indicative of pathway bias, a reflection of a better coupled cell signalling system (system bias), or an artefact of a more sensitive assay system (observational bias), $Log(\tau/K_A)$ values were calculated. Using a modified equation of the Black and Leff operational model of agonism (see **Section 2.8.4**), $Log(\tau/K_A)$ values were generated to calculate pathway bias using the transduction coefficient parameter τ/K_A, which assessed the operational affinity and efficacy of each agonist to remove cell system and observational bias (Kenakin et al., 2012; Kenakin and Christopoulos, 2013). Tau (τ) represented agonist efficacy, receptor density, and coupling within the system, while the dissociation constant (K_A) represented the reciprocal of the conditional affinity of the full agonist in the functional system (Kenakin and Christopoulos, 2013).

The first column of **Table 4.3** presents the transduction coefficient ($Log(\tau/K_A)$) values for each agonist in the BRET-based β-arrestin-2 or IP-One assays. The second column, $\Delta Log(\tau/K_A)$, compares each agonist's transduction coefficient value with zaprinast, with a value <1 or >1 representing an agonist with a transduction coefficient less than or greater than zaprinast, respectively. The third column, $\Delta\Delta Log(\tau/K_A)$, compared the $\Delta Log(\tau/K_A)$ ratios generated from the IP-One assay with the BRET system to generate a single parameter of pathway bias, with ratios <1 or >1 indicating a β-arrestin-2 recruitment or IP_1 accumulation pathway bias, respectively (**Table 4.3**).

The $\Delta\Delta Log(\tau/K_A)$ values for compound 1 indicated that although a strong bias was displayed toward the β-arrestin-2 recruitment pathway at human GPR35, mouse and rat GPR35 displayed selectivity toward G protein coupling and IP_1 accumulation (**Table 4.3**). Calculation of bias profiles was not possible for compound 2 or compound 3 at the rodent orthologues due to their inactivity in the BRET assay, but at human GPR35 both compounds displayed at least some selectivity toward the β-arrestin-2 recruitment pathway (**Table 4.3**). Compound 4 meanwhile acted with some selectivity toward β-arrestin-2 recruitment at all three species orthologues, while compound 5 acted with bias toward IP_1 accumulation at human and β-arrestin-2 recruitment at rat (**Table 4.3**).

Table 4.3 Transduction coefficient ratios calculated between BRET and IP-One assays indicate some bias between β-arrestin-2 recruitment and IP_1 accumulation pathways

	FLAG-Human GPR35a-eYFP				
	$Log(\tau/K_A)^a$		$\Delta Log(\tau/K_A)^b$		$\Delta\Delta Log(\tau/K_A)^c$
Compound	**BRET**	**IP-One**	**BRET**	**IP-One**	
Zaprinast	**5.56**	7.05	**1**	**1**	1
1	**7.53**	7.95	**93.3**	7.94	0.09
2	**5.46**	6.59	**0.79**	0.35	0.44
3	**5.7**	6.67	**1.38**	0.42	0.3
4	**4.98**	5.64	**0.26**	0.04	0.15
5	**4.88**	5.87	**0.21**	0.66	3.14
	FLAG-Mouse GPR35-eYFP				
	$Log(\tau/K_A)^a$		$\Delta Log(\tau/K_A)^b$		$\Delta\Delta Log(\tau/K_A)^c$
Compound	**BRET**	**IP-One**	**BRET**	**IP-One**	
Zaprinast	**6.18**	7.78	**1**	1	1
1	**5.43**	6	**0.18**	0.66	3.67
2	**NA**	5.06	**-**	0.006	-
3	**NA**	NA	**-**	-	-
4	**4.62**	6.12	**0.03**	0.02	0.67
5	**NA**	4.93	**-**	0.001	-
	FLAG-Rat GPR35-eYFP				
	$Log(\tau/K_A)^a$		$\Delta Log(\tau/K_A)^b$		$\Delta\Delta Log(\tau/K_A)^c$
Compound	**BRET**	**IP-One**	**BRET**	**IP-One**	
Zaprinast	**7**	8.61	**1**	1	1
1	**4.84**	5.66	**0.007**	0.05	7.14
2	**NA**	5	**-**	0.0002	-
3	**NA**	NA	**-**	-	-
4	**4.35**	5.6	**0.002**	0.001	0.5
5	**5.03**	5.9	**0.01**	0.002	0.2

[a] $Log(\tau/K_A)$ ratios calculated using the formula described in **Section 2.8.4**

[b] Within pathway ratio $\Delta(Log(\tau/K_A)$ is the fold difference relative to zaprinast at each species orthologue

[c] Between pathway ratio $\Delta\Delta(Log(\tau/K_A)$ is the $\Delta(Log(\tau/K_A)$ from IP-One pathway divided by the $\Delta(Log(\tau/K_A)$ BRET; a value >1 indicates bias toward IP_1 accumulation, and <1 a bias toward β-arrestin-2 recruitment

NA, not applicable, -, not calculated

4.1.5 *Assessment of the interaction of MRCT compounds with human GPR35*

To assess whether the potent GPR35 antagonist ML-145 acted in a competitive manner with MRCT compounds 1-3, as has been previously indicated for GPR35 reference agonists zaprinast, pamoic acid, and cromolyn (Jenkins et al., 2010; Jenkins et al., 2012), Schild analysis was carried out using the global Gaddum/ Schild EC_{50} shift analysis (**Section 2.8.3**). This was carried out by an assessment of the competition for receptor binding between antagonist and agonist. Seven concentrations of agonist were assessed in the presence or absence of fixed, increasing, antagonist concentrations that had been pre-equilibrated with the receptor prior to application of agonist (**Section 2.8.3**). If the mode of action of the antagonist was competitive, and these compounds shared one overlapping ligand binding site, the analysis would produce a Schild slope of 1. This calculation also provided an estimate of antagonist potency by generation of the pA_2 value. The pA_2 is the negative logarithm of the concentration of antagonist that produces a 2-fold shift in the concentration response curve of the agonist. Since the endogenous ligand of GPR35 has not been agreed upon, these assessments cannot be used to state whether ligand binding is orthosteric, but can indicate if each agonist shares an overlapping binding pocket with the antagonist, and by default, the previously characterised GPR35 reference agonists.

In the BRET-based β-arrestin-2 recruitment assay, increasing, fixed, concentrations of ML-145 was associated with an increase in the concentration of compound 1 required to achieve half-maximal effect (**Table 4.4**); this was achieved in a fully surmountable manner (**Fig 4.3A**). ML-145 displayed similar properties, indicative of competitive antagonism (**Table 4.4**), when co-incubated with compound 2 (**Fig 4.3B**) or compound 3 (**Fig 4.3C**); however, due to limitation in the potency of each of the agonists, it was not possible to state whether ML-145 was fully surmountable. In the IP-One assay, as demonstrated previously (**Fig 3.9**), increasing ML-145 concentration was associated with a decrease to the basal signal as a result of GPR35's constitutive activity. This inverse agonism invalidated the Schild analysis and the values derived from such analysis; yet the data is provided for completeness (**Fig 4.4D-F**). In order to clearly present the rightward shifts caused by ML-145 in the IP-One system, the basal and maximal values were constrained at each set of concentration responses to 100% and 0%, respectively. Overall, and despite the inverse agonism issues,

ML-145 produced broadly similar effects as those observed in the BRET assay when assessed in terms of Schild slope and pA_2 values (**Table 4.4**).

As a result of this analysis, it is apparent that the MRCT agonist compounds 1-3 interact with human GPR35 in a manner similar to that described previously for well-characterised GPR35 agonists zaprinast, pamoic acid, and cromolyn (**Appendix A**). In summary, herein I have reported the activity of novel chemical compounds 1-5 in the BRET based β-arrestin-2 recruitment assay and the IP_1 accumulation assay for human, mouse and rat GPR35. These ligands were found to act with species selectivity, which in some cases was conditional upon the signalling pathway assessed. This data forms part a comprehensive story detailed in the publication authored by Neetoo-Isseljee et al., 2013 (**Appendix B**).

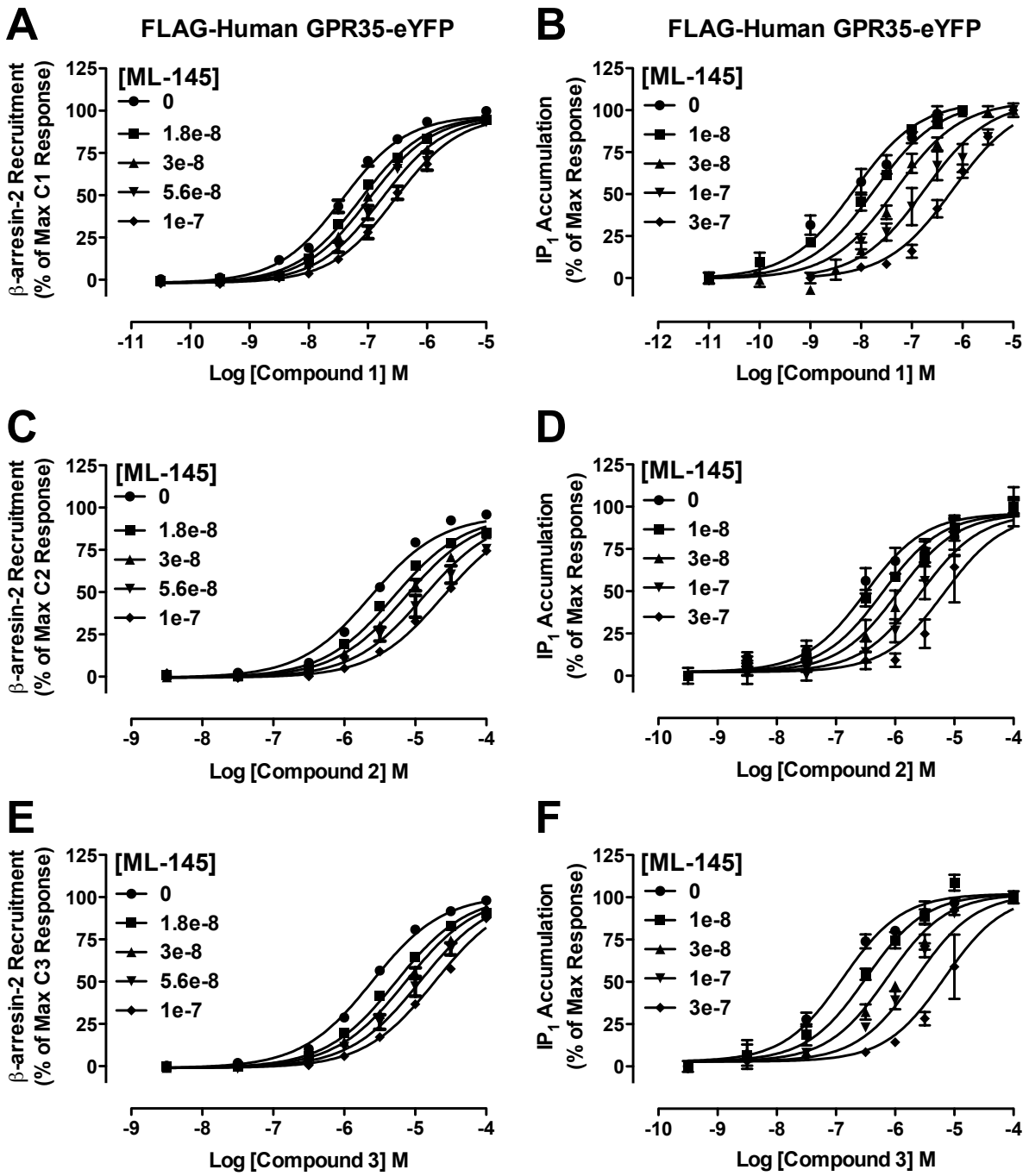

Figure 4.3 ML-145 acts in a competitive manner with compounds 1-3 in the BRET and IP-One assays
Concentration-response curves of compound 1 (**A**/**B**) compound 2 (**C**/**D**), and compound 3 (**E**/**F**) in the presence and absence of increasing ML-145 concentrations were assessed using global Schild analysis of agonist-induced BRET (**A**, **C**, **E**) or $G\alpha_{q13}$-mediated accumulation of IP_1 (**B**, **D**, **F**). BRET data are normalised to the maximum agonist only response, whilst IP-One data are normalised to both the maximum and minimum responses to correct for the inverse agonism of ML-145. Each dataset represents the mean ± SEM of a minimum of two independent experiments carried out in duplicate.

Table 4.4 ML-145 acts in a competitive manner with compounds 1-3

		BRET		IP-One	
Antagonist	**Agonist**	**Schild Slope**	**pA_2**	**Schild Slope**	**pA_2**
ML-145	Compound 1	1.09 ± 0.09	7.76 ± 0.07	1.19 ± 0.08	8.14 ± 0.11
	Compound 2	1.24 ± 0.08	7.79 ± 0.05	0.91 ± 0.14	7.96 ± 0.25
	Compound 3	1.01 ± 0.06	7.82 ± 0.05	1.04 ± 0.08	8.16 ± 0.13

Data represents the mean ± SEM of a minimum of two independent experiments carried out in duplicate

4.2 An assessment of mast cell stabilisers as GPR35 agonists

The anti-asthma medication cromolyn, the flavonoids luteolin, ellagic acid and quercetin, and the anti-allergy treatment amlexanox have been reported to function as mast cell stabilisers (Cox, 1971; Yazid et al., 2013; Theoharides et al., 2007; Kempuraj et al., 2008; Weng et al., 2012; Choi and Yan, 2009; Kimata et al., 2000; Makino et al., 1987; Rudd et al., 1983; Reiser et al., 1986), as well as GPR35 agonists. Thus, to assess whether there could be additional mast cell stabilisers that also acted with GPR35 agonism, a further drug discovery effort was carried out to assess the responses of marketed mast cell stabilisers as potential GPR35 agonists. The compounds assessed were lodoxamide and bufrolin, (neither of which are currently commercially available, but were synthesised by the MRCT and Novartis, respectively, **Section 2.1**), tranilast, doxantrazole, pemirolast, and ketotifen fumarate (**Fig 4.4**). The mast cell *activator* compound 48/80 was also assessed as a compound with distinct function (**Fig 4.4**). Additionally, the mast cell stabilisers and previously identified GPR35 agonists amlexanox and cromolyn were also assessed to determine if there were similarities in the responses generated by mast cell stabilisers that are also GPR35 agonists. As with previous experimental efforts, zaprinast was employed as the reference agonist.

4.2.1 *Mast cell stabilisers display species selectivity at GPR35 orthologues in the BRET assay*

The BRET-based β-arrestin-2 recruitment assay was employed to assess the ability of the mast cell stabilisers to activate human, mouse and rat GPR35. As reference agonist, zaprinast generated a species selectivity profile of r>m>h (**Fig 4.5A**; **Table 4.5**) as described previously. Despite a 3-fold difference in potency ($P \leq 0.001$) between human and rat, lodoxamide became the first agonist identified at GPR35 to act with high nM potency at both the human and rat orthologues (**Fig 4.5B**). However, at mouse GPR35, lodoxamide acted with 457-fold ($P \leq 0.001$) and 151-fold ($P \leq 0.001$) less potency than at human or rat, respectively (**Table 4.5**). Bufrolin generated a similar trend in species selectivity to lodoxamide, although the potency of human and rat was not statistically distinct and the potency at mouse was only 10 to 15-fold less potent ($P \leq 0.001$) than human or rat GPR35 (**Fig 4.5C**; **Table 4.5**). Cromolyn also displayed the h=r>m profile of species selectivity and generated responses some 3 to 6-fold more potent ($P \leq 0.001$) at human and rat than at

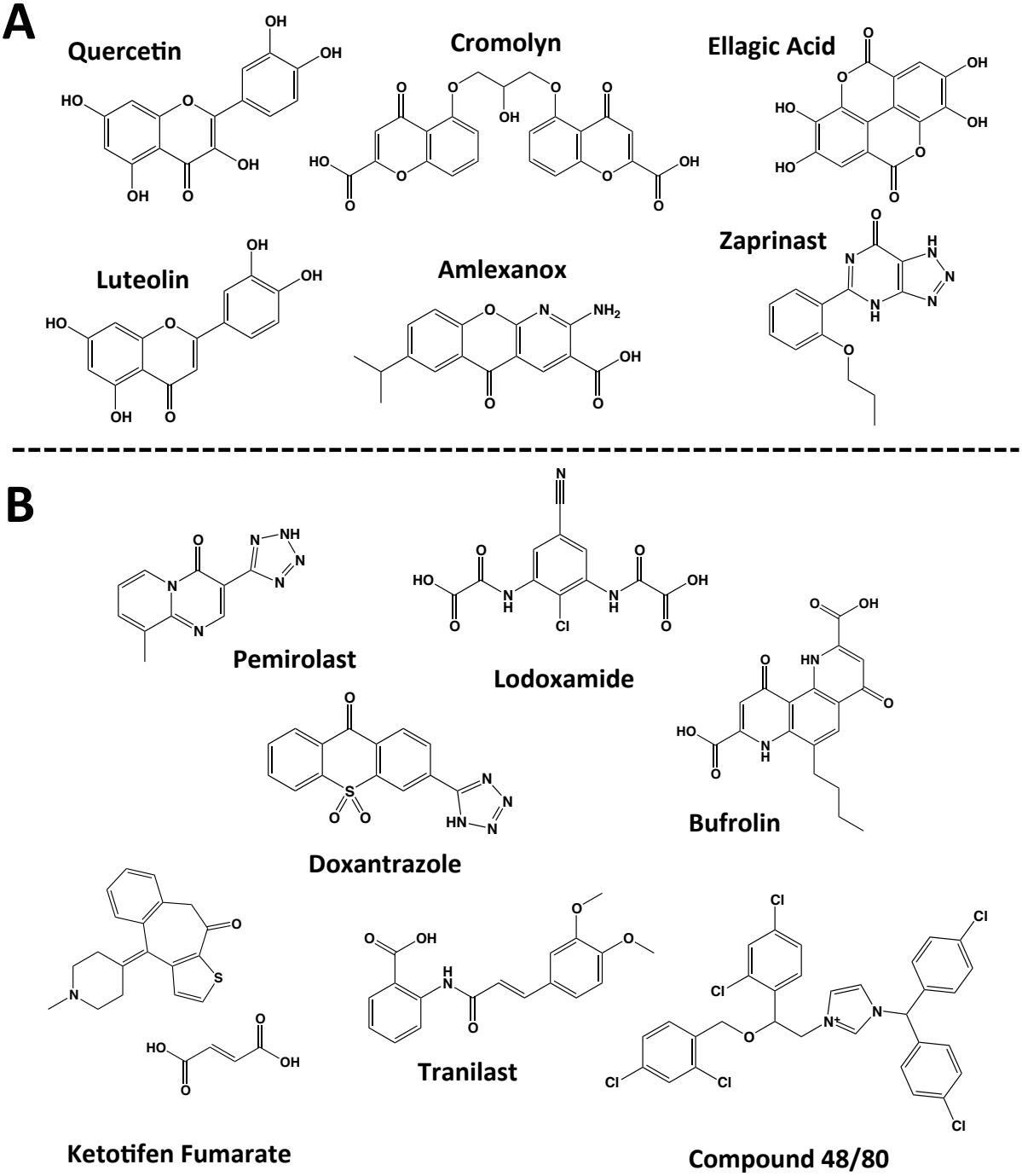

Figure 4.4 The chemical structure of mast cell stabilising compounds assessed for GPR35 agonism
The chemical structures of quercetin, luteolin, cromolyn, amlexanox, ellagic acid, and zaprinast, reported mast cell stabilisers and also GPR35 agonists (**A**). Mast cell stabilisers lodoxamide, bufrolin, pemirolast, doxantrazole, ketotifen fumarate, and tranilast are to be assessed herein for GPR35 activity, alongside the mast cell activator compound 48/80 (**B**).

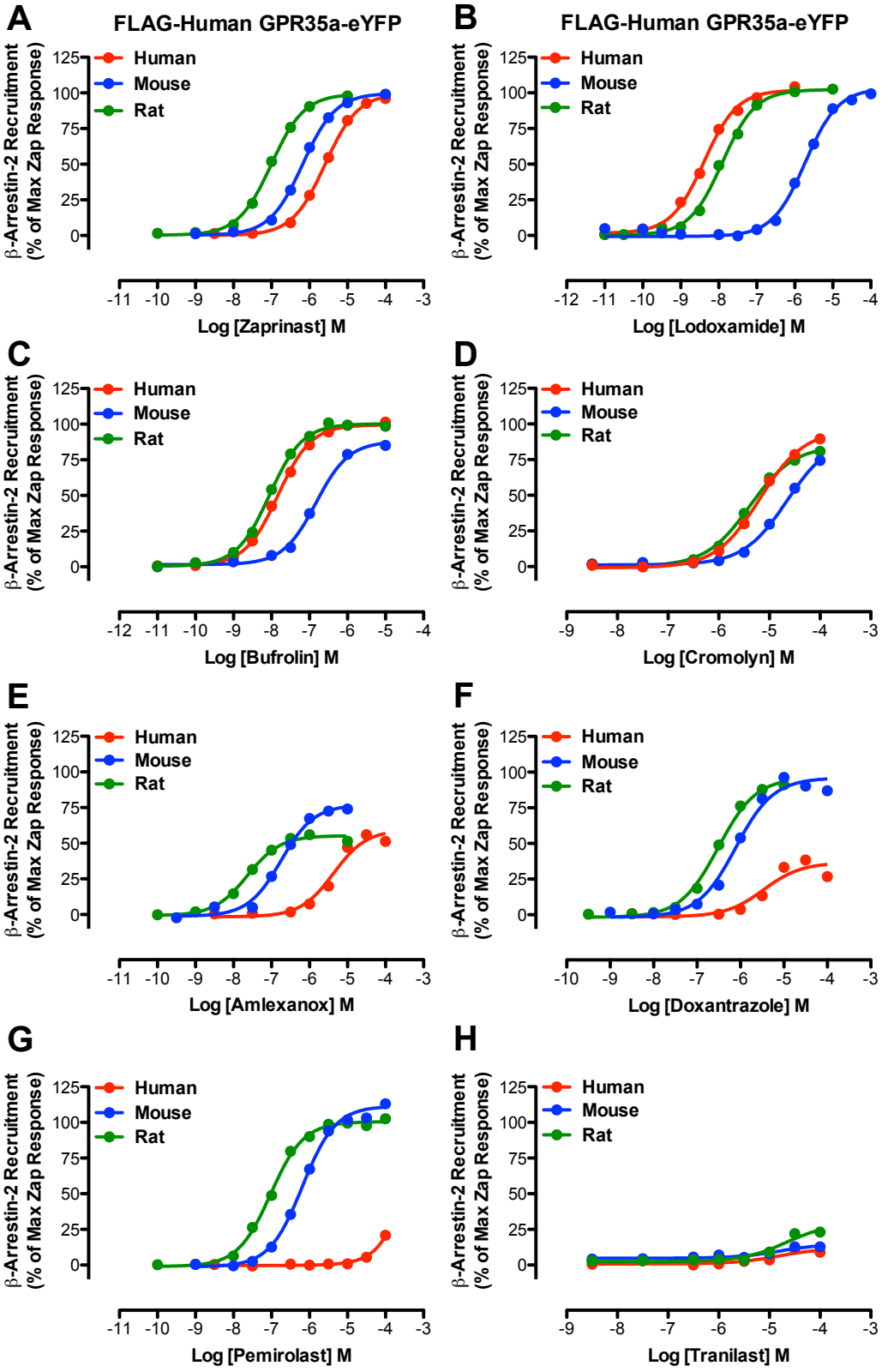

Figure 4.5 Mast cell stabilising compounds display species selectivity in the BRET assay The ability of zaprinast (**A**), lodoxamide (**B**), bufrolin (**C**), cromolyn (**D**), amlexanox (**E**), doxantrazole (**F**), pemirolast (**G**), and tranilast (**H**), to recruit β-arrestin-2 to GPR35 species orthologues is presented. Each dataset represents the mean of a minimum of three independent experiments carried out in duplicate ± SEM. Efficacy is normalised as a percentage of the maximal zaprinast response.

Table 4.5 Mast cell stabilisers display various species selectivity profiles at GPR35

Ligand	Human	Mouse	Rat	M-H	R-H	R-M	Selectivity
Zaprinast	pEC_{50} [a]			ΔpEC_{50} [b]			Rat
	5.59 ± 0.01	**6.18 ± 0.01**	**7.01 ± 0.02**	**+ 0.59 ± 0.02*****	**+ 1.42 ± 0.03*****	**+ 0.83 ± 0.03*****	
	E_{max} [c]			ΔE_{max} [d]			
	99.8 ± 0.7	99.8 ± 1.0	99.3 ± 0.9	NA	NA	NA	
Amlexanox	**5.38 ± 0.05*****	**6.75 ± 0.06*****	**7.63 ± 0.07*****	**+ 1.37 ± 0.11*****	**+ 2.25 ± 0.12*****	**+ 0.88 ± 0.11*****	Rat
	59.4 ± 1.5***	76.9 ± 1.5***	55.3 ± 0.1***	+ 17.5 ± 3.0***	- 4.1 ± 2.1	- 21.6 ± 2.1***	
Cromolyn	**5.20 ± 0.03*****	**4.71 ± 0.03*****	**5.39 ± 0.03*****	**- 0.49 ± 0.06*****	**+ 0.19 ± 0.06***	**+ 0.68 ± 0.06*****	Human and Rat
	95.5 ± 1.2*	91.2 ± 1.7**	84.8 ± 1.0***	- 4.3 ± 2.9	- 10.7 ± 2.2***	- 6.4* ± 2.8	
Bufrolin	**7.83 ± 0.02*****	**6.81 ± 0.04*****	**8.00 ± 0.02*****	**- 1.02 ± 0.06*****	**+ 0.17 ± 0.04**	**+ 1.19 ± 0.06*****	Human and Rat
	99.5 ± 0.9	91.8 ± 1.9**	100.6 ± 0.1	- 7.7 ± 3.0**	+ 1.1 ± 1.3	+ 8.8 ± 2.7***	
Lodoxamide	**8.38 ± 0.02*****	**5.72 ± 0.03*****	**7.90 ± 0.02*****	**- 2.66 ± 0.05*****	**- 0.48 ± 0.04*****	**+ 2.18 ± 0.05*****	Human and Rat
	102 ± 1.0	103.2 ± 1.7	102.3 ± 0.8	+ 1.2 ± 2.8	+ 0.2 ± 1.8	- 0.9 ± 2.7	
Doxantrazole	**5.47 ± 0.07***	**6.11 ± 0.03**	**6.51 ± 0.02*****	**+ 0.64 ± 0.11*****	**+ 1.04 ± 0.1*****	**+ 0.40 ± 0.05*****	Rat and Mouse
	36.5 ± 1.2***	96 ± 1.2	96.2 ± 1.0	+ 59.5 ± 2.4***	+ 59.7 ± 2.2***	+ 0.2 ± 2.2	
Pemirolast	**Inactive**	**6.19 ± 0.02**	**7.02 ± 0.03**	-	-	**+ 0.83 ± 0.05*****	Rat
	NA	111.5 ± 1.0***	100.5 ± 1.1	-	-	- 11.0 ± 2.1***	
Tranilast	**Inactive**	**Inactive**	**Inactive**	-	-	-	-
	NA	NA	NA	-	-	-	
Ketotifen Fumarate	**Inactive**	**Inactive**	**Inactive**	-	-	-	-
	NA	NA	NA	-	-	-	
Compound 48/80	**Inactive**	**Inactive**	**Inactive**	-	-	-	-
	NA	NA	NA	-	-	-	

[a] Statistically significant difference from the potency of zaprinast, *P* = *** ≤ 0.001, ** ≤ 0.01, * ≤ 0.05

[b] ΔpEC_{50} represents the difference in potency between species orthologues

[c] Statistically significant difference from the efficacy of zaprinast (%), *P* = *** ≤ 0.001, ** ≤ 0.01, * ≤ 0.05

[d] ΔE_{max} represents the difference in efficacy between species orthologues

NA, not applicable, -, not calculated

Data represents the mean ± SEM of a minimum of three independent experiments carried out in duplicate

mouse (**Fig 4.5D**; **Table 4.5**). The efficacy of cromolyn, however, did not reach full agonism at human ($P \leq 0.05$), mouse ($P \leq 0.01$) or rat ($P \leq 0.001$) GPR35 (**Table 4.5**). Amlexanox displayed partial agonism at all three species orthologues ($P \leq 0.001$), with potency at rat GPR35 being significantly greater than that at human ($P \leq 0.001$) or mouse ($P \leq 0.001$) (**Fig 4.5E**; **Table 4.5**). Meanwhile, doxantrazole displayed rat and mouse selectivity, with responses some 4 to 11-fold less potent ($P \leq 0.001$) than at human GPR35 (**Fig 4.5F**). Moreover, the efficacy of doxantrazole increased from partial agonism at human ($P \leq 0.001$), to full agonism at mouse and rat (**Table 4.5**). Pemirolast acted with rat selectivity ($P \leq 0.001$) and full agonism at the rodent orthologues, but it was inactive at human GPR35 (**Fig 4.5G**; **Table 4.5**). Tranilast (**Fig 4.5H**), ketotifen fumarate, and compound 48/80 (data not shown) meanwhile, were inactive at all three species orthologues in the BRET assay (**Table 4.5**).

4.2.2 *Mast cell stabilisers induce G protein coupling at human GPR35*

The IP-One assay was carried out with human GPR35 only, and this time in the absence of the addition of LiCl to cells during assay preparation to reduce constitutive activity (see **Section 2.7.2**). Zaprinast produced a pEC_{50} of 6.63 ± 0.09 when lithium chloride was added at the same time as test compound (**Table 4.6**) compared with a pEC_{50} of 7.00 ± 0.05 when lithium chloride was added before test compound (**Table 4.2**). Lodoxamide and bufrolin displayed a 6.2-fold ($P \leq 0.01$) and 14.8-fold ($P \leq 0.001$) increase in potency from the BRET assay (**Table 4.6**), to act with equal potency at human GPR35 in the IP-One assay (**Fig 4.6A/B**). Amlexanox generated full agonism in the IP-One system with a non-significant difference in potency between the two assay systems (**Fig 4.6C**), while cromolyn generated a 15.5-fold increase in potency ($P \leq 0.001$) between BRET and IP-One assays (**Fig 4.6D**). Akin to amlexanox, doxantrazole became a full agonist with potency not being significantly different between the BRET and IP-One assays (**Fig 4.6E**). Pemirolast, which was inactive in the BRET assay was active at human GPR35 in the IP-One format with a pEC_{50} of 4.73 ± 0.19 (**Fig 4.6F**).

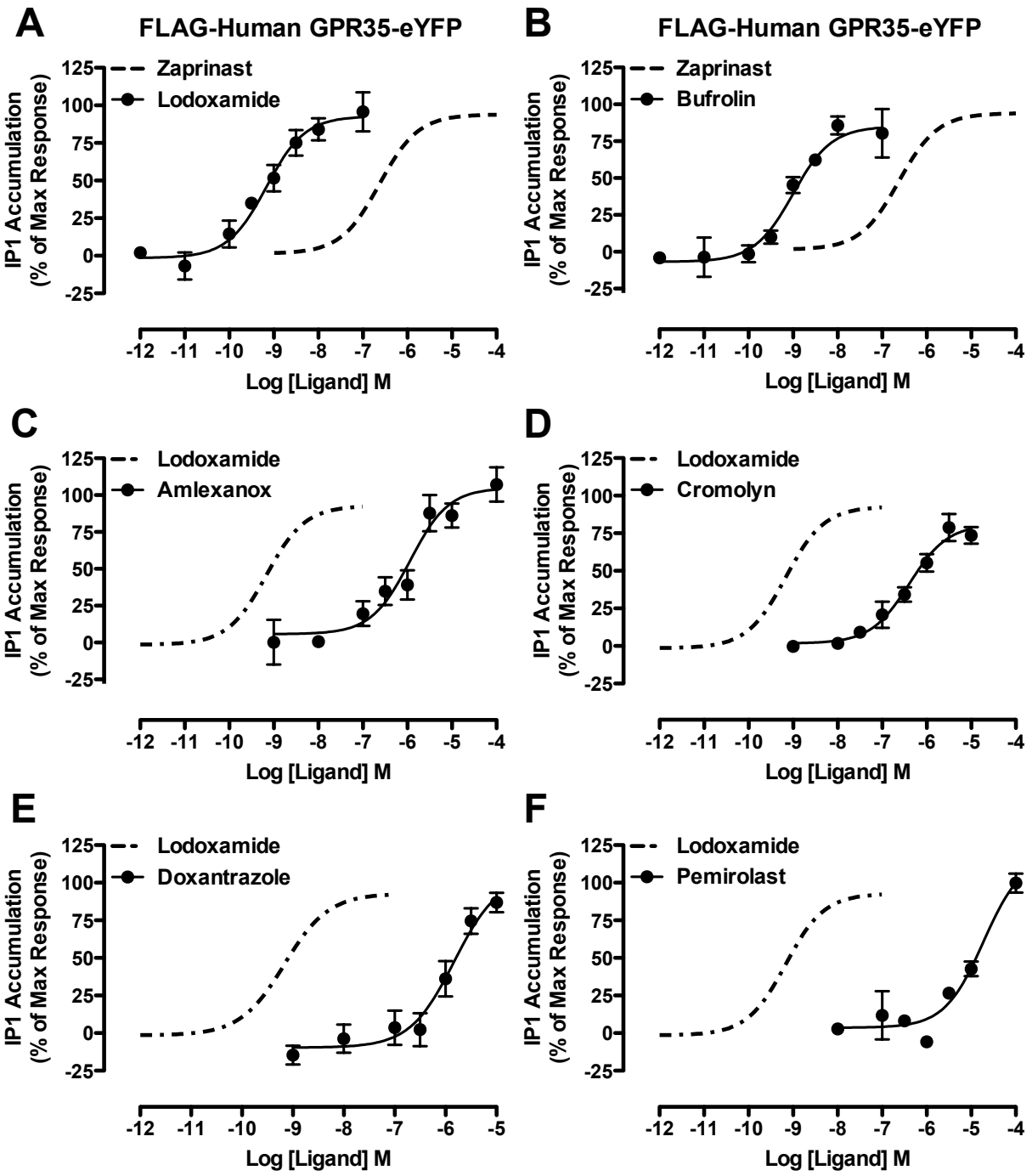

Figure 4.6 Mast cell stabilisers generate various responses in the IP-One assay IP_1 accumulation mediated by the $G\alpha_{q13}$ chimera and stimulation with lodoxamide (**A**), bufrolin (**B**), amlexanox (**C**), cromolyn (**D**), doxantrazole (**E**), or pemirolast (**F**), at human GPR35, is presented. Zaprinast (data shown in **Fig 3.8**) or lodoxamide (**A**) are presented as reference agonists (dashed lines). Each dataset represents the mean of a minimum of two independent experiments carried out in duplicate ± SEM with efficacy normalised as a percentage of the maximal zaprinast response.

Table 4.6 IP_1 accumulation responses of GPR35 agonist and mast cell stabilisers

		Human GPR35 IP_1 Accumulation		Human GPR35 β-arrestin-2 Recruitment		
Ligand	**Structure**	**pEC_{50} [a]**	**E_{max} (% max zap response) [b]**	**pEC_{50} [a]**	**E_{max} (% max zap response) [b]**	**ΔpEC_{50} [c]**
Zaprinast	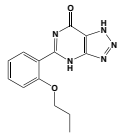	6.63 ± 0.09	92.6 ± 3.4	5.59 ± 0.01	99.8 ± 0.7	+ 1.03 ± 0.13
Amlexanox	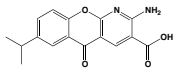	5.94 ± 0.18*	104.9 ± 7.8	5.38 ± 0.05***	59.4 ± 1.5***	+ 0.56 ± 0.26
Cromolyn	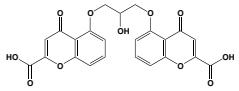	6.39 ± 0.15	81.1 ± 5.6	5.20 ± 0.03***	95.5 ± 1.2*	+ 1.19 ± 0.08
Bufrolin	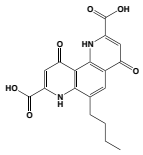	9.00 ± 0.20***	85.1 ± 7.7	7.83 ± 0.02***	99.5 ± 0.9	+ 1.17 ± 0.28
Lodoxamide	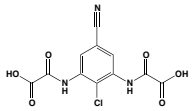	9.17 ± 0.16***	92.8 ± 6.0	8.38 ± 0.02***	102.0 ± 1.0	+ 0.79 ± 0.23
Doxantrazole	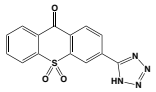	5.83 ± 0.19*	104.9 ± 14.1	5.47 ± 0.07*	36.5 ± 1.2***	+ 0.36 ± 0.29
Pemirolast	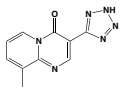	4.73 ± 0.19***	117.8 ± 13.8	Inactive	NA	-

[a] Statistically significant difference from the potency of zaprinast, *P* = *** ≤ 0.001, ** ≤ 0.01, * ≤ 0.05

[b] Statistically significant differences from zaprinast efficacy, *P* = *** ≤ 0.001, ** ≤ 0.01, * ≤ 0.05

[c] ΔpEC_{50} represents the difference in potency between IP-One and BRET assays

NA, not applicable; - , not calculated

Data represent the mean ± SEM of a minimum of two independent experiments carried out in duplicate

4.2.3 Transduction coefficients assess pathway bias between β-arrestin-2 and IP_1 pathways

Akin to the analysis performed with the MRCT compounds, transduction coefficients were calculated for the GPR35 agonist/mast cell stabilisers to determine if they displayed pathway bias. A $\Delta\Delta Log(\tau/K_A)$ ratio <1 was indicative of bias toward β-arrestin-2 recruitment, while >1 indicated bias toward IP_1 accumulation (**Table 4.7**). All of the compounds generated $\Delta\Delta Log(\tau/K_A)$ ratios that were close to 1, indicating that there was not a strong bias towards either pathway. Nonetheless, the data indicated that there was at least some preference of bufrolin toward G protein signalling and IP_1 accumulation, while lodoxamide displayed the opposite profile, toward β-arrestin-2 recruitment (**Table 4.7**). Amlexanox and cromolyn generated similar bias ratios, which were toward IP_1 accumulation, while doxantrazole acted with almost equal effect through both pathways (**Table 4.7**).

4.2.4 Lodoxamide and bufrolin do not conform to the rules of simple competitive antagonism

To assess whether ML-145 behaved in a competitive manner with lodoxamide and bufrolin, Schild analysis was carried out using various concentrations of agonist in the presence and absence of fixed antagonist concentration as described previously (**Section 4.1.5**). In the β-arrestin-2 recruitment assay, ML-145 acted in a manner consistent with competitive antagonism when assessed alongside zaprinast (**Fig 4.7A/B**), with increasing antagonist concentration increasing the concentration of zaprinast required to achieve an EC_{50} value (**Table 4.8**); however, the potency of zaprinast limited the opportunity to observe surmountability of the antagonist blockade. Due to the high potency of lodoxamide it was possible for this ligand to overcome ML-145's antagonism at all concentrations assessed (**Fig 4.7C**). This was not the case for bufrolin, however, which was limited by poor solubility and failed to achieve receptor occupancy at high antagonist concentrations (**Fig 4.7E**). In contrast to the competition observed between ML-145 and zaprinast, the global Gaddum/Schild analysis indicated that the competition between ML-145 and lodoxamide (**Fig 4.7C/D**) or bufrolin (**Fig 4.7E/F**) differed from unity (**Table 4.8**) – indicating a deviation from the model of simple competitive antagonism. Despite this, the reciprocal dose ratios indicate that the competition between ML-145, lodoxamide (**Fig 4.7D)** or bufrolin (**Fig 4.7F**) is linear, indicating that these compounds are not acting at distinct sites on the receptor.

Table 4.7 GPR35 agonists display limited pathway bias between β-arrestin-2 recruitment and IP_1 accumulation

	FLAG-Human GPR35-eYFP				
	$Log(\tau/K_A)^a$		$\Delta Log(\tau/K_A)^b$		$\Delta\Delta Log(\tau/K_A)^c$
Compound	**BRET**	**IP-One**	**BRET**	**IP-One**	
Zaprinast	**5.56**	6.40	**1.00**	1.00	1.00
Amlexanox	**5.12**	6.18	**0.36**	0.60	1.67
Bufrolin	**7.80**	8.79	**173.80**	245.50	1.41
Cromolyn	**5.14**	6.22	**0.38**	0.66	1.74
Doxantrazole	**5.01**	5.82	**0.28**	0.26	0.93
Lodoxamide	**8.40**	9.05	**691.80**	446.70	0.65
Pemirolast	**NA**	4.97	**-**	-	-

[a] $Log(\tau/K_A)$ calculated using the formula described in **Section 2.8.4**.

[b] Within pathway ratio, $\Delta(Log(\tau/K_A)$ is the fold difference relative to zaprinast at each species orthologue

[c] Between pathway ratio, $\Delta\Delta(Log(\tau/K_A)$ is the $\Delta(Log(\tau/K_A)$ from IP-One pathway divided by the $\Delta(Log(\tau/K_A)$ from BRET; a value >1 indicates bias toward the IP_1 accumulation pathway, and <1 a bias toward β-arrestin-2 recruitment pathway

NA, not applicable, -, not calculated

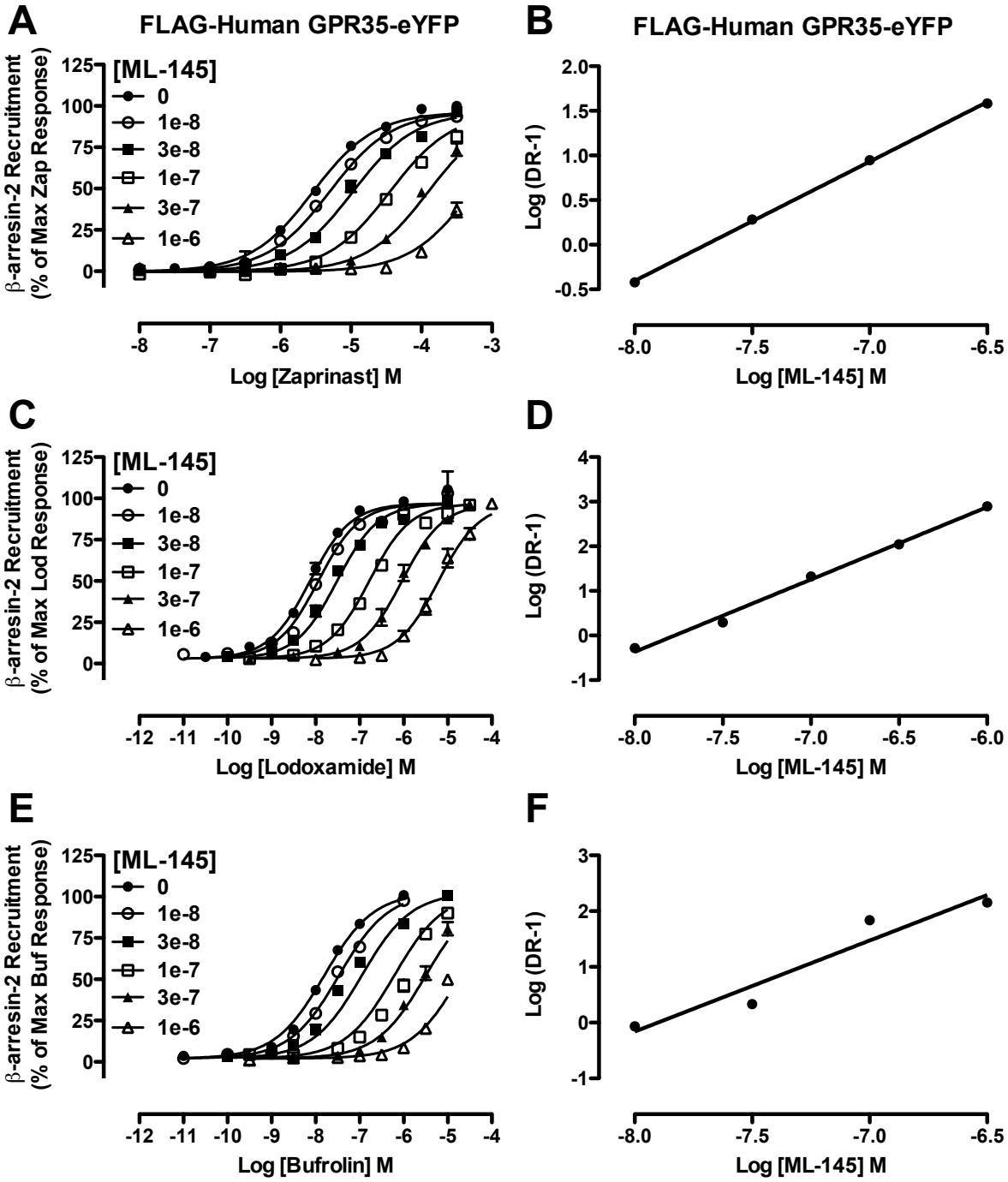

Figure 4.7 The antagonism of lodoxamide and bufrolin by ML-145 does not conform to the rules of competitive antagonism Concentration-responses of zaprinast (**A**), lodoxamide (**C**), and bufrolin (**E**) were assessed in the absence and presence of increasing ML-145 concentrations using the Gaddum/Schild EC_{50} shift global analysis in the β-arrestin-2 recruitment assay. To determine whether the antagonist competition was linear, the reciprocal of the log dose-ratio was plotted against the molar ML-145 concentration for zaprinast (**B**), lodoxamide (**D**) or bufrolin (**F**). Each dataset represents the mean of three independent experiments carried out in duplicate ± SEM, normalised to the maximum agonist only response.

Table 4.8 ML-145 does not appear to compete with lodoxamide or bufrolin in a simple competitive manner

		BRET	
Antagonist	**Agonist**	**Schild Slope**	**pA_2**
ML-145	Zaprinast	1.17 ± 0.04	7.90 ± 0.03
	Lodoxamide	1.59 ± 0.03	7.83 ± 0.03
	Bufrolin	1.49 ± 0.04	8.04 ± 0.05

Data are the mean ± SEM of three independent experiments carried out in duplicate

Thus, there appear to be other factors that are shifting the Schild slope to a value greater than 1, of which the transient nature of the interaction between receptor and β-arrestin-2 (**Figure 3.10**) and the lack of a steady state for BRET measurements to be taken appears a likely cause.

4.3 A pharmacological characterisation of GPR35 agonist responses in a cell system endogenously expressing *GPR35*

As the physiological function and associated signalling pathways have yet to be elucidated for GPR35, the label-free DMR platform provided a format for ligand-induced responses to be monitored in cell lines endogenously expressing *GPR35*. Since the pattern of ligand-induced DMR traces is reported to be deterministic of the G proteins involved in receptor coupling (Schröder et al., 2010) responses generated in DMR assays were compared with data obtained from the IP-One accumulation assay. Data were also compared between DMR and the BRET method of β-arrestin-2 recruitment since it has not been definitively demonstrated that DMR assays solely monitor G protein signalling.

4.3.1 *Profiling of GPR35 agonist responses in HT-29 cells using DMR technology*

MRCT compound 1 and the mast cell stabiliser/GPR35 agonists were assessed for their ability to induce DMR post ligand addition in the human colorectal adenocarcinoma HT-29 cell line that endogenously expresses *GPR35* (**Section 3.3.1**). All GPR35 agonists assessed generated comparable kinetic DMR traces with a positive DMR peak occurring immediately following agonist addition (**Fig 4.8**) with data extrapolated from the five min post ligand time point presented as concentration-response curves (**Fig 4.9**). Zaprinast generated comparable responses in the DMR and IP-One assays, being some 13.8-fold more potent ($P \leq 0.001$) than potency generated in the BRET system (**Table 4.9**). This was a trend observed for the majority of agonists assessed, in addition to all agonists generating full efficacy in the DMR system (**Fig 4.9**; **Table 4.9**). Compound 1 acted with potency some 15-fold ($P \leq 0.001$) and 51-fold ($P \leq 0.001$) more potent than in the IP-One and BRET assays, respectively (**Fig 4.9A**), and while the DMR response of bufrolin was not statistically distinct from IP-One, it was 14-fold ($P \leq 0.001$) more potent than in the BRET assay (**Fig 4.9B**). Lodoxamide did not

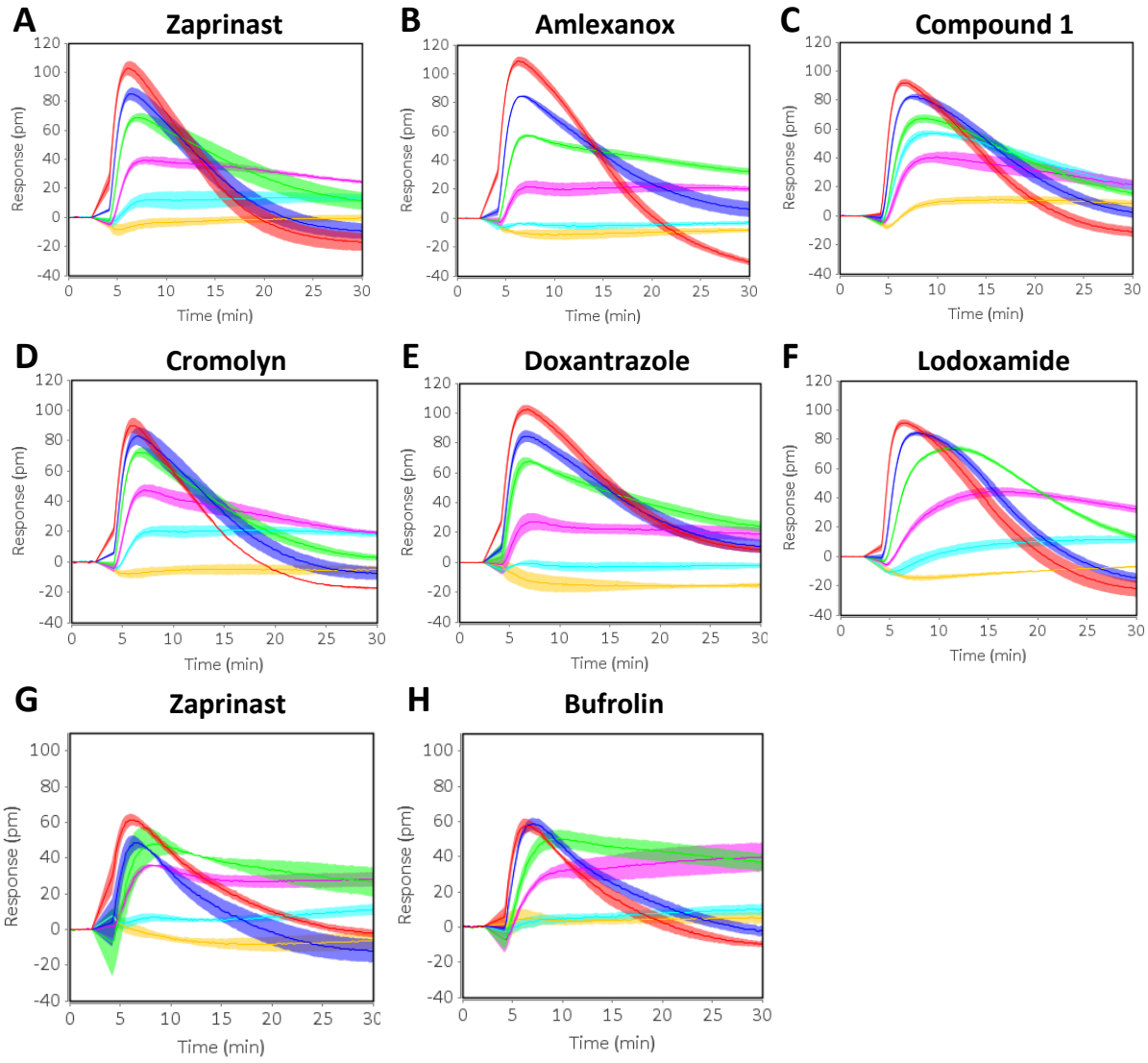

Figure 4.8 Different GPR35 agonists display similar kinetic traces in the DMR assay Kinetic DMR traces were monitored every 2 sec for 30 min, with agonist added following a 2 min baseline read. Positive DMR occurred in a concentration-dependent manner, with concentration-responses calculated from the above traces presented in **Fig 4.9**. All traces are baseline corrected from cells treated with vehicle only, with concentration-responses increasing from yellow (lowest concentration) to red (highest concentration). Concentrations used for each compound are indicated in **Fig 4.9**. **A – F** are traces taken from the same experiment, while **G – H** were assayed separately. Data are representative of three independent experiments carried out in quadruplicate, depicting a single experiment with traces and error of four individual wells.

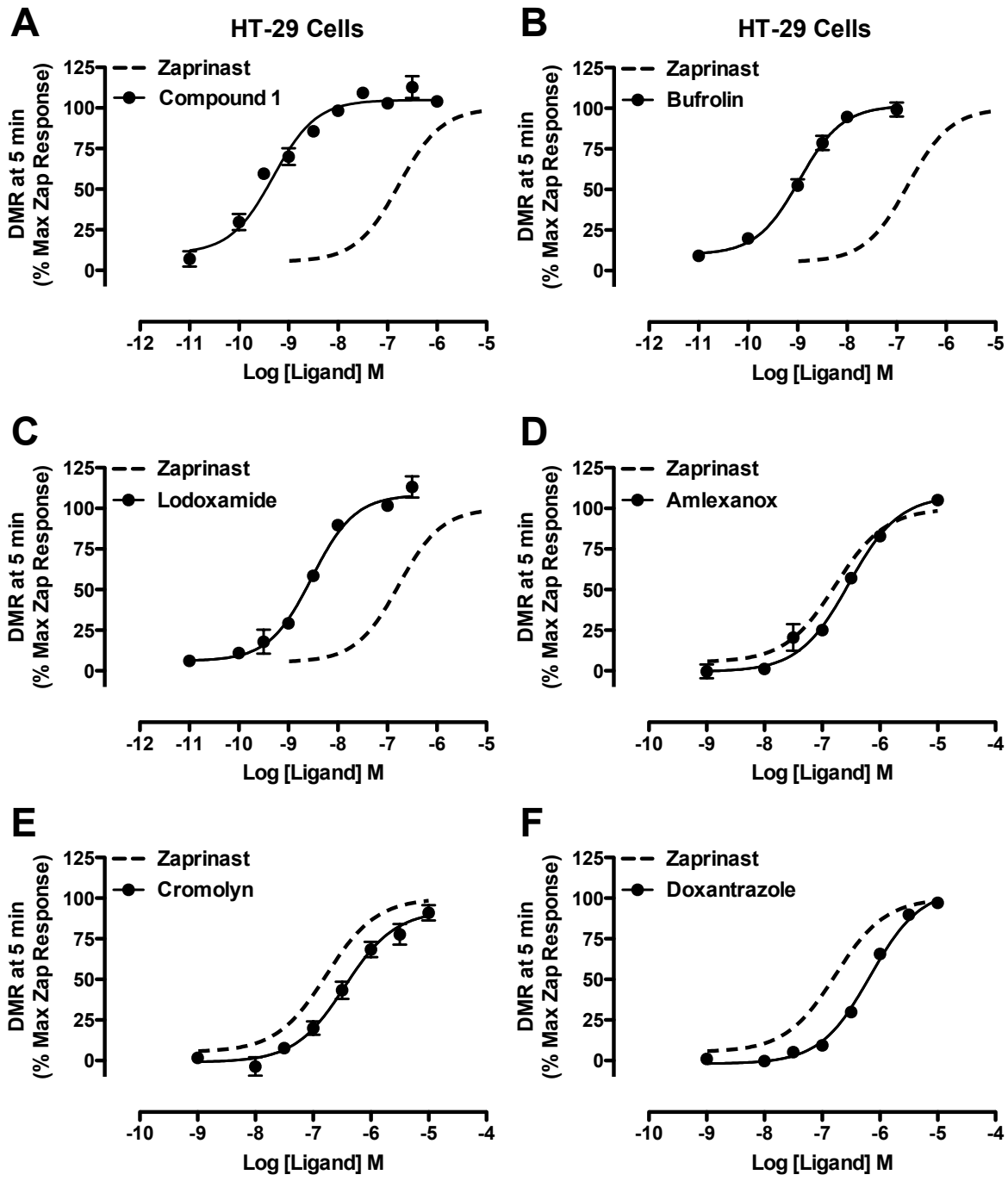

Figure 4.9 GPR35 agonists produce responses in a concentration-dependent manner in the DMR assay using HT-29 cells Human colorectal adenocarcinoma HT-29 cells endogenously expressing human GPR35 were incubated overnight in plates containing waveguide grated biosensors. DMR was monitored using the Epic BT® system, with positive DMR occurring 5 min post ligand addition plotted against ligand concentration. The ability of compound 1 (**A**), bufrolin (**B**), lodoxamide (**C**), amlexanox (**D**), cromolyn (**E**), and doxantrazole (**F**), to induce DMR is presented. Zaprinast (dashed lines) is presented as a reference agonist (originally shown in **Fig 3.13**). Each dataset represents the mean of three independent experiments carried out in quadruplicate ± SEM, with efficacy normalised as a percentage of the maximum zaprinast response.

Table 4.9 GPR35 agonists mediated DMR from HT-29 cells and a comparison with the IP-One and BRET systems in HEK293 cells

	HT-29 Cell DMR		IP-One: Human GPR35 IP_1 Accumulation		BRET: Human GPR35 β-arrestin-2 Recruitment	
Ligand	**pEC_{50} [a]**	**E_{max} [b]**	**pEC_{50} [a]**	**E_{max} [b]**	**pEC_{50} [a]**	**E_{max} [b]**
Zaprinast	6.77 ± 0.08	99. 9 ± 3.2	6.63 ± 0.09	92.6 ± 3.4	5.59 ± 0.01	99.8 ± 0.7
Amlexanox	6.54 ± 0.06	107.9 ± 3.3	5.94 ± 0.18*	104.9 ± 7.8	5.38 ± 0.05***	59.4 ± 1.5***
Compound 1	9.31 ± 0.09***	104.9 ± 2.5	8.13 ± 0.09***	86.0 ± 3.5	7.60 ± 0.03	100.2 ± 1.3
Cromolyn	6.45 ± 0.09*	92.3 ± 4.1	6.39 ± 0.15	81.1 ± 5.6	5.20 ± 0.03***	95.5 ± 1.2*
Bufrolin	8.97 ± 0.07***	101.7 ± 2.8	9.00 ± 0.20***	85.1 ± 7.7	7.83 ± 0.02***	99.5 ± 0.9
Lodoxamide	8.53 ± 0.05***	108.4 ± 2.2	9.17 ± 0.16***	92.8 ± 6.0	8.38 ± 0.02***	102.0 ± 1.0
Doxantrazole	6.17 ± 0.05***	105.6 ± 3.1	5.83 ± 0.19*	104.9 ± 14.1	5.47 ± 0.07*	36.5 ± 1.2***

[a] Statistically significant difference from the potency of zaprinast, *P* = *** ≤ 0.001, ** ≤ 0.01, * ≤ 0.05

[b] Statistically significant differences the efficacy of zaprinast, *P* = *** ≤ 0.001, ** ≤ 0.01, * ≤ 0.05

[c] ΔpEC_{50} represents the difference in potency between DMR and BRET assays

[d] ΔpEC_{50} represents the difference in potency between DMR and IP-One assays

Data are the mean ± SEM of a minimum of three independent experiments (DMR assays assessed in quadruplicate, IP-One and BRET, in duplicate)

act in a statistically different manner between DMR and BRET assays, but generated a 4.4-fold decrease ($P \leq 0.05$) between the DMR and IP-One assay systems (**Fig 4.9C**). For amlexanox, potency in the DMR system was some 4-fold higher ($P \leq 0.05$) than IP-One and 14-fold higher ($P \leq 0.001$) than in the BRET assay (**Fig 4.9D**; **Table 4.9**). Meanwhile, the potency of cromolyn and doxantrazole was not statistically different in the DMR or IP-One assays, but was some 18-fold ($P \leq 0.001$) and 5-fold ($P \leq 0.01$) more potent than in the BRET assay, respectively (**Fig 4.9E/F**).

4.3.2 *Confirmation that zaprinast and lodoxamide-induced signals are via GPR35 using ML-145 in the DMR assay*

One of the most important aspects of assessing ligand-induced signalling via HT-29 cells was to verify that the response generated was indeed emanating from GPR35. In order to assess this, Schild analysis was carried out using the GPR35 antagonist/ inverse agonist ML-145. However, since GPR35 displayed constitutive activity in the HT-29 cell system (data not shown), increasing ML-145 concentration was accompanied with a depression to the basal response. This negated the requirements of the Schild analysis and any analytical values generated by such processes. Akin to the Schild analysis carried out using the MRCT compounds in the IP-One assay (**Section 4.1.5**), zaprinast and lodoxamide were assessed in competition with ML-145 to confirm the specificity of the GPR35 agonist response in HT-29 cells in the DMR assay system. By constraining the basal and maximal DMR response of zaprinast and lodoxamide, it can be observed that incubation with fixed, increasing, concentrations of ML-145 rightward shifted the concentration response curves of both agonists (**Fig 4.10A/B**). This suggested that the DMR peaks of zaprinast and lodoxamide, therefore, were generated as a result of GPR35 agonism in the HT-29 cell system.

4.3.3 *A calculation of agonist bias between β-arrestin-2, IP_1 accumulation, and DMR pathways*

Transduction coefficients were calculated for compound 1 and the mast cell stabiliser/ GPR35 agonists to identify if pathway bias existed between the β-arrestin-2, IP_1 accumulation, or DMR pathways using zaprinast as reference agonist; the previously

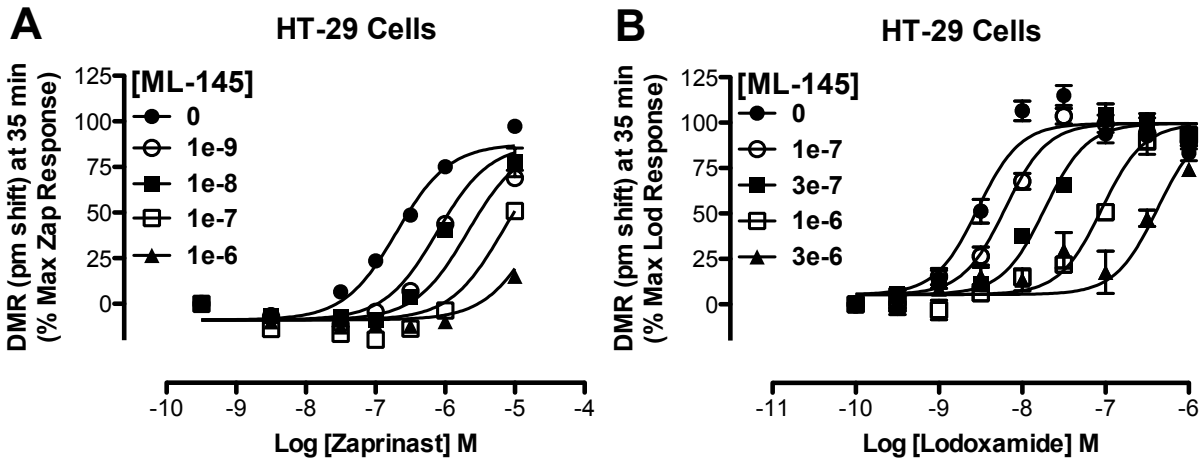

Figure 4.10 ML-145 is competitive with zaprinast and lodoxamide in the DMR assay ML-145 was pre-incubated with HT-29 cells for 30 min before the addition of zaprinast (**A**) or lodoxamide (**B**) for 5 min. Data are presented as the DMR responses at 35 min post initial antagonist addition. Zaprinast represents the mean ± SEM of two independent experiments, while lodoxamide represents an the mean ± SEM of four independent experiments with each condition assessed in duplicate. Data are presented relative to the maximum and minimum agonist-only response to correct for the inverse agonism associated with ML-145.

calculated pathway bias profile between IP-One and BRET assays was also displayed for comparison purposes although it is appropriate to note that the experimental analysis was carried out in distinct cell lines (**Table 4.10**). Interestingly, compound 1 acted with clear bias towards the DMR pathway with a $\Delta\Delta Log(\tau/K_A)$ value of 17 (**Table 4.10**). Amlexanox, bufrolin, and doxantrazole, with values close to 1 however, did not appear biased between the DMR or IP_1 accumulation pathways (**Table 4.10**). Cromolyn and lodoxamide meanwhile, displayed some bias toward the IP_1 accumulation pathway (**Table 4.10**). In comparison with the β-arrestin-2 pathway compound 1 and amlexanox, with ratios >1, displayed bias toward the DMR pathway (**Table 4.10**). Bufrolin, cromolyn, and doxantrazole, meanwhile acted without bias while lodoxamide displayed preference toward the β-arrestin-2 recruitment pathway (**Table 4.10**).

Thus, it appears that a subset of mast cell stabilisers also act with an ability to activate GPR35, and at human GPR35 this has been demonstrated to occur in a cell line endogenously expressing the receptor. Unlike the MRCT compounds presented herein however, lodoxamide and bufrolin do not appear to interact with the GPR35 antagonist ML-145 in a simple competitive manner. The characterisation of these ligands is presented fully in the publication authored by Mackenzie et al., 2014, which also presents the molecular homology modelling effort of these ligands in the proposed binding pocket of GPR35 as carried out by Dr. Gianluigi Caltabiano (**Appendix C**).

Table 4.10 An assessment of GPR35 agonist pathway bias generated through the BRET, IP-One and DMR assays

	$Log(\tau/K_A)^a$		$\Delta Log(\tau/K_A)^b$		$\Delta\Delta Log(\tau/K_A)^c$
Compound	**DMR**	**IP-One**	**DMR**	**IP-One**	
Zaprinast	**6.68**	6.4	**1**	1	**1**
Amlexanox	**6.56**	6.18	**0.76**	0.6	**1.27**
Bufrolin	**9.05**	8.79	**234.4**	245.5	**0.95**
Compound 1	**9.46**	7.95	**602.6**	35.5	**17**
Cromolyn	**6.27**	6.22	**0.39**	0.66	**0.59**
Doxantrazole	**6.14**	5.82	**0.29**	0.26	**1.11**
Lodoxamide	**8.63**	9.05	**89.1**	446.7	**0.2**
	$Log(\tau/K_A)^a$		$\Delta Log(\tau/K_A)^b$		$\Delta\Delta Log(\tau/K_A)^d$
Compound	**DMR**	**BRET**	**DMR**	**BRET**	
Zaprinast	**6.68**	5.56	**1**	1	**1**
Amlexanox	**6.56**	5.12	**0.76**	0.36	**2.11**
Bufrolin	**9.05**	7.8	**234.4**	173.8	**1.35**
Compound 1	**9.46**	7.53	**602.6**	93.3	**6.46**
Cromolyn	**6.27**	5.14	**0.39**	0.38	**1.02**
Doxantrazole	**6.14**	5.01	**0.29**	0.28	**1.03**
Lodoxamide	**8.63**	8.4	**89.1**	691.8	**0.13**

[a] $Log(\tau/K_A)$ values were calculated for the DMR, IP-One and BRET assays

[b] Within pathway ratio $\Delta(Log(\tau/K_A)$, fold difference relative to zaprinast at each species orthologue

[c] Between pathway ratio $\Delta\Delta(Log(\tau/K_A)$, $\Delta(Log(\tau/K_A)$ from DMR pathway divided by the $\Delta(Log(\tau/K_A)$ of IP-One; a value >1 indicates bias toward the DMR pathway, and <1 a bias toward IP_1 accumulation

[d] $\Delta(Log(\tau/K_A)$ from DMR pathway divided by the $\Delta(Log(\tau/K_A)$ of BRET; a value >1 indicates bias toward the DMR pathway, and <1 a bias toward the β-arrestin-2 recruitment pathway

4.4 Discussion

Originally, small molecule compound libraries were formed as a result of attempts to chemically enhance the structural and pharmacological properties of known endogenous ligands. However, as these efforts were based on a relatively small number of therapeutic targets, the molecules tended not to be structurally diverse and a large degree of structural overlap exists between these molecules. Furthermore, many of these compounds are not suitable as therapeutics and exist primarily as tool compounds for screening campaigns to elucidate common structural motifs that are important for activation of the receptor. Previous small molecule compound library screening efforts at GPR35 identified pamoic acid (Zhao et al., 2010; Jenkins et al., 2010), cromolyn (Yang et al., 2010; Jenkins et al., 2010), dicoumarol, luteolin, niflumic acid, quercetin and zaprinast (Jenkins et al., 2010) as agonists. However, most of these ligands were of modest potency, activated other biological targets with reasonable potency, and/or acted with marked species selectivity. As part of my PhD project, a collaborative study with the MRCT was initiated aiming to identify novel small molecule agonists of GPR35 that acted with high potency and activated human and rodent orthologues within a similar concentration range.

To this end, a screening campaign was initiated against the MRCT's internal collection of 100,000 small molecules using the DiscoveRx's PathHunter β-arrestin-2 translocation enzyme complementation assay, as detailed in Neetoo-Isseljee et al., 2013. From this effort, GPR35 hit compounds with distinct structural properties were profiled and assessed in a number of different pharmacological outputs against species orthologues of GPR35. This study culminated in the identification of 'compound 1' ((4-{(Z)-[(2Z)-2-(2-fluorobenzylidene)-4-oxo-1,3-thiazolidin-5-ylidene]methyl}benzoic acid)), which was the most potent agonist of GPR35 reported at that time, with a potency of 25 nM in the BRET assay. Previously, the most potent ligand that had been reported for human GPR35 was pamoic acid, which recorded an EC_{50} in the BRET β-arrestin-2 recruitment assay of 50 nM. However, although their potencies were within a similar range, pamoic acid acted only with partial efficacy in the β-arrestin-2 recruitment assay while compound 1 was a full agonist (Jenkins et al., 2010; Neetoo-Isseljee et al., 2013). Subsequently, lodoxamide and bufrolin, as reported herein and in Mackenzie et al., 2014, became the most potent ligands of GPR35, with EC_{50}s in the BRET β-arrestin-2 recruitment assay of 4.2 nM and 14.8 nM. More recently Funke et al.,

(2013) also reported a potent ligand of human GPR35, named PSB-13253. In the BRET β-arrestin-2 recruitment assay, PSB-13253 generates an EC_{50} of 35 nM (my unpublished finding). Thus, compound 1, PSB-13253, and pamoic acid act within a similar potency range at the human receptor. These compounds are reasonably potent and are useful for understanding of the pharmacology of the human receptor; however, their use is impractical in rodent studies since all three ligands act with marked human selectivity (Jenkins et al., 2012; Neetoo-Isseljee et al., 2013; Funke et al., 2013). Importantly, this is not the case for bufrolin or lodoxamide, which activate the human and rat orthologues of GPR35 with similar potency (Mackenzie et al., 2014). This Discussion will focus on the information these ligands have provided in terms of understanding GPR35 receptor pharmacology, functional selectivity (also known as pathway bias) and species selectivity.

4.4.1 *Screening of MRCT's compound library and assessment of a subset of mast cell stabilisers indicate that a carboxyl group is a common structural property of GPR35 ligands*

Compounds 1-5 are novel structures that are chemically diverse in nature (**Table 4.1**), although, with the exception of the tricyclic compound 5, they all share a carboxyl group. The mast cell stabilisers lodoxamide and bufrolin also contain carboxyl groups, but akin to pamoic acid and cromolyn they are dicarboxylates (**Fig 4.4**; **Fig 3.1**). This suggests that the carboxyl group of GPR35 ligands may be important for receptor recognition and/or activation (Jenkins et al., 2010; Deng and Fang 2012b; Deng et al., 2012d; Funke et al., 2013), however ligands that do not contain carboxylic acids can activate GPR35. These 'non-carboxylic acid' ligands include zaprinast (which contains a triazole group), doxantrazole and pemirolast, (which contain a tetrazole group) that act as carboxylic acid bioisosteres; phenols such as nitecapone, tolcapone (Deng et al., 2012b), quercetin, luteolin (Jenkins et al., 2010) and wedelolactone (Deng and Fang 2012a); and melanonitrile containing molecules (Deng et al., 2011b). Thus, although there is not an absolute requirement for a carboxyl group to bind or to activate human GPR35, at the very least GPR35 ligands appear to be negatively charged or are electron withdrawing (Jenkins et al., 2010; Deng et al., 2011b; 2012d; Deng and Fang, 2012b; Funke et al., 2013).

For ligands that contain a carboxyl group however, this group is imperative for function. An example to support this is demonstrated with the ethyl ester derivative of

kynurenic acid, which was inactive in a β-arrestin-2 recruitment assay at human and rat GPR35 (Jenkins et al., 2011). Structure activity relationship (SAR) studies performed by researchers based at Corning also indicated that changing the carboxylic acid to an ethyl ester rendered the novel structure [3,2-*b*]thiophene-2-carboxylic acid inactive (Deng et al., 2011b). However, Funke and colleagues indicated that human GPR35 relied less on the negative charge than either mouse or rat, as the ethyl ester of 8-benzamido-chromen-4-one-2-carboxylic acid was able to recruit β-arrestin-2 to human but not rodent GPR35 (Funke et al., 2013). Since data indicate that GPR35 ligands containing an acid bioisostere are significantly rodent selective (such as doxantrazole, pemirolast) (Mackenzie et al., 2014), it is likely that ligands with charge differences preferentially interact with one GPR35 species orthologue over the other.

In this context, since pamoic acid was a dicarboxylic acid with marked species selectivity toward human GPR35, it was suggested that human GPR35 was likely to contain two positively charged binding regions within the ligand binding pocket, with rat GPR35 only having one positively charged region. This theory however, was invalidated following the identification of lodoxamide and bufrolin as human and rat equipotent agonists. Thus, there must be distinct structural properties within these ligands that enable their cross-species activity. Indeed, site directed mutagenesis efforts (described in **Chapter Five**) used in conjunction with receptor homology modelling, indicated that the cyano group of lodoxamide and the propyl appendage of bufrolin interacted with a human specific valine residue at position 2.60 (Mackenzie et al., 2014). Therefore, it appeared that lodoxamide and bufrolin achieved their equipotent activity at human and rat GPR35 by binding differently between the two species of receptor. Understanding which residues are meditating these differences is of the utmost importance for the rational design of species equipotent antagonists, since neither ML-145 nor CID2745687 function at the rodent orthologues of GPR35 (**Fig 3.8**).

4.4.2 *What is the relevance of GPR35 ligands having mast cell stabilising properties?*

This body of work presented for the first time that certain known mast cell stabilisers amlexanox, lodoxamide, bufrolin, doxantrazole, and pemirolast potassium, activate GPR35 (**Fig 4.5**). Previously reported GPR35 agonists also display mast cell stabiliser functionality,

including luteolin, ellagic acid, gallic acid, morin, dicoumarol, quercetin, furosemide, nedrocromil, nivimedone, and cromolyn (Jenkins et al., 2010; Yang et al., 2010; Deng et al., 2012b; Deng and Fang 2012a; Yang et al., 2012; Neetoo-Isseljee et al., 2013; Mackenzie et al., 2014). Importantly, this body of work indicated that not all mast cell stabilisers are GPR35 agonists, as demonstrated by the lack of activity of ketotifen fumarate and tranilast at GPR35 (**Table 4.5**). Of the mast cell stabiliser compounds that activate GPR35, most have been marketed as ophthalmic solutions. These include cromolyn (Opticrom®), amlexanox (Elics®), lodoxamide tromethamine (Alomide®), nedrocromil sodium (Alocril®), and pemirolast potassium (Alamast®). Bufrolin and doxantrazole have not been marketed commercially. Unlike cromolyn and counterparts, the non-GPR35 agonist ketotifen fumarate (Zatidor®) is a second-generation histamine H_1 receptor antagonist and therefore displays dual function to stabilise mast cells (Abelson et al., 2011), and tranilast is a mast cell stabiliser and anti-allergy mediation (Rizaben®) with no obvious distinction from the GPR35 ligands.

The role of GPR35 in mast cell degranulation has not been reported, although *GPR35* is expressed by human mast cells and is upregulated following mast cell activation with anti-IgE antisera (Yang et al., 2010). Expression of *GPR35* in the immune system is not exclusive to mast cells however, as various reports indicate the presence of *GPR35* in basophils and eosinophils (Yang et al., 2010), natural killer cells (Fallarini et al., 2010), CD14+ monocytes, dendric cells, peripheral blood lymphocytes (Wang et al., 2006a), and neutrophils (Barth et al., 2009; Wang et al., 2006a). Furthermore, *GPR35* expression is upregulated following exposure of primary human macrophages to the polycyclic aromatic hydrocarbon benzo(a)pyrene (Sparfel et al., 2010). In mouse *GPR35* was found to be expressed to a higher level in pro-inflammatory thioglycollate elicited peritoneal macrophages following activation by LPS when compared with anti-inflammatory bone marrow derived macrophages (Lattin et al., 2008). Based on this information, it seems likely that the function of GPR35 is not exclusive to the modulation of mast cell responses. Indeed, the aforementioned GPR35 ligands can modulate the release of pro-inflammatory mediators including histamine and TNF-α from both mast cell and non-mast cell populations (Yanni et al., 1993; Yanni et al., 1997; Saijo et al., 1985; Yanagihara et al., 1988; Bissonnette et al., 1995; Haddad et al., 2002; Irie et al., 2001).

In order to clarify the role of GPR35 in immunity, therefore, future investigations may consider the use of a GPR35 antagonist to dissect whether the emanating responses are actually a result of GPR35-specific activation. Investigations should focus on pathways and processes that are shared amongst different immune cell populations and not simply by mast cells. GPR35 has been shown to play a direct role in leukocyte extravasation, as kynurenic acid induced adhesion of leukocytes to vascular endothelial cells and shedding of neutrophil L-selectin from human peripheral monocytes in a manner that was significantly reduced by short hairpin mediated silencing of GPR35 (Barth et al., 2009). Therefore, it appears that GPR35 may play a wider role in immune cell chemotaxis or adhesion, yet it is unclear whether GPR35 would function directly or through other targets to modulate these processes and further investigations will be required to answer this.

4.4.3 *Ligand bias at GPR35*

Derivatives of LPA have been indicated to act as endogenous ligands of human GPR35, with their activity leading to an increase in $[Ca^{2+}]_i$ (Oka et al., 2010). When GPR35 is present, the increase in $[Ca^{2+}]_i$ was greater than that observed in non-GPR35 transfected cells (Oka et al., 2010). Since GPR35 does not couple to $G\alpha_q$ (at least following treatment with zaprinast, Jenkins et al., 2012) and if LPA is directly interacting with GPR35, it must do so in a ligand biased manner. Further to this, application of LPA to cells expressing human GPR35 does not result in β-arrestin-2 recruitment (Southern et al., 2013), revealing, quite intriguingly, that ligands with this profile of ligand bias at GPR35 would not have been detected by widely used (β-arrestin-2 recruitment) assays for this receptor.

As the activation of GPR35 by LPA has never been confirmed by an independent source however, it is unclear whether the data presented by Oka et al., reflect a novel pathway of GPR35 activation or whether GPR35 is in some way upregulating the receptors that endogenously respond to LPA in HEK293 cells. Most recently however, a second study emerged that associated GPR35 with modulation of $[Ca^{2+}]_i$ (Berlinguer-Palmini et al., 2013). In this study, zaprinast and kynurenic acid altered $[Ca^{2+}]_i$ waves in rat hippocampal neurons and reduced excitatory post-synaptic currents (Berlinguer-Palmini et al., 2013). Importantly, CID-2745687 and small interfering RNAs were found to attenuate the kynurenic acid

response, therefore, as the authors suggested, this implicated GPR35 as a receptor modulating $[Ca^{2+}]_i$ release (Berlinguer-Palmini et al., 2013).

There is a discrepancy here however, since these two studies report distinct actions of GPR35 activation in the role of calcium mobilisation: LPA stimulates $[Ca^{2+}]_I$ release, while kynurenic acid and zaprinast reduce $[Ca^{2+}]_i$ mobilisation. However, it is possible that LPA acts as an antagonist of GPR35 to increase $[Ca^{2+}]_i$, as the mode of action of LPA has not been determined at GPR35. This may also explain why LPA did not stimulate recruitment of β-arrestin-2 (Southern et al., 2013). Further evidence to support the role of GPR35 in the modulation of $[Ca^{2+}]_i$ mobilisation was generated in a very recent paper that claims to have found the true endogenous ligand of GPR35: an orphan chemokine CXCL17 (Maravillas-Montero et al., 2014). Importantly this work (although it does not provide evidence of a direct association between the two proteins) indicates that in cells expressing GPR35 there is an increase in $[Ca^{2+}]_i$ mobilisation following application of CXCL17 to transfected human monocytic leukaemia THP-1 cells and transfected HEK293 cells (Maravillas-Montero et al., 2014). Importantly, and unlike the previous two papers, this study indicated that CXCL17 acted in a $G\alpha_{i/o}$ dependent manner, as the increase in $[Ca^{2+}]_i$ mobilisation was abolished following treatment of cells with Pertussis toxin (Maravillas-Montero et al., 2014). Placing this finding in context with the aforementioned LPA data therefore, a number of questions remain to be answered: primarily is GPR35 modulating calcium flux through $G\alpha_{i/o}$ associated $G\beta\gamma$ modulation of calcium flux (McCool et al., 1998)? Is CXCL17 a functionally biased ligand of GPR35? How is the apparently completely human selective antagonist CID-2745687 able to block $[Ca^{2+}]_i$ mobilisation at mouse and rat GPR35? Is CID-2745687 acting in a species selective, ligand biased manner?

Species selective ligand bias has not been widely reported, although one study detailed this for the κ-opioid receptor (κOR). Pentazocine, a κ-opioid receptor partial agonist, was found to be significantly more potent in the activation of p38 MAPK at human κOR compared with rat κOR, while both species orthologues responded equally to phosphorylate ERK when activated with the same ligand (Schattauer et al., 2012). My data present an interesting profile of functional selectivity, with the ligand bias of compound 1 being completely reversed between human and rodent orthologues of GPR35 (**Table 4.3**). At human GPR35, compound 1 strongly couples GPR35 to the β-arrestin-2 recruitment

pathway, while at mouse and rat compound 1 preferentially links GPR35 to G protein mediated IP_1 accumulation (importantly, through a $G\alpha_{q13}$ chimeric G protein). It is therefore plausible that, for some ligands, the rodent orthologues of GPR35 could selectively couple to G protein signalling pathways to elicit their responses. This does not help to explain how the rodent orthologues are responsive to CID-2745687 however, as neither CID-2745687 nor ML-145 substantially reduced the zaprinast signal at rat GPR35 in the presence of $G\alpha_{q13}$ in the IP-One assay (**Section 3.8**), other than perhaps full-length G proteins may be required. Thus, future studies may wish to assess CID-2745687 and ML-145 antagonism of cAMP responses in endogenously expressing cells at both the human and rodent orthologues of GPR35 to determine whether these antagonists are acting with ligand bias.

4.4.4 *Species selectivity at GPR35*

This project aimed to identify small molecule agonists of GPR35, of which there are now a large number of chemically diverse ligands available (**Table 1.3**; **Table 1.4**). Drug discovery efforts with the MRCT identified a large number of chemically diverse ligands that activated human GPR35, however most of these acted with relatively low potency at the human receptor and this pharmacology did not always translate to the rat and mouse species orthologues (Neetoo-Isseljee et al., 2013). Indeed, the majority of compounds failed to activate rat and mouse GPR35. This presented key issues for target validation efforts, and could have been a reflection of the stronger requirement for a negatively charged ligand for activation at the rodent receptors (Funke et al., 2013). So what are the differences between these receptors that are impacting upon GPR35 pharmacology, and why is species selectivity so pronounced at GPR35?

4.4.4.1 *Why is species selectivity so pronounced at GPR35?*

GPCRs are placed under considerable evolutionary pressure to maintain responsiveness to their endogenous ligand(s) in order to retain responsiveness to their biological cue(s). This is particularly apparent for receptors that modulate ancient and conserved evolutionary functions such energy homeostasis, reward, and wakefulness. A key molecule in these processes is orexin A. The amino acid sequence of orexin A is identical

between the human, rat, mouse, cow, sheep, dog and pig species orthologues, while the receptors that respond to orexin (OX_1 and OX_2) are 94% and 95% identical between human and rat (Tsujino and Sakurai, 2009). Perturbations to the orexin system cause narcolepsy in humans, dogs, and rodents, indicating that the orexin system plays an important signalling function that is conserved between species (Sakurai et al., 1998; Chemelli et al., 1999; Lin et al., 1999; Peyron et al., 2000). When a GPCR is involved in biological processes that have diverged over time however, the degree of evolutionary pressure to maintain the ligand-binding pocket is reduced and may be altered to meet the new and specific requirements of the organism. The most notable examples of this are receptors that are involved in immunity, exemplified mainly by studies involving the histamine, chemokine, and proteinase-activated receptors. Such marked species selectivity has been attributed to vastly different concentrations of the endogenous molecule produced between species, the absence of a rodent counterpart to the endogenous human ligand, or receptors carrying out completely distinct functions in different species (Strasser et al., 2013; Zlotnik et al., 2006; Coughlin, 2005; Nakanishi-Matsui et al., 2000; Steinhoff et al., 2005).

As described in **Section 4.4.3**, GPR35 appears to play a role in the chemotaxis or migration of leukocytes to the site of inflammation (Barth et al., 2009). It is therefore important to note that there are marked differences in the composition of these cells between human and mouse, with peripheral blood containing a ratio of 50-70 % neutrophils to 30-50% leukocytes, in human and 75-90 % leukocytes to 10-25 % neutrophils in the mouse (Mestas and Hughes, 2004). Furthermore, mice lack twenty-or so of the α-defensins present in rat and human, and completely lack expression of myeloid defensins in their neutrophil population (Eisenhauer et al., 1992; Shanahan et al., 2011). It is therefore quite plausible that if GPR35 is involved in leukocyte homing in human, then the endogenous molecule involved in initiating this process could differ in expression in the mouse.

This is exemplified by the fact that a number of chemokines that are involved in the movement of immune cells into and through tissues have been identified in humans but not mice (CXCL8, CXCL7, CXCL11, CCL13, CCL14, CCL15, CCL18, CCL23, and CCL24/CCL26), whilst yet others are unique to the mouse (CCL6, CCL9, CXCL15, and CCL12) (Olson and Ley, 2002; Zlotnik and Yoshie, 2000). Fittingly, the orphan chemokine CXCL17 was most recently reported as an endogenous ligand of human GPR35 (Maravillas-Montero et al., 2014). CXCL17 is an anti-inflammatory chemokine that acts in a manner critical to leukocyte

recruitment (Lee et al., 2013). Although *CXCL17* is expressed in human and rodent species, the protein sequence is not completely conserved (**Fig 4.11**), with human and rat CXCL17 sharing 62 % identity, human and mouse sharing 71 % identity, and rat-and-mouse sharing 80 % identity. Thus it is plausible that this ligand acts in a species selective manner at GPR35. This is not a foregone conclusion however, and it may be pertinent to note that although the histamine H_1, H_2, and H_3 receptors display significant species selectivity to synthetic molecules, there is actually only a half log order difference in potency between human, mouse, and rat in their responses to histamine (Strasser et al., 2013).

4.4.4.2 *What are the residues that are regulating species selectivity at GPR35?*

This body of work provided the first account of highly potent agonists that activate human and rat GPR35 in an equipotent manner (**Fig 4.5**). This is important as it indicates firstly that it is possible to achieve ligands that act in the same concentration range at GPR35, and secondly, it provides ligands that can be assessed in comparison with those displaying marked species selectivity to enable identification of residues important in ligand binding at GPR35. Indeed, although it has been well documented that species selectivity hinders the pathway towards assessment of pre-clinical efficacy, the differences in responses between species orthologues can also be looked upon as a useful means to help decipher receptor-ligand binding interactions. This approach has been successful in aiding characterisation of the free fatty acid receptors, namely FFA2 and FFA3, whereby a single negatively charged residue in ECL2 was found to differ between the human and mouse that differentially regulated the potency of the endogenous ligand propionate *and* also the level of ligand-free constitutive activity observed (Hudson et al., 2012a). Furthermore, a single residue between human and bovine FFA2 was identified and when reciprocally altered, generated pharmacology at the human receptor that was similar to bovine responses; addition of a second mutation to human FFA2 completely ablated responsiveness to endogenous ligands, but importantly, retained the ability to respond to synthetic ligands (Hudson et al., 2012b). This led to the development of a Receptor Activated Solely by Synthetic Ligands (RASSL), which enabled important distinctions to be made between the closely related FFA2 and FFA3 receptors. Thus, since most of the ligands of GPR35 act with marked species selectivity, I could use the differences in their responsiveness to mutations

```
Mouse           MKLLASPFLLLLPVMLMSMVFSSPNPGVARSHGDQHLAPRRWLLEGGQECECKDWFLQAP 60
Rat             MKLLASPFLLLLTGMFTATVSSSPNQEVARHHGDQHQAPRRWLWEGGQECDCKDWSLRVS 60
Human           MKVLISSLLLLLLPLMLMSMVSSSLNPGVARGHRDRGQASRRWLQEGGQECECKDWFLRAP 60
                **:* *.:****. *: : * ** *  *** * *:  *.**** ******:**** *:..

Mouse           KRKATAVLGPPRKQCPCDHVKGREKKNRHQKHHRKSQRPSRACQQFLKRCHLASFALPL  119
Rat             KRKTTAVLEPPRKQCPCDHVKGSEKKNRRQKHHRKSQRPSRTCQQFLKRCQLASFTLPL  119
Human           RRKFMTVSGLPKKQCPCDHFKGNVKKTRHQRHHRKPNKHSRACQQFLKQCQLRSFALPL  119
                :**  :*   *:*******.**  **.*:*:****.:: **:******:*:* **:***
```

Figure 4.11 CXCL17 sequence alignment indicates shared sequence between species Full-length protein sequences were downloaded from NCBI nucleotide for human, mouse, and rat CXCL17 (http://www.ncbi.nlm.nih.gov/nuccore) and aligned using the multiple sequence alignment function from ClustalW (http://www.ebi.ac.uk/Tools/msa/clustalw2). An asterisk indicates a conserved residue, a colon indicates a conservative alteration, and a full stop indicates a semi-conservative alteration.

made in the human or rat receptors to identify residues important in ligand binding. While no consensus had been reached on the endogenous ligand of GPR35 at the time of this analysis, I had a plethora of synthetic tool compounds with which to probe the pharmacology of ligand binding at human and rat GPR35, many of which were identified and described herein. **Chapter Five** is dedicated to these investigations.

Chapter Five

Investigating Species Orthologue Selectivity of Ligands at GPR35

5.1 Using GPR35 species selectivity to elucidate the basis of ligand-receptor interactions

Species selectivity surrounding GPR35 has been documented for almost all ligands reported. Most notably, the proposed endogenous ligand of GPR35, kynurenic acid, suffers from pronounced species selectivity, as although activating the rat orthologue at a concentration obtainable under physiological conditions (pEC_{50} 7.13 ± 0.16) (Wang et al., 2006a), at the human receptor kynurenic acid is close to inactive (Oka et al., 2010; Jenkins et al., 2011). Even the GPR35 reference compound, zaprinast, displays species selective characteristics (Taniguchi et al., 2006) with a receptor preference of rat>mouse>human (Jenkins et al., 2012).

Species selectivity is not unique to GPR35, and has been documented for various other GPCRs including the free fatty acid receptors FFA2 and FFA4 (Hudson et al., 2012a; 2012b; 2013a; 2013b; 2013c) and the histamine H_1, H_2, H_3 and H_4 receptors (Strasser et al., 2009, Preuss, 2007; Yao et al., 2003; Igel et al., 2010; Strasser et al. 2013). Comparisons between species orthologues are commonplace within the drug development process. Animal models, particularly rodents, are employed to validate the pharmacodynamic and toxicological profile of ligands prior to progression toward the latter stages of drug development (Hughes et al., 2011). Thus, early identification and understanding of species selectivity is key to the successful profiling of ligands during the later stages of drug development efforts.

5.1.1 *Investigating the mode of ligand binding using GPR35 ligands with various species selectivity profiles*

In some instances, for orthologues with high sequence similarity, the divergence of only one amino acid is sufficient to mediate species selective responses, such as for the RAMP/CRLR receptor (Mallee et al., 2002). Since there is only 71% sequence identity between human and rat GPR35, there are likely to be a number of residues that contribute to differences in ligand binding. In order to identify residues that may contribute to species selectivity at GPR35, various mutations were made using site directed mutagenesis, with the emanating responses characterised using six pharmacologically distinct ligands that could be grouped within ‘human selective’, ‘rat selective’ or ‘equipotent’ categories.

The human selective ligands were represented by the previously described GPR35 ligands pamoic acid (**Chapter Three**), and compound 1 (**Chapter Four**), which in the BRET-based β-arrestin-2 recruitment assay acted with partial and full efficacy, respectively, and generated species selective profiles of h>r>m (**Fig 5.1A/B**; **Table 5.1**). The rodent selective compounds chosen for investigation were zaprinast and amlexanox (**Chapter Four**), which acted with full and partial efficacy respectively, and generated species selectivity profiles of r>m>h (**Fig 5.1C/D**; **Table 5.1**). The human and rat equipotent pair of ligands chosen for assessment herein were the mast cell stabilisers and newly identified GPR35 agonists, described in **Chapter Four**, lodoxamide and bufrolin, which generated species selective profiles of h=r>m (**Fig 5.1E/F**; **Table 5.1**).

5.1.2 *Identification of residues involved in ligand binding at human and rat GPR35*

The presence of at least one carboxyl group or carboxylic acid isostere is a common feature of GPR35 ligands (**Fig 5.2**) (Jenkins et al., 2010; Deng et al., 2011b; 2012c; Deng and Fang, 2012a; 2012c; Funke et al., 2013; Neetoo-Isseljee et al., 2013), and for this reason sequence alignments were performed with other GPCRs that are activated by carboxylic acids (**Fig 5.3**). This sequence alignment indicated that R3.36 was conserved amongst the hydroxycarboxylic, oxoeicosanoid, and GPR35 receptors. The importance of this residue at carboxylic acid binding receptors has been documented previously, as, in each case, mutation of R3.36 to alanine (R3.36A) abolished ligand-mediated responses (He et al., 2004; Tunaru et al., 2005; Liu et al., 2009; Jenkins et al., 2011; Zhao et al., 2014). However, since R3.36 was conserved between species orthologues (**Fig 5.3B**), it seemed unlikely that R3.36, at least on its own, would define the observed differences in species selectivity.

As a result, other arginine residues that were present within possible GPR35 ligand binding regions and that were different between human and rat orthologues were chosen as residues that could interact with the ligand carboxyl group. To investigate this, I carried out a series of species swap mutations, whereby arginine residues were mutated to the non-arginine present in the opposite species orthologue. Four arginine residues: R4.62 in rat, R^{164} in human ECL2, R6.58 and R7.32 in human ECL3 (**Fig 5.4**), were altered to the non-arginine residue expressed in the opposite species orthologue, which created R^{161}S (human),

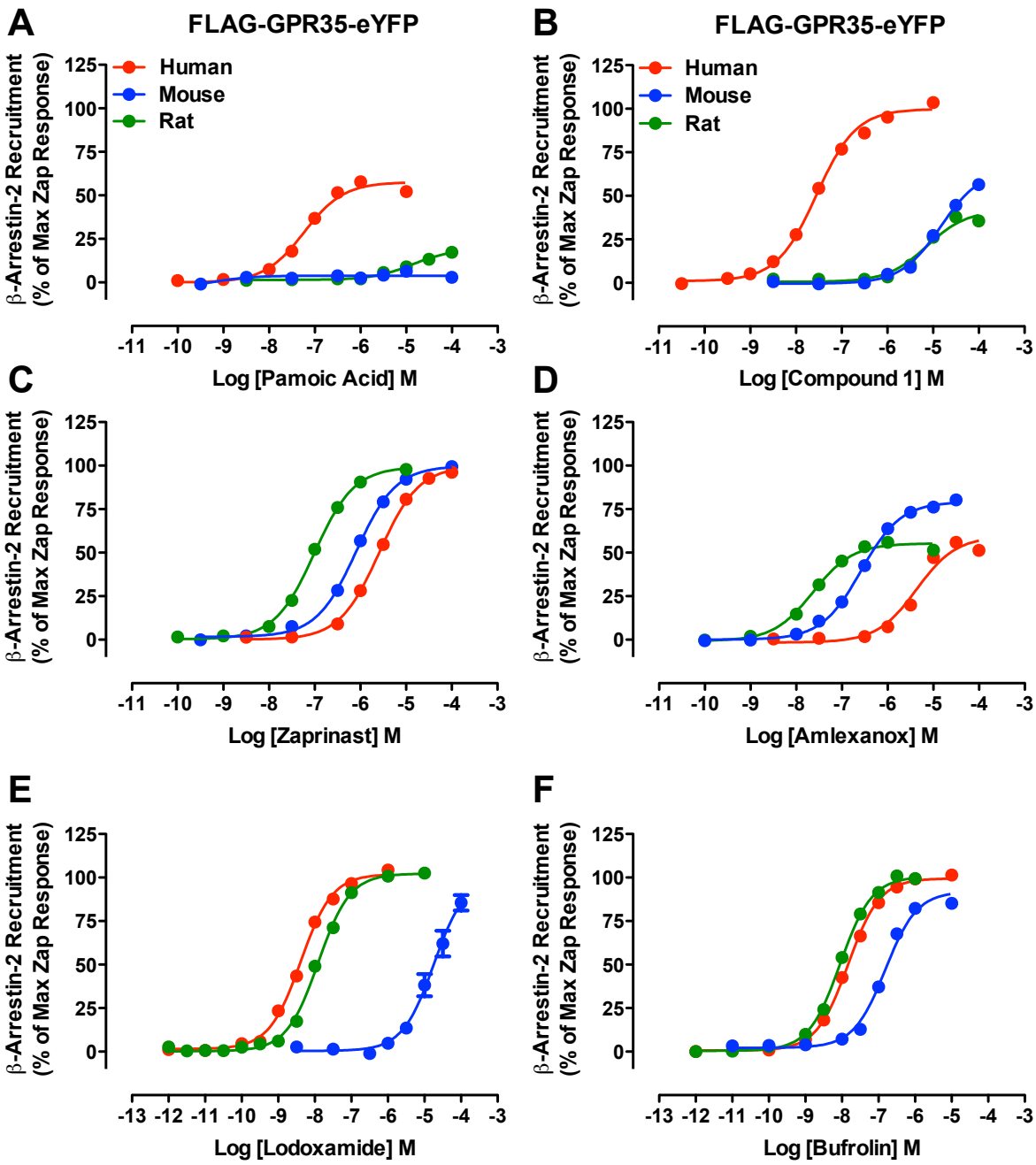

Figure 5.1 The species selectivity profiles of GPR35 agonists as displayed in the BRET assay Pamoic acid (**A**), compound 1 (**B**), zaprinast (**C**), amlexanox (**D**), lodoxamide (**E**), and bufrolin (**F**) were assessed using human (red), mouse (blue), or rat (green) FLAG-GPR35-eYFP constructs for their ability to recruit β-arrestin-2 using the BRET-based method of protein: protein interaction (see **Section 2.7.3** for details). Each dataset represents the mean of the minimum of three independent experiments carried out in duplicate ± SEM. Efficacy is presented relative to the reference compound zaprinast, which served as an internal control between experiments.

Table 5.1 GPR35 agonist potency and efficacy at human, mouse and rat orthologues in the β-arrestin-2 recruitment assay

	Ligand Potency (pEC_{50}), Efficacy (E_{max}) ± SEM, and ΔpEC_{50}							
	Human GPR35		Mouse GPR35			Rat GPR35		
Ligand	**pEC_{50}**	**E_{max} (% of zap max response)[a]**	**pEC_{50}[b]**	**E_{max} (% of zap max response)[a]**	**ΔpEC_{50}[c]**	**pEC_{50}[b]**	**E_{max} (% of zap max response)[a]**	**ΔpEC_{50}[c]**
Zaprinast	5.59 ± 0.01	99.8 ± 0.7	6.09 ± 0.03***	99.8 ± 1.0	+ 0.50	7.01 ± 0.02***	99.3 ± 0.9	+ 1.42
Amlexanox	5.38 ± 0.05	59.4 ± 1.5***	6.58 ± 0.04***	79.3 ± 1.5***	+ 1.20	7.63 ± 0.07***	55.3 ± 0.1***	+ 2.25
Pamoic Acid	7.25 ± 0.05	57.6 ± 1.7***	Inactive	NR	NA	4.87 ± 0.10***	19.2 ± 1.3***	- 2.38
Compound 1	7.55 ± 0.03	99.9 ± 1.1	4.83 ± 0.06***	65.1 ± 2.5***	- 2.72	5.14 ± 0.08***	41.7 ± 1.8***	- 2.41
Lodoxamide	8.38 ± 0.02	102.0 ± 1.0	4.74 ± 0.09	100.5 ± 6.7	- 3.64	7.90 ± 0.02***	102.3 ± 0.8	- 0.48
Bufrolin	7.83 ± 0.02	99.5 ± 0.9	6.81 ± 0.04***	91.8 ± 1.9	- 1.02	8.00 ± 0.02	100.6 ± 0.9	+ 0.17

[a] Statistically significant difference in efficacy from zaprinast response denoted as *P* *** = ≤ 0.001

[b] Statistically significant difference in potency between species, *P* values = *** ≤ 0.001, ** ≤ 0.01, * ≤ 0.05

[c] ΔpEC_{50} represents mouse or rat pEC_{50} – human pEC_{50}

NR, no response; NA, not applicable

Data are the mean ± SEM of a minimum of three independent experiments carried out in duplicate

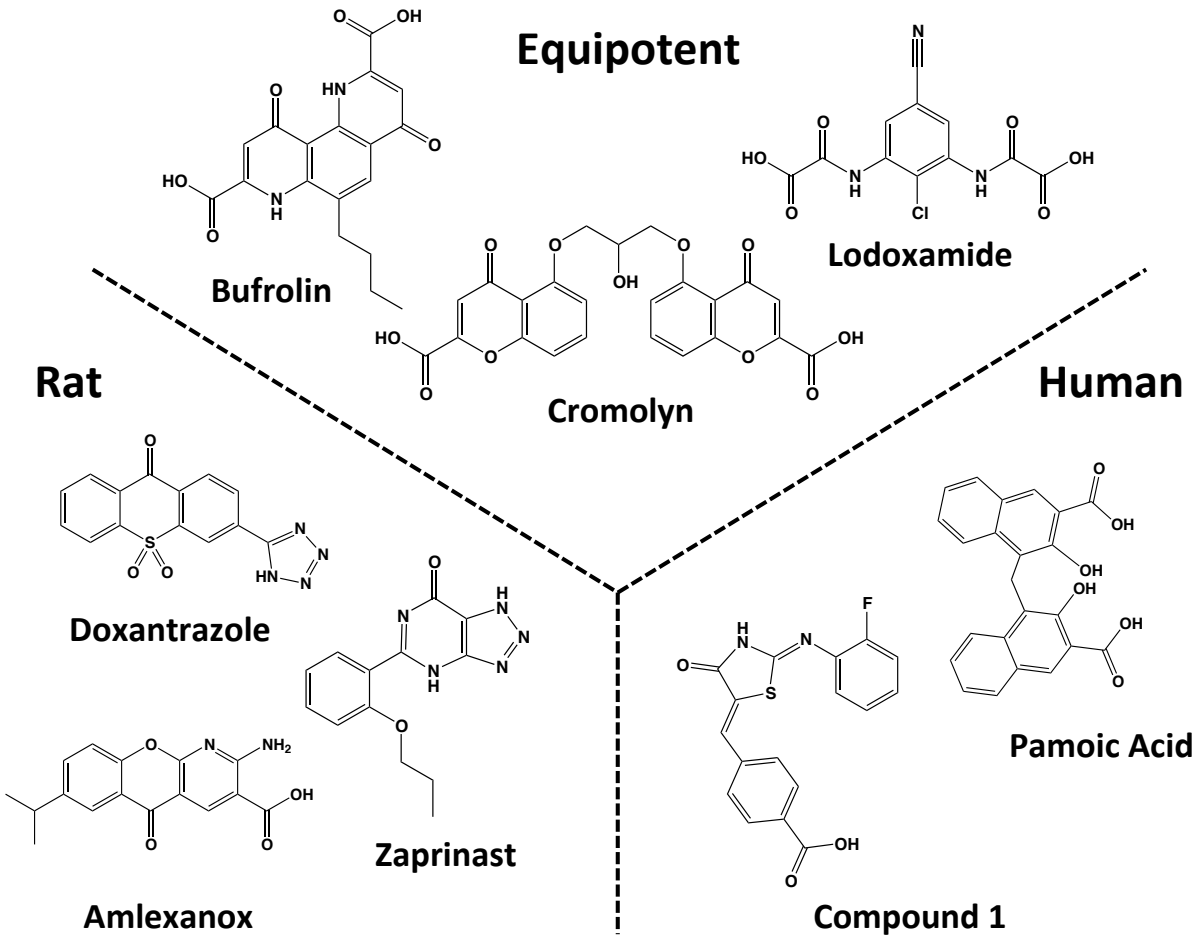

Figure 5.2 GPR35 ligands tend to contain a carboxyl group or a carboxylic acid isostere Ligands have been depicted structurally and grouped in terms of their species selective properties between human and rat GPR35: equipotent, human-selective, or rat-selective. Of note are the carboxylic acid isostere of doxantrazole, and the tricyclic structure of amlexanox, which are representative of a number of rat-selective ligands, versus the dicarboxylic acid, and (for some) symmetrical structures of the equipotent and human selective ligands.

A

```
hGPR35  IYLTNRYMSISLVTAIAVDRYV
HCA1    TLAMNRAGSIVFLTVVAADRYF
HCA2    MLAMNRQGSIIFLTVVAVDRYF
HCA3    MFAMNRQGSIIFLTVVAVDRYF
OXE     MLSTNRTASVVFLTAIALNRYL
             **  *: ::*.:* :**.
```

B

```
hGPR35  IYLTNRYMSISLVTAIAVDRYV
mGPR35  IYLANRYMSISLVTAIAVDRYV
rGPR35  IYLVNRYMSISLVTAIAVDRYV
        ***.******************
```

Figure 5.3 Arginine 3.36 is conserved at the hydroxycarboxylic, oxoeicosanoid, and GPR35 receptors Full-length protein sequences were downloaded from NCBI nucleotide (http://www.ncbi.nlm.nih.gov/nuccore) and aligned using the multiple sequence alignment function from ClustalW (http://www.ebi.ac.uk/Tools/msa/clustalw2) to provide sequence alignments between a segment of transmembrane domain 3 containing the arginine 3.36 residue for human GPR35, hydroxycarboxylic acid (HCA_1, HCA_2, and HCA_3), and oxoeicosanoid (OXE) receptors (**A**). R3.36 is also conserved between human, mouse, and rat orthologues of GPR35 (**B**). The highly conserved DRY sequence of the class A family of GPCRs is also indicated in bold. An asterisk indicates a conserved residue, a colon indicates a conservative alteration, and a full stop indicates a semi-conservative alteration.

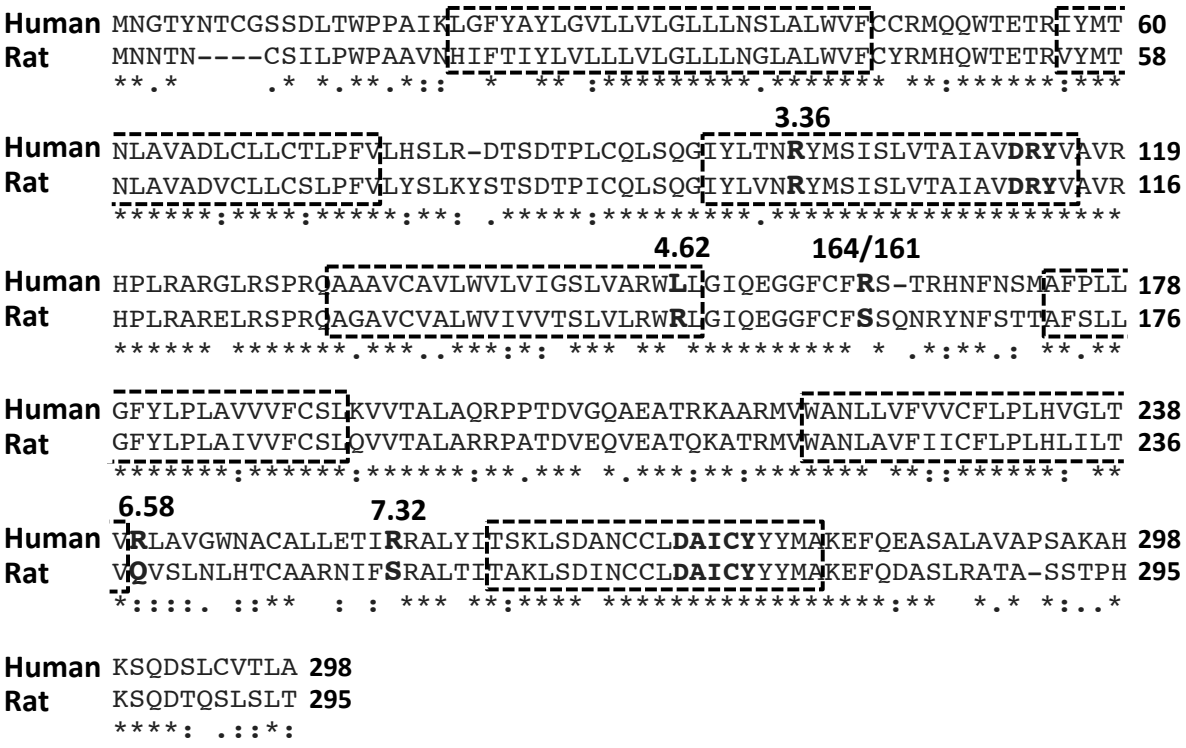

Figure 5.4 Arginine residues that differ in sequence between human and rat GPR35 Full-length human GPR35a and rat GPR35 protein sequences were downloaded from NCBI nucleotide and aligned using the multiple sequence alignment function from ClustalW. Amino acids with shared identity are marked *, conserved amino acids are indicated with a colon and semi-conserved amino acids with a full stop. Predicted transmembrane domain regions are boxed. The DRY domain and NPxxY motif, two defining features of Class A GPCRs, are highlighted in bold. Also highlighted in bold is R3.36, alongside the arginine residues chosen for analysis herein: R4.62 (rat), R^{164} (human), R6.58 (human) and R7.32 (human).

R4.62L (rat), R6.58Q (human), and R7.32S (human). Additionally, and since it was hypothesised that R6.58 and R7.32 were acting together at the top of the human binding pocket, a double mutant was created that encoded R6.58Q and R7.32S in human GPR35. Equally, gain of arginine mutants were generated by reversing the species swaps, such that $S^{164}R$ (rat), L4.62R (human), Q6.58R (rat), S7.32R (rat) and the double mutant Q6.58R and S7.32R (rat) were generated. Each mutant receptor was confirmed, using the FLAG N-terminal epitope tag with cell surface ELISA, as being expressed at the cell surface. To assess the effect of each mutation on ligand binding and species selectivity, the BRET-based β-arrestin-2 recruitment assay was employed since it provided an assay system that reflected receptor occupancy and was free from signal amplification.

5.1.3 *Arginine residues 164, 6.58, and 7.32 play a role in ligand binding in human GPR35*

To determine whether loss of arginine residues $R^{164}S$, R6.58Q, and R7.32S affected ligand binding at human GPR35, each category of ligands was assessed in terms of losses or gains of potency which, using the β-arrestin-2 recruitment assay, could be utilised as a surrogate measure of affinity. Although both pamoic acid and compound 1 were similar in that they acted with significant human selectivity, they responded in a different manner at each of the mutations presented herein. The potency of pamoic acid was most affected by expression of R6.58Q human GPR35, with a 17.8-fold loss in potency ($P \leq 0.001$) from wild type, while there was a 15.1-fold loss in potency at $R^{164}S$ ($P \leq 0.001$) and a 8.1-fold loss at R7.32S ($P \leq 0.001$) (**Fig 5.5A**; **Table 5.2**). For compound 1 however, the greatest reduction in potency was observed at R7.32S (51-fold, $P \leq 0.001$), while at $R^{164}S$ and R6.58Q compound 1 was substantially less affected, with losses in potency of 11.7-fold ($P \leq 0.001$) and 4.1-fold ($P \leq 0.001$), respectively (**Fig 5.5B**; **Table 5.2**). The potency of the rodent selective ligands zaprinast and amlexanox was less affected by the $R^{164}S$, R6.58Q, and R7.32S forms of human GPR35. At R6.58Q human GPR35 zaprinast generated a small but significant ($P \leq 0.001$) 3-fold decrease in potency from wild type, while at R7.32S there was a small but significant 2.5-fold increase ($P \leq 0.001$). Expression of $R^{164}S$, meanwhile, did not significantly affect the ability of zaprinast to recruit β-arrestin-2 (**Fig 5.5C**; **Table 5.2**). For amlexanox, the β-arrestin-2 recruitment responses were not significantly affected by changes to R^{164}, R6.58, or R7.32 human GPR35 (**Fig 5.5D**; **Table 5.2**).

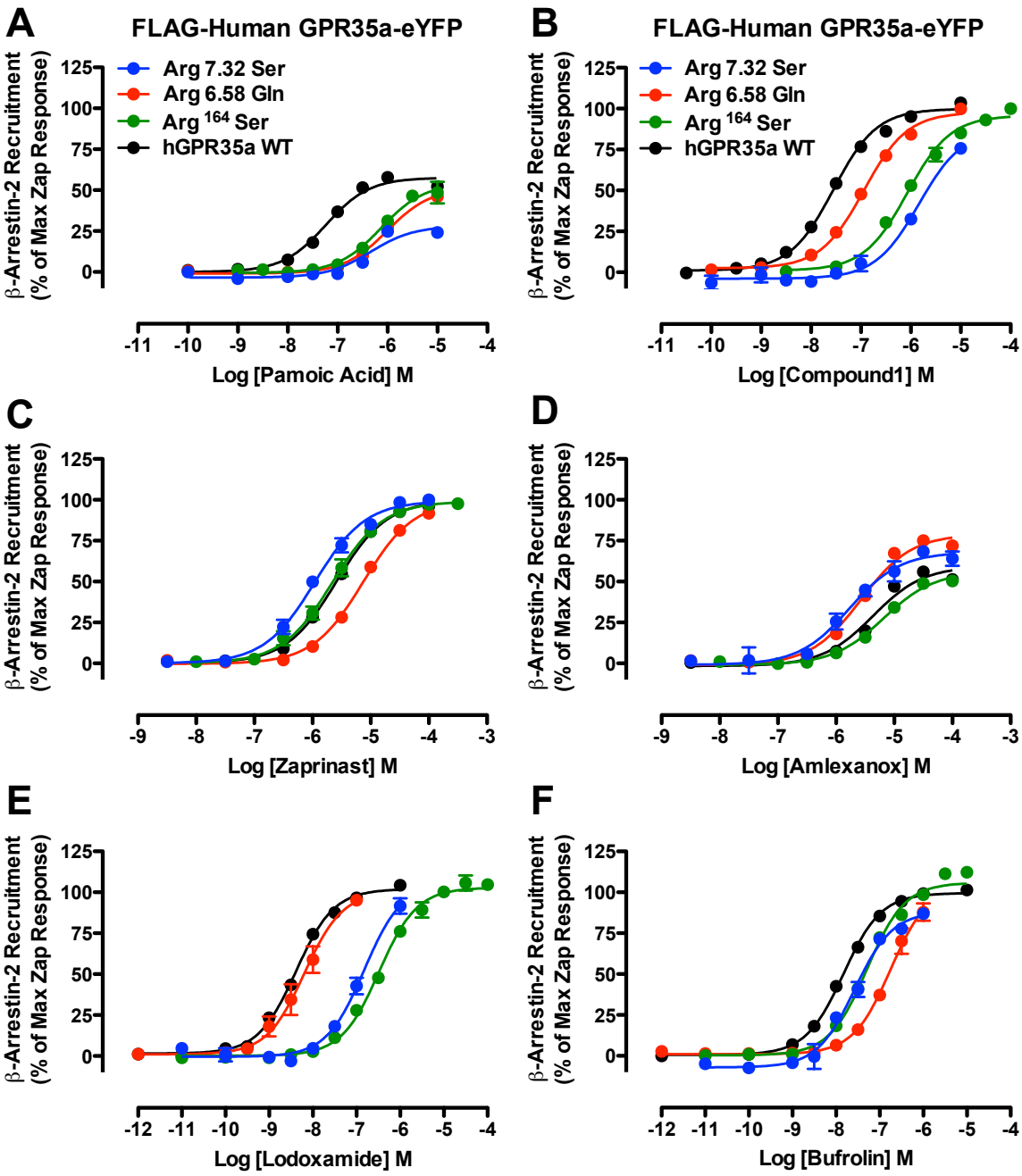

Figure 5.5 Arg^{164}, R6.58 and R7.32 play a role in ligand selectivity at human GPR35 The effect of wild type (black), R^{164}S (green), R6.58Q (red), R7.32S (blue) on response to pamoic acid (**A**), compound 1 (**B**), zaprinast (**C**), amlexanox (**D**) lodoxamide (**E**), and bufrolin (**F**) is illustrated using the BRET-based β-arrestin-2 recruitment assay. Data represent the mean ± SEM of a minimum of three independent experiments carried out in duplicate. Efficacy was normalised as a percentage of the maximal zaprinast response generated at each individual mutant.

Table 5.2 $R^{164}S$, R6.58Q, and R7.32 play a role in human GPR35 ligand selectivity in the β-arrestin-2 recruitment assay.

	Cell Surface Expression, Ligand Potency (pEC_{50}), ± SEM, and ΔpEC_{50}						
	Wild Type	**Arg 6.58 Gln**		**Arg 7.32 Ser**		**Arg ^{164} Ser**	
Cell Surface[a]	100.0 ± 20.4	97.1 ± 10.5		95.9 ± 13.1		104.4 ± 3.3	
Ligand	pEC_{50}	pEC_{50}[b]	ΔpEC_{50}[c]	pEC_{50}[b]	ΔpEC_{50}[c]	pEC_{50}[b]	ΔpEC_{50}[c]
Pamoic Acid	7.25 ± 0.05	6.00 ± 0.04***	- 1.25	6.34 ± 0.15 ***	- 0.91	6.07 ± 0.05***	- 1.48
Compound 1	7.55 ± 0.03	6.94 ± 0.04***	- 0.61	5.84 ± 0.09***	- 1.71	6.48 ± 0.03***	- 1.90
Zaprinast	5.59 ± 0.01	5.11 ± 0.05***	- 0.48	5.99 ± 0.09***	+ 0.40	5.65 ± 0.04	+ 0.06
Amlexanox	5.38 ± 0.05	5.54 ± 0.11	+ 0.16	5.86 ± 0.15*	+ 0.47	5.18 ± 0.08	- 0.20
Lodoxamide	8.38 ± 0.02	8.19 ± 0.09	- 0.19	6.83 ± 0.01***	- 1.55	6.13 ± 0.11***	- 1.12
Bufrolin	7.83 ± 0.02	6.75 ± 0.06***	- 1.08	7.57 ± 0.06*	- 0.26	7.29 ± 0.03***	- 0.54

[a] Cell surface expression presented as a percentage of wild type

[b] Statistically significant difference in potency from wild type pEC_{50}, *P* values = *** ≤ 0.001, ** ≤ 0.01, * ≤ 0.05

[c] ΔpEC_{50} represents mutant pEC_{50} - wild type pEC_{50}

Data represent the mean ± SEM of a minimum of three independent experiments carried out in duplicate

The human and rat equipotent ligands lodoxamide and bufrolin responded with a different order and magnitude of β-arrestin-2 recruitment from each other at $R^{164}S$, R6.58Q, and R7.32S human GPR35. The potency of lodoxamide was most affected by alteration to R^{164}, with a 177.8-fold ($P \leq 0.001$) decrease in potency; with comparatively less effect, 35.5-fold decrease in potency ($P \leq 0.001$) at R7.32S, while this ligand was not affected by the R6.58Q mutation (**Fig 5.5E**; **Table 5.2**). The potency of bufrolin, by comparison, was affected to a lesser extent than lodoxamide and showed a 12-fold ($P \leq 0.001$) reduction in potency at R6.58Q, a 3.5-fold reduction ($P \leq 0.001$) at $R^{164}S$, and a 1.8-fold reduction ($P \leq 0.01$) at R7.32S (**Fig 5.5F**; **Table 5.2**).

5.1.4 *Arginine residues 6.58 and 7.32 act to mediate ligand responses at human GPR35*

Since the arginine residues positioned at 6.58 and 7.32 were believed to be acting with R3.36 to coordinate ligand binding between the top and bottom of the binding pocket, respectively, and given their close proximity within ECL3, I decided to test whether R6.58 and R7.32 were acting together to orchestrate β-arrestin-2 recruitment at human GPR35. The effect of pamoic acid was completely ablated following expression of the R6.58Q/R7.32S construct, equating to a ≥ 1778-fold reduction in potency, while for compound 1 the reduction in potency was 200-fold ($P \leq 0.001$) (**Fig 5.6A/B**; **Table 5.3**). The rodent selective ligands zaprinast and amlexanox conversely were not affected to a similar extent, and generated only a 3.2-fold ($P \leq 0.001$) or non-significant reduction in potency at R6.58Q/R7.32S human GPR35, respectively (**Fig 5.6C/D**; **Table 5.3**). For lodoxamide, potency was almost completely abolished (≥ 24,000-fold), while for bufrolin there was a 120-fold ($P \leq 0.001$) reduction in potency at R6.58Q/R7.32S human GPR35 (**Fig 5.6E/F**; **Table 5.3**).

5.1.5 *Addition of arginine residues 161, 6.58 and 7.32 increase human selective ligand potency at rat GPR35*

Equivalent mutations were made using site-directed mutagenesis to generate species swaps at rat GPR35. Addition of arginine residues Q6.58R, S7.32R and the double Q6.58R/S7.32R mutant to rat GPR35 increased the potency of the human selective ligands pamoic acid and compound 1 at this orthologue. The double Q6.58R/S7.32R mutation had

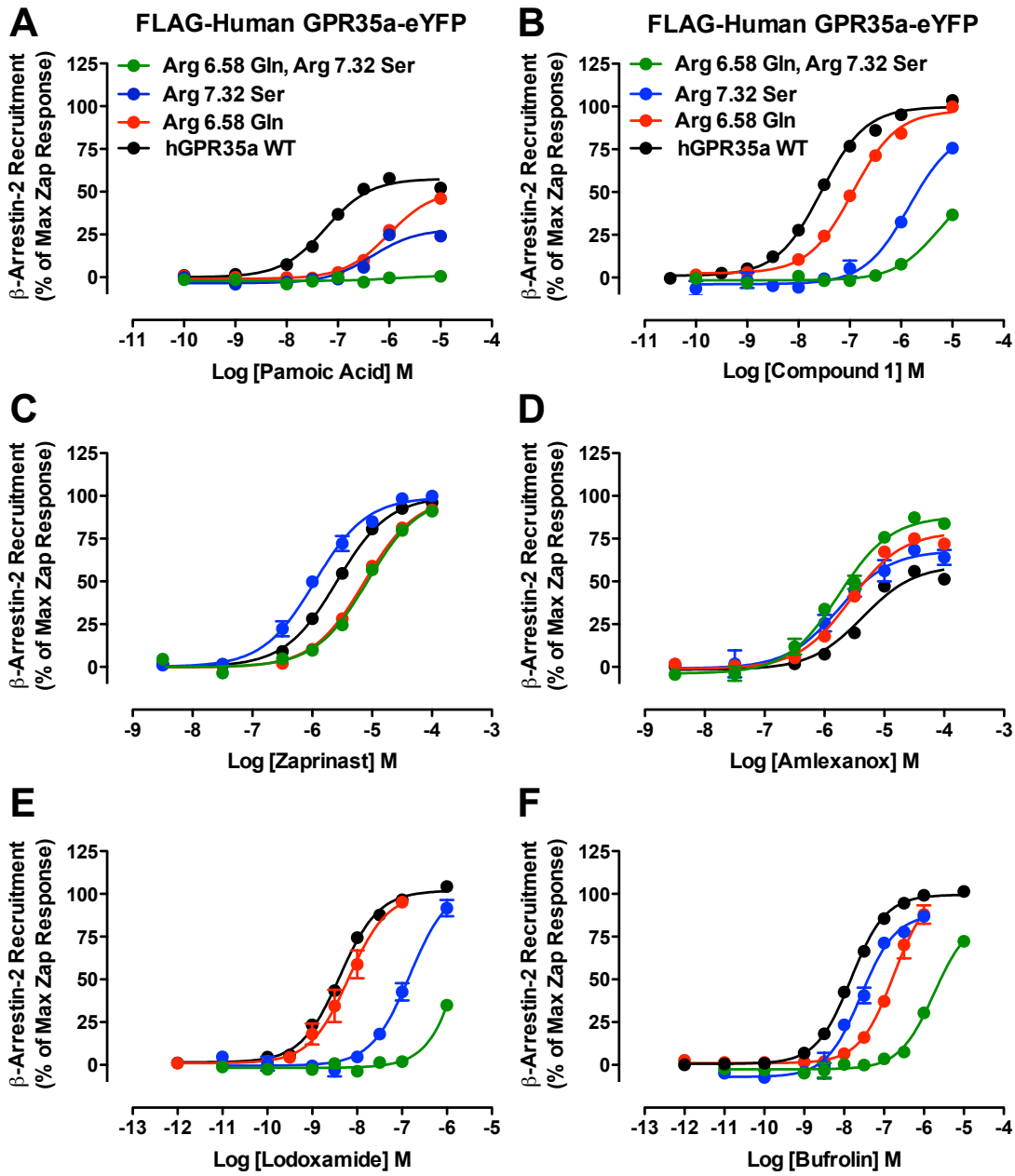

Figure 5.6 R6.58 and R7.32 act together at human GPR35 to recruit β-arrestin-2 Using the BRET-based methodology of β-arrestin-2 recruitment, the effect of wild type (black), R6.58Q (red), R7.32S (blue) and R6.58Q/R7.32S (green) was monitored on response to pamoic acid (**A**), compound 1 (**B**), zaprinast (**C**), amlexanox (**D**) lodoxamide (**E**), and bufrolin (**F**). Data are the mean ± SEM of a minimum of three independent experiments carried out in duplicate. Efficacy was normalised as a percentage of the maximal zaprinast response generated at each individual mutant.

Table 5.3 R6.58Q and R7.32 act together to mediate ligand responses at human GPR35

	Cell Surface Expression, Ligand Potency (pEC_{50}), ± SEM, and ΔpEC_{50}						
	Wild Type	**Arg 6.58 Gln**		**Arg 7.32 Ser**		**Arg 6.58 Gln, Arg 7.32 Ser**	
Cell Surface	100.0 ± 20.4	97.14 ± 10.5		95.97 ± 13.1		112.3 ± 4.04**	
Pamoic Acid	7.25 ± 0.05	6.00 ± 0.04***	- 1.25	6.34 ± 0.15***	- 0.91	<4	N/A
Compound 1	7.55 ± 0.03	6.94 ± 0.04***	- 0.61	5.84 ± 0.09***	- 1.71	5.25 ± 0.20***	- 2.30
Zaprinast	5.59 ± 0.01	5.11 ± 0.05***	- 0.48	5.99 ± 0.09***	+ 0.40	5.08 ± 0.05***	- 0.51
Amlexanox	5.38 ± 0.05	5.54 ± 0.11	+ 0.15	5.86 ± 0.15*	+ 0.47	5.74 ± 0.11	+ 0.35
Lodoxamide	8.38 ± 0.02	8.19 ± 0.09	- 0.19	6.83 ± 0.01***	- 1.55	<4	N/A
Bufrolin	7.83 ± 0.02	6.75 ± 0.06***	- 1.08	7.57 ± 0.06*	- 0.26	5.75 ± 0.07***	- 2.08

[a] Cell surface expression presented as a percentage of wild type, *P* value ** ≤ 0.01

[b] Statistically significant difference in potency from wild type pEC_{50}, *P* values *** ≤ 0.001, ** ≤ 0.01, * ≤ 0.05

[c] ΔpEC_{50} represents mutant pEC_{50} - wild type pEC_{50}

NR, no response; NA, not applicable

Data are the mean ± SEM of a minimum of three independent experiments carried out in duplicate

the greatest effect on ligand potency, and recorded gains of 34.7-fold ($P \leq 0.001$) for pamoic acid and 34-fold ($P \leq 0.001$) for compound 1 (**Fig 5.7A/B**; **Table 5.4**). However, although alteration to Q6.58R/S7.32R increased the potency of compound 1 and pamoic acid by a similar extent, the effect of each single mutation was different. At Q6.58R rat GPR35 pamoic acid recorded 9.1-fold increase in potency ($P \leq 0.05$), while for compound 1 there was a 24-fold increase ($P \leq 0.001$). At S7.32R rat GPR35 there was a 21.6-fold increase ($P \leq 0.001$) for pamoic acid, while for compound 1 this was 6.8-fold ($P \leq 0.01$). Expression of the $S^{161}R$ mutant increased the potency of pamoic acid 5.1-fold ($P \leq 0.05$) at rat GPR35, while for compound 1 there was no alteration of the potency from the wild type response (**Fig 5.7A/B**; **Table 5.4**). Although the potency was increased for pamoic acid following mutation of Q6.58R, S7.32R and the double Q6.58R/S7.32R mutant, the efficacy was low ($E_{max} < 20$ %) for all but the S7.32R mutant (E_{max} 57.6 ± 1.2 %) (**Fig 5.7A**). Compound 1 also acted with partial efficacy at rat GPR35 (E_{max} 41.7 ± 1.8 %), but the efficacy generated at each mutant was higher than that associated with pamoic acid (**Fig 5.7B**).

Expression of the single or double Q6.58R and S7.32R mutants did not significantly affect the responses of zaprinast or amlexanox, although both ligands were affected by expression of $S^{161}R$, with a 3.8-fold ($P \leq 0.01$) and 3.2-fold ($P \leq 0.05$) reduction in the potency for β-arrestin-2 recruitment, respectively (**Fig 5.7C/D**; **Table 5.4**). Interestingly, expression of the single or double Q6.58R and S7.32R mutants at rat GPR35 was also without effect on the lodoxamide and bufrolin responses (**Fig 5.7E/F**; **Table 5.4**). At $S^{161}R$ rat GPR35 a reduction in potency of 2.8-fold ($P \leq 0.05$) was generated for lodoxamide, but bufrolin was not significantly affected (**Fig 5.7E/F**; **Table 5.4**).

5.1.6 *Arginine 4.62 plays an important role in ligand binding at rat GPR35*

The last species selective arginine residue assessed was rat R4.62 (L4.62 at human GPR35) and following site directed mutagenesis, constructs that expressed R4.62L (rat) or L4.62R (human) were generated. Although pamoic acid and compound 1 did not display high potency at wild type rat GPR35, expression of R4.62L completely ablated such responses (**Fig 5.8A/B**; **Table 5.5**). Expression of the equivalent mutation at human GPR35 (L4.62R) did not, however, significantly affect the potency of pamoic acid or compound 1 (**Table 5.5**). Lodoxamide recorded a 21-fold reduction in potency ($P \leq 0.001$) at R4.62L rat

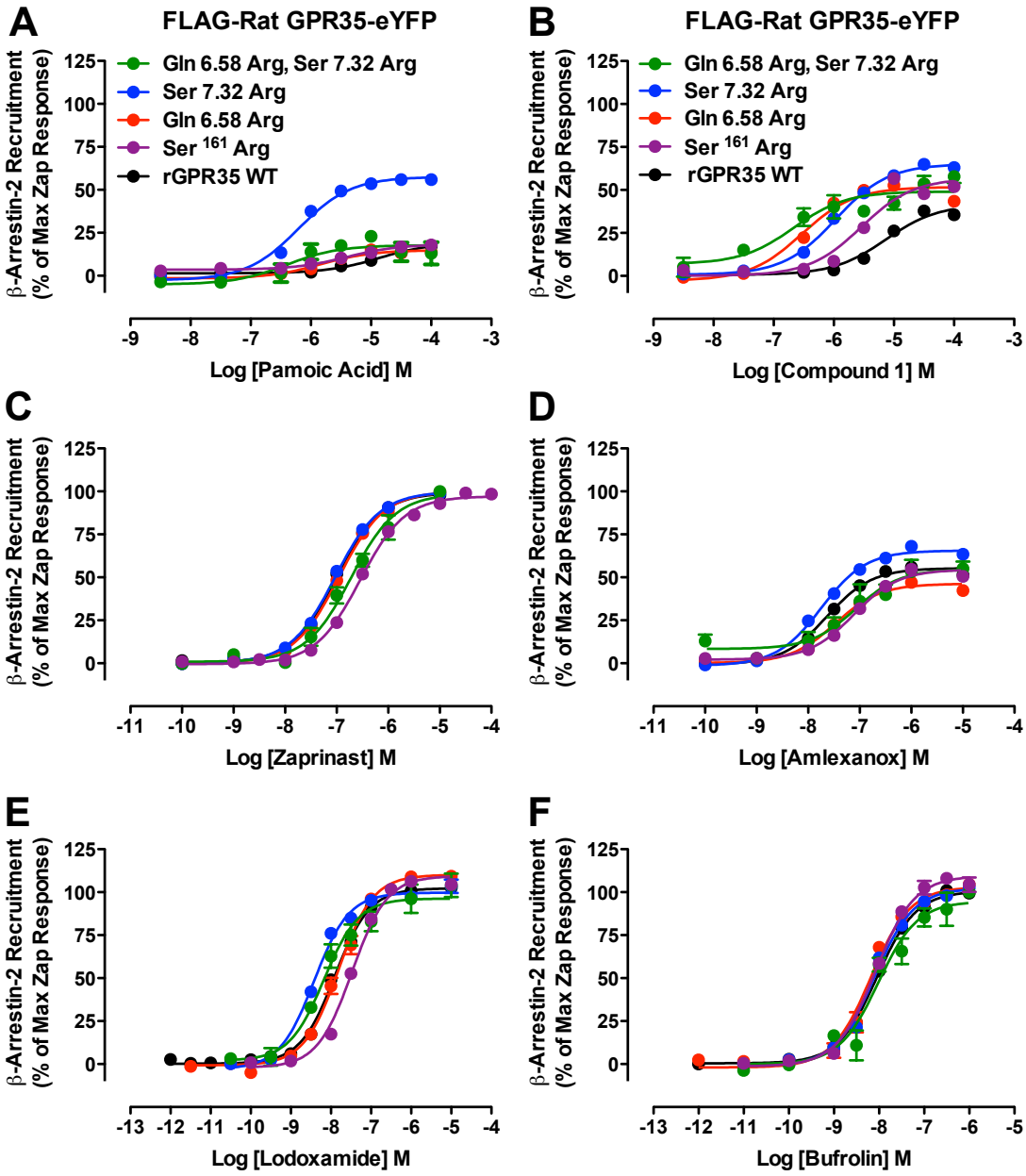

Figure 5.7 Expression of $S^{161}R$, Q6.58R and S7.32R improve human-selective ligand potency at rat GPR35 β-arrestin-2 recruitment at wild type (black), $S^{161}R$ (purple), R6.58Q (red), R7.32S (blue) and R6.58Q/R7.32S (green) was assessed on response to pamoic acid (**A**), compound 1 (**B**), zaprinast (**C**), amlexanox (**D**) lodoxamide (**E**), and bufrolin (**F**). Data are the mean ± SEM of a minimum of three independent experiments carried out in duplicate. Efficacy was normalised as a percentage of the maximal zaprinast response generated at each individual mutant.

Table 5.4 Human selective ligands increase in potency following expression of $S^{161}R$, Q6.58R and S7.32R at rat GPR35

	Cell Surface Expression, Ligand Potency (pEC_{50}), ± SEM, and ΔpEC_{50}								
	Wild Type	Gln 6.58 Arg		Ser 7.32 Arg		Gln 6.58 Arg, Ser 7.32 Arg		Ser ^{161} Arg	
Cell Surface[a]	100.0 ± 20.7	143.9 ± 19.5**		148.6 ± 7.3*		163.8 ± 16.9***		71.2 ± 5.2***	
Ligand	pEC_{50}	pEC_{50} [b]	ΔpEC_{50} [c]	pEC_{50} [b]	ΔpEC_{50} [c]	pEC_{50} [b]	ΔpEC_{50} [c]	pEC_{50} [b]	ΔpEC_{50} [c]
Pamoic Acid	4.87 ± 0.10	5.83 ± 0.14*	+ 0.96	6.20 ± 0.06***	+ 1.33	6.41 ± 0.35***	+ 1.54	5.58 ± 0.17	+ 0.71
Compound 1	5.14 ± 0.08	6.52 ± 0.08***	+ 1.38	5.97 ± 0.04**	+ 0.83	6.67 ± 0.24***	+ 1.53	5.31 ± 0.17	+ 0.17
Zaprinast	7.01 ± 0.02	6.97 ± 0.08	- 0.04	7.03 ± 0.06	+ 0.02	6.77 ± 0.20	- 0.24	6.43 ± 0.04**	- 0.58
Amlexanox	7.63 ± 0.07	7.47 ± 0.06	- 0.16	7.75 ± 0.08	+ 0.12	7.21 ± 0.21	- 0.42	7.12 ± 0.05*	- 0.51
Lodoxamide	7.90 ± 0.02	8.09 ± 0.08	+ 0.19	8.25 ± 0.08	+ 0.35	8.15 ± 0.20	+ 0.25	7.45 ± 0.03*	- 0.45
Bufrolin	8.00 ± 0.02	8.18 ± 0.05	+ 0.18	8.10 ± 0.04	+ 0.10	8.02 ± 0.11	+ 0.02	8.05 ± 0.02	+ 0.05

[a] Cell surface expression presented as a percentage of wild type, *P* values *** ≤ 0.001, ** ≤ 0.01, * ≤ 0.05

[b] Statistically significant difference in potency from wild type pEC_{50}, *P* values *** ≤ 0.001, ** ≤ 0.01, * ≤ 0.05

[c] ΔpEC_{50} represents mutant pEC_{50} - wild type pEC_{50}

Data are the mean ± SEM of a minimum of three independent experiments carried out in duplicate

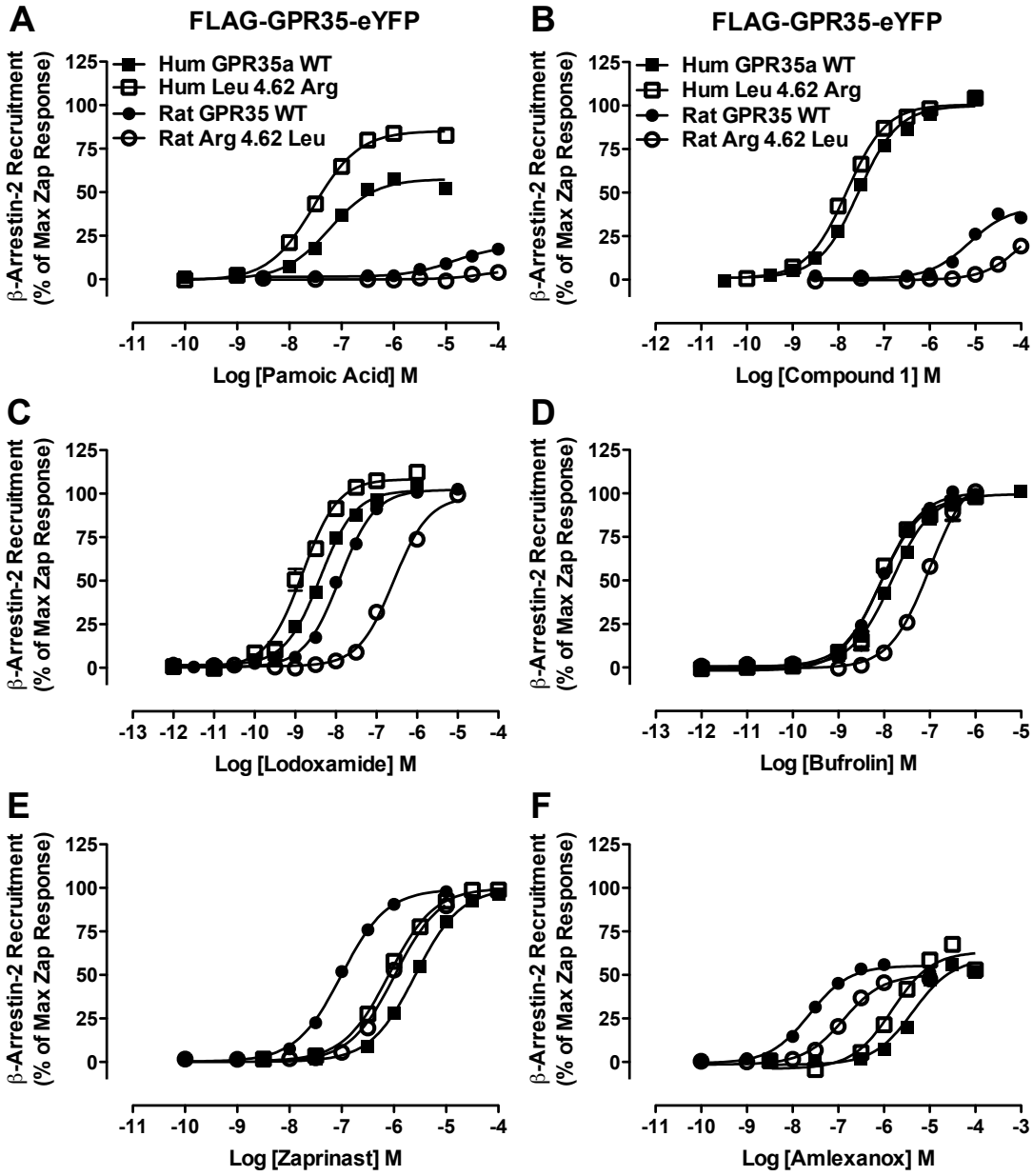

Figure 5.8 R4.62 plays a role in ligand-induced β-arrestin-2 recruitment at rat GPR35 The effect of human (filled squares), rat (filled circles), human L4.62R (open squares) and the rat R4.62L (open circles) GPR35 was measured on response to pamoic acid (**A**), compound 1 (**B**), lodoxamide (**C**), bufrolin (**D**) zaprinast (**E**), and amlexanox (**F**) using the BRET-based β-arrestin-2 recruitment assay. Data are the mean ± SEM of a minimum of three independent experiments carried out in duplicate. Efficacy was normalised as a percentage of the maximal zaprinast response generated at each individual mutant.

Table 5.5 Expression of R4.62 enhanced β-arrestin-2 recruitment at rat GPR35

	Ligand Potency (pEC_{50}) ± SEM and ΔpEC_{50}					
	FLAG-Human GPR35-eYFP			FLAG-Rat GPR35-eYFP		
	Wild Type	Leu 4.62 Arg		Wild Type	Arg 4.62 Leu	
Cell Surface	100.0 ± 20.4	86.8 ± 11.1		100 ± 20.7	112.3 ± 4.0**	
Pamoic Acid	7.25 ± 0.05	7.53 ± 0.03	+ 0.28	4.87 ± 0.10	<4	NA
Compound 1	7.55 ± 0.03	7.81 ± 0.03	+ 0.26	5.14 ± 0.08	<4	NA
Lodoxamide	8.38 ± 0.02	8.82 ± 0.05***	+ 0.44	7.90 ± 0.02	6.58 ± 0.07***	- 1.32
Bufrolin	7.83 ± 0.02	8.09 ± 0.05*	+ 0.26	8.00 ± 0.02	7.00 ± 0.04***	- 1.00
Zaprinast	5.59 ± 0.01	6.01 ± 0.02***	+ 0.42	7.01 ± 0.02	5.98 ± 0.02***	- 1.03
Amlexanox	5.38 ± 0.05	5.89 ± 0.09**	+ 0.51	7.63 ± 0.07	6.89 ± 0.06***	- 0.74

[a] Cell surface expression presented as a percentage of wild type, *P* value ** ≤ 0.01

[b] Statistically significant difference in potency from wild type pEC_{50}, *P* values *** ≤ 0.001, ** ≤ 0.01, * ≤ 0.05

[c] ΔpEC_{50} represents mutant pEC_{50} - wild type pEC_{50}

NR, no response; NA, not applicable

Data are the mean ± SEM of a minimum of three independent experiments carried out in duplicate

GPR35 (**Fig 5.8C**; **Table 5.5**). This was in contrast to a small, but significant 2.8-fold ($P \leq 0.01$) increase in the potency for lodoxamide following expression of L4.62R human GPR35 (**Fig 5.8C**; **Table 5.5**). Similarly, bufrolin recorded a 10-fold ($P \leq 0.001$) reduction in potency following expression of R4.62L rat GPR35 and a 1.8-fold increase in potency ($P \leq 0.05$) following expression of L4.62R human GPR35 (**Fig 5.8D**; **Table 5.5**). This trend was observed in the potencies of zaprinast and amlexanox. Zaprinast showed a 10.7-fold ($P \leq 0.001$) reduction in potency at R4.62L, while at human L4.62R potency increased 2.6-fold ($P \leq 0.001$) (**Fig 5.8E**; **Table 5.5**). At R4.62L the potency of amlexanox was reduced 5.5-fold ($P \leq 0.001$), while a 3.9-fold ($P \leq 0.01$) increase was observed at human L4.62R (**Fig 5.8F**; **Table 5.5**).

5.2 A conserved network of residues at GPR35 act in a species selective manner

In order to place the activity of the species selective ligands in the context of general ligand binding, species conserved residues were identified via receptor modelling efforts based on the β2-adrenergic receptor (Rasmussen et al., 2007; Cherezov et al., 2007), and more recently, the PAR1 receptor (Zang et al., 2012) that were likely to be involved in ligand binding at human GPR35. Residues at positions 3.32, 3.36, 4.60 and 7.43 were chosen for analysis, and to assess their role in ligand binding and contribution to species selectivity, each residue was mutated to alanine or, in the case where this produced a non-functional receptor, an amino acid with different functional properties to the endogenous residue. As for the species selective arginine residues, the ability of each mutant to recruit β-arrestin-2 was assessed via BRET technology and the effect on cell surface expression quantified using cell surface ELISA with FLAG antisera.

5.2.1 *Mutation of Y3.32L perturbs ligand induced β-arrestin-2 recruitment at human and rat GPR35*

Previous research efforts undertaken within our laboratory indicated the importance of R3.36 and Y3.32 at human and rat GPR35, with mutation to alanine completely abolishing ligand induced β-arrestin-2 recruitment (Jenkins et al., 2011). Indeed, while R3.36 was mutated to both alanine and methionine, and despite delivery to the cell surface, β-arrestin-

2 recruitment was completely abolished for all of the ligands assessed herein at both human and rat GPR35 (data not shown). As described by Jenkins et al., (2011), however, the non-conservative mutation of Y3.32L abolished β-arrestin-2 recruitment at human but not rat GPR35 (Jenkins et al., 2011). For this reason therefore, Y3.32L was retested with the current selection of ligands to assess its role in ligand binding at rat GPR35. At Y3.32L rat GPR35, the potency of zaprinast was reduced 89-fold ($P \leq 0.001$) and amlexanox 50-fold ($P \leq 0.001$) (**Fig 5.9A/B**; **Table 5.6**). Pamoic acid, conversely, was unaffected by expression of Y3.32L, while compound 1 recorded a 4.1-fold reduction in potency ($P \leq 0.05$) (**Fig 5.9C/D**; **Table 5.6**). Lodoxamide, akin to the rodent selective ligands, recorded a 81-fold ($P \leq 0.001$) reduction in potency at Y3.32L, while bufrolin was not tested at this mutant (**Fig 5.9E**; **Table 5.6**).

5.2.2 *R4.60 expression is critical for β-arrestin-2 recruitment at both human and rat GPR35*

Since the R4.60A mutant was found to be unresponsive in the β-arrestin-2 recruitment assay (data not shown), an R4.60M mutant was generated and assessed herein. The ability of zaprinast (**Fig 5.10A**) to recruit β-arrestin-2 was completely abolished at R4.60M human GPR35, although all of the other ligands tested retained at least some functionality at this form of GPR35 (**Table 5.7**). It is for this reason that the data presented in **Figure 5.10** for human GPR35 were normalised to the maximal wild type response to zaprinast. At R4.60M rat GPR35 zaprinast retained some functionality, but it displayed a 81-fold reduction in potency ($P \leq 0.001$) (**Fig 5.10A**; **Table 5.7**). Conversely, although amlexanox showed a 11-fold reduction in potency ($P \leq 0.001$) at R4.60M human GPR35, the equivalent mutation at rat GPR35 completely ablated the ability of amlexanox to recruit β-arrestin-2 (**Fig 5.10B**; **Table 5.7**). Pamoic acid meanwhile generated a 33-fold ($P \leq 0.001$) reduction in potency at R4.60M human GPR35 but was not significantly affected by the equivalent mutation at rat (**Fig 5.10C**; **Table 5.7**). Similarly, compound 1 recorded a 190-fold ($P \leq 0.001$) reduction in potency at R4.60M human GPR35 and was not significantly affected by expression of R4.60M rat GPR35 (**Fig 5.10D**; **Table 5.7**). Unlike the human-selective ligands, however, the potencies of lodoxamide (**Fig 5.10E**) and bufrolin (**Fig 5.10F**) were significantly reduced following mutation of R4.60M in both human and rat GPR35 (**Table 5.7**). Lodoxamide recorded a 170-fold decrease in potency ($P \leq 0.001$) at R4.60M human GPR35, while at R4.60M rat GPR35 there was a 525-fold decrease ($P \leq 0.001$) in

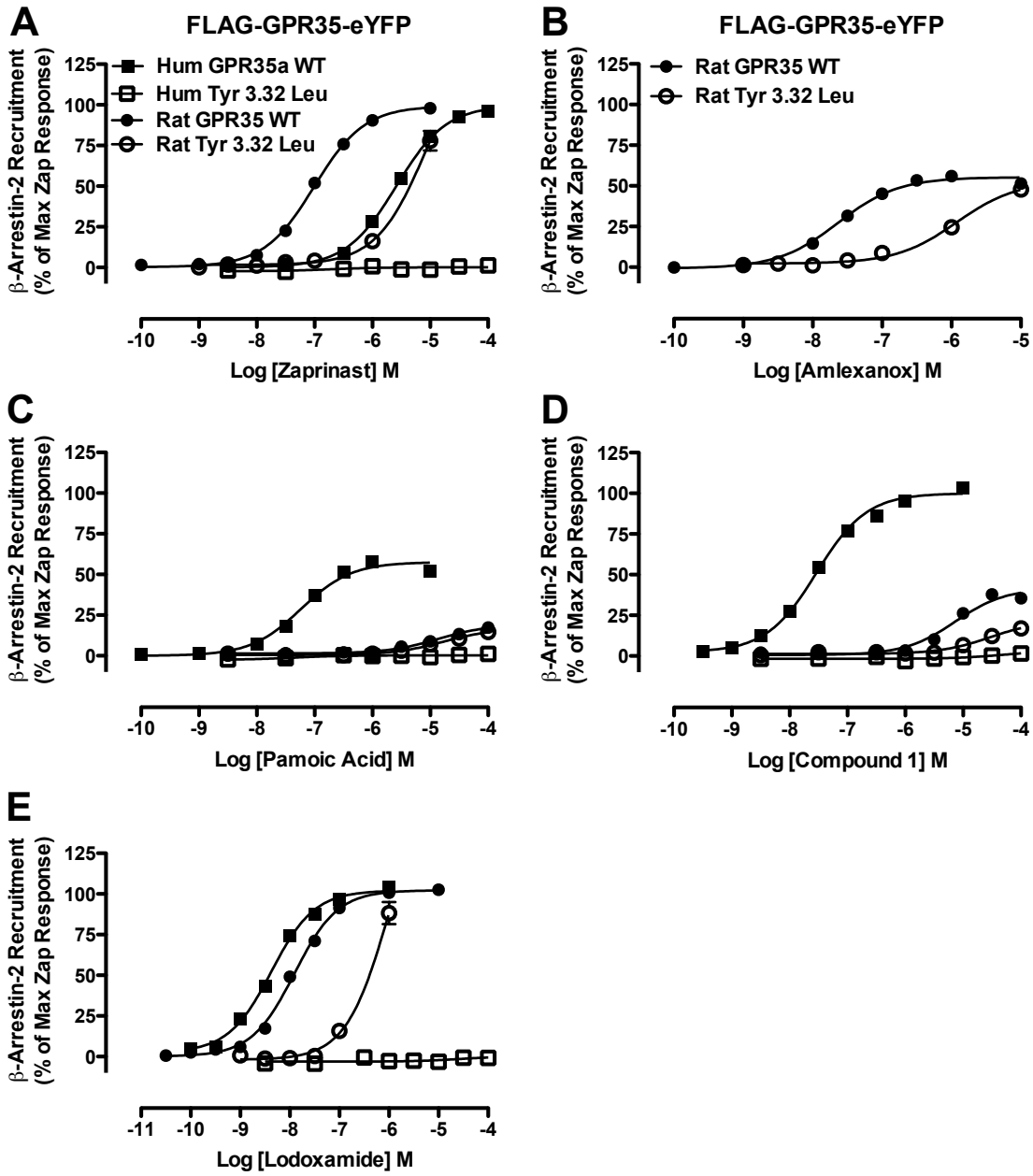

Figure 5.9 Y3.32 plays a role in ligand-induced β-arrestin-2 recruitment at human and rat GPR35 β-arrestin-2-*Renilla* luciferase and mutant or wild type human or rat FLAG-GPR35-eYFP constructs were employed in the BRET-based methodology of β-arrestin-2 recruitment. The effects of wild type human (filled squares), wild type rat (filled circles), human R4.60M (open squares), or rat R4.60M (open circles) were measured on response to zaprinast (**A**), amlexanox (**B**), pamoic acid (**C**), compound 1 (**D**), and lodoxamide (**E**). Data are the mean ± SEM of a minimum of three independent experiments carried out in duplicate. Efficacy was normalised to the percentage of the maximal zaprinast response generated at each individual mutant (rat) or the maximal wild type zaprinast response (human).

Table 5.6 Y3.32 plays a role in ligand induced β-arrestin-2 recruitment at human and rat GPR35

	Cell Surface Expression, Ligand Potency (pEC_{50}) ± SEM, and ΔpEC_{50}					
	FLAG-Human GPR35-eYFP			FLAG-Rat GPR35-eYFP		
	Wild Type	Tyr 3.32 Leu		Wild Type	Tyr 3.32 Leu	
Cell Surface[a]	100.0 ± 20.4	90.7 ± 8.7		100.0 ± 20.7	89.2 ± 6.4**	
Ligand	pEC_{50}	pEC_{50}[b]	ΔpEC_{50}[c]	pEC_{50}	pEC_{50}[b]	ΔpEC_{50}[c]
Zaprinast	5.59 ± 0.01	Inactive	NR	7.01 ± 0.02	5.06 ± 0.18***	- 1.95
Amlexanox	5.38 ± 0.05	NT	NA	7.63 ± 0.07	5.93 ± 0.08***	- 1.70
Pamoic Acid	7.25 ± 0.05	Inactive	NR	4.87 ± 0.10	4.77 ± 0.16	- 0.10
Compound 1	7.55 ± 0.03	Inactive	NR	5.14 ± 0.08	4.53 ± 0.17*	- 0.61
Lodoxamide	8.38 ± 0.02	Inactive	NR	7.90 ± 0.02	5.99 ± 0.21***	- 1.91
Bufrolin	7.83 ± 0.02	NT	NA	8.00 ± 0.02	NT	NA

[a] Cell surface expression presented as a percentage of wild type, *P* value ** ≤ 0.01

[b] Statistically significant difference in potency from wild type pEC_{50}, *P* values *** ≤ 0.001, ** ≤ 0.01, * ≤ 0.05

[c] ΔpEC_{50} represents mutant pEC_{50} - wild type pEC_{50}

NR, no response; NA, not applicable; NT, not tested

Data are the mean ± SEM of a minimum of three independent experiments carried out in duplicate

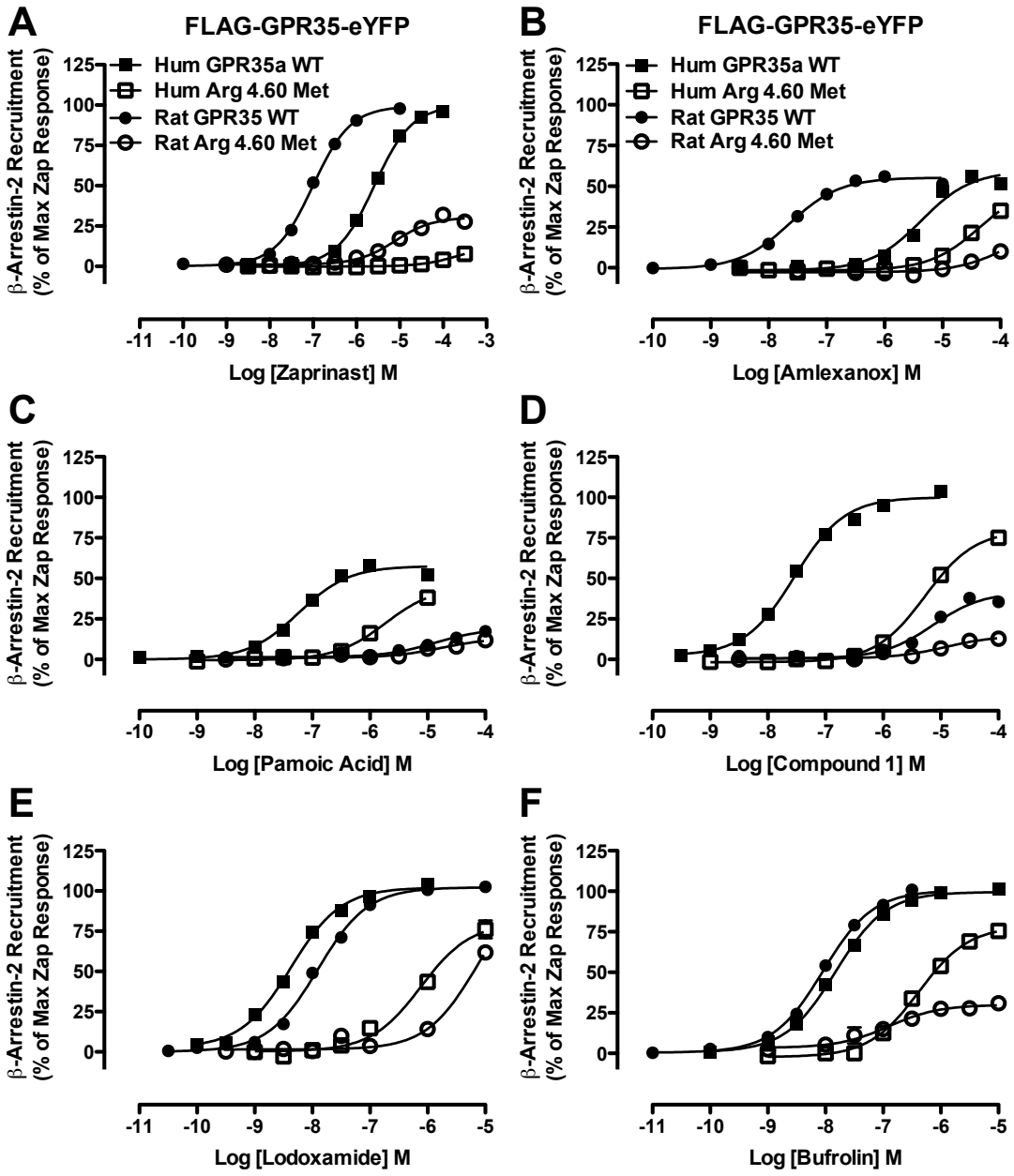

Figure 5.10 Expression of R4.60 is critical for β-arrestin-2 recruitment at human and rat GPR35 HEK293T cells transiently co-transfected with β-arrestin-2-*Renilla* luciferase and mutant or wild type human or rat FLAG-GPR35-eYFP constructs were assessed using the BRET-based methodology of β-arrestin-2 recruitment. The response of wild type human (filled squares), wild type rat (filled circles) human R4.60M (open squares) or rat R4.60M (open circles) were measured on response to zaprinast (**A**), amlexanox (**B**), pamoic acid (**C**), compound 1 (**D**) lodoxamide (**E**), and bufrolin (**F**) as illustrated. Data are the mean ± SEM of a minimum of three independent experiments carried out in duplicate and were normalised to the percentage of the maximal zaprinast response generated at each individual mutant (rat) or the maximal wild type zaprinast response (human).

Table 5.7 R4.60 is involved in ligand-induced β-arrestin-2 recruitment at human and rat GPR35

	Cell Surface Expression, Ligand Potency (pEC_{50}) ± SEM, and ΔpEC_{50}					
	FLAG-Human GPR35-eYFP			FLAG-Rat GPR35-eYFP		
	Wild Type	Arg 4.60 Met		Wild Type	Arg 4.60 Met	
Cell Surface[a]	100.0 ± 20.4	110.7 ± 9.60		100.0 ± 20.7	80.0 ± 1.5***	
Ligand	pEC_{50}	pEC_{50}[b]	ΔpEC_{50}[c]	pEC_{50}	pEC_{50}[b]	ΔpEC_{50}[c]
Zaprinast	5.59 ± 0.01	Inactive	NR	7.01 ± 0.02	5.10 ± 0.06***	- 1.91
Amlexanox	5.38 ± 0.05	4.35 ± 0.08***	- 1.03	7.63 ± 0.07	Inactive	NR
Pamoic Acid	7.25 ± 0.05	5.73 ± 0.06***	- 1.52	4.87 ± 0.10	4.76 ± 0.30	- 0.11
Compound 1	7.55 ± 0.03	5.27 ± 0.06***	- 2.28	5.14 ± 0.08	4.92 ± 0.20	- 0.22
Lodoxamide	8.38 ± 0.02	6.15 ± 0.05***	- 2.23	7.90 ± 0.02	5.18 ± 0.13***	- 2.72
Bufrolin	7.83 ± 0.02	6.37 ± 0.04***	- 1.46	8.00 ± 0.02	6.90 ± 0.14 ***	- 1.10

[a] Cell surface expression presented as a percentage of wild type, *P* value *** ≤ 0.001

[b] Statistically significant difference in potency from wild type pEC_{50}, *P* values *** ≤ 0.001, ** ≤ 0.01, * ≤ 0.05

[c] ΔpEC_{50} represents mutant pEC_{50} - wild type pEC_{50}

NR, no response; NA, not applicable

Data are the mean ± SEM of a minimum of three independent experiments carried out in duplicate

potency (**Fig 5.10E**; **Table 5.7**). Expression of R4.60M also affected the bufrolin response with a 29-fold ($P \leq 0.001$) and 13-fold ($P \leq 0.001$) reduction in potency at human and rat GPR35, respectively (**Fig 5.10F**; **Table 5.7**).

5.2.3 *Mutation of D7.43A affects responses at rat GPR35 on a ligand-specific basis*

In previous mutagenesis efforts at GPR35, D7.43 had been mutated to both alanine and asparagine residues. Although β-arrestin-2 responses generated from the D7.43A and D7.43N mutants were generally equivalent in terms of potency (data not shown), the D7.43A mutant was subsequently chosen for the study presented herein (**Fig 5.11**). In a similar vein to the Y3.32L and R3.36A mutations however, alteration to the human wild type D7.43 sequence completely abolished β-arrestin-2 recruitment for all ligands assessed herein, despite receptor delivery to the cell surface (**Fig 5.11**; **Table 5.8**). Following expression D7.43A rat GPR35 zaprinast recorded a 5.8-fold increase ($P \leq 0.001$) in potency, while amlexanox was not significantly affected (**Fig 5.11A/B**; **Table 5.8**). For pamoic acid the E_{max} increased to 69.8 ± 3.3 % ($P \leq 0.001$) from 19.2 ± 1.3 %, but potency was not significantly affected (**Fig 5.11C**). Compound 1 also recorded an increase in efficacy (E_{max} 94.6 ± 1.9 % from 41.7 ± 1.8 %) ($P \leq 0.001$) and was associated with a 380-fold increase in potency ($P \leq 0.001$) following expression of D7.43A (**Fig 5.11D**; **Table 5.8**). This increase actually abolished the species selective difference between human and rat GPR35 for compound 1 (**Table 5.8**). Lodoxamide, meanwhile, was not significantly affected by expression of the D7.43A mutant, while the potency of bufrolin was reduced 3-fold ($P \leq 0.001$) (**Fig 5.11E/F**; **Table 5.8**).

5.2.4 *Site directed mutagenesis efforts reveal residues involved in the activation of rat GPR35*

In addition to altering the potency and efficacy of some GPR35 ligands at rat GPR35, expression of D7.43A also resulted in a significant increase to the BRET signal in the absence of ligand, consistent with enhanced constitutive activity of the receptor. However, the equivalent mutation of the human receptor (D7.43A) was not constitutively active (**Fig 5.12B**). This phenomenon extended to residues other than D7.43A, and included Q6.58R, S7.32R and the double Q6.58R/S7.32R mutant, which all displayed various levels of

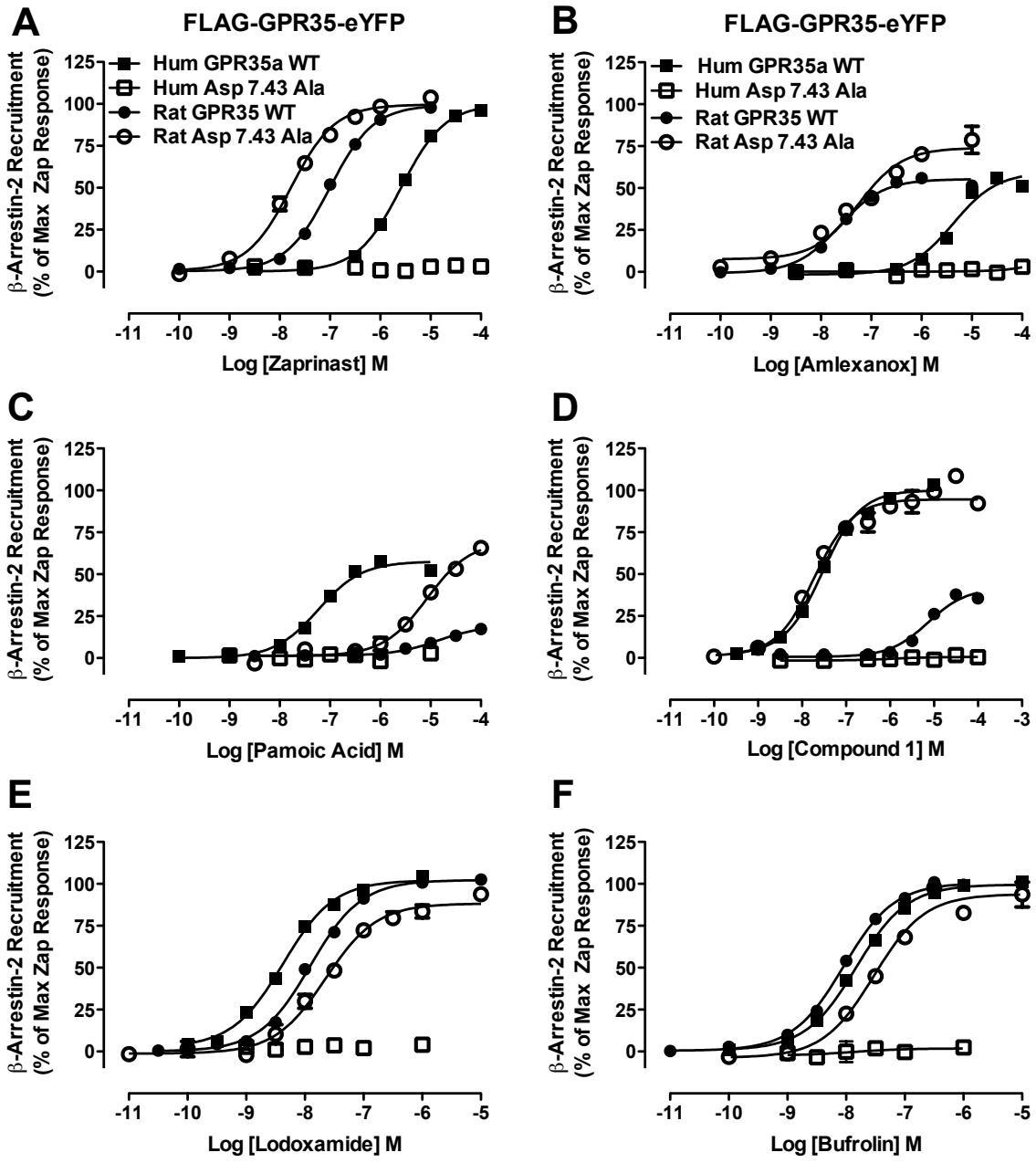

Figure 5.11 D7.43A has various effects on ligand responses at rat GPR35 HEK293T cells transiently co-transfected with β-arrestin-2-*Renilla* luciferase and mutant or wild type FLAG-GPR35-eYFP constructs were assessed using the BRET-based methodology of β-arrestin-2 recruitment. The effect of human GPR35 (filled squares), rat GPR35 (filled circles), human D7.43A (open squares) and rat D7.43A (open circles) was measured on response to zaprinast (**A**), amlexanox (**B**), pamoic acid (**C**), compound 1 (**D**) lodoxamide (**E**), and bufrolin (**F**). Data are the mean ± SEM of a minimum of three independent experiments carried out in duplicate. Efficacy was normalised to the percentage of the maximal zaprinast response generated at each individual mutant (rat) or the wild type zaprinast response (human).

Table 5.8 D7.43A plays a variable role in ligand induced β-arrestin-2 recruitment at rat GPR35

	Cell Surface Expression, Ligand Potency (pEC_{50}) ± SEM, and ΔpEC_{50}					
	FLAG-Human GPR35-eYFP			FLAG-Rat GPR35-eYFP		
	Wild Type	Asp 7.43 Ala		Wild Type	Asp 7.43 Ala	
Cell Surface[a]	100.0 ± 20.4	107.7 ± 11.6		100.0 ± 20.7	76.8 ± 1.5***	
Ligand	pEC_{50}	pEC_{50}[b]	ΔpEC_{50}[c]	pEC_{50}	pEC_{50}[b]	ΔpEC_{50}[c]
Zaprinast	5.59 ± 0.01	Inactive	NR	7.01 ± 0.02	7.77 ± 0.05***	+ 0.76
Amlexanox	5.38 ± 0.05	Inactive	NR	7.63 ± 0.07	7.23 ± 0.11	- 0.40
Pamoic Acid	7.25 ± 0.05	Inactive	NR	4.87 ± 0.10	5.07 ± 0.09	+ 0.20
Compound 1	7.55 ± 0.03	Inactive	NR	5.14 ± 0.08	7.72 ± 0.09***	+ 2.58
Lodoxamide	8.38 ± 0.02	Inactive	NR	7.90 ± 0.02	7.67 ± 0.06	- 0.23
Bufrolin	7.83 ± 0.02	Inactive	NR	8.00 ± 0.02	7.53 ± 0.07***	- 0.47

[a] Cell surface expression presented as a percentage of wild type, *P* value *** ≤ 0.001

[b] Statistically significant difference in potency from wild type pEC_{50}, *P* values *** ≤ 0.001, ** ≤ 0.01, * ≤ 0.05

[c] ΔpEC_{50} represents mutant pEC_{50} - wild type pEC_{50}

NR, no response; NA, not applicable

Data are the mean ± SEM of a minimum of three independent experiments carried out in duplicate

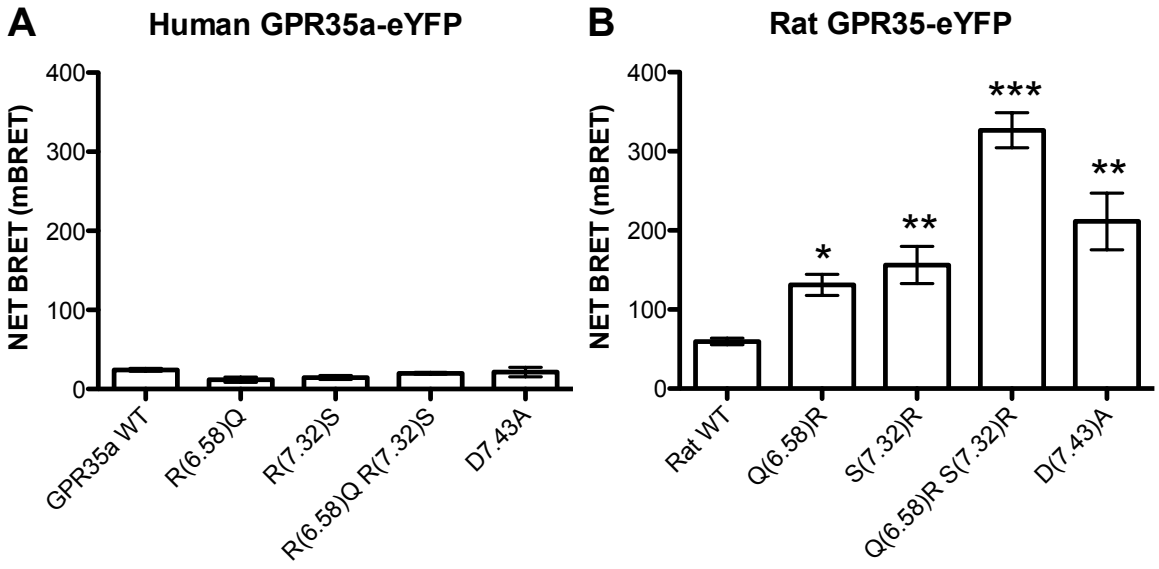

Figure 5.12 Alterations of GPR35 sequence can induce constitutive activity at rat but not human GPR35 Species swap mutations that were carried out via site directed mutagenesis at residues 6.58, 7.32 and 7.43 had no effect on the basal BRET signal at human GPR35 (**A**) but induce constitutive activity at rat GPR35 (**B**). In order to show changes in efficacy, NET mBRET was calculated from the basal β-arrestin-2 recruitment readings from three individual experiments and presented ± SEM. A statistically significant difference from wild type is denoted as *P* = *** ≤ 0.001, ** ≤ 0.01, * ≤ 0.05.

constitutive activity at rat but not human GPR35 (**Fig 5.12A**).

5.3 Discussion

The differences in species selectivity displayed by selected GPR35 ligands were assessed upon response to 'species swap' mutations in an effort to identify residues important for ligand function. Since there was no radiolabelled ligand available at this time, all mutants were assessed by means of β-arrestin-2 recruitment to human or rat GPR35 using BRET technology. The β-arrestin-2 recruitment assay generates EC_{50}s that are similar to the K_D values obtained in receptor binding assays (Funke et al., 2013) since this format is assumed to lack signal amplification and is therefore suitable for this purpose. The results presented herein indicated for the first time the reliance of the human selective ligands pamoic acid and compound 1 on positively charged arginine residues in ELC2 (R^{164}) and ELC3 (R6.58 and R7.32). Reciprocal mutations made at these residues increased the potency of pamoic acid and compound 1 at rat GPR35, and therefore presented the first molecular evidence for the basis of species selectivity at GPR35.

By assessing the responses of the human and rat equipotent ligands lodoxamide and bufrolin it became apparent that their equipotent responses were achieved by binding in a manner akin to pamoic acid and compound 1 at the human receptor and to zaprinast and amlexanox at rat (**Fig 5.13**). This is important as it indicated that lodoxamide and bufrolin do not interact with a series of conserved residues to result in their equipotency between species, and therefore it is quite remarkable that two ligands with such high potency at both human and rat orthologues of GPR35 have been identified. The majority of reciprocal mutations generated did not affect the potency of zaprinast and amlexanox to any great extent, with the exception of the species conserved residue R4.60, which when mutated to methionine completely ablated zaprinast's ability to recruit β-arrestin-2 at human GPR35. Mutation of R4.60M also completely ablated ligand response at rat GPR35. Alteration to the rat sequence was often associated with a substantial increase in tonic receptor activity that was not observed for human GPR35. These findings, taken together, strongly indicate that the residues involved in ligand binding and receptor activation at human and rat GPR35 are acting in a distinct manner. This discussion places the findings presented herein in the context of those generated from mutagenesis efforts of others studying carboxylic acid

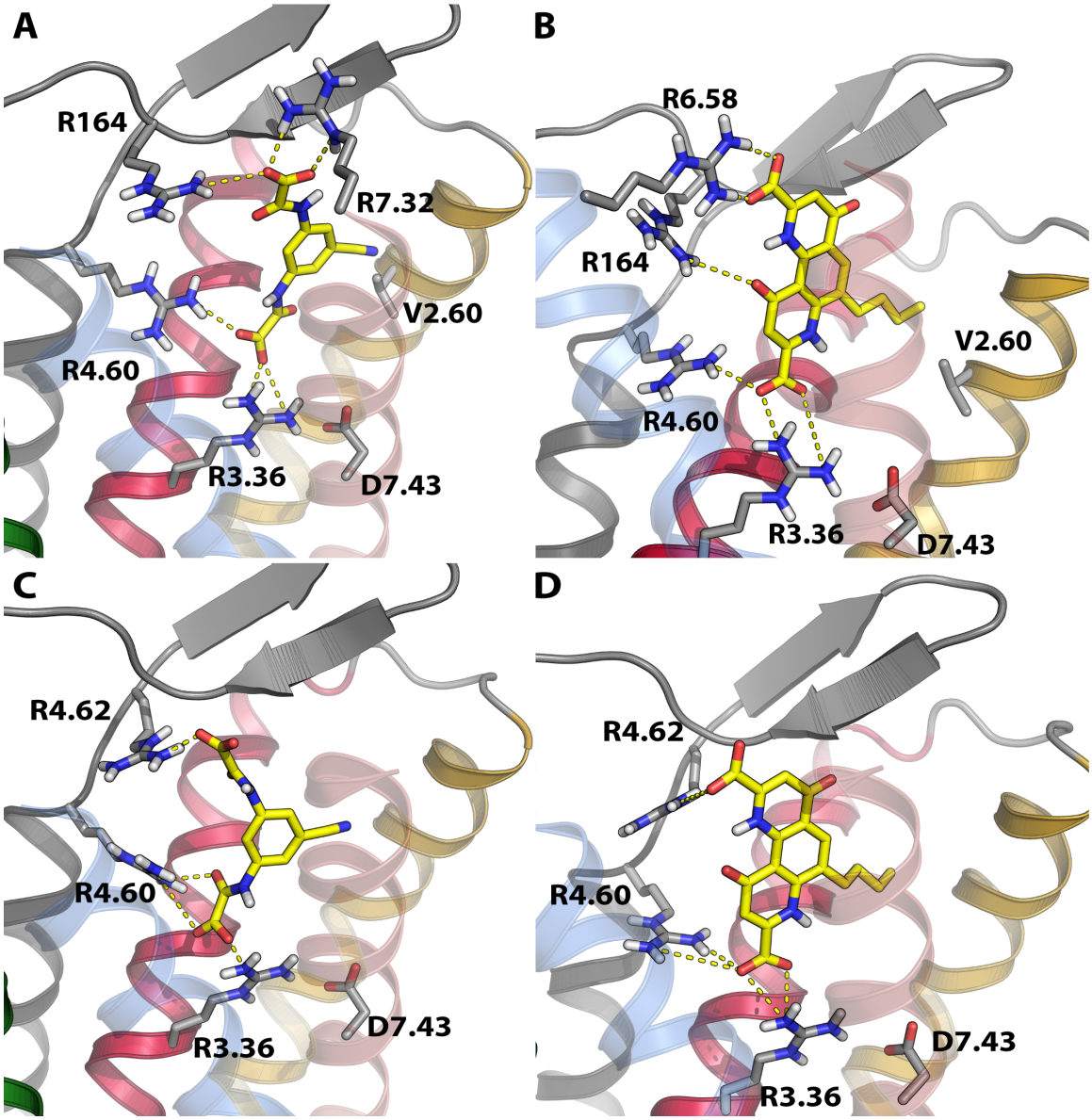

Figure 5.13 Lodoxamide and bufrolin interact with a distinct subset of residues between species to achieve their equipotent responses Receptor homology models for human (**A/B**) and rat (**C/D**) GPR35 in complex with lodoxamide (**A/C**) or bufrolin (**B/D**) based on the crystal structure of the PAR1 receptor (Zhang et al., 2012), generated by my collaborator Dr. Gianluigi Caltabiano (Mackenzie et al., 2014). Species conserved residues R3.36 and R4.60 act alongside D7.43 at the base of the binding pocket to tether the carboxylic acid moiety of each agonist. At human GPR35, residues in ECL2 (R^{164}) and ECL3 (R6.58 and R7.32) coordinate ligand binding at the top of the binding pocket. Rat GPR35 does not contain arginine residues in these positions and relies on an arginine residue at the top of TM4/ bottom of ECL2 (R4.62) for ligand binding. Valine 2.60 is a residue present in human GPR35 that has been reported as a single nucleotide polymorphism that negatively affects ligand potency (Mackenzie et al., 2014).

binding GPCRs, which include the HCA_{1-3}, FFAR, succinate and oxoglutarate, receptors.

5.3.1 *A conserved carboxylic acid binding arginine residue at position 3.36*

In GPR35, R3.36 is widely conserved between species including the fruit bat, whale, cow, rodents, and man suggesting that it plays an important and conserved function (data not shown). Indeed, for both human and rat GPR35, mutation of R3.36A completely abolishes all ligand responses without ablating cell surface delivery (Jenkins et al., 2011; Mackenzie et al., 2014). This finding was also observed upon mutation of R3.36A in the HCA_1 and HCA_2 receptors, with the suggestion that R3.36 is critical for carboxylic acid binding of lactate and nicotinic acid, respectively (Liu et al., 2009; Tunaru et al., 2005; Kuei et al., 2011). For this reason therefore, it was hypothesised that R3.36 was a residue critical for carboxylic acid binding at the base of the ligand binding pocket at both human and rat GPR35. In an independent study, R3.36 was also described as a residue that played a role in maintaining the structural integrity of GPR35 as well as making ligand contacts that are important for function (Zhao et al., 2014).

In this study Zhao et al. found that human R3.36A was retained within the cytoplasm and did not reach the cell surface following expression in a U2OS cell line. Incubation with the GPR35 inverse agonist CID-2745687 restored cell surface expression of GPR35 R3.36A by acting as a pharmacological chaperone, indicating that the R3.36A mutation affected folding and cell surface delivery of the receptor (Zhao et al., 2014). The ability of CID-2745687 to rescue cell surface expression of GPR35 R3.36A indicated that R3.36 is not critical for CID-2745687 interaction with GPR35. In this context, it would be of interest to determine whether expression of R3.36A could also be rescued by ML-145, since ML-145 contains a carboxyl group and may require R3.36 for ligand binding (whereas CID-2745687 contains only an ethyl ester). This group also indicated that R3.36 is not directly involved in ligand binding in rat GPR35, as an alteration in sequence from P5.43 at human to S5.43 in rat is predicted to shift TM5 by approximately 4 Å to a position unfavourable for R3.36 ligand interaction (Lane, 2011). This is distinct from the model generated from the data presented herein based on homology modelling with the PAR1 receptor, and is perhaps a reflection that receptor homology modelling based on the crystal structure of the β2-AR (Mackenzie et al., 2014; Zhang et al., 2012).

The hydroxycarboxylic acid receptor family consists of the HCA_{1-3} receptors that respond endogenously to 2-hydroxy-propanoic acid (lactate), 2-hydroxy-butyric acid (a keytone), and 3-hydroxy-octanoic acid (a β-oxidation intermediate), respectively (Ahmed, 2011). In terms of sequence similarity, GPR35, the oxoeicosanoid (OXE) and GPR31 receptors are closely related to this family, and these receptors are unique amongst class A GPCRs in that they all contain the residue R3.36. The OXE and GPR31 receptors, akin to HCA_{1-3}, are activated by endogenous hydroxycarboxylic acids derived from lipoxygenase activity, namely 5-oxo-6,8,11,14-eicosatetraenoic acid and 12-(S)-hydroxy-5,8,10,14-eicosatetraenoic acid, respectively (Hosoi et al., 2002; Jones et al., 2003; Guo et al., 2011). R3.36 therefore appears to be a central feature of hydroxycarboxylic acid-binding GPCRs, but it is of interest to note that hydroxycarboxylic acid ligands have not been suggested as agonists of GPR35. Although GPR35 responds to numerous carboxylic acid and dicarboxylic acid ligands, a conserved arginine residue at position 3.36 is not a required feature for general carboxylic acid binding, and this residue is not present in the FFAR or the dicarboxylic acid binding succinate and oxoglutarate receptors (**Fig 5.14**). From these observations, therefore, it may be pertinent to assess hydroxycarboxylic acids as endogenous ligands of GPR35, given the presence of this unusual residue within the binding pocket.

5.3.2 *ECL2 plays a role in ligand binding at human GPR35*

In addition to R3.36, the HCA_{1-3} receptors also require the presence of an arginine residue in TM6 and a conserved sequence motif (CxSF) in ECL2 (**Fig 5.15**) for ligand binding (Tunaru et al., 2005; Liu et al., 2009). The cysteine residue of ECL2 forms a highly conserved disulphide bond with C3.25 in most family A GPCRs that effectively tethers ECL2 to the helical bundle, provides conformational constraint, and can influence ligand entry into the binding pocket (Wheatley et al., 2012). This sequence is CFRS in human GPR35 and CFSS in rat GPR35, and was investigated herein by reciprocal mutation of $R^{164}S$ and $S^{161}R$ at human and rat GPR35, respectively. R^{164} was found to be important for ligand function at human GPR35 for the human selective and equipotent but not rat selective ligands (**Fig 5.5**; **Table 5.2**), while the reciprocal mutation at rat GPR35 ($S^{161}R$) actually significantly reduced the potency of zaprinast, amlexanox, and lodoxamide (**Fig 5.7**; **Table 5.4**). This indicates that

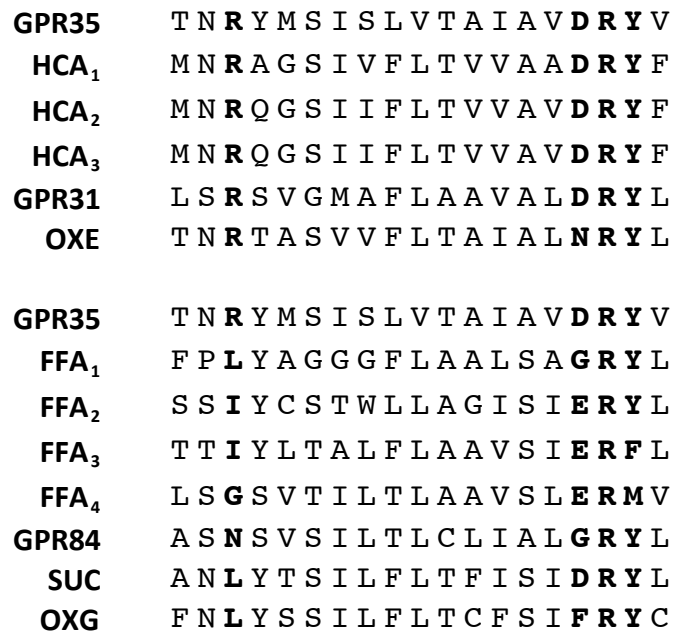

Figure 5.14 Hydroxycarboxylic acid binding GPCRs contain a conserved arginine residue at position 3.36 that is not conserved across all carboxylic acid-binding GPCRs Sequence alignments of TM3 including the 'DRY' motif or equivalent sequence in bold, alongside the conserved arginine residue at position 3.36 that is thirteen residues preceding the DRY motif, in bold. Those containing R3.36 are the hydroxycarboxylic acid receptors HCA_1 (GPR81), HCA_2 (GPR109A), HCA_3 (GPR109B), GPR31 and the oxoeicosanoid (OXE) receptor 1; class A carboxylic acid ligand binding GPCRs that do not contain the R3.36 residue include the free fatty acid receptors 1-4 and GPR84, the succinate (GPR91) and oxoglutarate (GPR99) receptors.

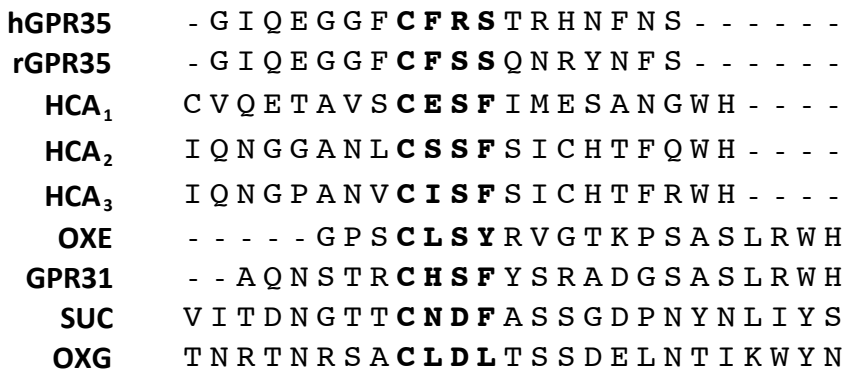

Figure 5.15 Hydroxycarboxylic acid binding GPCRs contain a 'CxSF' motif in ECL2 that is critical for ligand function The highly conserved cysteine residue in ECL2 forms a disulphide bond in many class A GPCRs that is critical for receptor stability and function. The HCA_{1-3}, GPR31 and OXE receptors that bind hydroxycarboxylic acid ligands all contain the CxSF motif (bold); these amino acids are present in human (h) and rat (r) GPR35 but not in the same order: human 'CFRS' and rat 'CFSS'. The succinate and oxoglutarate receptors do not contain this motif in their ECL2 region.

ECL2 plays a different role between GPR35 species orthologues and that the equipotent ligands rely on distinct contacts to modulate binding between species. Further differences in this region between species are likely based on sequence, as rat GPR35 contains an N-linked glycosylation consensus sequence (N-X-S/T) that is absent from the ECL2 of human. Oligosaccharide chains can orient ELC2 away from the binding pocket (Wheatley et al., 2012), such that ECL2 may play less of a role in mediating entry of the ligand into the binding pocket. Receptor homology modelling efforts at GPR35 reflect this, with the β-hairpin loop of human – but not rat – forming a lid over the binding pocket and playing a role in ligand binding (**Fig 5.13**) (Mackenzie et al., 2014).

ELC2 has also been implicated as a negative regulator of constitutive activity, with various ionic locks forming between ECL2, TM5 and TM7 that maintain receptors in an inactive state (Massotte and Kieffer, 2005; Klco et al., 2005). Constitutive activity has only been confirmed for human GPR35 in the IP-One assay (**Fig 3.9**), since the inverse agonists ML-145 and CID-2745687 are markedly human selective and do not block agonist induced responses at the rodent orthologues. Despite this, however, it is likely that human and rodent orthologues of GPR35 display constitutive activity. This is based on findings obtained from the BRET-based β-arrestin-2 recruitment assay that showed that rat GPR35 generated a significantly higher level of basal BRET than human GPR35 and many of the reciprocal mutations generated at rat further increased this activity (**Fig 5.12**). Interestingly, of the few reciprocal mutations assessed herein that did *not* induce constitutive activity of rat GPR35, both were within the region of ECL2 ($S^{161}R$ and R4.62L), which could indicate that the ECL2 of rat GPR35 is not involved in modulating rat GPR35 receptor activation.

5.3.3 *ECL3 is critical for ligand binding at human GPR35*

Interestingly, although a number of GPCRs use topological residues at the top of TM6 and TM7 for ligand binding, the only crystal structures that involve the topological residue at 6.58 for ligand contact are the human PAR1, human CXCR4, rat neurotensin receptor, mouse μ-opioid and δ-opioid receptors, all of which are peptide-binding GPCRs (Venkatakrishnan et al., 2013). Moreover, PAR1 is the only crystalised GPCR that has been shown to contact the ligand at both positions 6.58 and 7.32 (Zhang et al., 2012; Venkatakrishnan et al., 2013). The requirement of 6.58 and 7.32 for ligand binding at human GPR35 does not translate to the

rat species orthologue, since reciprocal mutations at 6.58 and 7.32 ablate ligand functionality of the human-selective and equipotent ligands at human GPR35 (**Fig 5.6**; **Table 5.3**), but there is little effect on ligand binding at rat GPR35 following alteration to this sequence (**Fig 5.7**; **Table 5.4**). This is with the exception of the human-selective ligands pamoic acid and compound 1, which significantly gain potency over the wild type response following mutation of both Q6.58R and S7.32R in rat GPR35. This suggests that R6.58 and R7.32 are the major drivers of human-selective ligand induced species selectivity between human and rat GPR35. Interestingly, based on homology modelling with the β2-AR, Zhao et al. suggest that R6.58 shields R7.32 and that only R6.58 plays a direct role in ligand binding under wild type conditions; mutation of only one of these arginine residues therefore, in this case, could be compensated for by the second arginine residue (Zhao et al., 2014).

The dicarboxylic acid receptors succinate and oxoglutarate also require two arginine residues at the top of TM6 and TM7 (R6.55, R7.36), in addition to two basic residues at the base of the binding pocket (R3.29, H3.33), that coordinate dicarboxylic acid ligand binding (He et al., 2004). They therefore form a mechanism of dicarboxylic acid binding that utilises residues that are distinct from human GPR35. Molecular homology modelling efforts indicate that human GPR35 contains R3.36 and R4.60 at the base of the binding pocket (R4.60 is a unique residue of GPR35 amongst all the carboxylic acid-binding GPCRs), and R^{164}, R6.58 and R7.32 at the top (Mackenzie et al., 2014). Interestingly rat GPR35 is again distinct in that it contains R3.36 and R4.60 at the base but only R4.62 at the top of the binding pocket, since rat GPR35 lacks the two arginine residues in ECL3 (**Fig 5.4**) (Mackenzie et al., 2014). However, it is important to note that rat GPR35 contains a unique histidine residue in ECL3 (H6.64) that could perhaps coordinate dicarboxylic acid binding with R4.62 at this species orthologue. There are also additional arginine residues that are conserved between human and rat GPR35 that were not investigated as part of this study, namely in ECL2 (R167 in human, R165 in rat) and in TM7 (R7.33 in human and rat) (**Fig 5.4**). Therefore it is possible that, given the different results generated between species orthologues with previously described species conserved residues, human and rat GPR35 will interact and rely to different extents upon alteration of R165/R167 and R7.33, although this remains to be assessed directly.

In accordance with the involvement of ECL2 and since both R6.58 and R7.32 appear to be located within ECL3 it is apparent that (at least human) GPR35 relies heavily on the

extracellular loops to coordinate ligand binding. For this reason it is very interesting that the crystal structures of the closely related $P2Y_{12}$ receptor (which was not available during receptor homology efforts as part of this project) and the CXCR4 receptor (which did not appear to be relevant to GPR35 until the recent suggestion of CXCL17 as an endogenous ligand of GPR35) indicate the involvement of an 'ECL4' in ligand binding (Wu et al., 2010; Zhang et al., 2014). ECL4 is created as the result of the formation of a disulphide bond between a cysteine residue in the N-terminal region and a conserved cysteine residue in ECL3, which acts to pull ECL4 over the ligand-binding pocket (Szpakowska et al., 2014). The conserved cysteine is present in ECL3 of both human and rat GPR35, but the cysteine residue in the N-terminus is differentially positioned between the species orthologues (human C8, and rat C6, from the N-terminus). Furthermore, since the N-terminus of rat is four residues shorter than human GPR35a, it is likely that the exact positioning and structure of ECL4 would be distinct between the two species orthologues of GPR35. In light of this, it would be very interesting to determine the role of ECL4 in ligand binding and species selectivity, especially since this disulphide bond does not appear to be critical to GPCR structural stability (Zhang et al., 2014) and, therefore, this can be assessed directly. **Figure 5.16** depicts the formation of ECL4 over the binding pocket of human GPR35, as generated by Dr. Gianluigi Caltabiano by modification of the previously generated GPR35 model based on the PAR1 crystal structure.

5.3.4 *Y3.32 and D7.43 are species conserved residues at human and rat GPR35 that are generally involved in GPCR activation*

In both the S1P1 and PAR1 crystal structures, a residue within TMD3 forms a stabilising hydrogen bond network with TM7, often referred to as the '3-7 lock', breakage of which is depicted as the first molecular event associated with agonist-induced activation of the receptor (Hulme, 2013; Trzaskowski et al., 2012). In the PAR1 crystal structure (Zhang et al. 2014), Y3.33 and Y7.35 form a hydrogen bond that forms the base of the orthosteric-binding pocket. These residues are present in human GPR35 at positions Y3.32, and Y7.36, but rat GPR35 does not contain a tyrosine residue in this position in TM7. Mutation to Y3.32A and Y3.32L completely ablates ligand function at human but not rat GPR35, which retains activity at Y3.32L (**Fig 5.9**; **Table 5.6**). This suggests that the base of the human and

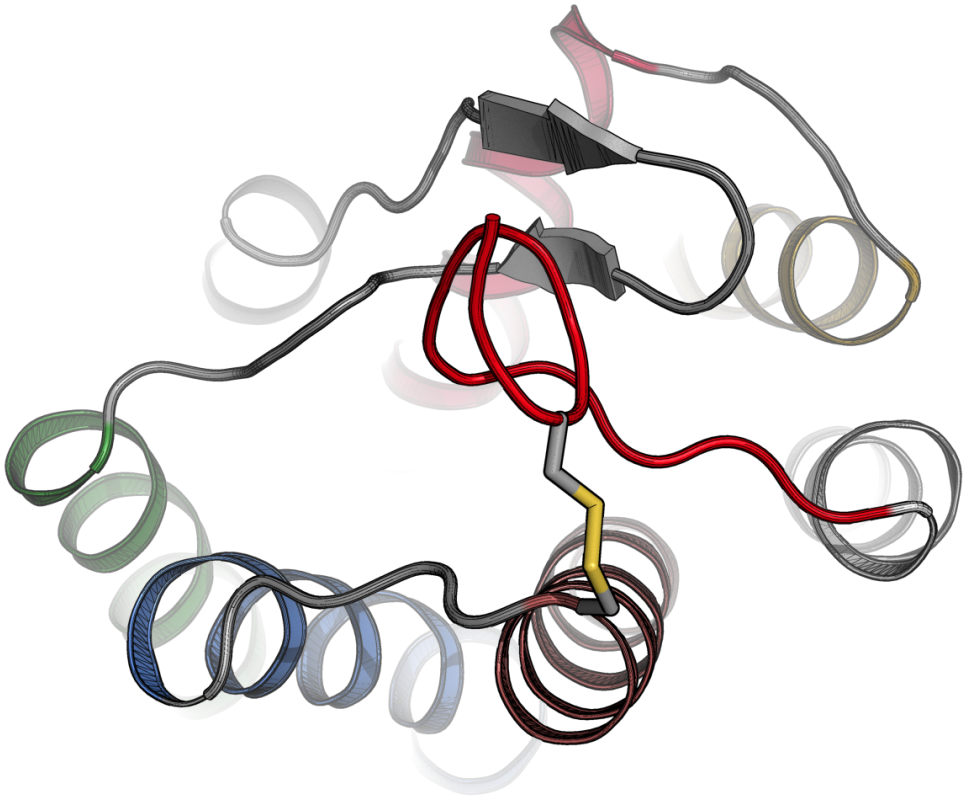

Figure 5.16 Receptor homology model of human GPR35 based on PAR1 with 'ECL4' depicted The N-terminal region of human GPR35 (red) shown in association with ECL3 through the formation of a disulphide bond. ECL2 is shown in grey as a β-hairpin loop. Image generated by Dr. Gianluigi Caltabiano.

rat binding pockets may be distinct, with Y3.32 forming critical structural and functional contacts at human GPR35.

The topological residue at 7.43 is implicated in the binding of both agonist and antagonist compounds of class A GPCRs, suggesting that it plays a role in the transition toward the active state (Rezmann-Vitti et al., 2006; Doré et al., 2011; Xu et al., 2011; Deupi and Standfuss 2011). At rat GPR35 the mutation D7.33A led to a significant increase in basal β-arrestin-2 interaction, indicative of constitutive activity (**Fig 5.12B**). This suggests that the role of D7.43 and the residues required to hold GPR35 in an inactive position differ between species, or simply that the BRET-based β-arrestin-2 assay is not suitable for assessment of constitutive activity at human GPR35 since the equivalent D7.43A mutation at human did not lead to constitutive β-arrestin-2 recruitment in the BRET assay (**Fig 5.12A**). Mutation of D7.43A also affected ligand binding, which completely ablated all responses at the human orthologue without affecting cell surface delivery. Most interestingly, at rat GPR35, compound 1 displayed a 2.6 log increase in potency (an EC_{50} of 7.2 μM at wild type to 1.9 nM at D7.43A) and a 67 % gain in efficacy (E_{max} 42 % at wild type, 109 % at D7.43A) to record a response that was now akin to that generated at human GPR35 (EC_{50} 2.8 nM, E_{max} 100 %) (**Fig 5.11**; **Table 5.8**). Interestingly, the GPR35 ligands containing a protonated nitrogen residue – compound 1, zaprinast, doxantrazole, and pemirolast – all displayed significant increases in potency upon the loss of D7.43 (Mackenzie et al., 2014), suggesting that this residue limited potency and/or efficacy at rat GPR35.

5.3.5 *Conclusions*

In order to progress the understanding of the physiological role of GPR35, ligands that display similar binding and signal transduction properties at human and rodent orthologues are necessary. This study aimed to progress toward a better understanding of the species differences that exist between human and rat GPR35 by employing mutagenesis efforts to determine residues important for each of human-selectivity, rodent-selectivity and equipotency. Specifically, arginine residues expressed in the human receptor (R^{164}, R6.58 and R7.32) were found to be necessary for human selective and equipotent ligand-induced β-arrestin-2 recruitment. Addition of these arginine residues, moreover, increased the potency of human-selective ligands at the rat receptor, suggesting that the lack of

expression of R6.58 and R7.32 in the rat orthologue contributes to species selectivity. This study led to the first molecular characterisation of ligand binding at GPR35 and, in conjunction with receptor homology efforts based on the crystal structure of the PAR1 receptor, indicated that while both human and rat GPR35 coordinate ligand binding using R3.36, R4.60, D7.43 and Y3.32 at the base of the ligand binding pocket, at the top the binding pocket human GPR35 relies on R^{164}, R6.58 and R7.32, while rat GPR35 utilises R4.62. It will be of interest now to determine whether 'ECL4' is involved in ligand binding at GPR35 and what effect mutation of this region may have on the potency and efficacy of GPR35 ligand responses. Verification of CXCL17 as an endogenous ligand of GPR35 will offer the opportunity to further investigate ligand binding at GPR35, with particular focus on negatively charged residues in the N-terminal and extracellular loops of the receptor. Since peptide ligands tend to bind to the extracellular surface of the GPCR, verification of CXCL17 as an endogenous ligand of GPR35 could indicate that the small molecule binding site of GPR35 is in fact an allosteric, rather than orthosteric, binding site. Investigation of GPR35 signalling in the presence of CXCL17 and whether small molecule agonists act as positive or negative modulators of this response would also be an interesting avenue of research to pursue.

Chapter Six

Final Discussion

6.1 General comments, findings, and future perspectives

GPR35 is an class A orphan G protein-coupled receptor that has attracted interest as a potential therapeutic target based on its expression profile and genetic associations with diseases including heart disease, inflammatory bowel disease and primary sclerosing cholangitis, in addition to physiological ligand/receptor association studies that have linked GPR35 to antinociception and anti-inflammatory disease states (Mackenzie et al., 2011). However, the basic physiological function of GPR35 has remained poorly characterised, sixteen years after the initial discovery of GPR35 as a GPCR (O' Dowd et al., 1998). This is mainly a result of a lack of consensus on the endogenous ligand, as many of the putative ligands either act with potency that is unlikely to be achieved under normal physiological conditions, and/or act with prominent effects at other biological targets (**Table 1.2**). Because of this, a number of large-scale high-throughput screening efforts were carried out by both the academic and industrial sectors, and have yielded a large array of chemically diverse small molecule agonists of GPR35 (**Table 1.3**; **Table 1.4**). One of the major issues surrounding the characterisation of GPR35 *in vivo* has been a result of the marked profiles of species selectivity displayed by the majority of GPR35 ligands, many of which also act with prominent off-target effects that are associated with their biological function. To this end, this project was successful in that it discovered the only highly potent agonist molecules of human and rat GPR35, which can now feasibly be employed to translate human *in vitro* research efforts into rodent *in vivo* disease models.

To begin this research effort, I initially assessed a number of *in vitro* pharmacological test systems to identify a format that would be suitable for drug discovery efforts at GPR35 (**Chapter Three**). From this, I found a number of assay formats that would be suitable for ligand characterisation including the [^{35}S]GTPγS with immunoprecipitation assay for assessment of full-length Gα_{13} responses emanating from GPR35; the IP-One assay with chimeric Gα_q subunits that routed GPR35 responses through the IP_3 pathway; a high-content imaging platform using ArrayScan™ technology that monitored C-terminally eYFP-tagged receptor construct internalisation; and the label-free DMR platform that monitored receptor activation in cell lines endogenously expressing *GPR35*. Of the assay platforms assessed, the BRET-based β-arrestin-2 recruitment was found to be the most suited for drug-screening efforts at GPR35 as a result of the robustness, low-cost, and throughput achievable with this

technology. For this reason initial screening efforts were carried out using the BRET-based β-arrestin-2 recruitment assay, followed by the IP-One assay for assessment of G protein responses, and the DMR format to ensure responses correlated with those generated in cells endogenously-expressing *GPR35* (**Chapter Four**).

In the process of characterising assay outputs for assessment of GPR35 function I found that the GPR35 antagonists ML-145 and CID2745687 acted as inverse agonists in systems displaying constitutive activity, and that the interaction between β-arrestin-1 or β-arrestin-2 and GPR35 was short-lived rather than sustained. Future research efforts may wish to determine whether GPR35 is constitutively active in endogenously expressing cell lines, which could be assessed by application of the inverse agonists CID2745687 or ML-145 and monitoring responses using DMR technology. If GPR35 is found to be constitutively active under native physiological conditions, it may be pertinent to question whether the endogenous ligand of GPR35 may in fact be an inverse agonist rather than agonists such as kynurenic acid or LPA. Assessment of inverse agonism has previously not been possible using the standard screening format, the BRET-based β-arrestin-2 recruitment assay, as human GPR35 is not constitutively active in this system.

From my drug discovery effort carried out in conjunction with MRCT (**Chapter Four**), I identified and reported five chemically distinct and novel agonists of GPR35 that acted with different profiles of species selectivity. Of these, compound 1 became the most potent agonist reported for human GPR35 at that time (Neetoo-Isseljee et al., 2013), and was found to display unusual species selective pathway bias, preferentially interacting with β-arrestin-2 at human GPR35, but with $G\alpha_{q13}$ at rat and mouse. This raises the interesting question as to whether the human and rodent orthologues of GPR35 couple endogenously through the same pathways or whether compound 1 uniquely biases the receptor between different pathways. Ligand-induced pathway bias has yet to be comprehensively assessed at GPR35, mainly because the involvement of particular pathways emanating from this receptor and their subsequent physiological profiles remain to be clarified. However, from a pharmacological perspective, it would be of interest to use some of the ligands identified herein to perform an across-pathway assessment of their function and assess any potential pathway bias that may emanate from these responses. As yet no GPR35 ligand has been found that is completely biased for one pathway over another, but with the recent suggestion that the chemokine CXCL17 activates GPR35 to mobilise intracellular calcium, it

may be that the ligands identified through their ability to recruit β-arrestin-2 towards GPR35 act in a manner distinct from those able to induce calcium mobilisation.

The majority of GPR35 agonists identified from the compound library screen displayed marked human selectivity, and it was determined that mostly all of these ligands – although chemically diverse – contained a carboxylic acid group. For this reason GPR35 appears to be activated promiscuously by a wide-variety of ligands, many of which act with low potency. These have actually complicated understanding of GPR35 receptor biology since GPR35 is not likely to be the primary target of many of these ligands *in vivo*. By examination of the previously associated functions of the large number of ligands reported as agonists of GPR35, I began to question whether mast cell stabilisers were generally mediating function through activation of GPR35. To extend this, a number of mast cell stabilising compounds were assessed, including amlexanox, bufrolin, cromolyn, doxantrazole, lodoxamide, and pemirolast, tranilast, ketotifen fumarate, and the mast cell activator compound 48/80. Interestingly, only a subset of mast cell stabilisers was found to activate GPR35. This raises a number of intriguing questions for future research efforts, including those that focus on the basic biological profile of GPR35 in the context of the mast cell. Is the mechanism by which GPR35-active ligands prevent degranulation one that is associated with GPR35 or are these ligands all acting at distinct biological targets to carry out this function? In this context, it would be of interest to probe the role of mast cell activation and leukocyte adhesion in *GPR35* knockout mice, and to determine if there are any abnormalities arising in the immune system of these animals that could be subsequently associated with the lack of expression of *GPR35.*

The identification of two highly potent agonists – lodoxamide and bufrolin – of human and rat GPR35 as described herein was an important milestone for GPR35 research (Mackenzie et al., 2014). Identification of these ligands enabled the first detailed study of the receptor-binding pocket of GPR35 to be carried out, in which responses produced by ligands that acted with marked profiles of species selectivity between human and rat GPR35 were compared with the newly discovered species equipotent ligands at various receptor mutants (**Chapter Five**). My study of GPR35 species selectivity and ligand binding identified residues that are responsible for differences between species orthologues as a result of reciprocally mutating key arginine residues thought to be involved in ligand binding. These results may therefore be different to those that may arise from mutating the same residues

to alanine, due to the size and charge differences between these molecules, but should theoretically be more informative of the differences between the ligand binding pockets of the human and rat orthologues. Since the 'species swap' mutants were only assessed for their ability to recruit β-arrestin-2 to GPR35, it may be pertinent to now move towards assessment of these mutants with the newly reported GPR35 radiolabelled agonist PSB-13253 (Funke et al., 2013; Thimm et al., 2013), to determine if these mutations are affecting affinity of the ligand at the receptor, or simply the ability of the receptor to recruit β-arrestin-2. In the case of the latter, therefore, it could be worth probing the same mutants and their responses in the IP-One or $G\alpha_{13}$ [^{35}S]GTPγS systems to determine their effects on G protein recruitment. This may provide a more thorough understanding of the molecular links between ligand binding and distinct pathway signalling, which will help in assessing the physiological function and signalling pathways of GPR35.

Finally, the most pressing issue that requires attention with regards to future research efforts at GPR35 is the identification of antagonist molecules that block responses arising from the rodent receptors. This is particularly important since the majority of physiological function-based studies surrounding GPR35 have been carried out in rats or mice, with these studies using shRNA, RNAi, or actually applying the human-specific antagonist compounds to these systems to infer a function for GPR35. It is possible that these compounds act as biased inverse agonists that can prevent activation of the rodent receptors in various G protein-mediated outputs. Finding a suitable assay to assess such responses will be key to addressing this issue, but it will be one that is quite important for the future elucidation of the function of GPR35.

References

Abdellah, Z. (2004) International Human Genome Sequencing Consortium. Finishing the euchromatic sequence of the human genome. *Nature*, 431, 931-945.

Adjobo-Hermans, M.J., Goedhart, J., van Weeren, L., Nijmeijer, S., Manders, E.M., Offermanns, S., Gadella, T.W.^{Jr} (2011) Real-time visualization of heterotrimeric G protein Gq activation in living cells. *BMC Biol.,* 9, 32.

Abelson, M.B., McLaughlin, J.T., Gomes, P.J. (2011) Antihistamines in ocular allergy: are they all created equal? *Curr. Allergy Asthma Rep.*, 11, 205-211.

Ahmed, K. (2011) Biological roles and therapeutic potential of hydroxy-carboxylic acid receptors. *Front. Endocrinol. (Lausanne)*, 2:51.

Albuquerque, E.X., Schwarcz, R. (2013) Kynurenic acid as an antagonist of α7 nicotinic acetylcholine receptors in the brain: facts and challenges. *Biochem. Pharmacol.*, 85, 1027-1032.

Alkondon, M., Pereira, E.F.R., Eisenberg, H.M., Kajii, Y., Schwarcz, R., Albuquerque, E.X. (2011) Age dependency of inhibition of a7 nicotinic receptors and tonically active Nmethyl-D-aspartate receptors by endogenously produced kynurenic acid in the brain. *J. Pharmacol. Exp. Ther.*, 337, 572-582.

Ames, R.S., Sarau, H.M., Chambers, J.K., Willette, R.N., Aiyar, N.V., Romanic, A.M., Louden, C.S., Foley, J.J., Sauermelch, C.F., Coatney, R.W., Ao, Z., Disa, J., Holmes, S.D., Stadel, J.M., Martin, J.D., Liu, W.S., Glover, G.I., Wilson, S., McNulty, D.E., Ellis, C.E., Elshourbagy, N.A., Shabon, U., Trill, J.J., Hay, D.W., Ohlstein, E.H., Bergsma, D.J., Douglas, S.A. (1999) Human urotensin-II is a potent vasoconstrictor and agonist for the orphan receptor GPR14. *Nature,* 401, 282-286.

Amori, L., Wu, H.Q., Marinozzi, M., Pellicciari, R., Guidetti, P., Schwarcz, R. (2009) Specific inhibition of kynurenate synthesis enhances extracellular dopamine levels in the rodent striatum. *Neuroscience,* 159, 196-203.

An, S., Bleu, T., Huang, W., Hallmark, O.G., Coughlin, S.R., Goetzl, E.J. (1997) Identification of cDNAs encoding two G protein-coupled receptors for lysosphingolipids. *FEBS Lett.*, 417, 279-282.

An, S., Goetzl, E.J., Lee, H. (1998) Signaling mechanisms and molecular characteristics of G protein-coupled receptors for lysophosphatidic acid and sphingosine 1-phosphate. *J. Cell. Biochem. Suppl.,* 30, 147-157.

Anborgh, P.H., Seachrist, J.L., Dale, L.B., Ferguson, S.S. (2000) Receptor/beta-arrestin complex formation and the differential trafficking and resensitization of beta2-adrenergic and angiotensin II type 1A receptors. *Mol. Endocrinol.,* 14, 2040-2053.

Arnaiz-Cot, J.J., Gonzalez, J.C., Sobrado, M., Baldelli, P., Carbone, E., Gandia, L, García, A.G., Hernández-Guijo, J.M. (2008) Allosteric modulation of alpha 7 nicotinic receptors selectively depolarizes hippocampal interneurons, enhancing spontaneous GABAergic transmission. *Eur. J. Neurosci.*, 27, 1097-1110.

Arunlakshana, O., Schild, H.O. (1959) Some quantitative uses of drug antagonists. *Br. J. Pharmacol. Chemother.,* 14, 48-58.

Baker, K.E., Bonvini, S.J., Donovan, C., Foong, R.E., Han, B., Jha, A., Shaifta, Y., Smit, M., Johnson, J.R., Moir, L.M. (2014) Novel drug targets for asthma and COPD: Lessons learned from in vitro and in vivo models. *Pulm. Pharmacol. Ther.,* 29, 181-198.

Bakker, R.A., Wieland, K., Timmerman, H., Leurs, R. (2000) Constitutive activity of the histamine H(1) receptor reveals inverse agonism of histamine H(1) receptor antagonists. *Eur. J. Pharmacol.,* 387, 5-7.

Baldi, L., Hacker, D.L., Adam, M., Wurm, F.M. (2007) Recombinant protein production by large-scale transient gene expression in mammalian cells: state of the art and future perspectives. *Biotechnol. Lett.,* 29, 677-684.

Ballesteros, J.A., Weinstein, H. (1995). Integrated methods for modeling G-protein coupled receptors. *J. Neurosci. Methods,* 25, 366-428.

Baltoumas, F.A., Theodoropoulou, M.C., Hamodrakas, S.J. (2013) Interactions of the α-subunits of heterotrimeric G-proteins with GPCRs, effectors and RGS proteins: a critical review and analysis of interacting surfaces, conformational shifts, structural diversity and electrostatic potentials. *J. Struct. Biol.*, 182, 209-218.

Baran, H., Jellinger, K., Deecke, L. (1999) Kynurenine metabolism in Alzheimer's disease. *J. Neural. Transm.*, 106, 165-181.

Barker, A., Kettle, J.G., Nowak, T., Pease, J.E. (2013) Expanding medicinal chemistry space. *Drug Discov. Today,* 18, 298-304.

Barth, M.C., Ahluwalia, N., Anderson, T.J., Hardy, G.J., Sinha, S., Alvarez-Cardona, J.A., Pruitt, I.E., Rhee, E.P., Colvin, R.A., Gerszten, R.E. (2009) Kynurenic acid triggers firm arrest of leukocytes to vascular endothelium under flow conditions. *J. Biol. Chem.,* 284, 19189-19195.

Battey, J.F., Way, J.M., Corjay, M.H., Shapira, H., Kusano, K., Harkins, R., Wu, J.M., Slattery, T., Mann, E., Feldman, R.I. (1991) Molecular cloning of the bombesin/gastrin-releasing peptide receptor from Swiss 3T3 cells. *Proc. Natl. Acad. Sci. U.S.A*, 88, 395-399.

Beal, M.F., Matson, W.R., Swartz, K.J., Gamache, P.H., Bird, E.D. (1990) Kynurenine pathway measurements in Huntington's disease striatum: evidence for reduced formation of kynurenic acid. *J. Neurochem.,* 55, 1327-1339.

Bennett, M.R. One hundred years of adrenaline: the discovery of autoreceptors. *Clin. Auton. Res.*, 9, 145-159.

Berlinguer-Palmini, R., Masi, A., Narducci, R., Cavone, L., Maratea, D., Cozzi, A., Sili, M., Moroni, F., Mannaioni, G. (2013) GPR35 activation reduces Ca^{2+} transients and contributes to the kynurenic acid-dependent reduction of synaptic activity at CA3-CA1 synapses. *PLoS ONE,* 8: e82180.

Bertin, B., Freissmuth, M., Jockers, R., Strosberg, A.D., Marullo, S. (1994) Cellular signaling by an agonist-activated receptor/Gs alpha fusion protein. *Proc. Natl. Acad. Sci. U.S.A.,* 91, 8827-8831.

Bettica, P., Nucci, G., Pyke, C., Squassante, L., Zamuner, S., Ratti, E., Gomeni, R., Alexander, R. (2012) Phase I studies on the safety, tolerability, pharmacokinetics and pharmacodynamics of SB-649868, a novel dual orexin receptor antagonist. *J. Psychopharmacol. (Oxford)*, 26, 1058-1070.

Bhattacharya, S., Hall, S.E., Li, H., Vaidehi, N. (2008) Ligand-stabilized conformational states of human

beta(2) adrenergic receptor: insight into G-protein-coupled receptor activation. *Biophys. J.*, 94, 2027-2042.

Bhattacharya, S.K., Andrews, K., Beveridge, R., Cameron, K.O., Chen, C., Dunn, M., Fernando, D., Gao, H., Hepworth, D., Jackson, V.M., Khot, V., Kong, J., Kosa, R.E., Lapham, K., Loria, P.M., Londregan, A.T., McClure, K.F., Orr, S.T., Patel, J., Rose, C., Saenz, J., Stock, I.A., Storer, G., VanVolkenburg, M., Vrieze, D., Wang, G., Xiao, J., Zhang, Y. (2014) Discovery of PF-5190457, a Potent, Selective, and Orally Bioavailable Ghrelin Receptor Inverse Agonist Clinical Candidate. *ACS Med. Chem. Lett.*, 5, 474-479.

Bissonnette, E.Y., Enciso, J.A., Befus, A.D. (1995) Inhibition of tumour necrosis factor-alpha (TNF-alpha) release from mast cells by the anti-inflammatory drugs, sodium cromoglycate and nedocromil sodium. *Clin. Exp. Immunol.,* 102, 78-84.

Bockaert, J., Pin, J.P. (1999) Molecular tinkering of G protein-coupled receptors: an evolutionary success. *EMBO J.*, 18, 1723-1729.

Bockenhauer, S., Fürstenberg, A., Yao, X.J., Kobilka, B.K., Moerner, W.E. (2011) Conformational dynamics of single G protein-coupled receptors in solution. *J. Phys. Chem. B.*, 115, 13328-13338.

Bohn, L.M., Dykstra, L.A., Lefkowitz, R.J., Caron, M.G., Barak, L.S. (2004) Relative opioid efficacy is determined by the complements of the G protein-coupled receptor desensitization machinery. *Mol. Pharmacol.,* 66, 106-112.

Bolonna, A.A., Kerwin, R.W. (2005) Partial agonism and schizophrenia. *Int. J. Neuropsychopharmacol.*, 186, 7-10.

Bonander, N., Bill, R.M. (2012) Optimising yeast as a host for recombinant protein production (review). *Methods Mol. Biol.,* 866, 1-9.

Bouvier, M. (2014) Peripheral actions of GPCRs in energy homeostasis: view from the chair. *Int. J. Obes. Suppl.*, 4, S3-S4.

Branch, A. (1939) The clinical uses of histamine. *Can. Med. Assoc. J.,* 41, 73-75.

Briscoe, C.P., Tadayyon, M., Andrews, J.L., Benson, W.G., Chambers, J.K., Eilert, M.M., Ellis, C., Elshourbagy, N.A., Goetz, A.S., Minnick, D.T., Murdock, P.R., Sauls, H.R.^{Jr}, Shabon, U., Spinage, L.D., Strum, J.C., Szekeres, P.G., Tan, K.B., Way, J.M., Ignar, D.M., Wilson, S., Muir, A.I. (2003) The orphan G protein-coupled receptor GPR40 is activated by medium and long chain fatty acids. *J. Biol. Chem.*, 278, 11303-11311.

Broughton, B.J., Chaplen, P., Knowles, P., Lunt, E., Pain, D.L., Wooldridge, K.R., Ford, R., Marshall, S., Walker, J.L., Maxwell, D.R. (1974) New inhibitor of reagin-mediated anaphylaxis. *Nature*, 251, 650-652.

Brown, A.J., Goldsworthy, S.M., Barnes, A.A., Eilert, M.M., Tcheang, L., Daniels, D., Muir, A.I., Wigglesworth, M.J., Kinghorn, I., Fraser, N.J., Pike, N.B., Strum, J.C., Steplewski, K.M., Murdock, P.R., Holder, J.C., Marshall, F.H., Szekeres, P.G., Wilson, S., Ignar, D.M., Foord, S.M., Wise, A., Dowell, S.J. (2003) The Orphan G protein-coupled receptors GPR41 and GPR43 are activated by propionate and other short chain carboxylic acids. *J. Biol. Chem.*, 278, 11312-11319.

Brown, A.J., Daniels, D.A., Kassim, M., Brown, S., Haslam, C.P., Terrell, V.R., Brown, J., Nichols, P.L., Staton, P.C., Wise, A., Dowell, S.J. (2011) Pharmacology of GPR55 in yeast and identification of GSK494581A as a mixed-activity glycine transporter subtype 1 inhibitor and GPR55 agonist. *J. Pharmacol. Exp. Ther.,* 337, 236-246.

Burris, K.D., Molski, T.F., Xu, C., Ryan, E., Tottori, K., Kikuchi, T., Yocca, F.D., Molinoff, P.B. (2002) Aripiprazole, a novel antipsychotic, is a high-affinity partial agonist at human dopamine D2 receptors. *J. Pharmacol. Exp. Ther.*, 302, 381-389.

Butcher, A.J., Hudson, B.D., Shimpukade, B., Alvarez-Curto, E., Prihandoko, R., Ulven, T., Milligan, G., Tobin, A.B. (2014) Concomitant action of structural elements and receptor phosphorylation determines arrestin-3 interaction with the free fatty acid receptor FFA4. *J. Biol. Chem.,* 289, 18451-18465.

Cabrera-Vera, T.M., Vanhauwe, J., Thomas, T.O., Medkova, M., Preininger, A., Mazzoni, M.R., Hamm, H.E. (2003) Insights into G protein structure, function, and regulation. *Endocr. Rev.,* 24, 765-781.

Calebiro, D., Nikolaev, V.O., Persani, L., Lohse, M.J. (2010) Signaling by internalized G-protein-coupled receptors. *Trends Pharmacol. Sci.,* 31, 221-228.

Carmeci, C., Thompson, D.A., Ring, H.Z., Francke, U., Weigel, R.J. (1997) Identification of a gene (GPR30) with homology to the G-protein-coupled receptor superfamily associated with estrogen receptor expression in breast cancer. *Genomics*, 45, 607-617.

Carpenedo, R., Pittaluga, A., Cozzi, A., Attucci, S., Galli, A., Raiteri, M., Moroni, F. (2001) Presynaptic kynurenate-sensitive receptors inhibit glutamate release. *Eur. J. Neurosci.*, 13, 2141-2147.

Carpenedo, R., Meli, E., Peruginelli, F., Pellegrini-Giampietro, D.E., Moroni, F. (2002) Kynurenine 3-mono-oxygenase inhibitors attenuate post-ischemic neuronal death in organotypic hippocampal slice cultures. *J. Neurochem.,* 82, 1465-1471.

Carr, I.C., Burt, A.R., Jackson, V.N., Wright, J., Wise, A., Rees, S., Milligan, G. (1998) Quantitative analysis of a cysteine351glycine mutation in the G protein Gi1alpha: effect on alpha2A-adrenoceptor-Gi1alpha fusion protein activation. *FEBS Lett.,* 428, 17-22.

Chalmers, D.T., Behan, D.P. (2002) The use of constitutively active GPCRs in drug discovery and functional genomics. *Nat. Rev. Drug Discov.,* 1, 599-608.

Chang, J.C., Leung, J., Tang, T., Holzknecht, Z.E., Hartwig, M.G., Duane Davis, R., Parker, W., Abraham, S.N., Lin, S.S. (2014) Cromolyn ameliorates acute and chronic injury in a rat lung transplant model. *J. Heart Lung Transplant.*, 33, 749-757.

Chemelli, R.M., Willie, J.T., Sinton, C.M., Elmquist, J.K., Scammell, T., Lee, C., Richardson, J.A., Williams, S.C., Xiong, Y., Kisanuki, Y., Fitch, T.E., Nakazato, M., Hammer, R.E., Saper, C.B., Yanagisawa, M. (1999) Narcolepsy in orexin knockout mice: molecular genetics of sleep regulation. *Cell*, 98, 437-451.

Cherezov, V., Rosenbaum, D.M., Hanson, M.A., Rasmussen, S.G., Thian, F.S., Kobilka, T.S., Choi, H.J., Kuhn, P., Weis, W.I., Kobilka, B.K., Stevens, R.C. (2007) High-resolution crystal structure of an engineered human beta2-adrenergic G protein-coupled receptor. *Science*, 318, 1258-1265.

Choe, H.W., Kim, Y.J., Park, J.H., Morizumi, T., Pai, E.F., Krauss, N., Hofmann, K.P., Scheerer, P., Ernst, O.P. (2011) Crystal structure of metarhodopsin II. *Nature*, 471, 651-655.

Choi, J.H., Kim, D.H., Yun, I.J., Chang, J.H., Chun, B.G., Choi, S.H. (2007) Zaprinast inhibits hydrogen peroxide-induced lysosomal destabilization and cell death in astrocytes. *Eur. J. Pharmacol.*, 571, 106-115.

Choi, Y.H., Yan, G.H. (2009) Ellagic Acid attenuates immunoglobulin E-mediated allergic response in mast cells. *Biol. Pharm. Bull.,* 32, 1118-1121.

Chopra, I.J., Chopra, U., Smith, S.R., Reza, M., Solomon, D.H. (1975) Reciprocal changes in serum concentrations of 3,3',5-triiodothyronine (T3) in systemic illnesses. *J. Clin. Endocrinol. Metab.,* 41, 1043-1439.

Christopoulos, A., Christopoulos, G., Morfis, M., Udawela, M., Laburthe, M., Couvineau, A., Kuwasako, K., Tilakaratne, N., Sexton, P.M. (2003) Novel receptor partners and function of receptor activity-modifying proteins. *J. Biol. Chem.,* 278, 3293-3297.

Citrome, L. (2009) Olanzapine pamoate: a stick in time? A review of the efficacy and safety profile of a new depot formulation of a second-generation antipsychotic. *Int. J. Clin. Pract.*, 63, 140-150.

Civelli, O., Reinscheid, R.K., Zhang, Y., Wang, Z., Fredriksson, R., Schiöth, H.B. (2013) G protein-coupled receptor deorphanizations. *Annu. Rev. Pharmacol. Toxicol.*, 53, 127-146.

Coleman, D.E., Berghuis, A.M., Lee, E., Linder, M.E., Gilman, A.G., Sprang, S.R. (1994) Structures of active conformations of Gi alpha 1 and the mechanism of GTP hydrolysis. *Science*, 265, 1405-1412.

Correll, C.C., McKittrick, B.A. (2014) Biased Ligand Modulation of Seven Transmembrane Receptors (7TMRs): Functional Implications for Drug Discovery. *J. Med. Chem.,* 57, 6887-6896.

Cosi, C., Mannaioni, G., Cozzi, A., Carlà, V., Sili, M., Cavone, L., Maratea, D., Moroni, F. (2011) G-protein coupled receptor 35 (GPR35) activation and inflammatory pain: Studies on the antinociceptive effects of kynurenic acid and zaprinast. *Neuropharmacology,* 60, 1227-1231.

Costa, T., Herz, A. (1989) Antagonists with negative intrinsic activity at delta opioid receptors coupled to GTP-binding proteins. *Proc. Natl. Acad. Sci. U.S.A.*, 86, 7321-7325.

Coughlin, S.R. (2005) Protease-activated receptors in hemostasis, thrombosis and vascular biology. *J. Thromb. Haemost*., 3, 1800-1814.

Cox, J.S.G. (1971) Disodium cromoglycate - Mode of action and its possible relevance to the clinical use of the drug. *Br. J. Dis. Chest,* 65, 189-204.

Cox, C.D., Breslin, M.J., Whitman, D.B., Schreier, J.D., McGaughey, G.B., Bogusky, M.J., Roecker, A.J., Mercer, S.P., Bednar, R.A., Lemaire, W., Bruno, J.G., Reiss, D.R., Harrell, C.M., Murphy, K.L., Garson, S.L., Doran, S.M., Prueksaritanont, T., Anderson, W.B., Tang, C., Roller, S., Cabalu, T.D., Cui, D., Hartman, G.D., Young, S.D., Koblan, K.S., Winrow, C.J., Renger, J.J., Coleman, P.J. (2010) Discovery of the dual orexin receptor antagonist [(7R)-4-(5-chloro-1,3-benzoxazol-2-yl)-7-methyl-1,4-diazepan-1-yl][5-methyl-2-(2H-1,2,3-triazol-2-yl)phenyl]methanone (MK-4305) for the treatment of insomnia. *J. Med. Chem.*, 53, 5320-5332.

Cozzi, A., Carpenedo, R., Moroni, F. (1999) Kynurenine hydroxylase inhibitors reduce ischemic brain damage: studies with (m-nitrobenzoyl)-alanine (mNBA) and 3,4-dimethoxy-[-N-4-(nitrophenyl)thiazol-2yl]-benzenesulfonamide (Ro 61-8048) in models of focal or global brain ischemia. *J. Cereb. Blood Flow Metab.*, 19, 771-777.

Croset, A., Delafosse, L., Gaudry, J.P., Arod, C., Glez, L., Losberger, C., Begue, D., Krstanovic, A., Robert, F., Vilbois, F., Chevalet, L., Antonsson, B. (2012) Differences in the glycosylation of recombinant proteins expressed in HEK and CHO cells. *J. Biotechnol.,* 161, 336-348.

Davenport, A.P., Harmar, A.J. (2013) Evolving pharmacology of orphan GPCRs: IUPHAR Commentary. *Br. J. Pharmacol.*, 170, 693-695.

Davenport, A.P., Alexander, S., Sharman, J.L., Pawson, A.J., Benson, H.E., Monaghan, A.E., Chiy Liew, W., Mpamhanga, C., Battey, J., Benya, R.V., Jensen, R.T., Karnik, S., Kostenis, E., Spindel, E., Storjohann, L., Tirupula, K., Bonner, T.I., Neubig, R., Pin, J.P., Spedding, M., Harmar, A. (2014) Class A Orphans. Last modified on 09/05/2014. Accessed on 13/07/2014. IUPHAR database (IUPHAR-DB), http://www.iuphar-db.org/DATABASE/FamilyMenuForward?familyId=16

de Lecea, L., Kilduff, T.S., Peyron, C., Gao, X., Foye, P.E., Danielson, P.E., Fukuhara, C., Battenberg, E.L., Gautvik, V.T., Bartlett, F.S. [2nd], Frankel, W.N., van den Pol, A.N., Bloom, F.E., Gautvik, K.M., Sutcliffe, J.G. (1998) The hypocretins: hypothalamus-specific peptides with neuroexcitatory activity. *Proc. Natl. Acad. Sci. U.S.A.*, 95, 322-327.

Delhanty, P.J., Huisman, M., Baldeon-Rojas, L.Y., van den Berge, I., Grefhorst, A., Abribat, T., Leenen, P.J., Themmen, A.P., van der Lely, A.J. (2013) Des-acyl ghrelin analogs prevent high-fat-diet-induced dysregulation of glucose homeostasis. *FASEB J.*, 27, 1690-1700.

Delhanty, P.J., Huisman, M., Julien, M., Mouchain, K., Brune, P., Themmen, A.P., Abribat, T., van der Lely, A.J. (2014) The acylated (AG) to unacylated (UAG) ghrelin ratio in esterase inhibitor-treated blood is higher than previously described. *Clin. Endocrinol. (Oxf.), in press.*

de Ligt, R.A., Kourounakis, A.P., IJzerman, A.P. (2000) Inverse agonism at G protein-coupled receptors: (patho)physiological relevance and implications for drug discovery. *Br. J. Pharmacol.,* 130, 1-12.

Deng, H., Fang, Y. (2012a) Anti-inflammatory gallic acid and wedelolactone are G protein-coupled receptor-35 agonists. *Pharmacology,* 89, 211-219.

Deng, H., Fang, Y. (2012b) Synthesis and Agonistic Activity at the GPR35 of 5,6-Dihydroxyindole-2-carboxylic Acid Analogues. *ACS Med. Chem. Lett.,* 3, 550-554.

Deng, H., Fang, Y. (2012c) Aspirin metabolites are GPR35 agonists. *Naunyn Schmiedebergs Arch Pharmacol.,* 385, 729-737.

Deng, H., Hu, H., Fang, Y. (2011a) Tyrphostin analogs are GPR35 agonists. *FEBS Lett.,* 585, 1957-1962.

Deng, H., Hu, H., He, M., Hu, J., Niu, W., Ferrie, A.M., Fang, Y. (2011b) Discovery of 2-(4-methylfuran-2(5H)-ylidene)malononitrile and thieno[3,2-b]thiophene-2-carboxylic acid derivatives as G protein-coupled receptor 35 (GPR35) agonists. *J. Med. Chem.,* 54, 7385-7396.

Deng, H., Fang, Y., He, M., Hu, H., Niu, W., Sun, H. (2012a) Compositions and methods for the treatment of pathological condition(s) related to GPR35 and/or GPR35-HERG complex. United States Patent Application, # 20120022116

Deng, H., Hu, H., Ling, S., Ferrie, A.M., Fang, Y. (2012b) Discovery of natural phenols as G Protein-Coupled Receptor-35 (GPR35) Agonists. *ACS Med. Chem. Lett.,* 3, 165-169.

Deng, H., Hu, H., Fang, Y. (2012c) Multiple tyrosine metabolites are GPR35 agonists. *Sci. Rep.,* 2, 373.

Deng, H., Hu, J., Hu, H., He, M., Fang, Y. (2012d) Thieno[3,2-b]thiophene-2-carboxylic acid derivatives as GPR35 agonists. *Bioorg. Med. Chem. Lett*., 22, 4148-4152.

Deng, H., Fang, Y. (2013) The Three Catecholics Benserazide, Catechol and Pyrogallol are GPR35 Agonists. *Pharmaceuticals (Basel).,* 6, 500-559.

Deupi, X., Kobilka, B.K. (2010) Energy landscapes as a tool to integrate GPCR structure, dynamics, and function. *Physiology (Bethesda),* 25, 293-303.

Deupi, X., Standfuss, J. (2011) Structural insights into agonist-induced activation of G-protein-coupled receptors. *Curr. Opin. Struct. Biol.*, 21, 541-551.

DiMasi, J.A., Feldman, L., Seckler, A., Wilson, A. (2010) Trends in risks associated with new drug development: success rates for investigational drugs. *Clin. Pharmacol. Ther.*, 87, 272-277.

DiNatale, B.C., Murray, I.A., Schroeder, J.C., Flaveny, C.A., Lahoti, T.S., Laurenzana, E.M., Omiecinski, C.J., Perdew, G.H. (2010) Kynurenic acid is a potent endogenous aryl hydrocarbon receptor ligand that synergistically induces interleukin-6 in the presence of inflammatory signaling. *Toxicol. Sci.,* 115, 89-97.

Diniz Behn, C.G., Klerman, E.B., Mochizuki, T., Lin, S.C., Scammell, T.E. (2010) Abnormal sleep/wake dynamics in orexin knockout mice. *Sleep*, 33, 297-306.

Divorty, N., Mackenzie, A.E., Nicklin, S.A., Milligan, G. (2015) G protein-coupled receptor 35: an emerging target in inflammatory and cardiovascular disease. *Front. Pharmacol.,* 6, 41.

Dixon, R.A., Kobilka, B.K., Strader, D.J., Benovic, J.L., Dohlman, H.G., Frielle, T., Bolanowski, M.A., Bennett, C.D., Rands, E., Diehl, R.E., Mumford, R.A., Slater, E.E., Sigal, I.S., Caron, M.G., Lefkowitz, R.J., Strader, C.D. (1986) Cloning of the gene and cDNA for mammalian beta-adrenergic receptor and homology with rhodopsin. *Nature*, 321, 75-79.

Doré, A.S., Robertson, N., Errey, J.C., Ng, I., Hollenstein, K., Tehan, B., Hurrell, E., Bennett, K., Congreve, M., Magnani, F., Tate, C.G., Weir, M., Marshall, F.H. (2011) Structure of the adenosine A(2A) receptor in complex with ZM241385 and the xanthines XAC and caffeine. *Structure,* 19, 1283-1293.

Dowell, S.J., Brown, A.J. (2009) Yeast assays for G protein-coupled receptors. *Methods Mol. Biol.,* 552, 213-229.

Downes, G.B., Gautam, N. (1999) The G protein subunit gene families. *Genomics,* 62, 544-552.

Drews, J., Ryser, S. (1997) The role of innovation in drug development. *Nat. Biotechnol.*, 15, 1318-1319.

Drews, J. (2000) Drug discovery: a historical perspective. *Science,* 287, 1960-1964.

Du, J., Cleghorn, W.M., Contreras, L., Lindsay, K., Rountree, A.M., Chertov, A.O., Turner, S.J., Sahaboglu, A., Linton, J., Sadilek, M., Satrústegui, J., Sweet, I.R., Paquet-Durand, F., Hurley, J.B. (2013) Inhibition of mitochondrial pyruvate transport by zaprinast causes massive accumulation of aspartate at the expense of glutamate in the retina. *J. Biol. Chem.*, 288, 36129-36140.

Eisenhauer, P.B., Lehrer, R.I. (1992) Mouse neutrophils lack defensins. *Infect. Immun.,* 60, 3446-3447.

Ejskjaer, N., Dimcevski, G., Wo, J., Hellström, P.M., Gormsen, L.C., Sarosiek, I., Søfteland, E., Nowak, T., Pezzullo, J.C., Shaughnessy, L., Kosutic, G., McCallum, R. (2010) Safety and efficacy of ghrelin agonist TZP-101 in relieving symptoms in patients with diabetic gastroparesis: a randomized, placebo-controlled study. *Neurogastroenterol. Motil.*, 22, 1069-e281.

Ellinghaus, D., Folseraas, T., Holm, K., Ellinghaus, E., Melum, E., Balschun, T., Laerdahl, J.K., Shiryaev, A., Gotthardt, D.N., Weismüller, T.J., Schramm, C., Wittig, M., Bergquist, A., Björnsson, E., Marschall, H.U., Vatn, M., Teufel, A., Rust, C., Gieger, C., Wichmann, H.E., Runz, H., Sterneck, M., Rupp, C., Braun, F., Weersma, R.K., Wijmenga, C., Ponsioen, C.Y., Mathew, C.G., Rutgeerts, P., Vermeire, S., Schrumpf, E., Hov, J.R., Manns, M.P., Boberg, K.M., Schreiber, S., Franke, A., Karlsen, T.H. (2013) Genome-wide association analysis in primary sclerosing cholangitis and ulcerative colitis identifies risk loci at GPR35 and TCF4. *Hepatology*, 58, 1074-1083.

Erhardt, S., Blennow, K., Nordin, C., Skogh, E., Lindstrom, L.H., Engberg, G. (2001) Kynurenic acid levels are elevated in the cerebrospinal fluid of patients with schizophrenia. *Neurosci. Lett.*, 313, 96-98.

Erickson, J.R., Wu, J.J., Goddard, J.G., Tigyi, G., Kawanishi, K., Tomei, L.D., Kiefer, M.C. (1998) Edg-2/Vzg-1 couples to the yeast pheromone response pathway selectively in response to lysophosphatidic acid. *J. Biol. Chem.*, 273, 1506-1510.

Fallarini, S., Magliulo, L., Paoletti, T., de Lalla, C., Lombardi, G. (2010) Expression of functional GPR35 in human iNKT cells. *Biochem. Biophys. Res. Commun.,* 398, 420-425.

Fang, Y., Li, G., Ferrie, A.M. (2007) Non-invasive optical biosensor for assaying endogenous G protein-coupled receptors in adherent cells. *J. Pharmacol. Toxicol. Methods*, 55, 314-322.

Feng, Y., Zhu, Z., Chen, W., Prabakaran, P., Lin, K., Dimitrov, D.S., (2014) Conjugates of Small Molecule Drugs with Antibodies and Other Proteins. *Biomedicines*, 2, 1-13.

Filardo, E.J., Quinn, J.A., Bland, K.I., Frackelton, A.R.^{Jr} (2000) Estrogen-induced activation of Erk-1 and Erk-2 requires the G protein-coupled receptor homolog, GPR30, and occurs via trans-activation of the epidermal growth factor receptor through release of HB-EGF. *Mol. Endocrinol*., 14, 1649-1660.

Forrest, C.M., Youd, P., Kennedy, A., Gould, S.R., Darlington, L.G., Stone, T.W. (2002) Purine, kynurenine, neopterin and lipid peroxidation levels in inflammatory bowel disease. *Biomed. Sci.,* 9, 436-442.

Forrest, C.M., Gould, S.R., Darlington, L.G., Stone, T.W. (2003) Levels of purine, kynurenine and lipid peroxidation products in patients with inflammatory bowel disease. *Adv. Exp. Med. Biol.*, 527, 395-400.

Fredriksson, R., Lagerström, M.C., Lundin, L.G., Schiöth, H.B. (2003) The G-protein-coupled receptors in the human genome form five main families. Phylogenetic analysis, paralogon groups, and fingerprints. *Mol. Pharmacol.*, 63, 1256-1272.

Fredriksson R., Schioth, H.B. 2005. The Repertoire of G-Protein–Coupled Receptors in Fully Sequenced Genomes. *Mol. Pharmacol.,* 67, 1414-1425.

Friberg, L., Werner, S., Eggertsen, G., Ahnve, S. (2002) Rapid down-regulation of thyroid hormones in acute myocardial infarction: is it cardioprotective in patients with angina? *Arch. Intern. Med*., 162, 1388-1394.

Fujitsuka, N., Asakawa, A., Uezono, Y., Minami, K., Yamaguchi, T., Niijima, A., Yada, T., Maejima, Y., Sedbazar, U., Sakai, T., Hattori, T., Kase, Y., Inui, A. (2011) Potentiation of ghrelin signaling attenuates cancer anorexia-cachexia and prolongs survival. *Transl. Psychiatry*, 1:e23.

Funke, M., Thimm, D., Schiedel, A.C., Müller, C.E. (2013) 8-Benzamidochromen-4-one-2-carboxylic acids: potent and selective agonists for the orphan G protein-coupled receptor GPR35. *J. Med. Chem.,* 56, 5182-5197.

Garcia-Dorado, D., Agulló, L., Sartorio, C.L., Ruiz-Meana, M. (2009) Myocardial protection against reperfusion injury: the cGMP pathway. *Thromb. Haemost.,* 101, 635-642.

Garland, S.L. (2013) Are GPCRs still a source of new targets? *J. Biomol. Screen.,* 18, 947-966.

Gashaw, I., Ellinghaus, P., Sommer, A., Asadullah, K. (2011) What makes a good drug target? *Drug Discov. Today*, 17, S24-S30.

Gibson, A. (2001) Phosphodiesterase 5 inhibitors and nitrergic transmission-from zaprinast to sildenafil. *Eur. J. Pharmacol.*, 411, 1-10.

Golden, J.B. (2003) Prioritizing the human genome: knowledge management for drug discovery. *Curr. Opin. Drug Discov. Devel.,* 6, 310-316.

Gotoh, M., Fujiwara, Y., Yue, J., Liu, J., Lee, S., Fells, J., Uchiyama, A., Murakami-Murofushi, K., Kennel, S., Wall, J., Patil, R., Gupte, R., Balazs, L., Miller, D.D., Tigyi, G.J. (2012) Controlling cancer through the autotaxin-lysophosphatidic acid receptor axis. *Biochem. Soc. Trans.*, 40, 31-36.

Greene, S.J., Gheorghiade, M., Borlaug, B.A., Pieske, B., Vaduganathan, M., Burnett, J.C.^{Jr}, Roessig, L., Stasch, J.P., Solomon, S.D., Paulus, W.J., Butler, J. (2013) The cGMP signaling pathway as a therapeutic target in heart failure with preserved ejection fraction. *J. Am. Heart Assoc*., 2:e000536.

Grilli, M., Raiteri, L., Patti, L., Parodi, M., Robino, F., Raiteri, M., Marchi, M. (2006) Modulation of the function of presynaptic a7 and non-a7 nicotinic receptors by the tryptophan metabolites, 5-hydroxyindole and kynurenate in mouse brain. *Br. J. Pharmacol.*, 149, 724-732.

Groer, C.E., Tidgewell, K., Moyer, R.A., Harding, W.W., Rothman, R.B., Prisinzano, T.E., Bohn, L.M. (2007) An opioid agonist that does not induce mu-opioid receptor--arrestin interactions or receptor internalization. *Mol. Pharmacol.,* 71, 549-557.

Guan, X.M., Metzger, J.M., Yang, L., Raustad, K.A., Wang, S.P., Spann, S.K., Kosinski, J.A., Yu, H., Shearman, L.P., Faidley, T.D., Palyha, O., Kan, Y., Kelly, T.M., Sebhat, I., Lin, L.S., Dragovic, J., Lyons, K.A., Craw, S., Nargund, R.P., Marsh, D.J., Strack, A.M., Reitman, M.L. (2011) Antiobesity effect of MK-

5046, a novel bombesin receptor subtype-3 agonist. *J. Pharmacol. Exp. Ther.*, 336, 356-364.

Guo, J., Williams, D.J., Puhl III, H.L., Ikeda, S.R. (2008) Inhibition of N-Type Calcium Channels by Activation of GPR35, an Orphan Receptor, Heterologously Expressed in Rat Sympathetic Neurons. *J. Pharmacol. Exp. Ther.,* 324, 352-351.

Guo, Y., Zhang, W., Giroux, C., Cai, Y., Ekambaram, P., Dilly, A.K., Hsu, A., Zhou, S., Maddipati, K.R., Liu, J., Joshi, S., Tucker, S.C., Lee, M.J., Honn, K.V. (2011) Identification of the orphan G protein-coupled receptor GPR31 as a receptor for 12-(S)-hydroxyeicosatetraenoic acid. *J. Biol. Chem*., 286, 33832-33840.

Gutiérrez-de-Terán, H., Massink, A., Rodríguez, D., Liu, W., Han, G.W., Joseph, J.S., Katritch, I., Heitman, L.H., Xia, L., Ijzerman, A.P., Cherezov, V., Katritch, V., Stevens, R.C. (2013) The role of a sodium ion binding site in the allosteric modulation of the A(2A) adenosine G protein-coupled receptor. *Structure*, 21, 2175-2185.

Haddad, J.J., Land, S.C., Tarnow-Mordi, W.O., Zembala, M., Kowalczyk, D., Lauterbach, R. (2002) Immunopharmacological potential of selective phosphodiesterase inhibition. I. Differential regulation of lipopolysaccharide-mediated proinflammatory cytokine (interleukin-6 and tumor necrosis factor-alpha) biosynthesis in alveolar epithelial cells. *J Pharmacol Exp Ther*., 300, 559-566.

Hall, D.A., Strange, P.G. (1997) Evidence that antipsychotic drugs are inverse agonists at D2 dopamine receptors. *Br. J. Pharmacol.*, 121, 731-736.

Hall, J.L., O'Connell, T.D., Francis, G.S. (2014) Promising Small Molecule for Heart Failure Targeting Adrenal Catecholamine Release and β-Adrenergic Receptor Signaling in the Heart. *J. Am. Coll. Cardiol.*, 63, 2558-2559.

Hamilton, M.A., Stevenson, L.W., Luu, M., Walden, J.A. (1990) Altered thyroid hormone metabolism in advanced heart failure. *J. Am. Coll. Cardiol*., 16, 91-95.

Hamm, H.E. (1998) The many faces of G protein signaling. *J. Biol. Chem.*, 273, 669-672.

Hancock, A.A. (2006) The challenge of drug discovery of a GPCR target: analysis of preclinical pharmacology of histamine H3 antagonists/inverse agonists. *Biochem. Pharmacol.*, 71, 1103-1113.

Hansen, A.M., Ball, H.J., Mitchell, A.J., Miu, J., Takikawa, O., Hunt, N.H. (2004) Increased expression of indoleamine 2,3-dioxygenase in murine malaria infection is predominantly localised to the vascular endothelium. *Int. J. Parasitol*., 34, 1309-1319.

Hanyaloglu, A.C., von Zastrow, M. (2008) Regulation of GPCRs by endocytic membrane trafficking and its potential implications*. Annu. Rev. Pharmacol. Toxicol.,* 48, 537-568.

Hazan, C., Boudsocq, F., Gervais, V., Saurel, O., Ciais, M., Cazaux, C., Czaplicki, J., Milon, A. (2008) Structural insights on the pamoic acid and the 8 kDa domain of DNA polymerase beta complex: Towards the design of higher-affinity inhibitors. *BMC Struct. Biol.*, 8, 22-34.

He, W., Miao, F.J., Lin, D.C., Schwandner, R.T., Wang, Z., Gao, J., Chen, J.L., Tian, H., Ling, L. (2004) Citric acid cycle intermediates as ligands for orphan G-protein-coupled receptors. *Nature,* 429, 188-193.

Henderson, G., McKnight, A.T. (1997) The orphan opioid receptor and its endogenous ligand--nociceptin/orphanin FQ. *Trends Pharmacol. Sci.*, 18, 293-300.

Herrick-Davis, K., Grinde, E., Teitler, M. (2000) Inverse agonist activity of atypical antipsychotic drugs at human 5-hydroxytryptamine2C receptors. *J. Pharmacol. Exp. Ther.*, 295, 226-232.

Hewavitharana, T., Wedegaertner, P.B. (2012) Non-canonical signaling and localizations of heterotrimeric G proteins. *Cell. Signal.*, 24, 25-34.

Heynen-Genel, S., Dahl, R., Shi, S., Sauer, M., Hariharan, S., Sergienko, E., Dad, S., Chung, T.D.Y., Stonich, D., Su, Y., Caron, M.G., Zhao, P., Abood, M.E., Barak, L.S. (2010) Antagonists for the Orphan Receptor GPR35. Sanford-Burnham Centre for Chemical Genomics – Probe Report 1 & 2

Heynen-Genel, S., Dahl, R., Shi, S., Sauer, M., Hariharan, S., Sergienko, E., Dad, S., Chung, T.D.Y., Stonich, D., Su, Y., Zhao, P., Caron, M.G., Abood, M.E., Barak. L.S (2011) Antagonists for the Orphan Receptor GPR35. Sanford-Burnham Centre for Chemical Genomics – Probe Report 3.

Hilmas, C., Pereira, E.F., Alkondon, M., Rassoulpour, A., Schwarcz, R., Albuquerque, E.X. (2001) The brain metabolite kynurenic acid inhibits alpha7 nicotinic receptor activity and increases non-alpha7 nicotinic receptor expression: physiopathological implications. *J. Neurosci.,* 21, 7463-7473.

Hinkle, P.M., Gehret, A.U., Jones, B.W. (2012) Desensitization, trafficking, and resensitization of the pituitary thyrotropin-releasing hormone receptor. *Front. Neurosci.,* 6, 180.

Hirasawa, A., Tsumaya, K., Awaji, T., Katsuma, S., Adachi, T., Yamada, M., Sugimoto, Y., Miyazaki, S., Tsujimoto, G. (2005) Free fatty acids regulate gut incretin glucagon-like peptide-1 secretion through GPR120. *Nat. Med.*, 11, 90-94.

Holst, B., Cygankiewicz, A., Jensen, T.H., Ankersen, M., Schwartz, T.W. (2003) High constitutive signaling of the ghrelin receptor--identification of a potent inverse agonist. *Mol. Endocrinol.*, 17, 2201-2210.

Holst, B., Egerod, K.L., Schild, E., Vickers, S.P., Cheetham, S., Gerlach, L.O., Storjohann, L., Stidsen, C.E., Jones, R., Beck-Sickinger, A.G., Schwartz, T.W. (2007) GPR39 signaling is stimulated by zinc ions but not by obestatin. *Endocrinology*, 148, 13-20.

Holtze, M., Asp, L., Schwieler, L., Engberg, G., Karlsson, H. (2008) Induction of the kynurenine pathway by neurotropic influenza A virus infection. *J. Neurosci. Res.*, 86, 3674-3683.

Hopkins, A.L., Groom, C.R. (2002) The druggable genome. *Nat. Rev. Drug Discov.*, 1, 727-730.

Horikawa, Y., Oda, N., Cox, N.J., Li, X., Orho-Melander, M., Hara, M., Hinokio, Y., Lindner, T.H., Mashima, H., Schwarz, P.E., del Bosque-Plata, L., Horikawa, Y., Oda, Y., Yoshiuchi, I., Colilla, S., Polonsky, K.S., Wei, S., Concannon, P., Iwasaki, N., Schulze, J., Baier, L.J., Bogardus, C., Groop, L., Boerwinkle, E., Hanis, C.L., Bell, G.I. (2000) Genetic variation in the gene encoding calpain-10 is associated with type 2 diabetes mellitus. *Nat. Genet.*, 26, 163-175.

Hosoi, T., Sugikawa, E., Chikada, A., Koguchi, Y., Ohnuki, T. (2005) TG1019/OXE, a Galpha(i/o)-protein-coupled receptor, mediates 5-oxo-eicosatetraenoic acid-induced chemotaxis. *Biochem. Biophys. Res. Commun.*, 334, 987-995.

Hough, L.B. Genomics meets histamine receptors: new subtypes, new receptors. *Mol. Pharmacol.,* 59, 415-419.

Hoveyda, H.R., Marsault, E., Gagnon, R., Mathieu, A.P., Vézina, M., Landry, A., Wang, Z., Benakli, K., Beaubien, S., Saint-Louis, C., Brassard, M., Pinault, J.F., Ouellet, L., Bhat, S., Ramaseshan, M., Peng, X., Foucher, L., Beauchemin, S., Bhérer, P., Veber, D.F., Peterson, M.L., Fraser, G.L. (2011) Optimization of the potency and pharmacokinetic properties of a macrocyclic ghrelin receptor agonist (Part I): Development of ulimorelin (TZP-101) from hit to clinic. *J. Med. Chem.*, 54, 8305-8320.

Hu, H., Deng, H., Fang, Y. (2012) Label-free phenotypic profiling identified D-luciferin as a GPR35 agonist. *PLoS ONE,* 7: e34934.

Hu, H.Y., Horton, J.K., Gryk, M.R., Prasad, R., Naron, J.M., Sun, D.A., Hecht, S.M., Wilson, S.H., Mullen, G.P. (2004) Identification of small molecule synthetic inhibitors of DNA polymerase beta by NMR chemical shift mapping. *J. Biol. Chem.*, 279, 39736-39744.

Hudson, B.D., Tikhonova, I.G., Pandey, S.K., Ulven, T., Milligan, G. (2012a) Extracellular ionic locks determine variation in constitutive activity and ligand potency between species orthologs of the free fatty acid receptors FFA2 and FFA3. *J. Biol. Chem.*, 287, 41195-41209.

Hudson, B.D., Christiansen, E., Tikhonova, I.G., Grundmann, M., Kostenis, E., Adams, D.R., Ulven, T., Milligan, G. (2012b) Chemically engineering ligand selectivity at the free fatty acid receptor 2 based on pharmacological variation between species orthologs. *FASEB J.,* 26, 4951-4965.

Hudson, B.D., Due-Hansen, M.E., Christiansen, E., Hansen, A.M., Mackenzie, A.E., Murdoch, H., Pandey, S.K., Ward, R.J., Marquez, R., Tikhonova, I.G., Ulven, T., Milligan, G. (2013a) Defining the molecular basis for the first potent and selective orthosteric agonists of the FFA2 free fatty acid receptor. *J. Biol. Chem.*, 288, 17296-17312.

Hudson, B.D., Murdoch, H., Milligan, G. (2013b) The effects of species ortholog and SNP variation on receptors for free fatty acids. *Mol. Endocrinol.*, 27, 1177-1187.

Hudson, B.D., Shimpukade, B., Mackenzie, A.E., Butcher, A.J., Pediani, J.D., Christiansen, E., Heathcote, H., Tobin, A.B., Ulven, T., Milligan, G. (2013c) The pharmacology of TUG-891, a potent and selective agonist of the free fatty acid receptor 4 (FFA4/GPR120), demonstrates both potential opportunity and possible challenges to therapeutic agonism. *Mol. Pharmacol.*, 84, 710-725.

Hudson, B.D., Christiansen, E., Murdoch, H., Jenkins, L., Hansen, A.H., Madsen, O., Ulven, T., Milligan G. (2014) Complex pharmacology of novel allosteric free fatty acid 3 receptor ligands. *Mol. Pharmacol.,* 86, 200-210.

Hüfner, M., Grussendorf, M., Knöpfle, M. (1978) Plasma levels of 3,3', 5'-T3 (reverse-T3) under various functional thyroid conditions. *Acta Biol. Med. Ger.,* 37, 447-452.

Hughes, J.P., Rees, S., Kalindjian, S.B., Philpott, K.L. (2011) Principles of early drug discovery. *Br. J. Pharmacol.*, 162, 1239-1249.

Hulme, E.C. (2013) GPCR activation: a mutagenic spotlight on crystal structures. *Trends Pharmacol. Sci.*, 34, 67-84.

Iervasi, G., Pingitore, A., Landi, P., Raciti, M., Ripoli, A., Scarlattini, M., L'Abbate, A., Donato, L. (2003) Low-T3 syndrome: a strong prognostic predictor of death in patients with heart disease. *Circulation*, 107, 708-713.

Igel, P., Dove, S., Buschauer, A. (2010) Histamine H4 receptor agonists. *Bioorg. Med. Chem. Lett.*, 20, 7191-7199.

Iiri, T., Farfel, Z., Bourne, H.R. (1998) G-protein diseases furnish a model for the turn-on switch. *Nature*, 394, 35-38.

Im, D.S., Heise, C.E., Harding, M.A., George, S.R., O'Dowd, B.F., Theodorescu, D., Lynch, K.R. (2000) Molecular cloning and characterization of a lysophosphatidic acid receptor, Edg-7, expressed in prostate. *Mol Pharmacol.,* 57, 753-759.

Im, D.S. (2002) Orphan G protein-coupled receptors and beyond. *Jpn. J. Pharmacol.*, 90, 101-106.

Imielinski, M., Baldassano, R.N., Griffiths, A., Russell, R.K., Annese, V., Dubinsky, M., Kugathasan, S., Bradfield, J.P., Walters, T.D., Sleiman, P., Kim, C.E., Muise, A., Wang, K., Glessner, J.T., Saeed, S., Zhang, H., Frackelton, E.C. et al. (2009) Common variants at five new loci associated with early-onset inflammatory bowel disease. *Nat. Genet*., 41, 1335-1340.

Imming, P., Sinning, C., Meyer, A. (2006) Drugs, their targets and the nature and number of drug targets. *Nat. Rev. Drug Discov.,* 5, 821-834.

Irie, K., Fujii, E., Ishida, H., Wada, K., Suganuma, T., Nishikori, T., Yoshioka, T., Muraki, T. (2001) Inhibitory effects of cyclic AMP elevating agents on lipopolysaccharide (LPS)-induced microvascular permeability change in mouse skin. *Br. J. Pharmacol.*, 133, 237-242.

Itoh, Y., Kawamata, Y., Harada, M., Kobayashi, M., Fujii, R., Fukusumi, S., Ogi, K., Hosoya, M., Tanaka, Y., Uejima, H., Tanaka, H., Maruyama, M., Satoh, R., Okubo, S., Kizawa, H., Komatsu, H., Matsumura, F., Noguchi, Y., Shinohara, T., Hinuma, S., Fujisawa, Y., Fujino, M. (2003) Free fatty acids regulate insulin secretion from pancreatic beta cells through GPR40. *Nature,* 422, 173-176.

Jenkins, L., Brea, J., Smith, N.J., Hudson, B.D., Reilly, G., Bryant, N.J., Castro, M., Loza, M.I., Milligan, G. (2010) Identification of novel species-selective agonists of the G-protein-coupled receptor GPR35 that promote recruitment of β-arrestin-2 and activate Gα13. *Biochem. J.,* 432, 451-459.

Jenkins, L., Alvarez-Curto, E., Campbell, K., de Munnik, S., Canals, M., Schlyer, S., Milligan, G. (2011) Agonist activation of the G protein-coupled receptor GPR35 involves transmembrane domain III and is transduced via $G\alpha_{13}$ and β-arrestin-2. *Br. J. Pharmacol.,* 162, 733-748.

Jenkins, L., Harries, N., Lappin, J.E., MacKenzie, A.E., Neetoo-Isseljee, Z., Southern, C., McIver, E.G., Nicklin, S.A., Taylor, D.L., Milligan, G. (2012) Antagonists of GPR35 display high species ortholog selectivity and varying modes of action. *J. Pharmacol. Exp. Ther.,* 343, 683-695.

Jensen, B.C., O'Connell, T.D., Simpson, P.C. (2014) Alpha-1-adrenergic receptors in heart failure: the adaptive arm of the cardiac response to chronic catecholamine stimulation. *J. Cardiovasc. Pharmacol.*, 63, 291-301.

Jones, C.E., Holden, S., Tenaillon, L., Bhatia, U., Seuwen, K., Tranter, P., Turner, J., Kettle, R., Bouhelal, R., Charlton, S., Nirmala, N.R., Jarai, G., Finan, P. (2003) Expression and characterization of a 5-oxo-6E,8Z,11Z,14Z-eicosatetraenoic acid receptor highly expressed on human eosinophils and

neutrophils. *Mol. Pharmacol.,* 63, 471-477.

Josefsson, L.G. (1999) Evidence for kinship between diverse G-protein coupled receptors. *Gene*, 239, 333-340.

Kahsai, A.W., Xiao, K., Rajagopal, S., Ahn, S., Shukla, A.K., Sun, J., Oas, T.G., Lefkowitz, R.J. (2011) Multiple ligand-specific conformations of the β2-adrenergic receptor. *Nat. Chem. Biol.*, 7, 692-700.

Kang, D.S., Tian, X., Benovic, J.L. (2014) Role of β-arrestins and arrestin domain-containing proteins in G protein-coupled receptor trafficking. *Curr. Opin. Cell Biol.,* 27, 63-71.

Katritch, V., Cherezov, V., Stevens, R.C. (2013) Structure-function of the G protein-coupled receptor superfamily. *Annu. Rev. Pharmacol. Toxicol.*, 53, 531-556.

Kawano, T., Matsuse, H., Tsuchida, T., Fukahori, S., Fukushima, C., Nishino, T., Kohno, S. (2014) Cysteinyl leukotriene receptor antagonist regulates allergic airway inflammation in an organ- and cytokine-specific manner. *Med. Sci. Monit.*, 20, 297-302.

Kenakin, T. (2001) Inverse, protean, and ligand-selective agonism: matters of receptor conformation. *FASEB J.*, 15, 598-611.

Kenakin, T., Watson, C., Muniz-Medina, V., Christopoulos, A., Novick, S. (2012) A simple method for quantifying functional selectivity and agonist bias. *ACS Chem. Neurosci.,* 3, 193-203.

Kenakin, T. (2013) New concepts in pharmacological efficacy at 7TM receptors: IUPHAR review 2. *Br. J. Pharmacol.*, 168, 554-575.

Kenakin, T, Christopoulos, A. (2013) Signalling bias in new drug discovery: detection, quantification and therapeutic impact. *Nat. Rev. Drug. Discov.,* 12, 205-216.

Kempuraj, D., Tagen, M., Iliopoulou, B.P., Clemons, A., Vasiadi, M., Boucher, W., House, M., Wolfberg, A., Theoharides, T.C. (2008) Luteolin inhibits myelin basic protein-induced human mast cell activation and mast cell-dependent stimulation of Jurkat T cells. *Br. J. Pharmacol.,* 155, 1076-1084.

Khilnani, G., Khilnani, A.K. (2011) Inverse agonism and its therapeutic significance. *Indian J. Pharmacol.*, 43, 492-501.

Kilpatrick, L.E., Jakabovics, E., McCawley, L.J., Kane, L.H., Korchak, H.M. (1995) Cromolyn inhibits assembly of the NADPH oxidase and superoxide anion generation by human neutrophils. *J. Immunol.*, 154, 3429-3436.

Kimata, M., Shichijo, M., Miura, T., Serizawa, I., Inagaki, N., Nagai, H. (2000) Effects of luteolin, quercetin and baicalein on immunoglobulin E-mediated mediator release from human cultured mast cells. *Clin. Exp. Allergy.,* 30, 501-508.

Kimple, A.J., Bosch, D.E., Giguere, P.M., Siderovski, D.P. (2011) Regulators of G-protein signaling and their galpha substrates: promises and challenges in their use as drug discovery targets. *Pharmacol. Rev.,* 63, 728-749.

Kimple, M.E., Neuman, J.C., Linnemann, A.K., Casey, P.J. (2014) Inhibitory G proteins and their receptors: emerging therapeutic targets for obesity and diabetes. *Exp. Mol. Med.*, 46: e102.

Kishimoto, I., Tokudome, T., Hosoda, H., Miyazato, M., Kangawa, K. (2012) Ghrelin and cardiovascular diseases. *J. Cardiol.,* 59, 8-13.

Klco, J.M., Wiegand, C.B., Narzinski, K., Baranski, T.J. (2005) Essential role for the second extracellular loop in C5a receptor activation. *Nat. Struct. Mol. Biol.*, 12, 320-326.

Knight, P.J., Pfeifer, T.A., Grigliatti, T.A. (2003) A functional assay for G-protein-coupled receptors using stably transformed insect tissue culture cell lines. *Anal. Biochem.,* 320, 88-103.

Kohout, T.A., Lefkowitz, R.J. (2003) Regulation of G protein-coupled receptor kinases and arrestins during receptor desensitization. *Mol. Pharmacol.*, 63, 9-18.

Kojima, M., Hosoda, H., Date, Y., Nakazato, M., Matsuo, H., Kangawa, K. (1999) Ghrelin is a growth-hormone-releasing acylated peptide from stomach. *Nature,* 402, 656-660.

Kostenis, E., Waelbroeck, M., Milligan, G. (2005) Techniques: promiscuous Galpha proteins in basic research and drug discovery. *Trends Pharmacol. Sci.,* 26, 595-602.

Kotarsky, K., Nilsson, N.E., Flodgren, E., Owman, C., Olde, B. (2003) A human cell surface receptor activated by free fatty acids and thiazolidinedione drugs. *Biochem. Biophys. Res. Commun.*, 301, 406-410.

Kotarsky, K., Nilsson, N.E. (2004) Reverse pharmacology and the de-orphanization of 7TM receptors. *Drug Discov. Today Technol.*, 1, 99-104.

Krishnan, A., Almén, M.S., Fredriksson, R., Schiöth, H.B. (2012) The origin of GPCRs: identification of mammalian like Rhodopsin, Adhesion, Glutamate and Frizzled GPCRs in fungi. *PLoS ONE*, 7: e29817.

Kristiansen, K. (2004) Molecular mechanisms of ligand binding, signaling, and regulation within the superfamily of G-protein-coupled receptors: molecular modeling and mutagenesis approaches to receptor structure and function. *Pharmacol. Ther.,* 103, 21-80.

Kubo, T., Fukuda, K., Mikami, A., Maeda, A., Takahashi, H., Mishina, M., Haga, T., Haga, K., Ichiyama, A., Kangawa, K., Kojima, M., Matsuo, H., Hirose, T, Numa, S. (1986) Cloning, sequencing and expression of complementary DNA encoding the muscarinic acetylcholine receptor. *Nature,* 323, 411-416.

Kuc, D., Zgrajka, W., Parada-Turska, J., Urbanik-Sypniewska, T., Turski, W.A. (2008) Micromolar concentration of kynurenic acid in rat small intestine. *Amino Acids,* 35, 503-505.

Kuei, C., Yu, J., Zhu, J., Wu, J., Zhang, L., Shih, A., Mirzadegan, T., Lovenberg, T., Liu, C. (2011) Study of GPR81, the lactate receptor, from distant species identifies residues and motifs critical for GPR81 functions. *Mol. Pharmacol*., 80, 848-858.

Lander, E.S., Linton, L.M., Birren, B., Nusbaum, C., Zody, M.C., Baldwin, J., Devon, K., Dewar, K., Doyle, M., FitzHugh, W., Funke, R., Gage, D., Harris, K., Heaford, A., Howland, J., Kann, L., Lehoczky, J., LeVine, R., McEwan, P., McKernan, K., Meldrim, J., Mesirov, J.P., Miranda, C., Morris, W., Naylor, J., Raymond, C., Rosetti, M., Santos, R., Sheridan, A., Sougnez, C., Stange-Thomann, N., Stojanovic, N., Subramanian, A., Wyman, D. et al., (2001) Initial sequencing and analysis of the human genome. *Nature*, 409, 860-921.

Lane, J.R., Powney, B., Wise, A., Rees, S., Milligan, G. (2007) Protean agonism at the dopamine D2

receptor: (S)-3-(3-hydroxyphenyl)-N-propylpiperidine is an agonist for activation of Go1 but an antagonist/inverse agonist for Gi1, Gi2, and Gi3. *Mol. Pharmacol.,* 71, 1349-1359.

Lane, T.R. (2011) Building and Refinement of an in silico Homology Model of a Novel G Protein-Coupled Receptor: GPR35. Masters Dissertation, The University of North Carolina at Greensboro.

Langmead, C.J., Christopoulos, A. (2014) Functional and structural perspectives on allosteric modulation of GPCRs. *Curr. Opin. Cell Biol.*, 27, 94-101.

Lambright, D.G., Noel, J.P., Hamm, H.E., Sigler, P.B. (1994) Structural determinants for activation of the alpha-subunit of a heterotrimeric G protein. *Nature,* 369, 621–628.

Lambright, D.G., Sondek, J., Bohm, A., Skiba, N.P., Hamm, H.E., Sigler, P.B. (1996) The 2.0 Å crystal structure of a heterotrimeric G protein. *Nature,* 379, 311–319.

Lattin, J.E., Schroder, K., Su, A.I., Walker, J.R., Zhang, J., Wiltshire, T., Saijo, K., Glass, C.K., Hume, D.A., Kellie, S., Sweet, M.J. (2008) Expression analysis of G Protein-Coupled Receptors in mouse macrophages. *Immununome Res.,* 29, 4-5.

Laviano, A., Krznaric, Z., Sanchez-Lara, K., Preziosa, I., Cascino, A., Rossi Fanelli, F. (2010) Chronic renal failure, cachexia, and ghrelin. *Int. J. Pept.,* pii: 648045.

Lee, M.J., Van Brocklyn, J.R., Thangada, S., Liu, C.H., Hand, A.R., Menzeleev, R., Spiegel, S., Hla, T. (1998) Sphingosine-1-phosphate as a ligand for the G protein-coupled receptor EDG-1. *Science*, 279, 1552-1555.

Lee, W.Y., Wang, C.J., Lin, T.Y., Hsiao, C.L., Luo, C.W. (2013) CXCL17, an orphan chemokine, acts as a novel angiogenic and anti-inflammatory factor. *Am. J. Physiol. Endocrinol. Metab.*, 304, 32-40.

Lebon, G., Warne, T., Edwards, P.C., Bennett, K., Langmead, C.J., Leslie, A.G., Tate, C.G. (2011) Agonist-bound adenosine A2A receptor structures reveal common features of GPCR activation. *Nature,* 474, 521-525.

Le Poul, E., Loison, C., Struyf, S., Springael, J.Y., Lannoy, V., Decobecq, M.E., Brezillon, S., Dupriez, V., Vassart, G., Van Damme, J., Parmentier, M., Detheux, M. (2003) Functional characterization of human receptors for short chain fatty acids and their role in polymorphonuclear cell activation. *J. Biol. Chem.,* 278, 25481-25489.

Leurs, R., Church, M.K., Taglialatela, M. (2002) H1-antihistamines: inverse agonism, anti-inflammatory actions and cardiac effects. *Clin. Exp. Allergy,* 32, 489-498.

Levinson, B., Gertner, J. (2012) Randomized study of the efficacy and safety of SUN11031 (synthetic human ghrelin) in cachexia associated with chronic obstructive pulmonary disease. *E. Spen. Eur. E. J. Clin. Nutr. Metab.,* 7, 171-175.

Levoye, A., Dam, J., Ayoub, M.A., Guillaume, J.L., Jockers, R. (2006) Do orphan G-protein-coupled receptors have ligand-independent functions? New insights from receptor heterodimers. *EMBO Rep.,* 7, 1094-1098.

Levoye, A., Jockers, R. (2008) Alternative drug discovery approaches for orphan GPCRs. *Drug Discov. Today,* 13, 52-58.

Libert, F., Vassart, G., Parmentier, M. (1991) Current developments in G-protein-coupled receptors. *Curr. Opin. Cell Biol.,* 3, 218-223.

Lin, L., Faraco, J., Li, R., Kadotani, H., Rogers, W., Lin, X., Qiu, X., de Jong, P.J., Nishino, S., Mignot, E. (1999) The sleep disorder canine narcolepsy is caused by a mutation in the hypocretin (orexin) receptor 2 gene. *Cell,* 98, 365-376.

Lipinski, C.A., Lombardo, F., Dominy, B.W., Feeney, P.J. (1997) Experimental and computational approaches to estimate solubility and permeability in drug discovery and development settings. *Adv. Drug Deliv. Rev.*, 23, 3-25.

Liu, C., Ma, X., Jiang, X., Wilson, S.J., Hofstra, C.L., Blevitt, J., Pyati, J., Li, X., Chai, W., Carruthers, N., Lovenberg, T.W. (2001) Cloning and pharmacological characterization of a fourth histamine receptor (H(4)) expressed in bone marrow. *Mol. Pharmacol.*, 59, 420-426.

Liu, C., Wu, J., Zhu, J., Kuei, C., Yu, J., Shelton, J., Sutton, S.W., Li, X., Yun, S.J., Mirzadegan, T., Mazur, C., Kamme, F., Lovenberg, T.W. (2009) Lactate inhibits lipolysis in fat cells through activation of an orphan G-protein-coupled receptor, GPR81. *J. Biol. Chem.,* 284, 2811-2822.

Liu, Q., Pong, S.S., Zeng, Z., Zhang, Q., Howard, A.D., Williams, D.L.^{Jr}, Davidoff, M., Wang, R., Austin, C.P., McDonald, T.P., Bai, C., George, S.R., Evans, J.F., Caskey, C.T. (1999) Identification of urotensin II as the endogenous ligand for the orphan G-protein-coupled receptor GPR14. *Biochem. Biophys. Res. Commun.*, 266, 174-178.

Liu, W., Chun, E., Thompson, A.A., Chubukov, P., Xu, F., Katritch, V., Han, G.W., Roth, C.B., Heitman, L.H., IJzerman, A.P., Cherezov, V., Stevens, R.C. (2012) Structural basis for allosteric regulation of GPCRs by sodium ions. *Science,* 337, 232-236.

Lohse, M.J., Hoffmann, C. (2014) Arrestin interactions with G protein-coupled receptors. *Handb. Exp. Pharmacol.,* 219, 15-56.

Lomasney, J.W., Cotecchia, S., Lefkowitz, R.J., Caron, M.G. (1991) Molecular biology of alpha-adrenergic receptors: implications for receptor classification and for structure-function relationships. *Biochim. Biophys. Acta,* 1095, 127-39.

Lukowski, R., Krieg, T., Rybalkin, S.D., Beavo, J., Hofmann, F. (2014) Turning on cGMP-dependent pathways to treat cardiac dysfunctions: boom, bust, and beyond. *Trends Pharmacol. Sci.*, 35, 404-413.

Mackenzie, A.E., Lappin, J.E., Taylor, D.L., Nicklin, S.A., Milligan, G. (2011) GPR35 as a Novel Therapeutic Target. *Front. Endocrinol. (Lausanne)*, 2:68.

MacKenzie, A.E., Caltabiano, G., Kent, T.C., Jenkins, L., McCallum, J.E., Hudson, B.D., Nicklin, S.A., Fawcett, L., Markwick, R., Charlton, S.J., Milligan, G. (2014) The antiallergic mast cell stabilizers lodoxamide and bufrolin as the first high and equipotent agonists of human and rat GPR35. *Mol. Pharmacol*., 85, 91-104.

Mackenzie, A.E., Milligan, G. (2015) The emerging pharmacology and function of GPR35 in the nervous system. *Neuropharmacology, In Press.*

Makino, H., Saijo, T., Ashida, Y., Kuriki, H., Maki, Y. (1987) Mechanism of action of an antiallergic agent, amlexanox (AA-673), in inhibiting histamine release from mast cells. Acceleration of cAMP generation and inhibition of phosphodiesterase. *Int. Arch. Allergy Appl. Immunol.,* 82, 66-71.

Mallee, J.J., Salvatore, C.A., LeBourdelles, B., Oliver, K.R., Longmore, J., Koblan, K.S., Kane, S.A. (2002) Receptor activity-modifying protein 1 determines the species selectivity of non-peptide CGRP receptor antagonists. *J Biol Chem.*, 277, 14294-14298.

Manglik, A., Kobilka, B. (2014) The role of protein dynamics in GPCR function: insights from the β2AR and rhodopsin. *Curr. Opin. Cell Biol.*, 27, 136-143.

Maravillas-Montero, J.L., Burkhardt, A.M., Hevezi, P.A., Carnevale, C.D., Smit, M.J., Zlotnik, A. (2014) Cutting Edge: GPR35/CXCR8 is the Receptor of the Mucosal Chemokine CXCL17. *J. Immunol.*, pii: 1401704.

Marchi, M., Risso, F., Viola, C., Cavazzani, P., Raiteri, M. (2002) Direct evidence that release-stimulating α7* nicotinic cholinergic receptors are localized on human and rat brain glutamatergic axon terminals. *J. Neurochem.*, 80, 1071–1078.

Mason, J.S., Bortolato, A., Congreve, M., Marshall, F.H. (2012) New insights from structural biology into the druggability of G protein-coupled receptors. *Trends Pharmacol. Sci.*, 33, 249-260.

Massotte, D., Kieffer, B.L. (2005) The second extracellular loop: a damper for G protein-coupled receptors? *Nat. Struct. Mol. Biol.*, 12, 287-288.

McCarthy, J.S. (2014) Oxantel pamoate-albendazole for Trichuris trichiura infection. *N. Engl. J. Med.*, 370, 1952-1953.

McCool, B.A., Pin, J.P., Harpold, M.M., Brust, P.F., Stauderman, K.A., Lovinger, D.M. (1998) Rat group I metabotropic glutamate receptors inhibit neuronal Ca^{2+} channels via multiple signal transduction pathways in HEK 293 cells. *J. Neurophysiol.*, 79, 379-391.

McCudden, C.R., Hains, M.D., Kimple, R.J., Siderovski, D.P., Willard, F.S. (2005) G-protein signaling: back to the future. *Cell Mol. Life Sci.,* 62, 551-577.

Meltzer, H.Y., Massey, B.W. (2011) The role of serotonin receptors in the action of atypical antipsychotic drugs. *Curr. Opin. Pharmacol.*, 11, 59-67.

Mestas, J., Hughes, C.C. (2004) Of mice and not men: differences between mouse and human immunology. *J. Immunol.,* 172, 2731-2738.

Meunier, J.C., Mollereau, C., Toll, L., Suaudeau, C., Moisand, C., Alvinerie, P., Butour, J.L., Guillemot, J.C., Ferrara, P., Monsarrat, B, Mazarguil, H., Vassart, G., Parmentier, M, Costentin, J. (1995) Isolation and structure of the endogenous agonist of opioid receptor-like ORL1 receptor. *Nature,* 377, 532-535.

Michelson, D., Snyder, E., Paradis, E., Chengan-Liu, M., Snavely, D.B., Hutzelmann, J., Walsh, J.K., Krystal, A.D., Benca, R.M., Cohn, M., Lines, C., Roth, T., Herring, W.J. (2014) Safety and efficacy of suvorexant during 1-year treatment of insomnia with subsequent abrupt treatment discontinuation: a phase 3 randomised, double-blind, placebo-controlled trial. *Lancet Neurol.*, 13, 461-471.

Miki, K., Maekura, R., Nagaya, N., Kitada, S., Miki, M., Yoshimura, K., Tateishi, Y., Motone, M., Hiraga, T., Mori, M., Kangawa, K. (2013) Effects of ghrelin treatment on exercise capacity in underweight COPD patients: a substudy of a multicenter, randomized, double-blind, placebo-controlled trial of ghrelin treatment. *BMC Pulm. Med*., 13, 37.

Millan, M.J., Marin, P., Kamal, M., Jockers, R., Chanrion, B., Labasque, M., Bockaert, J., Mannoury, la Cour, C. (2011) The melatonergic agonist and clinically active antidepressant, agomelatine, is a neutral antagonist at 5-HT(2C) receptors. *Int. J. Neuropsychopharmacol.*, 14, 768-783.

Miller, L.J., Sexton, P.M., Dong, M., Harikumar, K.G. (2014) The class B G-protein-coupled GLP-1 receptor: an important target for the treatment of type-2 diabetes mellitus. *Int. J. Obes. Suppl.,* 4, S9-S13.

Milligan, G., Bond, R.A., Lee, M. (1995) Inverse agonism: pharmacological curiosity or potential therapeutic strategy? *Trends Pharmacol. Sci.*, 16, 10-13.

Milligan, G. (2000) Insights into ligand pharmacology using receptor-G-protein fusion proteins. *Trends Pharmacol. Sci.,* 21, 24-28.

Milligan, G. (2003a) Principles: extending the utility of [35S]GTP gamma S binding assays. *Trends Pharmacol. Sci.,* 24, 87-90.

Milligan, G. (2003b) Constitutive activity and inverse agonists of G protein-coupled receptors: a current perspective. *Mol. Pharmacol.*, 64, 1271-1276.

Milligan, G., Parenty, G., Stoddart, L.A., Lane, J.R. (2007) Novel pharmacological applications of G-protein-coupled receptor-G protein fusions. *Curr. Opin. Pharmacol.,* 7, 521-526.

Milligan, G. (2011) Orthologue selectivity and ligand bias: translating the pharmacology of GPR35. *Trends Pharmacol. Sci.*, 32, 317-325.

Milligan, G., Ulven, T., Murdoch, H., Hudson, B.D. (2014) G-protein-coupled receptors for free fatty acids: nutritional and therapeutic targets. *Br. J. Nutr.*, 111, S3-S7.

Min, K.D., Asakura, M., Liao, Y., Nakamaru, K., Okazaki, H., Takahashi, T., Fujimoto, K., Ito, S., Takahashi, A., Asanuma, H., Yamazaki, S., Minamino, T., Sanada, S., Seguchi, O., Nakano, A., Ando, Y., Otsuka, T., Furukawa, H., Isomura, T., Takashima, S., Mochizuki, N., Kitakaze, M. (2010). Identification of genes related to heart failure using global gene expression profiling of human failing myocardium. *Biochem. Biophys. Res. Commun.*, 393, 55-60.

Mizutani, K., Sugimoto, K., Okuda, T., Katsuya, T., Miyata, T., Tanabe, T., Higaki, J., Ogihara, T., Yamori, Y., Tsujita, Y., Tago, N., Iwai, N. (2002) Kynureninase is a novel candidate gene for hypertension in spontaneously hypertensive rats. *Hypertens. Res.*, 25, 135-140.

Mochizuki, T., Crocker, A., McCormack, S., Yanagisawa, M., Sakurai, T., Scammell, T.E. (2004) Behavioral state instability in orexin knock-out mice. *J. Neurosci.*, 24, 6291-6300.

Mollereau, C., Parmentier, M., Mailleux, P., Butour, J.L., Moisand, C., Chalon, P., Caput, D., Vassart, G., Meunier, J.C. (1994) ORL1, a novel member of the opioid receptor family. Cloning, functional expression and localization. *FEBS Lett.*, 341, 33-38.

Monajemzadeh, M., Mokhtari, S., Motamed, F., Shams, S., Ashtiani, M.T., Abbasi, A., Sani, M.N., Sadrian, E. (2013) Plasma ghrelin levels in children with cystic fibrosis and healthy children. *Arch. Med. Sci.*, 9, 93-97.

Moore, C.A., Milano, S.K., Benovic, J.L. (2007) Regulation of receptor trafficking by GRKs and arrestins. *Annu. Rev. Physiol.*, 69, 451-482.

Moroni, F., Russi, P., Lombardi, G., Beni, M., Carla, V. (1988) Presence of kynurenic acid in the mammalian brain. *J Neurochem.,* 51, 177-180.

Moroni, F., Carpenedo, R., Cozzi, A., Meli, E., Chiarugi, A., Pellegrini-Giampietro, D.E. (2003) Studies on the neuroprotective action of kynurenine mono-oxygenase inhibitors in post-ischemic brain damage. *Adv. Exp. Med. Biol.*, 527, 127-136.

Moroni, F., Cozzi, A., Sili, M., Mannaioni, G. (2012) Kynurenic acid: a metabolite with multiple actions and multiple targets in brain and periphery. *J. Neural Transm.*, 119, 133-139.

Morse, K.L., Behan, J., Laz, T.M., West, R.E.^{Jr}, Greenfeder, S.A., Anthes, J.C., Umland, S., Wan, Y., Hipkin, R.W., Gonsiorek, W., Shin, N., Gustafson, E.L., Qiao, X., Wang, S., Hedrick, J.A., Greene, J., Bayne, M., Monsma, F.J.^{Jr} (2001) Cloning and characterization of a novel human histamine receptor. *J. Pharmacol. Exp. Ther.,* 296, 1058-1066.

Motawi, T.M., Bustanji, Y., El-Maraghy, S., Taha, M.O., Al-Ghussein, M.A. (2014) Evaluation of naproxen and cromolyn activities against cancer cells viability, proliferation, apoptosis, p53 and gene expression of survivin and caspase-3. *J. Enzyme Inhib. Med. Chem.*, 29, 153-161.

Moukhametzianov, R., Warne, T., Edwards, P.C., Serrano-Vega, M.J., Leslie, A.G., Tate, C.G., Schertler, G.F. (2011) Two distinct conformations of helix 6 observed in antagonist-bound structures of a beta1-adrenergic receptor. *Proc. Natl. Acad. Sci. U.S.A.,* 108, 8228-8232.

Mullard, A. (2012) 2011 FDA drug approvals. *Nat. Rev. Drug Discov.*, 11, 91-94.

Mullard, A. (2013) 2012 FDA drug approvals. *Nat. Rev. Drug Discov.*, 12, 87-90.

Mullard, A. (2014) 2013 FDA drug approvals. *Nat. Rev. Drug Discov.*, 13, 85-99.

Müller, A., Kleinau, G., Piechowski, C.L., Müller, T.D., Finan, B., Pratzka, J., Grüters, A., Krude, H., Tschöp, M., Biebermann, H. (2013) G-protein coupled receptor 83 (GPR83) signaling determined by constitutive and zinc(II)-induced activity. *PLoS ONE*, 8: e53347.

Murad, J.P., Lin, O.A., Espinosa, E.V., Khasawneh, F.T. (2013) Current and experimental antibody-based therapeutics: insights, breakthroughs, setbacks and future directions. *Curr. Mol. Med.*, 13, 165-178.

Murakoshi, M., Saiki, K., Urayama, K., Sato, T.N. (2013) An anthelmintic drug, pyrvinium pamoate, thwarts fibrosis and ameliorates myocardial contractile dysfunction in a mouse model of myocardial infarction. *PLoS ONE*, 4: e79374.

Nakamura, T., Itadani, H., Hidaka, Y., Ohta, M., Tanaka, K. (2000) Molecular cloning and characterization of a new human histamine receptor, HH4R. *Biochem. Biophys. Res. Commun.*, 279, 615-620.

Nakanaga, K., Hama, K., Aoki, J. (2010) Autotaxin—an LPA producing enzyme with diverse functions. *J. Biochem.*, 148, 13-24.

Nakanishi-Matsui, M., Zheng, Y.W., Sulciner, D.J., Weiss, E.J., Ludeman, M.J., Coughlin, S.R. (2000) PAR3 is a cofactor for PAR4 activation by thrombin. *Nature*, 404, 609-613.

Neetoo-Isseljee, Z., MacKenzie, A.E., Southern, C., Jerman, J., McIver, E.G., Harries, N., Taylor, D.L., Milligan G. (2013) High-throughput identification and characterization of novel, species-selective GPR35 agonists. *J. Pharmacol. Exp. Ther.,* 344, 568-578.

Neubig, R.R. (2010) Mind your salts: when the inactive constituent isn't. *Mol. Pharmacol.,* 78, 558-559.

Nguyen, T., Shapiro, D.A., George, S.R., Setola, V., Lee, D.K., Cheng, R., Rauser, L., Lee, S.P., Lynch, K.R., Roth, B.L., O'Dowd, B.F. (2001) Discovery of a novel member of the histamine receptor family. *Mol. Pharmacol.*, 59, 427-433.

Nishimasu, H., Okudaira, S., Hama, K., Mihara, E., Dohmae, N., Inoue, A., Ishitani, R., Takagi, J., Aoki, J., Nureki, O. (2011) Crystal structure of autotaxin and insight into GPCR activation by lipid mediators. *Nat. Struct. Mol. Biol.*, 18, 205-212.

Nygaard, R., Zou, Y., Dror, R.O., Mildorf, T.J., Arlow, D.H., Manglik, A., Pan, A.C., Liu, C.W., Fung, J.J., Bokoch, M.P., Thian, F.S., Kobilka, T.S., Shaw, D.E., Mueller, L., Prosser, R.S., Kobilka, B.K. (2013) The dynamic process of β(2)-adrenergic receptor activation. *Cell*, 152, 532-542.

Oakley, R.H., Laporte, S.A., Holt, J.A., Caron, M.G., Barak, L.S. (2000) Differential affinities of visual arrestin, beta arrestin1, and beta arrestin2 for G protein-coupled receptors delineate two major classes of receptors. *J. Biol. Chem.*, 275, 17201-17210.

Oakley, R.H., Laporte, S.A., Holt, J.A., Barak, L.S., Caron, M.G. (2001) Molecular determinants underlying the formation of stable intracellular G protein-coupled receptor-beta-arrestin complexes after receptor endocytosis. *J. Biol. Chem*., 276, 19452-19460.

O'Dowd, B.F., Nguyen, T., Marchese, A., Cheng, R., Lynch, K.R., Heng, H.H., Kolakowski, L.F.^{Jr}, George, S.R. (1998) Discovery of three novel G-protein-coupled receptor genes. *Genomics,* 47, 310-313.

Offermanns, S., Wieland, T., Homann, D., Sandmann, J., Bombien, E., Spicher, K., Schultz, G., Jakobs, K.H. (1994) Transfected muscarinic acetylcholine receptors selectively couple to Gi-type G proteins and Gq/11. *Mol. Pharmacol.,* 45, 890-898.

O'Hayre, M., Degese, M.S., Gutkind, J.S. (2014) Novel insights into G protein and G protein-coupled receptor signaling in cancer. *Curr. Opin. Cell. Biol.,* 27, 126-135.

Ohki-Hamazaki, H., Watase, K., Yamamoto, K., Ogura, H., Yamano, M., Yamada, K., Maeno, H., Imaki, J., Kikuyama, S., Wada, E., Wada, K. (1997) Mice lacking bombesin receptor subtype-3 develop metabolic defects and obesity. *Nature,* 390, 165-169.

Ohshiro, H., Tonai-Kachi, H., Ichikawa, K. (2008) GPR35 is a functional receptor in rat dorsal root ganglion neurons. *Biochem. Biophys. Res. Commun.,* 365, 344-348.

Oka S, Ota R, Shima M, Yamashita A, Sugiura T. (2010) GPR35 is a novel lysophosphatidic acid receptor. *Biochem. Biophys. Res. Commun.,* 395, 232-237.

Oka, T., Kalesnikoff, J., Starkl, P., Tsai, M., Galli, S.J. (2012) Evidence questioning cromolyn's effectiveness and selectivity as a 'mast cell stabilizer' in mice. *Lab Invest.*, 92, 1472-1482.

Okumura, H., Nagaya, N., Enomoto, M., Nakagawa, E., Oya, H., Kangawa, K. (2002) Vasodilatory effect of ghrelin, an endogenous peptide from the stomach. *J. Cardiovasc. Pharmacol.*, 39, 779-783.

Okumura, S., Baba, H., Kumada, T., Nanmoku, K., Nakajima, H., Nakane, Y., Hioki, K., Ikenaka, K. (2004) Cloning of a G-protein-coupled receptor that shows an activity to transform NIH3T3 cells and is expressed in gastric cancer cells. *Cancer Sci.,* 95, 131-135.

Olson, T.S., Ley, K. (2002) Chemokines and chemokine receptors in leukocyte trafficking. *Am. J. Physiol. Regul. Integr. Comp. Physiol.,* 283, R7-28.

Otto, V.I., Schürpf, T., Folkers, G., Cummings, R.D. (2004) Sialylated complex-type N-glycans enhance the signaling activity of soluble intercellular adhesion molecule-1 in mouse astrocytes. *J. Biol. Chem.,* 279, 35201-35209.

Overington, J.P., Al-Lazikani, B., Hopkins, A.L. (2006) How many drug targets are there? *Nat. Rev. Drug Discov.*, 5, 993-996.

Paing, M.M., Stutts, A.B., Kohout, T.A., Lefkowitz, R.J., Trejo, J. (2002) beta-Arrestins regulate protease-activated receptor-1 desensitization but not internalization or Down-regulation. *J. Biol. Chem.,* 277, 1292-1300.

Patterson, A.D., Bonzo, J.A., Li, F., Krausz, K.W., Eichler, G.S., Aslam, S., Tigno, X., Weinstein, J.N., Hansen, B.C., Idle, J.R., Gonzalez, F.J. (2011) Metabolomics reveals attenuation of the SLC6A20 kidney transporter in nonhuman primate and mouse models of type 2 diabetes mellitus. *J. Biol. Chem*., 2286, 19511-19522.

Paul, S.M., Mytelka, D.S., Dunwiddie, C.T., Persinger, C.C., Munos, B.H., Lindborg, S.R., Schacht, A.L. (2010) How to improve R&D productivity: the pharmaceutical industry's grand challenge. *Nat. Rev. Drug Discov.*, 9, 203-214.

Pawlak, D., Tankiewicz, A., Buczko, W. (2001) Kynurenine and its metabolites in the rat with experimental renal insufficiency. *J. Physiol. Pharmacol.*, 52, 755-766.

Penn, R.B., Bond, R.A., Walker, J.K.L. (2014) GPCRs and Arrestins in Airways: Implications for Asthma. *Handb. Exp. Pharmacol.*, 219, 387-403.

Peyron, C., Faraco, J., Rogers, W., Ripley, B., Overeem, S., Charnay, Y., Nevsimalova, S., Aldrich, M., Reynolds, D., Albin, R., Li, R., Hungs, M., Pedrazzoli, M., Padigaru, M., Kucherlapati, M., Fan, J., Maki, R., Lammers, G.J., Bouras, C., Kucherlapati, R., Nishino, S., Mignot, E. (2000) A mutation in a case of early onset narcolepsy and a generalized absence of hypocretin peptides in human narcoleptic brains. *Nat. Med.*, 6, 991-997.

Pham, P.L., Kamen, A., Durocher, Y. (2006) Large-scale transfection of mammalian cells for the fast production of recombinant protein. *Mol. Biotechnol.,* 34, 225-237.

Piccart-Gebhart, M.J., Procter, M., Leyland-Jones, B., Goldhirsch, A., Untch, M., Smith, I., Gianni, L., Baselga, J., Bell, R., Jackisch, C., Cameron, D., Dowsett, M., Barrios, C.H., Steger, G., Huang, C.S., Andersson, M., Inbar, M., Lichinitser, M., Láng, I., Nitz, U., Iwata, H., Thomssen, C., Lohrisch, C., Suter,

T.M., Rüschoff, J., Süto T., Greatorex, V., Ward, C., Straehle, C., McFadden, E., Dolci, S., Gelber, R.D. (2005) Trastuzumab after Adjuvant Chemotherapy in HER2-Positive Breast Cancer. *New Engl. J. Med.,* 353, 16.

Plouffe, B., D'Aoust, J.P., Laquerre, V., Liang, B., Tiberi, M. (2010) Probing the constitutive activity among dopamine D1 and D5 receptors and their mutants. *Meth. Enzymol.,* 484, 295-328.

Prescott, C., Weeks, A.M., Staley, K.J., Partin, K.M. (2006) Kynurenic acid has a dual action on AMPA receptor responses. *Neurosci. Lett.,* 402, 108-112.

Prescott, R.W., Yeo, P.P., Watson, M.J., Johnston, I.D., Ratcliffe, J.G., Evered, D.C. (1979) Total and free thyroid hormone concentrations after elective surgery. *J. Clin. Pathol.,* 32, 321-324.

Preuss, H. (2007) Species-selective interactions of histamine H2 receptors with guanidine-type agonists: molecular modelling, site-directed mutagenesis and pharmacological analysis. Dissertation, Universität Regensburg.

Rahmeh, R., Damian, M., Cottet, M., Orcel, H., Mendre, C., Durroux, T., Sharma, K.S., Durand, G., Pucci, B., Trinquet, E., Zwier, J.M., Deupi, X., Bron, P., Banères, J.L., Mouillac, B., Granier, S. (2012) Structural insights into biased G protein-coupled receptor signaling revealed by fluorescence spectroscopy. *Proc. Natl. Acad. Sci. U.S.A*., 109, 6733-6738.

Rancoule, C., Dusaulcy, R., Tréguer, K., Grès, S., Attané, C., Saulnier-Blache, J.S. (2014) Involvement of autotaxin/lysophosphatidic acid signaling in obesity and impaired glucose homeostasis. *Biochimie,* 96, 140-143.

Rask-Andersen, M., Almén, M.S., Schiöth, H.B. (2011) Trends in the exploitation of novel drug targets. *Nat. Rev. Drug Discov.*, 10, 579-590.

Rasmussen, S.G., Choi, H.J., Rosenbaum, D.M., Kobilka, T.S., Thian, F.S., Edwards, P.C., Burghammer, M., Ratnala, V.R., Sanishvili, R., Fischetti, R.F., Schertler, G.F., Weis, W.I., Kobilka, B.K. (2007) Crystal structure of the human beta2 adrenergic G-protein-coupled receptor. *Nature*, 450, 383-387.

Rasmussen, S.G., DeVree, B.T., Zou, Y., Kruse, A.C., Chung, K.Y., Kobilka, T.S., Thian, F.S., Chae, P.S., Pardon, E., Calinski, D., Mathiesen, J.M., Shah, S.T., Lyons, J.A., Caffrey, M., Gellman, S.H., Steyaert, J., Skiniotis, G. Weis, W.I., Sunahara, R.K., Kobilka, B.K. (2011) Crystal structure of the beta2 adrenergic receptor-Gs protein complex. *Nature,* 477, 549-555.

Rassoulpour, A., Wu, H.Q., Ferre, S., Schwarcz, R. (2005) Nanomolar concentrations of kynurenic acid reduce extracellular dopamine levels in the striatum. *J. Neurochem.,* 93, 762-765.

Reilly, S.M., Chiang, S.H., Decker, S.J., Chang, L., Uhm, M., Larsen, M.J., Rubin, J.R., Mowers, J., White, N.M., Hochberg, I., Downes, M., Yu, R.T., Liddle, C., Evans, R.M., Oh, D., Li, P., Olefsky, J.M., Saltiel, A.R. (2013) An inhibitor of the protein kinases TBK1 and IKK-ε improves obesity-related metabolic dysfunctions in mice. *Nat. Med.,* 19, 313-321.

Reinscheid, R.K., Nothacker, H.P., Bourson, A., Ardati, A., Henningsen, R.A., Bunzow, J.R., Grandy, D.K., Langen, H., Monsma, F.J.^{Jr}, Civelli, O. (1995) Orphanin FQ: a neuropeptide that activates an opioidlike G protein-coupled receptor. *Science,* 270, 792-794.

Reiser, J., Yeang, Y., Warner, J.O. (1986) The effect of zaprinast (M&B 22,948, an orally absorbed mast cell stabilizer) on exercise-induced asthma in children. *Br. J. Dis. Chest.,* 80, 157-163.

Reitman, M.L., Dishy, V., Moreau, A., Denney, W.S., Liu, C., Kraft, W.K., Mejia, A.V., Matson, M.A., Stoch, S.A., Wagner, J.A., Lai, E. (2012) Pharmacokinetics and pharmacodynamics of MK-5046, a bombesin receptor subtype-3 (BRS-3) agonist, in healthy patients. *J. Clin. Pharmacol.,* 52, 1306-1316.

Renzulli, C., Nash, M., Wright, M., Thomas, S., Zamuner, S., Pellegatti, M., Bettica, P., Boyle, G. (2011) Disposition and metabolism of [14C]SB-649868, an orexin 1 and 2 receptor antagonist, in humans. *Drug Metab. Dispos.,* 39, 215-227.

Rezmann-Vitti, L.A., Nero, T.L., Jackman, G.P., Machida, C.A., Duke, B.J., Louis, W.J., Louis, S.N. (2006) Role of Tyr(356(7.43)) and Ser(190(4.57)) in antagonist binding in the rat beta1-adrenergic receptor. *J. Med. Chem.*, 49, 3467-3477.

Riemann, D., Spiegelhalder, K. (2014) Orexin receptor antagonists: a new treatment for insomnia? *Lancet Neurol.,* 13, 441-443.

Rives, M.L., Rossillo, M., Liu-Chen, L.Y., Javitch, J.A. (2012) 6'-Guanidinonaltrindole (6'-GNTI) is a G protein-biased κ-opioid receptor agonist that inhibits arrestin recruitment. *J. Biol. Chem.,* 287, 27050-27054.

Robinson, C.R., Sauer, R.T. (1998) Optimizing the stability of single-chain proteins by linker length and composition mutagenesis. *Proc. Natl. Acad. Sci. U.S.A.*, 95, 5929-5934.

Ronkainen, V.P., Tuomainen, T., Huusko, J., Laidinen, S., Malinen, M., Palvimo, J.J., Ylä-Herttuala, S., Vuolteenaho, O., Tavi, P. (2014) Hypoxia-inducible factor 1-induced G protein-coupled receptor 35 expression is an early marker of progressive cardiac remodelling. *Cardiovasc. Res.*, 101, 69-77.

Rosenkilde, M.M., Benned-Jensen, T., Frimurer, T.M., Schwartz, T.W. (2010) The minor binding pocket: a major player in 7TM receptor activation. *Trends Pharmacol. Sci.*, 31, 567-574.

Rouleau, A., Ligneau, X., Tardivel-Lacombe, J., Morisset, S., Gbahou, F., Schwartz, J.C., Arrang, J.M. (2002) Histamine H3-receptor-mediated [^{35}S]GTPγ[S] binding: evidence for constitutive activity of the recombinant and native rat and human H3 receptors. *Br. J. Pharmacol.*, 135, 383-392.

Roux, B.T., Cottrell, G.S. (2014) G protein-coupled receptors: what a difference a 'partner' makes. *Int. J. Mol. Sci.,* 15, 1112-1142.

Rudd, R.M., Gellert, A.R., Studdy, P.R., Geddes, D.M. (1983) Inhibition of exercise-induced asthma by an orally absorbed mast cell stabilizer (M&B 22,948). *Br. J. Dis. Chest.,* 77, 78-86.

Saijo, T., Kuriki, H., Ashida, Y., Makino, H., Maki, Y. (1985) Mechanism of the action of amoxanox (AA-673), an orally active antiallergic agent. *Int. Arch. Allergy Appl. Immunol.*, 78, 43-50.

Sakurai, T., Amemiya, A., Ishii, M., Matsuzaki, I., Chemelli, R.M., Tanaka, H., Williams, S.C., Richarson, J.A., Kozlowski, G.P., Wilson, S., Arch, J.R., Buckingham, R.E., Haynes, A.C., Carr, S.A., Annan, R.S., McNulty, D.E., Liu, W.S., Terrett, J.A., Elshourbagy, N.A., Bergsma, D.J., Yanagisawa, M. (1998) Orexins and orexin receptors: a family of hypothalamic neuropeptides and G protein-coupled receptors that regulate feeding behavior. *Cell*, 92, 573-585.

Sally, E.J., Xu, H., Dersch, C.M., Hsin, L.W., Chang, L.T., Prisinzano, T.E., Simpson, D.S., Giuvelis, D., Rice, K.C., Jacobson, A.E., Cheng, K., Bilsky, E.J., Rothman, R.B. (2010) Identification of a novel "almost

neutral" micro-opioid receptor antagonist in CHO cells expressing the cloned human mu-opioid receptor. *Synapse*, 64, 280-288.

Sams-Dodd, F. (2005) Target-based drug discovery: is something wrong? *Drug. Discov. Today,* 10, 139-147.

Sato, K., Ui, M., Okajima, F. (2000) Differential roles of Edg-1 and Edg-5, sphingosine 1-phosphate receptors, in the signaling pathways in C6 glioma cells. *Brain Res. Mol. Brain Res.*, 85, 151-160.

Scammell, T.E., Winrow, C.J. (2011) Orexin receptors: pharmacology and therapeutic opportunities. *Annu. Rev. Pharmacol. Toxicol.,* 51, 243-266.

Schattauer, S.S., Miyatake, M., Shankar, H., Zietz, C., Levin, J.R., Liu-Chen, L.Y., Gurevich, V.V., Rieder, M.J., Chavkin, C. (2012) Ligand directed signaling differences between rodent and human κ-opioid receptors. *J. Biol. Chem.*, 287, 41595-41607.

Scheerer, P., Park, J.H., Hildebrand, P.W., Kim, Y.J., Krauss, N., Choe, H.W., Hofmann, K.P., Ernst, O.P. (2008) Crystal structure of opsin in its G-protein-interacting conformation. *Nature,* 455, 497-502.

Shin, H.Y., Kim, J.S., An, N.H., Park, R.K., Kim, H.M. (2004) Effect of disodium cromoglycate on mast cell-mediated immediate-type allergic reactions. *Life Sci.,* 74, 2877-2887.

Schneider, E.H., Schnell, D., Papa, D., Seifert, R. (2009) High constitutive activity and a G-protein-independent high-affinity state of the human histamine H(4)-receptor. *Biochemistry*, 48, 1424-1438.

Schober, A., Siess, W. (2012) Lysophosphatidic acid in atherosclerotic diseases. *Br. J. Pharmacol.*, 167, 465-482.

Schöneberg, T., Hofreiter, M., Schulz, A., Römpler, H. (2007) Learning from the past: evolution of GPCR functions. *Trends Pharmacol. Sci.*, 28, 117-121.

Schröder, R., Janssen, N., Schmidt, J., Kebig, A., Merten, N., Hennen, S., Müller, A., Blättermann, S., Mohr-Andrä, M., Zahn, S., Wenzel, J., Smith, N.J., Gomeza, J., Drewke, C., Milligan, G., Mohr, K., Kostenis, E. (2010) Deconvolution of complex G protein-coupled receptor signaling in live cells using dynamic mass redistribution measurements. *Nat. Biotechnol.,* 28, 943-949.

Schwarcz, R., Rassoulpour, A., Wu, H.Q., Medoff, D., Tamminga, C.A., Roberts, R.C. (2001) Increased cortical kynurenate content in schizophrenia. *Biol. Psychiatry.*, 50, 521-530.

Schwartz, T.W., Frimurer, T.M., Holst, B., Rosenkilde, M.M., Elling, C.E. (2006) Molecular mechanism of 7TM receptor activation--a global toggle switch model. *Annu. Rev. Pharmacol*. *Toxicol.,* 46, 481-519.

Segura, V., Pérez-Aso, M., Montó, F., Carceller, E., Noguera, M.A., Pediani, J., Milligan, G., McGrath, I.C., D'Ocon, P. (2013) Differences in the signaling pathways of α(1A)- and α(1B)-adrenoceptors are related to different endosomal targeting. *PLoS ONE*, 8: e64996.

Seifert, R., Wenzel-Seifert, K., Gether, U., Lam, V.T., Kobilka, B.K. (1999a) Examining the efficiency of receptor/G-protein coupling with a cleavable beta2-adrenoceptor-Gsalpha fusion protein. *Eur. J. Biochem.,* 260, 661-666.

Seifert, R., Wenzel-Seifert, K., Kobilka, B.K. (1999b) GPCR-Galpha fusion proteins: molecular analysis of receptor-G-protein coupling. *Trends Pharmacol. Sci.,* 20, 383-389.

Selent, J., Sanz, F., Pastor, M., De Fabritiis, G. (2010) Induced effects of sodium ions on dopaminergic G-protein coupled receptors. *PLoS Comput. Biol.*, 12, 6.

Shanahan, M.T., Tanabe, H., Ouellette, A.J. (2011) Strain-specific polymorphisms in Paneth cell alpha-defensins of C57BL/6 mice and evidence of vestigial myeloid alpha-defensin pseudogenes. *Infect. Immun.,* 79, 459-473.

Sharma, I., Tan, D.S. (2013) Drug discovery: Diversifying complexity. *Nature Chem.*, 5, 157-158.

Shenoy, S.K., McDonald, P.H., Kohout, T.A., Lefkowitz, R.J. (2001) Regulation of receptor fate by ubiquitination of activated beta 2-adrenergic receptor and beta-arrestin. *Science,* 294, 1307-1313.

Shenoy, S.K., Lefkowitz, R.J. (2003a) Trafficking patterns of beta-arrestin and G protein-coupled receptors determined by the kinetics of beta-arrestin deubiquitination. *J. Biol. Chem.,* 278, 14498-144506.

Shenoy, S.K., Lefkowitz, R.J. (2003b) Multifaceted roles of beta-arrestins in the regulation of seven-membrane-spanning receptor trafficking and signalling. *Biochem. J.,* 375, 503-515.

Shin, A., Camilleri, M., Busciglio, I., Burton, D., Smith, S.A., Vella, A., Ryks, M., Rhoten, D., Zinsmeister, A.R. (2013) The ghrelin agonist RM-131 accelerates gastric emptying of solids and reduces symptoms in patients with type 1 diabetes mellitus. *Clin. Gastroenterol. Hepatol.*, 11, 1453-1459.

Shukla, A.K., Manglik, A., Kruse, A.C., Xiao, K., Reis, R.I., Tseng, W.C., Staus, D.P., Hilger, D., Uysal, S., Huang, L.Y., Paduch, M., Tripathi-Shukla, P., Koide, A., Koide, S., Weis, W.I., Kossiakoff, A.A., Kobilka, B.K., Lefkowitz, R.J. (2013) Structure of active β-arrestin-1 bound to a G-protein-coupled receptor phosphopeptide. *Nature,* 497, 137-141.

Sirohi, S., Dighe, S.V., Madia, P.A., Yoburn, B.C. (2009) The relative potency of inverse opioid agonists and a neutral opioid antagonist in precipitated withdrawal and antagonism of analgesia and toxicity. *J. Pharmacol. Exp. Ther.,* 330, 513-519.

Smith, N.J., Ward, R.J., Stoddart, L.A., Hudson, B.D., Kostenis, E., Ulven, T., Morris, J.C., Tränkle, C., Tikhonova, I.G., Adams, D.R., Milligan, G. (2011) Extracellular loop 2 of the free fatty acid receptor 2 mediates allosterism of a phenylacetamide ago-allosteric modulator. *Mol. Pharmacol.,* 80, 163-173.

Southern, C., Cook, J.M., Neetoo-Isseljee, Z., Taylor, D.L., Kettleborough, C.A., Merritt, A., Bassoni, D.L., Raab, W.J., Quinn, E., Wehrman, T.S., Davenport, A.P., Brown, A.J., Green, A., Wigglesworth, M.J., Rees, S. (2013) Screening β-arrestin recruitment for the identification of natural ligands for orphan G-protein-coupled receptors. *J. Biomol. Screen.*, 18, 599-609.

Sparfel, L., Pinel-Marie, M.-L., Boize, M., Koscielny, S., Desmots, S., Pery, A., Fardel, O. (2010) Transcriptional signature of human macrophages exposed to the environmental contaminant benzo(a)pyrene. *Toxicol. Sci.,* 114, 247-259.

Standfuss, J, Edwards, P.C., D'Antona, A., Fransen, M., Xie, G., Oprian, D.D., Schertler, G.F. (2011) The structural basis of agonist-induced activation in constitutively active rhodopsin. *Nature*, 471, 656-660.

Stambouli, N., Wei, N.N., Jlizi, A., Aissa, S., Abdelmalek, R., Kilani, B., Slim, A., Tiouiri, B.A., Dridi, M., Hamza, A., Ben Ammar Elgaied, A. (2014) Structural insight into a novel human CCR5-V130I variant associated with resistance to HIV-1 infection. *J. Biomol. Struct. Dyn.,* 32, 1202-1210.

Steinhoff, M., Buddenkotte, J., Shpacovitch, V., Rattenholl, A., Moormann, C., Vergnolle, N., Luger, T.A., Hollenberg, M.D. (2005) Proteinase-activated receptors: transducers of proteinase-mediated signaling in inflammation and immune response. *Endocr. Rev.,* 26, 1-43.

Stoddart, L.A., Brown, A.J., Milligan, G. (2007) Uncovering the pharmacology of the G protein-coupled receptor GPR40: high apparent constitutive activity in guanosine 5'-O-(3-[^{35}S]thio)triphosphate binding studies reflects binding of an endogenous agonist. *Mol. Pharmacol.,* 71, 994-1005.

Stoddart, L.A., Milligan, G. (2010) Constitutive activity of GPR40/FFA1 intrinsic or assay dependent? *Meth. Enzymol.*, 484, 569-590.

Stone, T.W. (2001) Kynurenines in the CNS: from endogenous obscurity to therapeutic importance. *Prog. Neurobiol.*, 64, 185-218.

Stone, T.W. (2007) Kynurenic acid blocks nicotinic synaptic transmission to hippocampal interneurons in young rats. *Eur. J. Neurosci.*, 25, 2656-2665.

Strasser, A., Wittmann, H. J., Kunze, M., Elz, S., Seifert, R. (2009) Molecular basis for the selective interaction of synthetic agonists with the human histamine H1-receptor compared with the guinea pig H1-receptor. *Mol Pharmacol.*, 75, 454-465.

Strasser, A., Wittmann, H.J., Buschauer, A., Schneider, E.H., Seifert, R. (2013) Species-dependent activities of G-protein-coupled receptor ligands: lessons from histamine receptor orthologs. *Trends Pharmacol. Sci.,* 34, 13-32.

Strasser, F. (2012) Clinical application of ghrelin. *Curr. Pharm. Des.,* 18, 4800-4812.

Strotmann, R., Schröck, K., Böselt, I., Stäubert, C., Russ, A., Schöneberg, T. (2011) Evolution of GPCR: change and continuity. *Mol. Cell Endocrinol.*, 331, 170-178.

Sun, Y., Asnicar, M., Saha, P.K., Chan, L., Smith, R.G. (2006) Ablation of ghrelin improves the diabetic but not obese phenotype of ob/ob mice. *Cell Metab.,* 3, 379-386.

Sun, Y., Butte, N.F., Garcia, J.M., Smith, R.G. (2008a) Characterization of adult ghrelin and ghrelin receptor knockout mice under positive and negative energy balance. *Endocrinology,* 149, 843-850.

Sun, Y.V., Bielak, L.F., Peyser, P.A., Turner, S.T., Sheedy, P.F.^{2nd}, Boerwinkle, E., Kardia, S.L. (2008b) Application of machine learning algorithms to predict coronary artery calcification with a sibship-based design. *Genet. Epidemiol.*, 32, 350-360.

Swaminath, G., Lee, T.W., Kobilka, B. (2003) Identification of an allosteric binding site for Zn^{2+} on the beta2 adrenergic receptor. *J. Biol. Chem.,* 278, 352-356.

Swartz, K.J., During, M.J., Freese, A., Beal, M.F. (1990) Cerebral synthesis and release of kynurenic acid: an endogenous antagonist of excitatory amino acid receptors. *J. Neurosci.*, 10, 2965-2773.

Szpakowska, M., Perez Bercoff, D., Chevigné, A. (2014) Closing the ring: a fourth extracellular loop in chemokine receptors. *Sci. Signal*., 7:pe21.

Taniguchi, Y., Tonai-Kachi, H., Shinjo, K. (2006) Zaprinast, a well-known cyclic guanosine monophosphate-specific phosphodiesterase inhibitor, is an agonist for GPR35. *FEBS Lett.,* 580, 5003-5008.

Tao, Y.X. (2008) Constitutive activation of G protein-coupled receptors and diseases: insights into mechanisms of activation and therapeutics. *Pharmacol. Ther.,* 120, 129-148.

Tao, Y.X. (2014) Constitutive activity in melanocortin-4 receptor: biased signaling of inverse agonists. *Adv. Pharmacol.*, 70, 135-154.

Tehan, B.G., Bortolato, A., Blaney, F.E., Weir, M.P., Mason, J.S. (2014) Unifying family A GPCR theories of activation. *Pharmacol. Ther.,* 143, 51-60.

Terrillon, S., Barberis, C., Bouvier, M. (2004) Heterodimerization of V1a and V2 vasopressin receptors determines the interaction with beta-arrestin and their trafficking patterns. *Proc. Natl. Acad. Sci. U.S.A.,* 101, 1548-1553.

Thannickal, T.C., Moore, R.Y., Nienhuis, R., Ramanathan, L., Gulyani, S., Aldrich, M., Cornford, M., Siegel, J.M. (2000) Reduced number of hypocretin neurons in human narcolepsy. *Neuron,* 27, 469-474.

Theoharides, T.C., Kempuraj, D., Iliopoulou, B.P. (2007) Mast cells, T cells, and inhibition by luteolin: implications for the pathogenesis and treatment of multiple sclerosis. *Adv. Exp. Med. Biol.,* 601, 423-430.

Thimm, D., Funke, M., Meyer, A., Müller, C.E. (2013) 6-Bromo-8-(4-[(3)H]methoxybenzamido)-4-oxo-4H-chromene-2-carboxylic acid: a powerful tool for studying orphan G protein-coupled receptor GPR35. *J. Med. Chem*., 56, 7084-7099.

Thorburn, A.N., Macia, L., Mackay, C.R. (2014) Diet, metabolites, and "western-lifestyle" inflammatory diseases. *Immunity,* 40, 833-842.

Threlfell, S., Exley, R., Cragg, S.J., Greenfield, S.A. (2008) Constitutive histamine H2 receptor activity regulates serotonin release in the substantia nigra. *J. Neurochem.*, 107, 745-755.

Tian, X., Kang, D.S., Benovic, J.L. (2014) β-arrestins and G protein-coupled receptor trafficking. *Handb. Exp. Pharmacol.,* 219, 173-186.

Tohgo, A., Choy, E.W., Gesty-Palmer, D., Pierce, K.L., Laporte, S., Oakley, R.H., Caron, M.G., Lefkowitz, R.J., Luttrell, L.M. (2003) The stability of the G protein-coupled receptor-β-arrestin interaction determines the mechanism and functional consequence of ERK activation. *J. Biol. Chem*., 278, 6258-6267.

Tomitsuka, E., Kita, K., Esumi, H. (2012) An anticancer agent, pyrvinium pamoate inhibits the NADH-fumarate reductase system--a unique mitochondrial energy metabolism in tumour microenvironments. *Biochem. J.,* 152, 171-183.

Trzaskowski, B., Latek, D., Yuan, S., Ghoshdastider, U., Debinski, A., Filipek, S. (2012) Action of molecular switches in GPCRs--theoretical and experimental studies. *Curr. Med. Chem.*, 19, 1090-1109.

Tsujino, N., Sakurai T. (2009) Orexin/hypocretin: a neuropeptide at the interface of sleep, energy homeostasis, and reward system. *Pharmacol. Rev.,* 61, 162-176.

Tulipano, G., Stumm, R., Pfeiffer, M., Kreienkamp, H.J., Höllt, V., Schulz, S. (2004) Differential beta-arrestin trafficking and endosomal sorting of somatostatin receptor subtypes. *J. Biol. Chem.,* 279, 21374-21382.

Tunaru, S., Lättig, J., Kero, J., Krause, G., Offermanns, S. (2005) Characterization of determinants of ligand binding to the nicotinic acid receptor GPR109A (HM74A/PUMA-G). *Mol. Pharmacol.,* 68, 1271-1280.

Turski, W.A., Schwarcz, R. (1988) On the disposition of intrahippocampally injected kynurenic acid in the rat. *Exp. Brain Res.*, 71, 563–567.

Ueda, H., Matsunaga, H., Olaposi, O., Nagai, J. (2013) Lysophosphatidic acid: chemical signature of neuropathic pain. *Biochim. Biophys. Acta*, 1831, 61-73.

Van der Ploeg, L., Laken, H., Sharma, S., Datta, R., Halem, H., Dong, J., Touvay, C., Teillot, M., Noonan, P., Tartaglia, L., Stoner, L., Henderson, B., Gottesdiener, K., Culler, M. (2014) Preclinical gastrointestinal prokinetic efficacy and endocrine effects of the ghrelin mimetic RM-131. *Life Sci.*, 109, 20-29.

van Heerebeek, L., Hamdani, N., Falcão-Pires, I., Leite-Moreira, A.F., Begieneman, M.P., Bronzwaer, J.G., van der Velden, J., Stienen, G.J., Laarman, G.J., Somsen, A., Verheugt, F.W., Niessen, H.W., Paulus, W.J. (2012) Low myocardial protein kinase G activity in heart failure with preserved ejection fraction. *Circulation,* 126, 830-839.

Venkatakrishnan, A.J., Deupi, X., Lebon, G., Tate, C.G., Schertler, G.F., Babu, M.M. (2013) Molecular signatures of G-protein-coupled receptors. *Nature,* 494, 185-194.

Venter, J.C., Adams, M.D., Myers, E.W., Li, P.W., Mural, R.J., Sutton, G.G., Smith, H.O., Yandell, M., Evans, C.A., Holt, R.A., Gocayne, J.D., Amanatides, P., Ballew, R.M., Huson, D.H., Wortman, J.R., Zhang, Q., Kodira, C.D., Zheng, X.H., Chen, L., Skupski, M., Subramanian, G., Thomas, P.D., Zhang, J., Gabor Miklos, G.L., Nelson, C., Broder, S., Clark, A.G., Nadeau, J., McKusick, V.A., Zinder, N., Levine, A.J., Roberts, R.J., Simon, M. et al. (2001) The sequence of the human genome. *Science*, 291, 1304-1351.

Vines, C.M., Revankar, C.M., Maestas, D.C., LaRusch, L.L., Cimino, D.F., Kohout, T.A., Lefkowitz, R.J., Prossnitz, E.R. (2003) N-formyl peptide receptors internalize but do not recycle in the absence of arrestins. *J. Biol. Chem.,* 278, 41581-41584.

Vischer, H.F., Siderius, M., Leurs, R., Smit, M.J. (2014) Herpesvirus-encoded GPCRs: neglected players in inflammatory and proliferative diseases? *Nat. Rev. Drug Discov.*, 13, 123-139.

Vogel, R., Mahalingam, M., Lüdeke, S., Huber, T., Siebert, F., Sakmar, T.P. (2008) Functional role of the "ionic lock"--an interhelical hydrogen-bond network in family A heptahelical receptors. *J. Mol. Biol.,* 380, 648-655.

Wall, M.A., Coleman, D.E., Lee, E., Iniguez-Lluhi, J.A., Posner, B.A., Gilman, A.G., Sprang, S.R. (1995) The structure of the G protein heterotrimer Gi alpha 1 beta 1 gamma 2. *Cell*, 83, 1047-1058.

Wallukat G. (2002) The beta-adrenergic receptors. *Herz*, 27, 683 - 690.

Wang, J., Simonavicius, N., Wu, X., Swaminath, G., Reagan, J., Tian, H., Ling, L. (2006a) Kynurenic acid as a ligand for orphan G protein-coupled receptor GPR35. *J. Biol. Chem*., 281, 22021-22018.

Wang, J., Wu, X., Simonavicius, N., Tian, H., Ling, L. (2006b) Medium-chain fatty acids as ligands for orphan G protein-coupled receptor GPR84. *J. Biol. Chem*., 281, 34457-34464.

Watari, K., Nakaya, M., Kurose, H. (2014) Multiple functions of G protein-coupled receptor kinases. *J. Mol. Signal.,* 9, 1.

Weng, Z., Zhang, B., Asadi, S., Sismanopoulos, N., Butcher, A., Fu, X., Katsarou-Katsari, A., Antoniou, C., Theoharides, T.C. (2012) Quercetin is more effective than cromolyn in blocking human mast cell cytokine release and inhibits contact dermatitis and photosensitivity in humans. *PLoS ONE,* 7: e33805.

West, G.M., Chien, E.Y., Katritch, V., Gatchalian, J., Chalmers, M.J., Stevens, R.C., Griffin, P.R. (2011) Ligand-dependent perturbation of the conformational ensemble for the GPCR β2 adrenergic receptor revealed by HDX. *Structure*, 19, 1424-1432.

Whalen, E.J., Rajagopal, S., Lefkowitz, R.J. (2011) Therapeutic potential of β-arrestin- and G protein-biased agonists. *Trends Mol. Med.*, 17, 126-139.

Wheatley, M., Wootten, D., Conner, M.T., Simms, J., Kendrick, R., Logan, R.T., Poyner, D.R., Barwell, J. (2012) Lifting the lid on GPCRs: the role of extracellular loops. *Br. J. Pharmacol.,* 165, 1688-1703.

Wide, L., Eriksson, K., Sluss, P.M., Hall, J.E. (2010) The common genetic variant of luteinizing hormone has a longer serum half-life than the wild type in heterozygous women. *J. Clin. Endocrinol. Metab.,* 95, 383-389.

Wifling, D., Löffel, K., Nordemann, U., Strasser, A., Bernhardt, G., Dove, S., Seifert, R., Buschauer, A. (2014) Molecular determinants for the high constitutive activity of the human histamine H4 receptor: functional studies on orthologues and mutants. *Br. J. Pharmacol., In press.*

Wildt, S., Gerngross, T.U. (2005) The humanization of N-glycosylation pathways in yeast. *Nat. Rev. Microbiol.*, 3, 119-128.

Williams, J.T., Ingram, S.L., Henderson, G., Chavkin, C., von Zastrow, M., Schulz, S., Koch, T., Evans, C.J., Christie, M.J. (2013) Regulation of μ-opioid receptors: desensitization, phosphorylation, internalization, and tolerance. *Pharmacol. Rev.,* 65, 223-254.

Wise, A., Sheehan, M., Rees, S., Lee, M., Milligan, G. (1999) Comparative analysis of the efficacy of A1 adenosine receptor activation of Gi/o alpha G proteins following coexpression of receptor and G protein and expression of A1 adenosine receptor-Gi/o alpha fusion proteins. *Biochemistry*, 38, 2272-2278.

Wise, A., Jupe, S.C., Rees, S. (2004) The identification of ligands at orphan G-protein coupled receptors. *Annu. Rev. Pharmacol. Toxicol.*, 44, 43-66.

Wisler, W., DeWire, S.M., Whalen, E.J., Violin, J.D., Drake, M.T., Ahn, S., Shenoy, S.K., Lefkowitz, R.J. (2007) A unique mechanism of beta-blocker action: carvedilol stimulates beta-arrestin signaling. *Proc. Natl. Acad. Sci. U.S.A.,* 104, 16657-16662.

Wisler, J.W., Xiao, K., Thomsen, A.R., Lefkowitz, R.J. (2014) Recent developments in biased agonism. *Curr. Opin. Cell Biol.,* 27, 18-24.

Woolf, P.J., Linderman, J.J. (2003) Untangling ligand induced activation and desensitization of G-protein-coupled receptors. *Biophys. J.,* 84, 3-13.

Wu, B., Chien, E.Y., Mol, C.D., Fenalti, G., Liu, W., Katritch, V., Abagyan, R., Brooun, A., Wells, P., Bi, F.C., Hamel, D.J., Kuhn, P., Handel, T.M., Cherezov, V., Stevens, R.C. (2010) Structures of the CXCR4 chemokine GPCR with small-molecule and cyclic peptide antagonists. *Science*, 330, 1066-1071.

Wu, H.Q., Schwarcz, R. (1996) Seizure activity causes elevation of endogenous extracellular kynurenic acid in the rat brain. *Brain Res. Bull.*, 39, 155-162.

Wu, H.Q., Rassoulpour, A., Schwarcz, R. (2007) Kynurenic acid leads, dopamine follows: a new case of volume transmission in the brain. *J. Neural. Transm.*, 114, 33-41.

Wu, H.Q., Pereira, E.F., Bruno, J.P., Pellicciari, R., Albuquerque, E.X., Schwarcz, R. (2010) The astrocyte-derived alpha7 nicotinic receptor antagonist kynurenic acid controls extracellular glutamate levels in the prefrontal cortex. *J. Mol. Neurosci.*, 40, 204-210.

Wurm, F., Bernard, A. (1999) Large-scale transient expression in mammalian cells for recombinant protein production. *Curr. Opin. Biotechnol.,* 10, 156-159.

Xu, F., Wu, H., Katritch, V., Han, G.W., Jacobson, K.A., Gao, Z.G., Cherezov, V., Stevens, R.C. (2011) Structure of an agonist-bound human A2A adenosine receptor. *Science*, 332, 322-337.

Xu, T.R., Yang, Y., Ward, R., Gao, L., Liu, Y. (2013a) Orexin receptors: multi-functional therapeutic targets for sleeping disorders, eating disorders, drug addiction, cancers and other physiological disorders. *Cell Signal.*, 25, 2413-2423.

Xu, W., Lacerda, L., Debeb, B.G., Atkinson, R.L., Solley, T.N., Li, L., Orton, D., McMurray, J.S., Hang, B.I., Lee, E., Klopp, A.H., Ueno, N.T., Reuben, J.M., Krishnamurthy, S., Woodward, W.A. (2013b) The antihelmintic drug pyrvinium pamoate targets aggressive breast cancer. *PLoS ONE*, 27: e71508.

Yanagihara, Y., Kasai, H., Shida, T. (1988) Immunopharmacological studies on TBX, a new antiallergic drug. Inhibitory effects on histamine release from peritoneal mast cells and lung fragments of rats. *Jpn. J. Pharmacol*., 48, 103-112.

Yang, Y., Lu, J.Y., Wu, X., Summer, S., Whoriskey, J., Saris, C., Reagan, J.D. (2010) G-protein-coupled receptor 35 is a target of the asthma drugs cromolyn disodium and nedocromil sodium. *Pharmacology*, 86, 1-5.

Yang, Y., Fu, A., Wu, X., Reagan, J.D. (2012) GPR35 is a target of the loop diuretic drugs bumetanide and furosemide. *Pharmacology,* 89, 13-17.

Yanni, J.M., Weimer, L.K., Glaser, R.L., Lang, L.S., Robertson, S.M., Spellman, J.M. (1993) Effect of lodoxamide on in vitro and in vivo conjunctival immediate hypersensitivity responses in rats. *Int. Arch. Allergy Immunol.,* 101, 102-106.

Yanni, J.M., Miller, S.T., Gamache. D.A., Spellman, J.M., Xu, S., Sharif, N.A. (1997) Comparative effects of topical ocular anti-allergy drugs on human conjunctival mast cells. *Ann. Allergy Asthma Immunol.*, 79, 541-545.

Yao, B.B., Hutchins, C.W., Carr, T.L., Cassar, S., Masters, J.N., Bennani, Y.L., Esbenshade, T.A., Hancock, A.A. (2003) Molecular modeling and pharmacological analysis of species-related histamine H(3) receptor heterogeneity. *Neuropharmacology*, 44, 773-786.

Yatomi, Y., Igarashi, K., Nakamura, K., Ohkawa, R., Masuda, A., Suzuki, A., Kishimoto, T., Ikeda, H., Aoki, J. (2013) Clinical Introduction of Lysophosphatidic Acid (LPA) and Autotaxin Assays. Lysophospholipid Receptors: Signaling and Biochemistry, First Edition. Chapter 33, pages 709-733.

Yazid, S., Sinniah, A., Solito, E., Calder, V., Flower, R.J. (2013) Anti-allergic cromones inhibit histamine and eicosanoid release from activated human and murine mast cells by releasing Annexin A1. *PLoS ONE,* 8: e58963.

Yoon, M.H., Choi, J.I., Bae, H.B., Jeong, S.W., Chung, S.S., Yoo, K.Y., Jeong, C.Y., Kim, S.J., Chung, S.T., Kim, C.M. (2005) Lack of the nitric oxide-cyclic GMP-potassium channel pathway for the antinociceptive effect of intrathecal zaprinast in a rat formalin test. *Neurosci. Lett.*, 390, 114-117.

Yoshida, M., Miyazato, M., Kangawa, K. (2012) Orphan GPCRs and methods for identifying their ligands. *Meth. Enzymol.,* 514, 33-44.

Yuan, H.T., Khankin, E.V., Karumanchi, S.A., Parikh, S.M. (2009) Angiopoietin 2 is a partial agonist/antagonist of Tie2 signaling in the endothelium. *Mol. Cell Biol.*, 29, 2011-2022.

Zambrowicz, B.P., Sands, A.T. (2003) Knockouts model the 100 best-selling drugs--will they model the next 100? *Nat. Rev. Drug Discov.*, 2, 38-51.

Zampeli, E., Tiligada, E. (2009) The role of histamine H4 receptor in immune and inflammatory disorders. *Br. J. Pharmacol.*, 157, 24-33.

Zhang, C., Srinivasan, Y., Arlow, D.H., Fung, J.J., Palmer, D., Zheng, Y., Green, H.F., Pandey, A., Dror, R.O., Shaw, D.E., Weis, W.I., Coughlin, S.R., Kobilka, B.K. (2012) High-resolution crystal structure of human protease-activated receptor 1. *Nature,* 492, 387-392.

Zhang, L., DiLizio, C., Kim, D., Smyth, E.M., Manning, D.R. (2006) The G12 family of G proteins as a reporter of thromboxane A2 receptor activity. *Mol. Pharmacol.,* 69, 1433-1440.

Zhang, X., Feng, Q., and Cote, R.H. (2005) Efficacy and selectivity of phosphodiesterase-targeted drugs in inhibiting photoreceptor phosphodiesterase (PDE6) in retinal photoreceptors. *Invest. Ophthalmol. Vis. Sci.,* 46, 3060-3066.

Zhao, P., Sharir, H., Kapur, A., Cowan, A., Geller, E.B., Adler, M.W., Seltzman, H.H., Reggio, P.H., Heynen-Genel, S., Sauer, M., Chung, T.D., Bai, Y., Chen, W., Caron, M.G., Barak, L.S., Abood, M.E. (2010) Targeting of the orphan receptor GPR35 by pamoic acid: a potent activator of extracellular signal-regulated kinase and β-arrestin2 with antinociceptive activity. *Mol. Pharmacol.*, 78, 560-568.

Zhao, P., Lane, T.R., Gao, H.G., Hurst, D.P., Kotsikorou, E., Le, L., Brailoiu, E., Reggio, P.H., Abood, M.E. (2014) Crucial positively charged residues for ligand activation of the GPR35 receptor. *J. Biol. Chem.*, 289, 3625-3638.

Zhu, Y., Michalovich, D., Wu, H., Tan, K.B., Dytko, G.M., Mannan, I.J., Boyce, R., Alston, J., Tierney, L.A., Li, X., Herrity, N.C., Vawter, L., Sarau, H.M., Ames, R.S., Davenport, C.M., Hieble, J.P., Wilson, S., Bergsma, D.J., Fitzgerald, L.R. (2001) Cloning, expression, and pharmacological characterization of a novel human histamine receptor. *Mol. Pharmacol.*, 59, 434-441.

Zlotnik, A., Yoshie, O. (2000) Chemokines: a new classification system and their role in immunity. *Immunity,* 12, 121-127.

Zlotnik, A., Yoshie, O., Nomiyama, H. (2006) The chemokine and chemokine receptor superfamilies and their molecular evolution. *Genome Biol.*, 7, 243.

Zmarowski, A., Wu, H.Q., Brooks, J.M., Potter, M.C., Pellicciari, R., Schwarcz, R., Bruno, J.P. (2009) Astrocyte-derived kynurenic acid modulates basal and evoked cortical acetylcholine release. *Eur. J. Neurosci.*, 29, 529-538.

Appendices